

DESIGN AND FABRICATION OF THREE-DIMENSIONAL SCAFFOLDS FOR BREAST CANCER STEM CELL EXPANSION AND MOLECULAR CHARACTERIZATION

Marc Rabionet Diaz

Per citar o enllaçar aquest document:
Para citar o enlazar este documento:
Use this url to cite or link to this publication:
<http://hdl.handle.net/10803/674042>

ADVERTIMENT. L'accés als continguts d'aquesta tesi doctoral i la seva utilització ha de respectar els drets de la persona autora. Pot ser utilitzada per a consulta o estudi personal, així com en activitats o materials d'investigació i docència en els termes establerts a l'art. 32 del Text Refós de la Llei de Propietat Intel·lectual (RDL 1/1996). Per altres utilitzacions es requereix l'autorització prèvia i expressa de la persona autora. En qualsevol cas, en la utilització dels seus continguts caldrà indicar de forma clara el nom i cognoms de la persona autora i el títol de la tesi doctoral. No s'autoritza la seva reproducció o altres formes d'explotació efectuades amb finalitats de lucre ni la seva comunicació pública des d'un lloc aliè al servei TDX. Tampoc s'autoritza la presentació del seu contingut en una finestra o marc aliè a TDX (framing). Aquesta reserva de drets afecta tant als continguts de la tesi com als seus resums i índexs.

ADVERTENCIA. El acceso a los contenidos de esta tesis doctoral y su utilización debe respetar los derechos de la persona autora. Puede ser utilizada para consulta o estudio personal, así como en actividades o materiales de investigación y docencia en los términos establecidos en el art. 32 del Texto Refundido de la Ley de Propiedad Intelectual (RDL 1/1996). Para otros usos se requiere la autorización previa y expresa de la persona autora. En cualquier caso, en la utilización de sus contenidos se deberá indicar de forma clara el nombre y apellidos de la persona autora y el título de la tesis doctoral. No se autoriza su reproducción u otras formas de explotación efectuadas con fines lucrativos ni su comunicación pública desde un sitio ajeno al servicio TDR. Tampoco se autoriza la presentación de su contenido en una ventana o marco ajeno a TDR (framing). Esta reserva de derechos afecta tanto al contenido de la tesis como a sus resúmenes e índices.

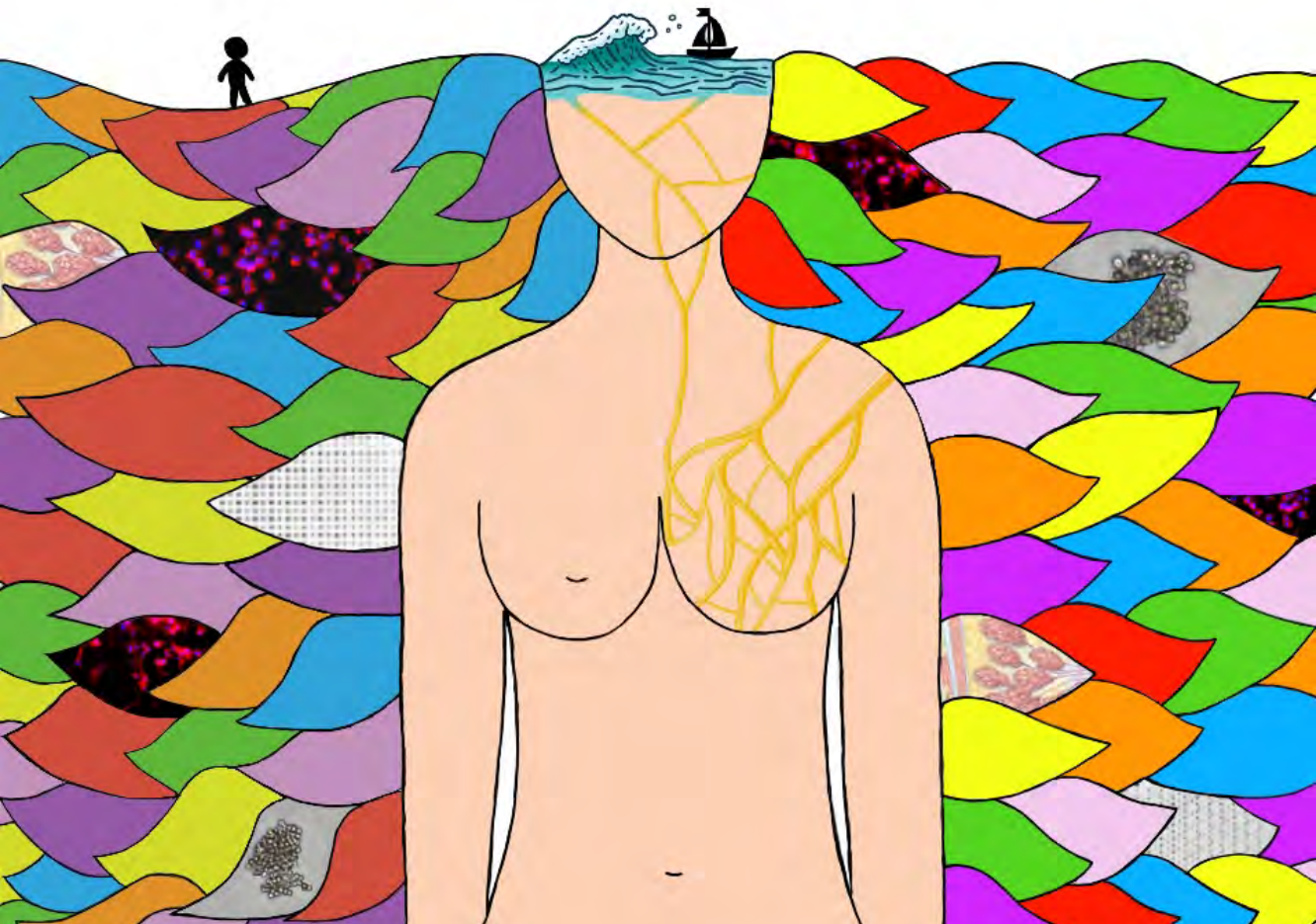
WARNING. Access to the contents of this doctoral thesis and its use must respect the rights of the author. It can be used for reference or private study, as well as research and learning activities or materials in the terms established by the 32nd article of the Spanish Consolidated Copyright Act (RDL 1/1996). Express and previous authorization of the author is required for any other uses. In any case, when using its content, full name of the author and title of the thesis must be clearly indicated. Reproduction or other forms of for profit use or public communication from outside TDX service is not allowed. Presentation of its content in a window or frame external to TDX (framing) is not authorized either. These rights affect both the content of the thesis and its abstracts and indexes.

DOCTORAL THESIS

DESIGN AND FABRICATION OF THREE-DIMENSIONAL
SCAFFOLDS FOR BREAST CANCER STEM CELL
EXPANSION AND MOLECULAR CHARACTERIZATION

Marc Rabionet Diaz

2021





DOCTORAL THESIS

DESIGN AND FABRICATION OF THREE-
DIMENSIONAL SCAFFOLDS FOR BREAST
CANCER STEM CELL EXPANSION AND
MOLECULAR CHARACTERIZATION

MARC RABIONET DIAZ

2021



DOCTORAL THESIS

DESIGN AND FABRICATION OF THREE-
DIMENSIONAL SCAFFOLDS FOR BREAST
CANCER STEM CELL EXPANSION AND
MOLECULAR CHARACTERIZATION

MARC RABIONET DIAZ

2021

Doctoral Program in Molecular Biology, Biomedicine and Health

Advised by Dr. Joaquim de Ciurana Gay and Dr. Teresa Puig Miquel

This thesis submitted in fulfillment of the requirements to obtain the doctoral degree
from the University of Girona

This PhD thesis contains one annex

Dr. Joaquim de Ciurana Gay, Full Professor at the Department of Mechanical Engineering and Industrial Construction of the University of Girona, and Dr. Teresa Puig Miquel, Full Professor at the Department of Medical Sciences of the University of Girona,

CERTIFY:

That the thesis entitled *Design and fabrication of three-dimensional scaffolds for breast cancer stem cell expansion and molecular characterization*, presented by Marc Rabionet Diaz to obtain a doctoral degree with recognition as an international doctorate, has been completed under our supervision and meets the requirements to aim for an International Doctorate.

For all intents and purposes, we hereby sign this document.



Dr. Joaquim de Ciurana Gay



Dr. Teresa Puig Miquel

*A totes les mares, àvies, ties, germanes, filles i amigues que els hi ha tocat ser
valentes.*

*A les que han guanyat la batalla i a les que, malauradament, s'han quedat enrere.
I, sobretot, a tu mama.*

Acknowledgments

Quan tanques una etapa sempre és bo tirar la vista enrere i agrair a totes les persones que han format part del teu camí.

Primer de tot, haig de donar les gràcies als meus directores de tesi per haver-me brindat l'oportunitat de començar i desenvolupar aquest projecte. M'heu permès néixer i créixer com a investigador. Quim, gràcies per aportar la part racional, pràctica i més tecnològica al projecte. Teresa, gràcies per tots els consells, ajuda i per representar la part biològica de la col·laboració. A part de "jefes", sempre sereu els meus "pares científics".

Gràcies Isabel, Jordi, Inés i Maria Luisa per obrir-me les portes del GREP. Un món nou per mi en el qual m'heu anat ajudant i acompanyant. Antonio, muchas gracias por toda tu ayuda y por el buen tándem ingeniero-biotecnólogo que formamos. Tu energía e inquietudes son contagiosas. Enric, tot i que ens hem conegut a la part final del meu camí, gràcies pel teu bon rollo, ajuda i docència cervesera. Espero no haver de dormir al sofà. Alba, la nostra *doodleler* oficial. Gràcies per la teva ajuda i el teu "petardeo". Ja saps que m'hauràs d'ajudar a organitzar una bona festa eh ;)

Adriana, tu em vas obrir les portes de TargetsLab. Gràcies per tot el que em vas ensenyar i per la teva paciència. Ariadna Giró (aka AG), crec que em vas ensenyar, a parts iguals, protocols i cançons de l'Enrique Iglesias. Gràcies per les dues coses. Ariadna Sarrats (aka AS), gràcies pel teu suport i consells durant el temps que vam compartir. Núria, gràcies per tots els moments viscuts. Només dir-te que a hores d'ara encara no tenim escombra.

Sònia, sé que quan vaig entrar per la porta no era la persona que esperaves. Però ara després de tant de temps penses el mateix? Bueno, per si de cas no responguis... (hahahahah). Fora bromes, hem fet gran part d'aquest camí junts i t'has convertit en una persona molt especial per mi. M'has ensenyat moltes coses, a nivell professional i personal. La passió pel que fas i les teves ganes d'aprenentatge són contagioses. Si us plau, que no s'acabin els vermuts, l'accent sud-americà ni les teves bromes.

Emma, la meva *sibiling*, què dir-te... Gràcies per ser el *ying* del meu *yang*, per fer-me costat i ensenyar-me tant. Per poder cantar junts Britney Spears i Oques Grasses a cultius durant la mateixa tarda. Trobaré a faltar la teva dislèxia i la teva visió racional a parts iguals. T'ho he dit més d'una vegada, en unes altres condicions ja t'hagués demanat per casar-te amb mi.

Irene, vas entrar més tard al grup però de seguida et vas fer un lloc dins els nostres cors. Gràcies per l'il·limitat número de fotos i vídeos compromesos, i la teva manera tan fidedigne de relatar qualsevol cosa. Però, sobretot, gràcies pels moments de complicitat i la germanor i estima que desprens. I ja saps, sempre més amunt Girona!

Santi, sempre dius que no et caic bé, però sé que és mentida. Gràcies per les birres, les notes de flamenco, les passejades amb moto i tota l'ajuda al llarg d'aquests anys. Encara que finalitzi aquesta etapa, la nostra competició de *crushes* no s'acaba!

Gràcies als altres estudiants predoctorals del grup, Xavier, David i Andreu. Alguns esteu a punt d'acabar i d'altres just comenceu aquest camí. Gràcies per tots els moments viscuts.

També voldria agrair a tots els estudiants amb els quals he coincidit durant aquests anys: Ander, Paula B, Maria del Mar, Adrià, Joan, Marina, Tess, Bea, Toni... Gràcies pel bon rollo que heu aportat al grup. Sobretot agrair a la Jessica, la Paula C i la Sabina. Va ser un plaer ensenyar-vos el que bonament sabia i poder treballar amb vosaltres. Espero que guardeu un bon record i que el vostre pas pel grup fos només l'inici d'una gran carrera.

Com no, també haig d'agrair la gent de NEOMA. Beltran, aun a día de hoy no puedo olvidar tus calzoncillos. Gracias por tus visitas sorpresas al laboratorio y tu sabiduría, tan infinita como diversa. Txell, gràcies pels cafès i les "reunions" al llarg d'aquests anys. I per últim Anna, ja ens coneixíem d'abans però fer junts el camí de la tesi ha estat un autèntic plaer. De compartir apunts a la carrera, a compartir penes (i alegries!) del doctorat. Gràcies per la teva bondat i somriures eterns, els nostres debats de *Drag Race*, els vídeos de l'Aramís i els teus pensaments extrems. No canviïs mai.

També m'agradaria donar les gràcies a en Marc Yeste. Sempre que hem anat al teu laboratori ens has fet sentir com un més. Gràcies per tota l'ajuda i consells durant aquests anys, tant a nivell científic com personal.

I also want to thank you all the people I met in Delaware. April, thanks for bringing me the opportunity to come to the UD and your group. I really appreciate all the kindness and help I got from you throughout all my stay. Jennifer, I still remember that the first paper my supervisors gave me to focus my project was one of yours. So eventually being in your research group felt like a full circle. Thanks for your teaching, guidance, and empathy. We all know they were hard times to be abroad, but you both helped me and made it easier. I also want to show gratitude to all the April Kloxin Group Members. Thanks Samantha and Lina for all the things you taught me, from making a hydrogel to the campfire roasted marshmallows. Thanks Amber, Paige, Bryan, Kartik, Eden, DeVonte, Phillip, Kimberly, and Kat (me debes un café en Torroella ☺) for making me feel welcome. I also have to thank all the people from ChristianaCare. Lynn, I learnt from you plenty of things about cytometry (apart from your huge patience with my endless samples). Thanks to Daniel, Steficah, and Kader, for being the best labmates and making me feel a part of your group. Daniel, you owe me a beer in Main Street once covid is over. I also want to thank you the other people in the lab, especially Caroline, Natalia, and

Shirin. Thanks for all your help and empathy. Caroline and Natalia, I still remember the taste of all those cheesecakes!

Joy, you were such an amazing roommate and support during all the stay. Thanks for all the trips (both to state parks and the liquor store), the basement parties... I hope you are still listening "Kitt y los coches del pasado" while drinking Martini.

Dre, thanks for being so supportive and friendly. Thanks for all the dinners, bike trips... I'm still waiting for you in Catalonia!

Ryan, fuiste todo un descubrimiento. Gracias por todo lo que me enseñaste y por ser mi apoyo en estos tiempos tan raros. No sabes hasta qué punto me ayudaste. Ya con ganas de verte este verano en Madrid! Espero no acabar igual que en Grotto.

Elena y Alberto, mis compañeros españoles en Delaware. Encontraros fue una gran suerte. Gracias por todas las cenas y paseos!

També em toca agrair a tots els meus amics que han hagut d'aguantar les "xapes" de la tesi. Gràcies a la gent de l'uni: Xènia, Gerard, Tina, Fuse, Laura, Irene, Mercè, Arnau. Gràcies per totes les birres, calçotades, Catans, abraçades, més birres, *escape rooms*, excursions i viatges. Irene, de parella de pràctiques durant la carrera a doctors. Moltes gràcies per tota l'ajuda. Només dir-te que m'has deixat el llistó molt alt!

Gràcies a la gent de Cassà: Sílvia, Susi, Sara, Marc... També heu hagut d'escoltar drames (i "salseo") de la tesi, però amb vosaltres es fa molt més passatger. Gràcies pels sopars, partits de pàdel, festes, *skypes* covid...

Gràcies Mònica i Sara per tots els vostres consells, vermuts, nits d'hipotèrmia als Pirineus, festes al Casino... Ja sigui per escoltar drames o celebrar qualsevol cosa, fer-ho amb vosaltres és màgic.

Grazie mille a quelli della macchina. Gràcies per tot el suport i preocupació i, sobretot, per donar-me la millor rebuda possible al tornar de Delaware.

I ja per acabar, moltes gràcies a la família. Moltes gràcies tiets, avis... per tot el suport i interès. Meritxell, gràcies per la portada, és immillorable. Mama, papa, David... Mareta meva, vosaltres sí que heu hagut d'escoltar drames de la tesi. Moltes gràcies per ser-hi i fer-me sempre costat, sigui a casa, a 10 o a 6,400 km. Gràcies mama per escoltar-me quan preparo seminaris, poder parlar de la malaltia i veure que realment el que faig té un impacte. Gràcies papa per alegrar-te de tots els passets que vaig fent i per posar-me una cervesa en fred quan veus que la necessito. Gràcies David per posar-te amb mi per riure, però després demanar-me consell. Si he fet tot el que he fet, ha sigut perquè hi éreu vosaltres. Us estimo.

Funding and technical support

This work has been supported by Spanish grants from Fundación Ramón Areces, Instituto de Salud Carlos III (PI1400329), Ministerio de Economía y Competitividad (MINECO; DPI2013-45201-P, DPI2016-77156-R), Universitat de Girona (MPCUdG2016/036) and the Catalanian government (2014SGR00868, 2017SGR00385). Financial support was also provided by Fundació Oncolliga and RadikalSwim (OncoSwim).

Marc Rabionet Diaz was the recipient of a pre-doctoral and mobility grant, both from Universitat de Girona (IFUdG2017/62 and MOB2019, respectively).

The authors thank the researcher Sabina Couto-Ovejero, TechnoSperm, and the Research Technical Services, both entities from the Universitat de Girona.

The authors are also grateful to Lynn Opendaker and the flow cytometry core at the Cawley Center for Translational Research, Helen F Graham Cancer Center, which is supported by the Delaware INBRE program, with a grant from the National Institute of General Medical Sciences (NIGMS; P20 GM103446) from the National Institutes of Health and the State of Delaware.

Publications resulted from this thesis

This thesis is presented as a compendium of manuscripts. Some studies published before PhD enrolment are presented in this thesis and described in the following publications.

Title Optimization of poly(ϵ -caprolactone) scaffolds suitable for 3D cancer cell culture (Proceeding)
Authors Ariadna Giró-Perafita, Marc Rabionet, Teresa Puig*, Joaquim Ciurana*
Journal Procedia CIRP
Publication year 2016
CiteScore ₂₀₁₆ 1.8 (65th percentile in Industrial and Manufacturing Engineering; position 106 of 304)
DOI 10.1016/j.procir.2015.07.031

Title Breast cancer stem cell culture and enrichment using poly(ϵ -caprolactone) scaffolds
Authors Sònia Palomeras[†], Marc Rabionet[†], Inés Ferrer, Ariadna Sarrats, Maria Luisa Garcia-Romeu, Teresa Puig*, Joaquim Ciurana*
Journal Molecules
Publication year 2016
Impact Factor ₂₀₁₆ 2.861 (Q2 in Chemistry, Organic; position 17 of 59)
DOI 10.3390/molecules21040537

Studies published during PhD enrolment are represented in the following publications. Papers to be considered for compendium of publications format are underlined.

Title Electrospinning parameters selection to manufacture polycaprolactone scaffolds for three-dimensional breast cancer cell culture and enrichment (Proceeding)
Authors Marc Rabionet, Teresa Puig*, Joaquim Ciurana*
Journal Procedia CIRP
Publication year 2017
CiteScore ₂₀₁₇ 2.4 (74th percentile in Industrial and Manufacturing Engineering; position 85 of 328)

DOI	10.1016/j.procir.2017.03.341
Title	<u>Electrospinning PCL scaffolds manufacture for three-dimensional breast cancer cell culture</u>
Authors	Marc Rabionet, Marc Yeste, Teresa Puig*, Joaquim Ciurana*
Journal	Polymers
Publication year	2017
Impact Factor ₂₀₁₇	2.935 (Q1 in Polymer Science; position 19 of 87)
DOI	10.3390/polym9080328
Title	<u>Design of a scaffold parameter selection system with additive manufacturing for a biomedical cell culture</u>
Authors	Marc Rabionet, Emma Polonio-Alcalá, Antonio J. Guerra, Jessica Martin, Teresa Puig*, Joaquim Ciurana*
Journal	Materials
Publication year	2018
Impact Factor ₂₀₁₈	2.972 (Q2 in Materials Science, Multidisciplinary; position 102 of 293)
DOI	10.3390/ma11081427
Title	<u>EGCG-derivative G28 shows high efficacy inhibiting the mammosphere-forming capacity of sensitive and resistant TNBC models</u>
Authors	Ariadna Giró-Perafita [†] , Marc Rabionet [†] , Marta Planas, Lidia Feliu, Joaquim Ciurana, Santiago Ruiz-Martínez*, Teresa Puig*
Journal	Molecules
Publication year	2019
Impact Factor ₂₀₁₉	3.267 (Q2 in Chemistry, Multidisciplinary; position 70 of 177)
DOI	10.3390/molecules24061027
Title	Manufacture of PCL scaffolds through electrospinning technology to accommodate triple negative breast cancer cells culture (Proceeding)

Authors Marc Rabionet, Teresa Puig*, Joaquim Ciurana*
Journal Procedia CIRP
Publication year 2020
CiteScore ₂₀₂₀ 3.3 (68th percentile in Industrial and Manufacturing Engineering; position 107 of 336)
DOI 10.1016/j.procir.2020.05.124

Title Fatty acid synthase as a novel biomarker for triple negative breast cancer stem cell subpopulation cultured on electrospun scaffolds

Authors Marc Rabionet, Emma Polonio-Alcalá, Joana Relat, Marc Yeste, Jennifer Sims-Mourtada, April M. Kloxin, Marta Planas, Lidia Feliu, Joaquim Ciurana*, Teresa Puig*
Journal Under review on Materials Today Bio
Publication year -
Impact Factor ₂₀₂₀ 7.348 (Q1 in Materials Science, Biomaterials; position 6 of 40)
DOI -

A review published during PhD enrolment is represented in the following publication (see Annex).

Title Three-dimensional manufactured supports for breast cancer stem cell population characterization
Authors Emma Polonio-Alcalá[†], Marc Rabionet[†], Santiago Ruiz-Martínez, Joaquim Ciurana, Teresa Puig*
Journal Current Drug Targets
Publication year 2019
Impact Factor ₂₀₁₉ 2.632 (Q3 in Pharmacology & Pharmacy; position 145 of 271)
DOI 10.2174/1389450120666181122113300

Additional unrelated studies performed during PhD enrolment will not be presented in this thesis and are represented in the following publications.

Title 3D-printed tubular scaffolds for vascular tissue engineering (Proceeding)
Authors Marc Rabionet[†], Antonio J. Guerra[†], Teresa Puig*, Joaquim Ciurana*
Journal Procedia CIRP
Publication year 2018
CiteScore 2018 2.7 (73rd percentile in Industrial and Manufacturing Engineering; position 88 of 335)
DOI 10.1016/j.procir.2017.12.094

Title Effects of different sterilization processes on the properties of a novel 3D-printed polycaprolactone stent
Authors Antonio J. Guerra*, Paula Cano, Marc Rabionet, Teresa Puig, Joaquim Ciurana
Journal Polymers for Advanced Technologies
Publication year 2018
Impact Factor 2018 2.162 (Q2 in Polymer Science; position 36 of 87)
DOI 10.1002/pat.4344

Title 3D-printed PCL/PLA composite stents: towards a new solution to cardiovascular problems
Authors Antonio J. Guerra, Paula Cano, Marc Rabionet, Teresa Puig, Joaquim Ciurana*
Journal Materials
Publication year 2018
Impact Factor 2018 2.972 (Q2 in Materials Science, Multidisciplinary; position 102 of 293)
DOI 10.3390/ma11091679

Title Screening of additive manufactured scaffolds designs for triple negative breast cancer 3D cell culture and stem-like expansion

Authors Emma Polonio-Alcalá, Marc Rabionet, Antonio J. Guerra, Marc Yeste, Joaquim Ciurana*, Teresa Puig*
Journal International Journal of Molecular Sciences
Publication year 2018
Impact Factor ₂₀₁₈ 4.183 (Q2 in Biochemistry & Molecular Biology; position 78 of 299)
DOI 10.3390/ijms19103148

Title PLA electrospun scaffolds for three-dimensional triple-negative breast cancer cell culture
Authors Emma Polonio-Alcalá[†], Marc Rabionet[†], Xavier Gallardo, David Angelats, Joaquim Ciurana, Santiago Ruiz-Martínez*, Teresa Puig*
Journal Polymers
Publication year 2019
Impact Factor ₂₀₁₉ 3.426 (Q1 in Polymer Science; position 16 of 89)
DOI 10.3390/polym11050916

_ Paper to be considered for compendium of publications format

* Corresponding author

[†] These authors contributed equally to this manuscript

Abbreviations

#

2D	Two-dimensional
3D	Three-dimensional
7-AAD	7-AminoActinoMycin D

A

A	Androgen
ABC	ATP-Binding Cassette
ACACA	Acetyl-CoA Carboxylase
ACLY	ATP Citrate LYase
AKT	Protein kinase B
ALDH1	Aldehyde DeHydrogenase 1
AM	Additive Manufacturing
AML	Acute Myeloid Leukemia
AMPK	5' Adenosine Monophosphate-activated Protein Kinase
AmR	AmphiRegulin
APC	AlloPhycoCyanin
AR	Androgen Receptor
ATCC	American Type Culture Collection
ATM	Ataxia Telangiectasia Mutated
ATP	Adenosine TriPhosphate
ATRA	All- <i>Trans</i> Retinoic Acid

B

B27	B27 supplement
BAAA	BODIPY-AminoAcetAldehyde
BAA	BODIPY-AminoAcate
BC	Breast Cancer
BCSC	Breast Cancer Stem Cell
BRCA1	BReast CAncer type 1 susceptibility protein
BRCA2	BReast CAncer type 2 susceptibility protein
BSA	Bovine Serum Albumin
BTC	BeTaCellulin

C

c-Src	cellular Src
-------	--------------

CAD	Computer-Aided Design
CAM	Computer-Aided Manufacturing
CAR-T	Chimeric Antigen Receptor T cell
CD	Cluster of Differentiation
cDNA	complementary DNA
CK	CytoKeratin
CL	Claudin-Low
CPT1	Carnitine PalmitoylTransferase 1
CSC	Cancer Stem Cell
CTC	Circulating Tumor Cell
CTLA-4	Cytotoxic T-Lymphocyte-Associated protein 4

D

DAPI	4,6-DiAmidino-2-PhenylIndole
DEAB	DiEthylAminoBenzaldehyde
DDR	DNA Damage Response
DMA	Dynamic Mechanical Analysis
DMEM	Dulbecco's Modified Eagle's Medium
DMEM/F12	Dulbecco's Modified Eagle's Medium nutrient mixture F12
DMF	DiMethyl Formamide
DMSO	DiMethyl SulfOxide
DNA	DeoxyriboNucleic Acid
DSC	Differential Scanning Calorimetry
DXR	DoXorubicin Resistant

E

E2	oEstradiol
ECM	ExtraCellular Matrix
EDTA	EthyleneDiamineTetraacetic Acid
EdU	5-Ethynyl-2'-deoxyUridine
EGCG	(-)-EpiGalloCatechin-3-Gallate
EGF	Epidermal Growth Factor
EGFR	Epidermal Growth Factor Receptor (HER1, ERBB1)
EMT	Epithelial-to-Mesenchymal Transition
EPG	EPiGen
EPR	EPiRegulin
ER	Estrogen Receptor
ERBB	Human epidermal growth factor receptor

ERBB1	Human epidermal growth factor receptor 1 (HER1, EGFR)
ERBB2	Human epidermal growth factor receptor 2 (HER2, Neu)
ERBB3	Human epidermal growth factor receptor 3 (HER3)
ERBB4	Human epidermal growth factor receptor 4 (HER4)
ERK	Extracellular signal-Regulated Kinase
ESA	Epithelial-Specific Antigen
EV	Electronic Volume

F

FA	Fatty Acid
FASN	Fatty Acid SyNthase
FBS	Fetal Bovine Serum
FDA	Food and Drug Administration
FDM	Fused Deposition Modeling
FFF	Fused Filament Fabrication
FGF	Fibroblast Growth Factor
FITC	Fluorescein IsoThioCyanate
FL1	Fluorescent channel 1

G

G28	G28UCM
GAPDH	GlycerAldehyde 3-Phosphatase DeHydrogenase
GF	Growth Factor
GFR	Growth Factor Receptor
GTPase	Guanosine TriPhosphatase

H

H ⁺	Hydron (hydrogen)
HA	Hyaluronic Acid
HB-EGF	Heparin-Binding EGF-like Growth Factor
HBMSC	Human Bone Marrow Stromal Cell
HER	Human Epidermal growth factor Receptor
HER1	Human Epidermal growth factor Receptor 1 (ERBB1, EGFR)
HER2	Human Epidermal growth factor Receptor 2 (ERBB2, Neu)
HER2-OE	Human Epidermal growth factor Receptor 2 OverExpressing
HER3	Human Epidermal growth factor Receptor 3 (ERBB3)
HER4	Human Epidermal growth factor Receptor 4 (ERBB4)

HMSC	Human Mesenchymal Stem Cell
HRP	HorseRadish Peroxidase
I	
IC	Inhibitory Concentration
IGF-1R	Insulin-like Growth Factor 1 Receptor
IHC	ImmunoHistoChemistry
IRS	Insulin Receptor Substrate
K	
KRAS	K-RAS
L	
LDH	Lactate DeHydrogenase
LDS	Lithium Dodecyl Sulfate
LKB1	Liver Kinase B1
LMD	List-Mode Data
M	
MAPK	Mitogen Activated Protein Kinase
MAPKK	Mitogen Activated Protein Kinase Kinase
MAPKKK	Mitogen Activated Protein Kinase Kinase Kinase
MEK	MAPK/ERK Kinase
MET	Mesenchymal-to-Epithelial Transition
MFA	Mammosphere Forming Assay
MFI	Mammosphere Forming Index
MFin	Mammosphere Forming Inhibition
ML	Mesenchymal-Like
mRNA	messenger RiboNucleic Acid
mTOR	mammalian Target Of Rapamycin
mTORC1	mammalian Target Of Rapamycin Complex 1
mTORC2	mammalian Target Of Rapamycin Complex 2
MTT	3-(4,5-diMethylThiazol-2-yl)-2,5-diphenylTetrazolium bromide

N

NADPH	Nicotinamide Adenine Dinucleotide Phosphate Hydrogen
NDF	Neu Differentiation Factor
NF- κ B	Nuclear Factor κ B
NOD/SCID	NonObese Diabetic / Severe Combined ImmunoDeficiency
NRG	NeuReGulin

O

OCT3/4	OCTamer-binding transcription factor β
--------	--

P

P	Progesterin
PARP	Poly (ADP-Ribose) Polymerase
PBS	Phosphate-Buffered Saline
PBS-T	Phosphate-Buffered Saline Tween
PCL	Poly(ϵ -CaproLactone)
PCR	Polymerase Chain Reaction
PD-1	Programmed cell Death protein 1
PD-L1	Programmed cell Death-Ligand 1
PE	PhycoErythrin
PFA	ParaFormAldehyde
pHEMA	polyHydroxyEthylMethAcrylate
PI3K	Phospholinositide-3-Kinase
PIP2	Phosphatidylinositol 4,5-biPhosphate
PIP3	Phosphatidylinositol 3,4,5-triPhosphate
PLA	PolyLactic Acid
PMSF	PhenylMethylSulfonyl Fluoride
PR	Progesterone Receptor
PROCR	PROtein C Receptor
PS	PolyStyrene
PTEN	Phosphatase and Tensin homolog
PTR	PacliTaxel Resistant

R

RAF	Rapidly Accelerated Fibrosarcoma
RAS	RAt Sarcoma

RHEB	Ras Homolog Enriched in Brain
RNA	RiboNucleic Acid
ROS	Reactive Oxygen Species
RPMI	Roswell Park Memorial Institute
RSK	Ribosomal S6 Kinase
RT-PCR	Real Time-Polymerase Chain Reaction

S

SDS-PAGE	Sodium Dodecyl Sulphate-PolyAcrylamide Gel Electrophoresis
SE	Standard Error
SEM	Scanning Electron Microscopy
SEM	Standard Error of the Mean
SOX2	Sex determining region Y HMG-bOX 2
SOX4	Sex determining region Y HMG-bOX 4
Sp1	Stimulatory protein 1
Sp3	Stimulatory protein 3
SREBP1	Sterol Regulatory Element Binding Protein 1
SS	Side Scatter
STL	STereoLithography

T

TBS-T	Tris-Buffered Saline Tween
TE	Tissue Engineering
TGA	Thermal Gravimetric Analysis
TGF- α	Transforming Growth Factor alfa
TGF- β	Transforming Growth Factor beta
TK	Tyrosine Kinase
TKI	Tyrosine Kinase Inhibitor
TNBC	Triple Negative Breast Cancer
TSC1	Tuberous SCLerosis protein 1
TSC2	Tuberous SCLerosis protein 2

U

USF	Upstream Stimulatory Factor
UV	UltraViolet

V

VEGF Vascular Endothelial Growth Factor

W

WHO World Health Organization

Index of figures and tables

Index of figures

Figure 1. The hallmarks of cancer	18
Figure 2. Female breast anatomy	20
Figure 3. Human epidermal growth factor receptors (HER) family	25
Figure 4. Intracellular signaling via the mitogen activated protein kinase (MAPK) and phosphoinositide 3-kinase (PI3K)/ mammalian target of rapamycin (mTOR) pathways	27
Figure 5. Distribution of clinical-pathological categories relative to the intrinsic subtypes of breast cancer	31
Figure 6. Two general models of heterogeneity in solid cancer cells	39
Figure 7. Schematic representation of tumor cell heterogeneity in an aggressive breast cancer	43
Figure 8. Epithelial-to-mesenchymal transition (EMT).....	48
Figure 9. Model of epithelial-to-mesenchymal transition (EMT) and mesenchymal-to-epithelial transition (MET) in driving the plasticity of breast cancer stem cells (BCSCs).....	49
Figure 10. Representation of the putative association between breast cancer molecular subtypes and the expression pattern of breast cancer stem cell (BCSC) biomarkers.....	50
Figure 11. Connecting glucose metabolism and fatty acid (FA) biosynthesis pathways in tumor cells	52
Figure 12. Regulation of fatty acid synthase (FASN) expression in cancer cells....	54
Figure 13. Fatty acid synthase (FASN) inhibition and cancer cell death	56
Figure 14. Schematic comparison between monolayer two-dimensional (2D) and three-dimensional (3D) breast cancer cell culture.....	58
Figure 15. Schematic representation of triple negative breast cancer (TNBC) cell metabolism modulation within three-dimensional (3D) electrospinning (ES) poly(ϵ -caprolactone) (PCL) scaffold culture.....	222

Index of tables

Table 1. Main features of breast cancer molecular subtypes and concordance with their immunohistochemical profile	23
Table 2. Comparison of different cell culture supports used in worldwide laboratories	60
Table 3. Comparison of different technologies used to manufacture scaffolds for 3D cell culture.....	63

Index

Acknowledgments.....	i
Publications resulted from this thesis.....	vii
Abbreviations.....	xv
Index of figures and tables.....	xxv
Summary	1
CHAPTER 1 Introduction	13
1 <i>Cancer</i>	17
2 <i>Breast cancer</i>	19
2.1 Breast cancer classification	20
2.2 Relevant cell signaling in breast cancer	23
3 <i>Triple negative breast cancer</i>	28
3.1 Triple negative breast cancer prognosis	29
3.2 Molecular classification of triple negative breast cancer.....	30
3.3 Triple negative breast cancer treatment	30
3.4 Targeted therapy of triple negative breast cancer and potential treatment regimens	34
4 <i>Cancer stem cells</i>	38
4.1 Breast cancer stem cell identification.....	39
4.2 Breast cancer stem cells and chemoresistance	42
4.3 Novel approaches against breast cancer stem cells.....	44
4.4 Epithelial-to-mesenchymal transition.....	46
4.5 Breast cancer stem cell plasticity.....	48
4.6 Breast cancer stem cells and triple negative breast cancer	50
5. <i>Fatty acid synthase</i>	51
5.1 Fatty acid synthase function	51
5.2 Fatty acid synthase regulation	52
5.3 Fatty acid synthase inhibition and cancer	54
6. <i>Cancer cell culture</i>	57
6.1 Three-dimensional cell culture supports	59
6.2 Technologies to manufacture three-dimensional scaffolds.....	61
6.3 Available biomaterials for scaffold manufacture.....	64
6.4 Breast cancer stem cell population in three-dimensional culture	66
CHAPTER 2 Hypothesis and Objectives	69

CHAPTER 3 Results I Use and optimization of fused filament fabrication technology to manufacture PCL scaffolds for 3D cell culture and stemness expansion	75
CHAPTER 4 Results II Use and optimization of electrospinning technology to manufacture PCL scaffolds for 3D cell culture and stemness expansion	115
CHAPTER 5 Results III Evaluation of BCSC and FASN role in chemosensitive and chemoresistant MDA-MB-231 TNBC cells	127
CHAPTER 6 Results IV Enrichment of BCSCs in the TNBC cell models MDA-MB-231 (mesenchymal-like) and MDA-MB-468 (basal-like) within 3D ES PCL scaffold culture	149
CHAPTER 7 Discussion	207
<i>Discussion</i>	209
CHAPTER 3	209
CHAPTER 4	212
CHAPTER 5	215
CHAPTER 6	217
Concluding remarks	223
<i>Limitations of the study</i>	224
CHAPTER 8 Conclusions	227
CHAPTER 9 Future directions	233
CHAPTER 10 References	237
CHAPTER 11 Annex	265

Summary

Resum

Actualment no existeix una teràpia dirigida contra el càncer de mama triple negatiu (*triple negative breast cancer*, TNBC), el qual representa el 15-20% dels tumors mamaris i mostra un perfil agressiu i amb mal pronòstic. Tot i una bona resposta inicial a la quimioteràpia, el 30% de les pacients recauen durant els següents 5 anys posttractament. L'aparició de recaigudes i el fracàs terapèutic són causats, en part, per a la presència d'una subpoblació cel·lular en el tumor amb propietats similars a les cèl·lules mare, anomenades, per aquest motiu, cèl·lules mare del càncer de mama (*breast cancer stem cells*, BCSCs). Tot i la seva importància, el seu estudi és dificultós degut a la seva poca representació dins el tumor o línia cel·lular i, també, al fet que el cultiu cel·lular tradicional *in vitro* en 2 dimensions (2D) induïx la seva diferenciació, transformant-les en cèl·lules canceroses no-mare. Així doncs, han aparegut diferents models de cultiu cel·lular en 3 dimensions (3D) com a alternativa per restablir un entorn similar al fisiològic i resoldre els problemes descrits anteriorment. Entre ells, els *scaffolds* ("bastida" traduït literalment) ofereixen una estructura física formada per un entramat de filaments polimèrics, el qual mimetitzava l'arquitectura de la matriu extracel·lular.

La principal hipòtesi d'aquesta tesi és que l'ús de *scaffolds* 3D permetrà l'expansió i caracterització de la subpoblació de BCSCs en mostres TNBC i, així doncs, facilitarà el desenvolupament de teràpies dirigides contra cèl·lules mare tumorals. Amb aquest objectiu, en la primera part del treball s'han optimitzat dues tecnologies diferents, la fabricació per filament fos (*fused filament fabrication*, FFF) i l'electrofilat (*electrospinning*, ES), per tal de fabricar *scaffolds* amb el polímer àmpliament utilitzat poli(ϵ -caprolactona) (PCL). Diversos paràmetres de les dues tecnologies han estat optimitzats segons l'estabilitat del procés de fabricació. Els *scaffolds* produïts amb un aparell FFF estaven formats per fibres micromètriques, mentre que les malles ES presentaven una estructura nanofilamentosa tova i elàstica. Quan s'han testat amb la línia cel·lular de referència de càncer de mama

MCF-7, els *scaffolds* ES han mostrat el major potencial pel que fa a proliferació cel·lular i expansió de BCSCs tenint en compte la capacitat de formació de mamosferes.

El propòsit de la següent part de la tesi va ser discernir una possible relació entre les BCSCs i la sintasa d'àcids grassos (*fatty acid synthase*, FASN), un enzim lipogènic sobreexpressat en diversos tumors, utilitzant un model d'adquisició de quimiorresistència. Per tant, s'han utilitzat el model TNBC MDA-MB-231 i els seus derivats resistents a doxorubicina (231DXR) i paclitaxel (231PTR). Els resultats han mostrat una proporció més elevada de BCSCs en el model resistent a doxorubicina, així com un increment de l'expressió de FASN després de l'addició de l'agent quimioterapèutic. D'entre els inhibidors de FASN analitzats, el G28 és el que ha mostrat un major efecte antiproliferatiu en condicions de monocapa i en el cultiu de mamosferes enriquides amb BCSCs, en tots els models cel·lulars. Així doncs, aquests resultats senten les bases de futures investigacions en què s'utilitzin inhibidors de FASN per atacar les BCSCs en pacients TNBC.

Finalment, s'han emprat *scaffolds* ES per cultivar els models cel·lulars MDA-MB-231 i MDA-MB-468, els quals pertanyen als dos subtipus moleculars de TNBC, *mesenchymal-like* i *basal-like*, respectivament. Les cèl·lules TNBC han presentat un citoplasma més allargat quan estaven cultivades en l'*scaffold* ES de 15% PCL i, curiosament, també un augment de diverses característiques pròpies de les cèl·lules mare tumorals. A part, les cèl·lules cultivades en *scaffolds* han mostrat una inactivació de la via de senyalització MAPK, una estimulació de la cascada PI3K/AKT/mTOR i una activació d'EGFR i HER2, fets que doten d'un perfil cel·lular quiescent i *stem-like*. Per últim, FASN s'ha trobat hiperactivada en les mostres 3D enriquides amb BCSCs i la seva inhibició farmacològica ha portat a una disminució de les característiques de cèl·lules mare tumorals, suprimint l'expansió de BCSCs aconseguida en el cultiu 3D.

En resum, els nostres resultats demostren la idoneïtat de les tecnologies FFF i ES quant a la fabricació de *scaffolds* de PCL per aplicacions de cultiu cel·lular *in vitro* 3D. Malgrat s'han aconseguit fabricar amb èxit diversos models de *scaffolds* utilitzant aquestes dues tecnologies, l'*scaffold* ES de 15% PCL és el que ha mostrat un major potencial per expandir la població BCSCs. Segons el nostre coneixement, som els primers en definir una hiperactivació de FASN en mostres TNBC enriquides amb BCSCs cultivades en estructures 3D. Tot i això, es necessiten més estudis per determinar el potencial de FASN i el seu bloqueig farmacològic com a nova estratègia contra les BCSCs en TNBC. Com a conclusió general, els *scaffolds* ES de PCL poden facilitar la investigació en l'àrea de les cèl·lules mare tumorals, ja que es necessiten identificar nous biomarcadors i desenvolupar nous tractaments per atacar les BCSCs juntament amb la resta del tumor per tal de millorar el pronòstic de les pacients TNBC, entre altres tipus de càncer.

Resumen

Actualmente no existe una terapia dirigida contra el cáncer de mama triple negativo (*triple negative breast cancer*, TNBC), el cual representa el 15-20% de los tumores mamarios y muestra un perfil agresivo y con mal pronóstico. A pesar de una buena respuesta inicial a la quimioterapia, el 30% de las pacientes recaen durante los siguientes 5 años posttratamiento. La aparición de recaídas y el fracaso terapéutico son causados, en parte, por la presencia de una subpoblación celular en el tumor con propiedades similares a las células madre, llamadas, por este motivo, células madre del cáncer de mama (*breast cancer stem cells*, BCSCs). Pese a su importancia, su estudio es difícil debido a su poca representación dentro el tumor o línea celular y, también, al hecho que el cultivo celular tradicional *in vitro* en 2 dimensiones (2D) induce su diferenciación, transformándolas en células cancerosas no-madre. Así pues, han aparecido distintos modelos para el cultivo celular en 3 dimensiones (3D) como alternativa para restablecer un entorno similar al fisiológico y resolver los problemas descritos anteriormente. Entre ellos, los *scaffolds* (“andamio” traducido directamente) ofrecen una estructura física formada por un entramado de filamentos poliméricos, el cual mimetiza la arquitectura de la matriz extracelular.

La principal hipótesis de esta tesis es que el uso de *scaffolds* 3D permitirá la expansión y caracterización de la subpoblación de BCSCs en muestras TNBC y, así pues, facilitará el desarrollo de terapias dirigidas contra células madre tumorales. Con este objetivo, en la primera parte del trabajo se han optimizado dos tecnologías diferentes, la fabricación por filamento fundido (*fused filament fabrication*, FFF) y el electrohilado (*electrospinning*, ES), para fabricar *scaffolds* con el polímero ampliamente utilizado poli(ϵ -caprolactona) (PCL). Distintos parámetros de las dos tecnologías han sido optimizados según la estabilidad del proceso de fabricación. Los *scaffolds* producidos con un aparato FFF estaban formados por fibras micrométricas, mientras que las mallas ES presentaban una estructura

nanofilamentosa blanda y elástica. Cuando se han testado con la línea celular de referencia de cáncer de mama MCF-7, los *scaffolds* ES han mostrado el mayor potencial en cuanto a proliferación celular y expansión de BCSCs teniendo en cuenta la capacidad de formación de mamosferas.

El propósito de la siguiente parte de la tesis fue discernir una posible relación entre las BCSCs y la sintasa de ácidos grasos (*fatty acid synthase*, FASN), una enzima lipogénica sobreexpresada en distintos tumores, utilizando un modelo de adquisición de quimioresistencia. Por lo tanto, se han utilizado el modelo TNBC MDA-MB-231 y sus derivados resistentes a doxorrubicina (231DXR) y paclitaxel (231PTR). Los resultados han mostrado una proporción más elevada de BCSCs en el modelo resistente a doxorrubicina, así como un incremento de la expresión de FASN después de la adición del agente quimioterapéutico. De entre los inhibidores de FASN analizados, el G28 es el que ha mostrado un mayor efecto antiproliferativo en condiciones de monocapa y en el cultivo de mamosferas enriquecidas con BCSCs, en todos los modelos celulares. Así pues, estos resultados sientan las bases de futuras investigaciones en que se utilicen inhibidores de FASN para atacar las BCSCs en pacientes TNBC.

Finalmente, se han usado *scaffolds* ES para cultivar los modelos celulares MDA-MB-231 y MDA-MB-468, los cuales pertenecen a los dos subtipos moleculares de TNBC, *mesenchymal-like* y *basal-like*, respectivamente. Las células TNBC han presentado un citoplasma más alargado cuando estaban cultivadas en el *scaffold* ES de 15% PCL y, curiosamente, también un aumento de distintas características propias de las células madre tumorales. Aparte, las células cultivadas en *scaffolds* han mostrado una inactivación de la vía de señalización MAPK, una estimulación de la cascada PI3K/AKT/mTOR y una activación de EGFR y HER2, hechos que dotan de un perfil quiescente y *stem-like*. Por último, FASN se ha encontrado hiperactivada en las muestras 3D enriquecidas con BCSCs y su inhibición farmacológica ha llevado a una disminución de las características de células madre tumorales, suprimiendo la expansión de BCSCs conseguida en el cultivo 3D.

En resumen, nuestros resultados demuestran la idoneidad de las tecnologías FFF y ES en cuanto a la fabricación de *scaffolds* de PCL para aplicaciones de cultivo celular *in vitro* 3D. Pese a conseguir fabricar con éxito distintos modelos de *scaffolds* utilizando estas dos tecnologías, el *scaffold* ES de 15% PCL es el que ha mostrado un mayor potencial para expandir la población BCSCs. Según nuestro conocimiento, somos los primeros en definir una hiperactivación de FASN en muestras TNBC enriquecidas con BCSCs cultivadas en estructuras 3D. A pesar de eso, se necesitan más estudios para determinar el potencial de FASN y su bloqueo farmacológico como nueva estrategia contra las BCSCs en TNBC. Como conclusión general, los *scaffolds* ES de PCL pueden facilitar la investigación en el área de las células madre tumorales, ya que se necesita identificar nuevos biomarcadores y desarrollar nuevos tratamientos para atacar las BCSCs juntamente con el resto del tumor para mejorar el pronóstico de las pacientes TNBC, entre otros tipos de cáncer.

Summary

There is no targeted therapy for triple negative breast cancer (TNBC), which accounts for 15-20% of the breast cancer cases and displays a very aggressive profile and poor prognosis. Despite a good initial chemotherapy response, there is a 30% of relapse risk within 5 years after treatment. Relapse appearance and therapeutic failure are caused, in part, by a rare cell population within the tumor that displays stem-like properties, thus termed breast cancer stem cells (BCSCs). Regardless of their importance, their study is challenging due to their low representation within the tumor or cell line and the fact that traditional *in vitro* two-dimensional (2D) cell culture induces their differentiation, transforming them to non-stem cancer cells. For this reason, three-dimensional (3D) cell culture supports have emerged as an alternative to reinstate a physiological-like structure and overcome the above-mentioned issues. Among them, scaffolds offer a physical structure made by a network of polymeric filaments, which mimics the extracellular matrix architecture.

The main hypothesis of this thesis is that the use of 3D scaffolds will enable the expansion and characterization of the BCSC subpopulation of TNBC samples and, therefore, facilitate the development of targeted therapies against cancer stem-like cells. For that purpose, in the first part of this work we optimized two distinct technologies to manufacture scaffolds, fused filament fabrication (FFF) and electrospinning (ES), using the widely used polymer poly(ϵ -caprolactone) (PCL). Several parameters of both technologies were optimized in accordance to manufacturing process stability. Scaffolds produced with an FFF apparatus were composed by micrometric fibers while ES meshes exhibited a soft and elastic nanofilamentous structure. When tested with the reference breast cancer cell model MCF-7, ES scaffolds displayed the highest potential regarding cell growth rate and expansion of BCSCs in terms of mammosphere forming capacity.

The purpose of the next part of the thesis was to discern a possible link between BCSCs and fatty acid synthase (FASN), a lipogenic enzyme overexpressed in several carcinomas, using a chemoresistance-acquisition model. Thus, the TNBC cells MDA-MB-231 and their derivatives resistant to doxorubicin (231DXR) and paclitaxel (231PTR) were used. Results showed a larger proportion of BCSCs in the doxorubicin-resistant model, as well as an increase of FASN expression after drug addition. Among the tested FASN inhibitors, G28 exhibited a greater antiproliferative effect in monolayer conditions and in the BCSC-enriched mammospheres culture in all cell models. Therefore, this data set up the basis for further investigation using FASN inhibitors to target BCSCs in TNBC patients.

Finally, ES scaffolds were used to culture MDA-MB-231 and MDA-MB-468 cells, which belong to the two main molecular TNBC subtypes, mesenchymal-like and basal-like, respectively. TNBC cells showed a more elongated cytoplasm when cultured in the 15% PCL ES mesh and, interestingly, an upregulation of several stemness features that proved a BCSC expansion. Other than that, scaffold-cultured cells displayed a shift from MAPK to PI3K/AKT/mTOR signaling pathways, alongside an enhanced EGFR and HER2 activation, which supports a quiescent and stem-like profile. Ultimately, FASN was found hyperactivated in BCSC-enriched 3D samples and its pharmacological inhibition led to a stemness diminishment, overcoming the BCSC expansion achieved in 3D culture.

In summary, our results prove the suitability of FFF and ES technologies regarding the manufacture of PCL scaffolds for *in vitro* 3D cell culture applications. Although distinct scaffold models were successfully produced using these two technologies, 15% PCL ES scaffold showed the greatest potential to expand BCSC niche. To the best of our knowledge, we are the first to define a FASN hyperactivation in stemness-enriched breast cancer cells cultured on 3D structures. However, further studies are required to discern the potential of FASN and its pharmacological blocking as a novel approach for BCSC niche in TNBC disease. As general conclusion, ES PCL scaffolds may facilitate research in the cancer stem-like cells

field, since novel biomarkers and treatments need to be developed to target BCSCs as well as the tumor bulk to improve the prognosis of the TNBC patients, among other cancer types.

CHAPTER 1 Introduction

Part of this chapter has been expanded, adapted, and published as a review in the following publication (see Annex)

Title	Three-dimensional manufactured supports for breast cancer stem cell population characterization
Authors	Emma Polonio-Alcalá [†] , Marc Rabionet [†] , Santiago Ruiz-Martínez, Joaquim Ciurana, Teresa Puig*
Journal	Current Drug Targets
Publication year	2019
Impact Factor <small>2019</small>	2.632 (Q3 in Pharmacology & Pharmacy; position 145 of 271)
DOI	10.2174/1389450120666181122113300

* Corresponding author

[†] These authors contributed equally to this manuscript

1 Cancer

According to the World Health Organization (WHO), cancer is “a large group of diseases that can start in almost any organ or tissue of the body when abnormal cells grow uncontrollably, go beyond their usual boundaries to invade adjoining parts of the body and/or spread to other organs” (1). The last process is referred to as metastasis, which represents the major cause of death from cancer (2). Cancer is considered a genetic disease since it is caused by changes to genes that control cell functions such as growth and division. Genetic changes can be inherited from progenitors, caused as a result of errors that occur as cells divide or arise from certain environmental exposures known as carcinogens (2). Other risk factors involved in tumor development are aging, obesity, unhealthy diet and lack of physical activity (1).

Types of cancer are usually named after the organs or tissues where they are originated, such as breast, lung and colorectum cancer. Moreover, cancers can also be described by the type of cell that formed them, originating 6 main categories: the most common are the carcinomas, which are formed by epithelial cells including the skin and tissues that cover internal organs; sarcomas, that start in the bone or soft tissues such as muscle, fat, and fibrous tissue; leukemia, which begins in the blood-forming tissue of the bone marrow; lymphomas and myelomas that occur when cells of the immune system divide uncontrollably; melanoma, which develops from the melanin-producing cells known as melanocytes; and central nervous system cancers which comprise tumors originated in the brain or spinal (2).

1 in 5 people will develop cancer before the age of 75 (1). Globally, cancer is nowadays the second leading cause of death, being responsible of 1 in 6 deaths (1). Cancer incidence and mortality are rapidly growing worldwide due to the growth and aging of the population as well as the increasing prevalence of risk

factors. For instance, there were an estimated 19.3 million new cases and 10 million cancer deaths worldwide in 2020. Assuming constant rates, a predicted 28.4 million new cancer cases are projected to occur in 2040, being a 47% increase from 2020 (3). In Spain, more than 282,000 of new cancer cases were diagnosed in 2020 (which represents the 0.6% of the total population), whereas approximately 113,000 cancer deaths occurred (3). More specifically, there were up to 36,000 cancer cases in Catalonia in 2015, and almost 17,000 cancer deaths were recorded (4).

In an attempt to rationalize the complexities of cancer, Hanahan and Weinberg first described in 2000 the biological capabilities acquired by cancer cells during the development of human tumors (**Figure 1**). These features, known as **hallmarks of cancer**, provide cells advantage to survive, proliferate, and disseminate and are the following: sustaining proliferative signaling, evading growth suppressors, resisting cell death, enabling replicative immortality, inducing angiogenesis, and activating invasion and metastasis (5). The authors revised their work in 2011 and they included two more emerging hallmarks, being deregulating cellular energetics and avoiding immune destruction, and two more enabling characteristics, such as genome instability and mutation and tumor-promoting inflammation (6).



Figure 1. The hallmarks of cancer. This schematic representation encompasses the ten hallmark capabilities described in cancer. Adapted from Hanahan, D. *et al.* 2011 (6).

2 Breast cancer

Breast cancer (BC) is the disease in which malignant cancer cells form in the tissues of the breast. Due to anatomical differences between genders, it is hardly surprising that more than 99% of all breast cancer cases are female patients (2). The incidence of female breast cancer has increased in most countries because of the growing exposure to specific risk factors, such as age of menarche, late period of first pregnancy, hormonal status, a later menopause, family history of breast cancer, fewer pregnancies, and shorter or no periods of breastfeeding (7, 8). In fact, in 2020 female breast cancer has surpassed lung cancer as the most commonly diagnosed cancer, with an estimated 2.3 million new cases worldwide (which accounts for the 11.7% of total new cases), and represents the fifth leading cause of cancer mortality (6.9%), after lung, colorectal, liver and stomach cancer (3). In the Spanish scenario, 34,088 new breast cancer cases were diagnosed in 2020 (12.1%), with a 6,606 breast cancer linked deaths (5.8%). In Catalonia, an estimated 4,500 new breast cancer cases were diagnosed in 2015 (12.5%), with 1,023 related deaths (6.1%). Despite the global high incidence, the number of breast cancer survivors has increased over the last decade thanks to early detection and the development of novel treatment strategies (9).

The female breast is composed by predominantly two types of structures: adipose tissue and glandular tissue, which affects the lactation functions (**Figure 2**). Glandular tissue is organized into 15 to 20 sections called lobes that, in turn, are formed by smaller structures known as lobules. The milk is produced in the lobules and travels through a network of thin tubes called ducts. The ducts connect and eventually exit the skin in the nipple. Therefore, breast cancer can be differently named depending on the zone of origin. The most prevalent is the one originated in the cells of the ducts, thus called ductal carcinoma. On the other hand, the lobular carcinoma starts in the lobes or lobules and, interestingly, is more often originated in both breasts than the other types (2).

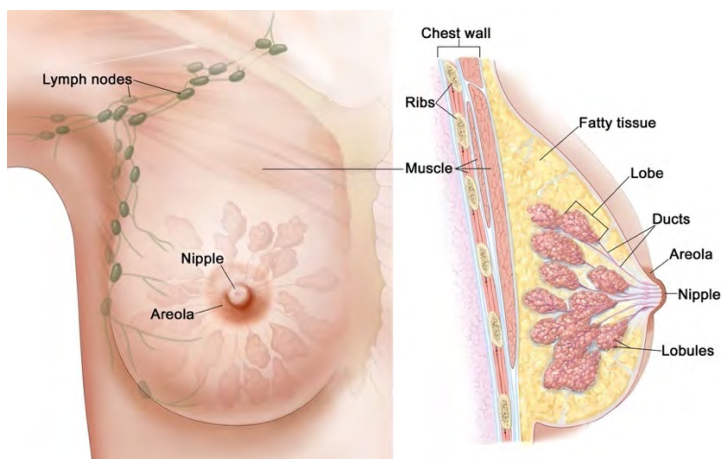


Figure 2. Female breast anatomy. Adapted from National Cancer Institute (2).

2.1 Breast cancer classification

Altogether with its counterparts, breast cancer is a very heterogeneous disease that can be organized in distinct clinical and molecular subtypes (10). In **clinics**, breast cancer is habitually classified depending on the presence or absence of three different cell membrane receptors, resulting in three groups. The hormone positive breast cancer is characterized by the overexpression of estrogen receptor (ER) and/or progesterone receptor (PR), responsible for permanent activation of proliferation pathways that triggers cell division. It stands for the most common breast cancer group with a representation of 60-70%, and patients have a better prognosis among the other types (11). Some targeted therapies are available, such as selective estrogen receptor modulators (SERMs; e.g., tamoxifen) and aromatase inhibitors (e.g., anastrozole) (12, 13). The HER2 positive breast cancer accounts for the 20-30% of breast cancer patients and presents an amplification of the human epidermal growth factor receptor 2 (HER2 or ERBB2). Patients diagnosed with HER2 positive breast cancer display poor prognosis and high risk of metastasis (14, 15). Different targeted therapies have been developed against HER2 receptor, including monoclonal antibodies (e.g., trastuzumab) and small molecule tyrosine-kinase inhibitors (e.g., lapatinib) (16). Finally, the triple negative breast cancer (TNBC) is characterized by the lack of hormone receptors and no overexpression

of HER2 (17). Although is the less frequent (it accounts for 15-20% of all breast cancer cases), TNBC runs an aggressive course and has a poor prognosis (18). TNBC patients are younger and exhibit a great incidence of metastasis and higher mortality among BC subtypes (18). The absence of the aforementioned biomarkers prevents the use of targeted therapies and leaves systemic chemotherapy as the sole treatment for TNBC patients, mainly with anthracyclines and taxanes (19). Unfortunately, despite a very good initial treatment response, the recurrence rate within 5 years following diagnosis is about 30%, the highest relapse rate compared to other BC types (20). In order to assess this clinical classification, immunohistochemistry (IHC) of the primary tumor biopsy is performed to determine the expression levels of the aforementioned receptors.

Described classification is used by clinicians to predict prognosis and decide treatment strategies, but do not provide a completely understanding of the disease. In order to further elucidate BC diversity, in 2000 Perou *et al.* analyzed the gene expression of several breast tumors and, by gene-clustering analysis, identified four different molecular subtypes within BC tumors (21). New data obtained in a following study executed by Perou and colleagues allowed them to divide one category into two groups (22) and, ultimately, a new subgroup was added thanks to a major comprehensive analysis (23). Taking all this in consideration, a **molecular** classification was depicted including 5 intrinsic BC subtypes, summarized in **Table 1**. The luminal A and B subtypes constitute the group which was divided in the following study. Luminal categories depict the majority of breast cancer tumors (40% and 10%, respectively (11)). Tumors formed by luminal cells are usually hormone positive (ER and PR overexpression) and are classified as low-grade. Luminal A tumors usually display increased expression of ER- and PR-regulated genes, no amplification of HER2 cluster (which is variable in luminal B tumors), and low expression of proliferation-associated genes (22). On the other hand, luminal B cells show a more proliferative profile and lower expression of ER- and PR-regulated genes (22). HER2-enriched group stands for, approximately, the 10% of the breast cancer patients. It is characterized by the

overexpression of HER2 gene and/or protein levels, low expression of hormone receptor-regulated gene cluster and basal-like genes. HER2-enriched tumors are generally classified as high-grade (24). The identification of the following two molecular subtypes, basal- and mesenchymal-like, caused a great impact on the BC classification since both belong to the TNBC clinical group. Therefore, TNBC were hereinafter not identified as a unique disease, contrary to hormone- and HER2-positive BC. In fact, many studies referred to TNBC as basal-like, since this intrinsic molecular subtype represents the majority of TNBC cases (specifically 75% (25)) until the identification of the mesenchymal-like subtype (23). Basal-like molecular group displays low to absent expression of HER2-, ER-, and PR-related genes, high expression of proliferation genes and a unique cluster of genes called basal cluster (which includes several cytokeratins and the epidermal growth factor receptor, EGFR). Basal-like subtype displays the poorest prognosis among groups (25, 26). Otherwise, mesenchymal-like was the latest intrinsic subgroup to be identified and is the least frequent subtype (5-10% of all breast tumors (27)). This subtype presents some characteristics similar to the basal-like group, including low HER2 expression and luminal cytokeratins. However, mesenchymal-like cells also display low proliferation phenotype and low expression of genes related to cell-cell adhesion (claudin genes), thus this subtype is also known as claudin-low (23). Moreover, mesenchymal-like tumors are enriched with immune system response and mesenchymal genes (23, 28). Finally, some authors include the normal-like group in this classification, not without controversy. In fact, some researchers point out that normal-like cases are tumor samples contaminated with healthy breast tissue since gene expression profile has similarities to adipose tissue. Regardless, normal-like cases are defined as normal breast samples from reduction mammoplasties or tumor samples that showed less than 50% of malignant cells. This subtype is similar to luminal A group due to their common low proliferation rate and high expression of the luminal cluster (22). Concerning tumors outcome, luminal A has the best prognosis among all intrinsic subtypes while an intermediate prognosis has been established for luminal B. In contrast, normal-like, HER2-enriched, and TNBC display the poorest one (22) (**Table 1**).

As explained before, intrinsic molecular groups can be correlated with classical subtypes since they differentially express ER, PR, and HER2 clusters (**Table 1**). However, it is worth noting that both classifications do not completely overlap (25, 29, 30).

Table 1. Main features of breast cancer molecular subtypes and concordance with their immunohistochemical profile (21, 23, 29, 31, 32).

Molecular subtypes	Cellular composition	Proliferative rate	Outcome	Classical IHC classification
Luminal A	luminal	low	good	ER+/PR+/HER2-
Luminal B	luminal	high	intermediate	ER+/PR+/HER2+ or ER+/PR+/HER2-
HER2-enriched	luminal/basal	high	poor	ER-/PR-/HER2+
Basal-like	basal	high	poor	ER-/PR-/HER2-
Mesenchymal-like	basal	low	poor	ER-/PR-/HER2-

2.2 Relevant cell signaling in breast cancer

Several cell functions such as growth, differentiation, motility, and survival are determined by receptor tyrosine kinases (33). The **HER protein tyrosine kinases** (TKs), also known as ERBB, are the most-studied cell signaling family in biology (**Figure 3**). This family is ubiquitously expressed in a wide range of cell types, including epithelial, mesenchymal, cardiac, neuronal cells, and their cellular progenitors (34). Their deregulation by overexpression, amplification, or mutation on critical pathway components can result in a hyperproliferative disease such as cancer (35). This family is composed by four known members: epidermal growth factor receptor (EGFR, also known as ERBB1 or HER1) was the first to be discovered, followed by HER2 (ERBB2 or Neu), HER3 (ERBB3) and HER4 (ERBB4) (36), displayed in **Figure 3A**. Like the other protein-tyrosine kinase receptors, ERBB family functions mainly as dimers, being possible the formation of homo- and heterodimers with all members of the family (37). Each receptor possesses an

extracellular portion that has four parts. Extracellular domains I and III participate in ligand binding, while domain II is involved in dimer formation and, altogether with domain IV, in disulfide bond formation as well. A typical HER member also displays a single transmembrane segment that anchors the receptor to cell membrane. Lastly, the intracellular portion has a juxtamembrane segment, a protein kinase domain, and a carboxyterminal tail. This intracellular segment is responsible for kinase activation and following activation of cell signaling pathways (37, 38). All four members possess a similar protein kinase domain except from HER3, which has its TK domain inactivated (39). Broadly, the activation mechanism of HER family receptors involves the ligands or growth factors binding to the extracellular domain, inducing the formation of an activated dimerization state (**Figure 3B**) (40). EGFR, HER3, and HER4 have been described to possess seven ligands: epidermal growth factor (EGF), transforming growth factor alpha (TGF- α), amphiregulin (AmR), betacellulin (BTC), epiregulin (EPR), heparin-binding EGF-like growth factor (HB-EGF), epigen (EPG), neuregulins (NRGs), and Neu differentiation factors (NDFs) (40–42). On the other hand, HER2 has no known natural ligand to date, so it is identified as an orphan receptor. HER2 presents, therefore, a fixed active conformation and it is permanently available for dimerization (44). Nevertheless, HER2 can act as a co-receptor with high affinity for EGFR, HER3, and HER4, thus forming heterodimers (45, 46). The HER2-HER3 heterodimer is actually considered to be the most active HER signaling dimer regarding strong interaction, ligand-induced tyrosine phosphorylation and downstream signaling (47, 48). The ligand binding leads to a receptor conformational change that enable the homo- or heterodimerization with another HER family member. In consequence, dimerization allows TK domains phosphorylation and the following activation of different intracellular pathways, including the mitogen activated protein kinase (MAPK) pathway, involved in cell proliferation, and the phosphoinositide 3-kinase (PI3K)/ mammalian target of rapamycin (mTOR) cascade, which regulates cell survival (44). Overall, these and other HER signaling cascades participate in angiogenesis, cell adhesion, motility, development, and organogenesis (49).

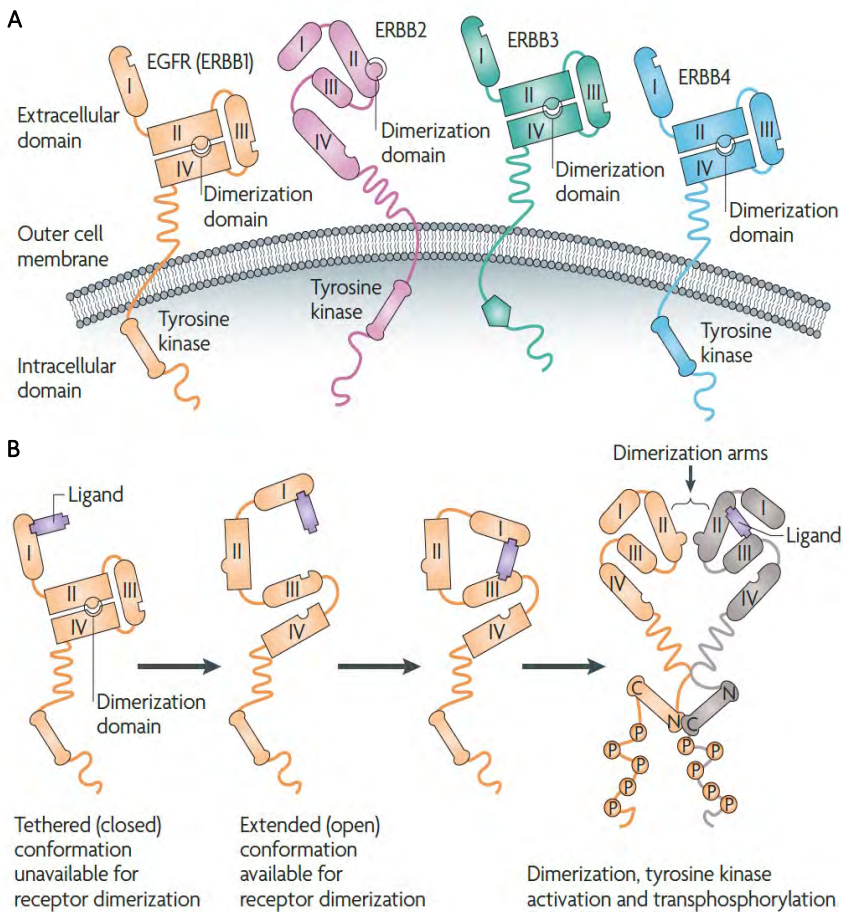


Figure 3. Human epidermal growth factor receptors (HER) family. **A** Schematic representation of the structural basis of the four HER family members: ERBB1 (epidermal growth factor receptor [EGFR] or HER1), ERBB2 (HER2), ERBB3 (HER3), and ERBB4 (HER4). Each receptor is composed of three functional segments: an extracellular region responsible for ligand binding, a transmembrane segment, and the intracellular protein tyrosine kinase domain that also contains motifs and residues that mediate interactions with intracellular signaling molecules. In normal conditions, ERBB1, ERBB3, and ERBB4 exist in a closed conformation. ERBB2 has no known ligand and, therefore, it is fixed in the active conformation and is permanently available for dimerization. In addition, ERBB3 has an inactive kinase domain (TK). **B** The ligand binding to receptor induces a conformational change in the folded structure of the receptor and the dimer formation, a crucial step for receptor activation. After dimerization, the intracellular kinase domains' cross-phosphorylate residues are found in the C-terminal receptor tail. Once HER-dimers are activated, their signal goes through different cascades. Taken from Baselga and Swain 2009 (43).

Despite the establishment of the activation mechanism, some ligand-independent mechanisms can activate HER pathways, including:

- i. Alterations in HER downstream proteins which can activate the pathway regardless ligand binding (32)
- ii. HER dimerization with other receptors such as the insulin-like growth factor 1 receptor (IGF-1R) (50)
- iii. Homodimerization and downstream signaling activation due to high levels of HER2 (51)

As previously said, different intracellular pathways are triggered due to TK domains phosphorylation, being MAPK and PI3K/mTOR the most relevant ones (**Figure 4**). For instance, activation of MAPK signaling pathway is typically mediated by EGFR and HER2. All MAPK cascades follow a common signal-relay mechanism that involves the sequential phosphorylation of three kinases. It consists of an initial guanosine triphosphatase (GTPase)- regulated kinase (a mitogen activated protein kinase kinase kinase; MAPKKK), that activates and intermediate kinase (a mitogen activated protein kinase kinase; MAPKK), which in turn phosphorylates an effector kinase (MAPK). The first MAPK signaling to be characterized in vertebrates was the extracellular signal-regulated kinase (ERK)/MAPK cascade (52). ERK/MAPK cascade is initiated by the activation of the small GTPase rat sarcoma (RAS), which phosphorylates the MAPKKK rapidly accelerated fibrosarcoma (RAF). Activated RAF later phosphorylates the MAPKK MEK (MAPK/ERK kinase) leading to its activation. Subsequently, activated MEK catalyzes the dual phosphorylation of the MAPK ERK. This signal transduction continues through the phosphorylation of cytoplasmic signaling proteins, such as p90 ribosomal S6 kinase (RSK), and end-point effectors including transcription factors. Eventually, MAPK pathway is involved in both physiological and pathological cell functions, including cell proliferation, differentiation, cell survival, oncogenesis, and tumor progression (53).

On the other hand, the PI3K/mTOR cascade represents another key mechanism for controlling cell metabolism. PI3K is recruited to the cell membrane by adaptor proteins, such as insulin receptor substrate (IRS) family members, that interact with these activated receptors, resulting in the phosphorylation of

phosphatidylinositol 4,5-bisphosphate (PIP₂) to generate phosphatidylinositol 3,4,5-triphosphate (PIP₃). PIP₃ activates protein kinase B (AKT), which in turn dissociates the tuberous sclerosis protein 1 and 2 (TSC1-TSC2) complex. This disruption results in the activation of mTOR complex 1 (mTORC1) and, eventually, in increased protein and lipid synthesis and decreased autophagy, which lead to cell growth and proliferation. Overall, the PI3K/mTOR cascade plays a key role in several physiological and pathological conditions, including cell proliferation, angiogenesis, metabolism, differentiation, and survival (54).

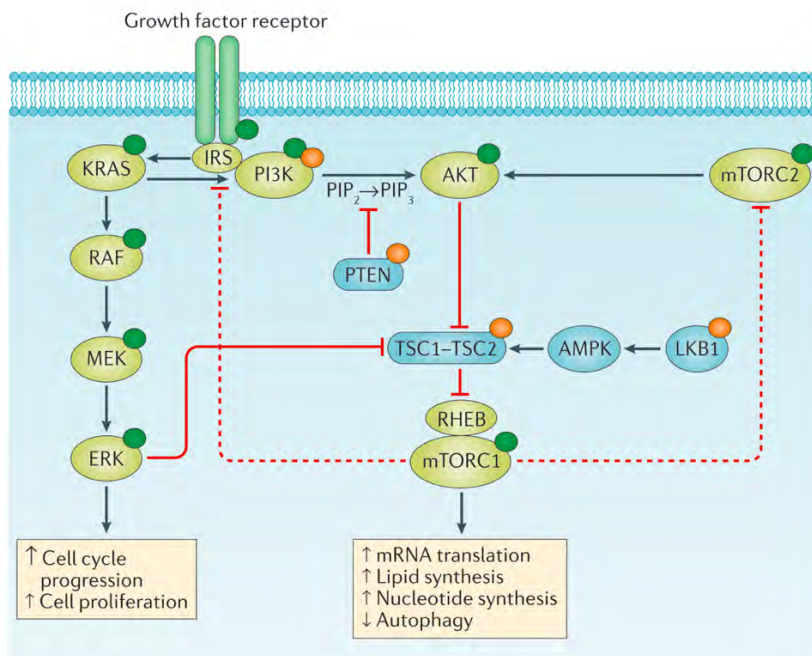


Figure 4. Intracellular signaling via the mitogen activated protein kinase (MAPK) and phosphoinositide 3-kinase (PI3K)/ mammalian target of rapamycin (mTOR) pathways. Induction of these signaling cascades is triggered by the activation of various growth factor receptor tyrosine kinases or G protein-coupled receptors (not shown). mTOR complex 1 (mTORC1) is involved in a negative feedback loop depicted with dashed red lines. Signaling of these pathways can be upregulated by gain-of-function alterations (depicted by green circles) or by loss-of-function alterations (orange circles). **Abbreviations:** AKT (protein kinase B), AMPK (5' adenosine monophosphate-activated protein kinase), ERK (Extracellular signal-Regulated Kinase), IRS (insulin receptor substrate), KRAS (K-rat sarcoma), LKB1 (liver kinase B1), MEK (MAPK/ERK kinase), mRNA (messenger ribonucleic acid), mTORC2 (mammalian target of rapamycin complex 2), PI3K (phosphoinositide-3-kinase), PIP₂ (phosphatidylinositol 4,5-bisphosphate), PIP₃ (phosphatidylinositol 3,4,5-triphosphate), PTEN (phosphatase and tensin homolog), RAF (rapidly accelerated fibrosarcoma), RHEB (Ras homolog enriched in brain), TSC1-TSC2 (tuberous sclerosis protein 1 and 2). Taken from Janku *et al.* 2018 (55).

3 Triple negative breast cancer

As explained in the previous section, TNBC is defined by the absence of ER/PR expression and HER2 amplification, and it accounts for the 15-20% of all breast cancer cases. TNBC exhibits an aggressive phenotype and poor prognosis when compared with other breast cancer subtypes (21). The main characteristics of TNBC are the following (56):

- i. Frequently seen in premenopausal younger women (less than 50 years) (57)
- ii. More frequent in African-American women and black ethnicities
- iii. High chemosensitivity
- iv. More aggressive with higher chance of brain metastases
- v. High chance of recurrence during the first and third year after diagnosis
- vi. Shorter survival following first metastatic event

Regarding its **clinical features**, TNBC is usually diagnosed as a palpable tumor since it frequently arises at ages younger than that at which breast cancer screening programs started. Moreover, TNBC usually displays higher grade, larger tumor size, and lymph node positivity (18). The majority of TNBC cases, approximately 90%, are unifocal and invasive ductal carcinomas (58). They preferentially spread hematogenously, resulting in metastatic deposits in the brain and lungs (59). Multiparity, young age at first pregnancy, and a higher waist/hip ratio are associated with an increased **risk of developing TNBC** (60). Whereas breastfeeding, a higher number of children breastfed, and nulliparity reduce this risk (56, 61). This apparently reduction of developing TNBC may be partially explained by the fact that these factors are more strongly associated with hormone-positive tumors as compared to hormone-negative tumors (62). At a genetic level, 75% of tumors with a mutated breast cancer type 1 susceptibility protein (BRCA1), a human tumor suppressor gene responsible for repairing DNA, show a TNBC phenotype (63, 64).

BRCA1-positive TNBC cases have been proved to be enriched for a family history of breast (50%) and ovarian cancers (18%) (65), denoting the importance of heredity in this breast cancer subtype. However, at the time of primary diagnosis TNBC exhibits a wide and continuous spectrum of genomic evolution, indicating that TNBC cases may be at a very different phase of molecular progression (66). Ethnicity represents an independent prognostic factor with black women having inferior prognosis (67). In fact, it has been proved that Black and Hispanic populations have a high likelihood of carrying mutations on the BRCA1 and breast cancer type 2 susceptibility protein (BRCA2) genes (11, 68). Interestingly, prognosis in TNBC patients older than 70 years has been reported to be better as compared to younger patients (69).

3.1 Triple negative breast cancer prognosis

Following TNBC diagnosis, there is a rapid rise in the risk of recurrence and approximately 46% of TNBC patients will have distant metastasis. Concretely, TNBC relapse rates are high during the first few years following surgery with a peak recurrence risk at 3 years after surgery (70). Survival after metastatic relapse is also shorter in TNBC compared to other subtypes. The majority of deaths occur in the first 5 years, when the mortality rate is 40%, and there is a rapid progression from distant recurrence to death (18). In fact, median survival time after metastasis is only 13.3 months and mortality rate within 3 months after recurrence is as high as 75%. This can be explained by the predilection for visceral, lung, and brain TNBC metastasis compared with hormonal positive breast cancers that are more likely to relapse in the bone and skin (71, 72). Overall, TNBC is at increased risk for locoregional relapse, distant metastasis, and death compared with other subtypes, even after mastectomy (73, 74).

3.2 Molecular classification of triple negative breast cancer

TNBC is mainly composed by basal-like and mesenchymal-like molecular subtypes, representing the 49% and 30%, respectively (**Figure 5A**). It should be recalled that clinic classification of breast tumors (ER, PR, and HER2) do not have a complete coincidence with the molecular classification as seen in **Figure 5B** (25, 29, 30). The identification of the two molecular TNBC subtypes at the time of diagnosis is challenging since both share negative expression for the common biomarkers (ER, PR, and HER2) by using IHC. Besides, the use of complementary deoxyribonucleic acid (cDNA) microarrays to molecularly classify breast cancer is still not a common technique in the clinic. To overcome this issue, some markers are added in IHC procedures in order to improve breast cancer categorization. The addition of the specific markers cytokeratins 5/6 (CK5/6) and EGFR to the classical ones has more prognostic value to identify basal-like subtype (26, 75, 76). On the other hand, mesenchymal-like identification can benefit from the addition of high levels of vimentin and other claudin proteins, and low expression of E-cadherin in IHC (77, 78).

3.3 Triple negative breast cancer treatment

Compared to other types of breast cancer, TNBC has limited treatment options, including surgery for operable tumors, radiotherapy, and chemotherapy. TNBC local treatment is similar to the other invasive breast cancers. Breast-conservative **surgery** is the default procedure for small tumors in contrast to mastectomy for larger and/or multifocal tumors. TNBC patients with large tumor mass can benefit from neoadjuvant chemotherapy, that is to say prior to surgery (79).

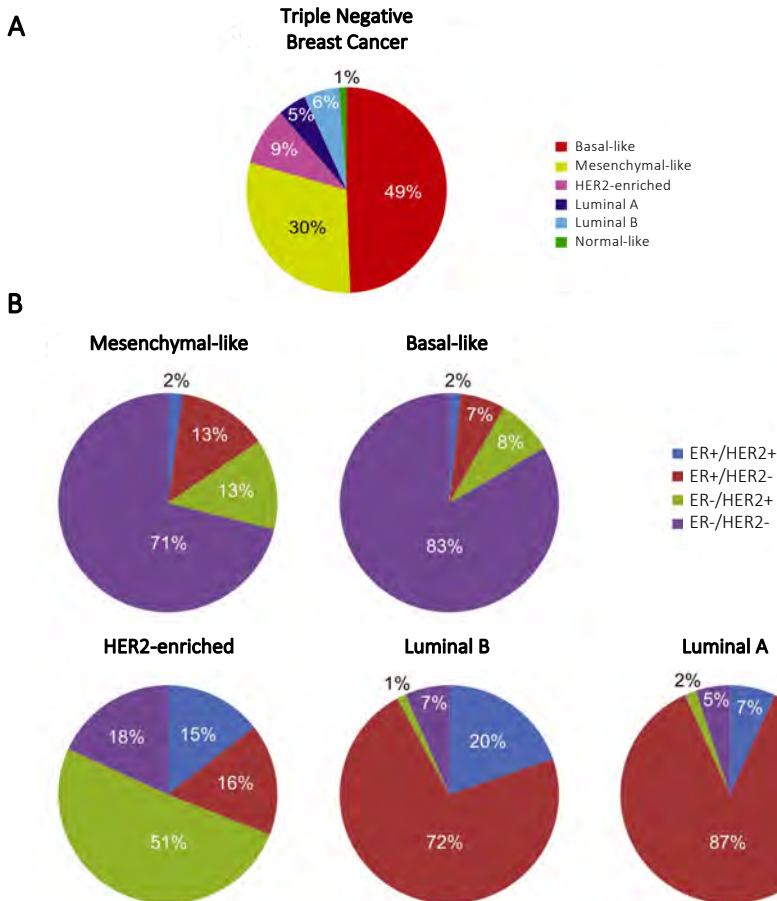


Figure 5. Distribution of clinical-pathological categories relative to the intrinsic subtypes of breast cancer. A Intrinsic subtype distribution within the triple negative tumor category. **B** Distribution of ER+/HER2+, ER+/HER2-, ER-/HER2+, ER-/HER2- clinical groups in the mesenchymal-like, basal-like, HER2-enriched, luminal B, and luminal A within each subtype. Abbreviations: ER (estrogen receptor), HER2 (human epidermal growth factor receptor 2). Modified from Prat *et al.* 2011 (29).

Radiotherapy is also an essential component of TNBC treatment, and its protocol depends upon the extent of surgery and lymph node status as for other breast cancer subtypes. Radiotherapy is generally performed in combination with the breast-conserving therapy, and it is not recommended after a mastectomy procedure according to current guidelines (80, 81). Cancer patients that undergo radiotherapy present a better long-term outcome. However, some authors suggested a relative radioresistance of TNBC tumors given their ER-negative status.

The expression of ER decreases cell cycle duration hence also the time available to repair deoxyribonucleic acid (DNA) damage caused by radiation, and in ER-negative tumors such as TNBC, DNA repair can further progress during a slower cell cycle (82).

Since a therapeutic target is not yet identified, **chemotherapy** is currently the only approved systemic treatment that improves TNBC outcome. In the meantime, various other systemic treatments options, such as molecular-directed targeted therapies or immunotherapy, are currently under scrutiny (56). Mounting data has shown that the administration of neoadjuvant chemotherapy significantly improves the prognosis of TNBC patients (20, 79, 83). As pointed before, TNBC shows high chemosensitivity. For example, response to neoadjuvant treatments can be very rapid in TNBC patients, even after only two cycles of therapy (84). Lack of ER expression predicts a greater response to chemotherapy as compared to ER-positive cases (85, 86). For operable tumors, neoadjuvant therapy decreases the size of the tumor, allowing a breast-conservative surgery and reducing the need for a mastectomy. Usually, combination regimens are used for TNBC treatment, based on taxanes, anthracyclines, cyclophosphamide, platinum agents, and fluorouracil. The taxanes is a group of chemotherapy drugs whose mechanism of action is mainly through the inhibition of microtubule depolymerization, thereby inhibiting cell division. For this reason, taxanes are categorized as mitotic inhibitors. Besides, their antitumor function is also associated with apoptosis induction and macrophages activation (87). Taxanes are proved to be more efficient on the basal-like TNBC subtype given its active expression of proliferation-related and DNA repair genes. For instance, after taxane-based treatment in TNBC patients, basal-like subtype has four times higher clinical remission rates than the mesenchymal-like group (88, 89). Some examples of taxanes are paclitaxel and docetaxel. Anthracyclines are one of the most used chemotherapeutic drugs. Their mechanism of action is based on intercalating with DNA, which inhibits DNA and ribonucleic acid (RNA) synthesis and blocks transcription and replication processes (90). Anthracyclines possess a broad antitumor spectrum and is the

chemotherapeutic drug that treats more types of cancer, including leukemia, lymphoma, breast cancer, uterine cancer, ovarian cancer, and lung cancer (91). The efficacy of anthracycline displays no significant difference among breast cancer subtypes (92). Clinically, the most relevant anthracyclines are doxorubicin, daunorubicin, epirubicin, and idarubicin. Anthracycline-/taxane-based regimens constitute current standard treatment for breast cancer patients (93) and have been proved to be highly active also in TNBC cases (94). More specifically, some authors pointed out that TNBC responds better to taxane- than anthracycline-based therapy compared with other breast cancer subtypes (95, 96). This fact would reduce the number of unnecessary anthracycline treatment, avoiding its inherent cardiotoxicity (97). However, both drugs are still given in combination in current practice. The following type of chemotherapeutic group available for TNBC patients is the alkylating agent cyclophosphamide, which attaches an alkyl group to the guanine base of DNA leading to cell death. In the liver, this compound is converted to the active metabolites aldophosphamide and phosphoramide mustard, the last one the main responsible of the DNA-alkylating effects (87). Cyclophosphamide is, moreover, a potent immunosuppressor that decrease the number of T and B lymphocytes, and antibody production (98). At present, a combination regimen of docetaxel and cyclophosphamide is used as neoadjuvant therapy for HER2-negative breast cancers, but has limited efficacy in treating other breast cancer subtypes (99). As discussed before, TNBC is strongly related with BRCA1 mutations. Interestingly, cells with BRCA1 mutations are deficient in DNA repair mechanisms, making them sensitive to platinum agents. Platinum salts bind to DNA, causing DNA cross-linking that elicits DNA repair mechanisms (93, 100). Deficiency of this repair mechanism results in cell apoptosis rather than repair. Due to their mechanism of action, platinum-based chemotherapeutic drugs are sometimes described as “alkylating-like”, because they act in a similar manner despite the absence of an alkyl group. Different studies determined the efficacy of platinum-based agents, e.g. cisplatin and carboplatin, on metastatic TNBC patients, particularly patients with basal-like subtypes (101–103). Finally, fluorouracil belongs to the antimetabolites group, composed by small and weakly acidic

molecules that inhibit cellular metabolism by acting as false substrates during RNA and DNA synthesis. Fluorouracil drugs are proven to be suitable for further treatment of advanced primary or metastatic breast cancer which display taxanes or anthracyclines resistance (104). In fact, with the widespread application of taxanes and anthracyclines for breast cancer treatment, an increasing number of patients develop resistance to the aforementioned drugs, which has become an urgent problem in clinical practice.

Concerning **metastatic relapse** in TNBC, chemotherapy remains the backbone treatment even though its prognosis after treatment is inferior compared to other breast cancer subtypes (20, 72). There can be a receptor status switch between the primary breast tumor and the metastatic lesion for ER, PR, and HER2, but only a few TNBC patients are proved to undergo this rearrangement and, therefore, gain extra treatment options (105). There is no evidence that some chemotherapeutic drug is superior to others depending on the breast cancer classification. TNBC patients with advanced disease usually respond poorly to current chemotherapeutic treatment and, after an initial good response, there is a rapid disease progression (56). For that reason, novel targeted therapies are urgently needed for TNBC patients, regardless of the disease stage.

3.4 Targeted therapy of triple negative breast cancer and potential treatment regimens

Owing to the high heterogeneity of TNBC disease, it is particularly difficult to discover new therapeutic biomarkers and develop targeted therapies. Nevertheless, a large number of clinical trials targeting specific receptors or pathways are currently ongoing.

TNBC is a highly proliferative tumor with an elevated angiogenesis activity throughout all the stages of its development (106). Therefore, **vascular endothelial**

growth factor (VEGF), a protein that stimulates the formation of blood vessels, has been proposed as a novel therapeutic target for TNBC. VEGF inhibitors hinder the development of tumor neovasculature. For instance, the anti-VEGF monoclonal antibody bevacizumab was found to be beneficial for TNBC patients when combined with chemotherapy (107, 108). Despite this initial good report, further clinical studies could not find a benefit for TNBC cases (109, 110). This fact, along with its increased toxicity (111), caused the Food and Drug Administration (FDA) to deny its approval for breast cancer (56). Other antiangiogenic agents targeting VEGF receptor instead of VEGF itself are currently under investigation (112).

Between 50-70% of TNBC cases have been related to high expression of **EGFR** (75, 113), which was linked to poor prognosis (114, 115). More accurately, EGFR expression is more associated to the basal-like TNBC subtype (75), making it a possible therapeutic target in TNBC. Unfortunately, the use of EGFR-targeted treatment in clinical trials did not improve TNBC patients outcome (116) and EGFR downstream signaling pathways were still activated in most patients after EGFR blocking, possibly due to a bypass activation caused by other pathways involved (117). Therefore, EGFR-targeted treatment alone cannot achieve significant efficacy. When combined with carboplatin, the anti-EGFR monoclonal antibody cetuximab displayed an interesting activity in TNBC patients (116), and its derivative panitumumab is already under investigation in a clinical trial in combination with carboplatin and paclitaxel (112). Small-molecule tyrosine kinase inhibitors (TKIs) against EGFR are also being tested in TNBC. For instance, gefitinib showed minimal single-agent activity (118), but promising results have been obtained when combined with docetaxel or carboplatin in TNBC cell models (119). Therefore, current clinical trials are focused on the use of EGFR TKIs in combination with chemotherapy (112).

Poly (ADP-ribose) polymerase (PARP), a class of DNA repair enzymes, has also been postulated as a possible therapeutic target in TNBC. Their inhibition causes a loss of DNA repair function and enhances the therapeutic effects of radio- and

chemotherapy (120). Moreover, PARP inhibitors have significant antitumor effects, notably on BRCA1/2-mutated tumors. However, recent studies did not observe a clinical benefit from the administration of the PARP inhibitors iniparib and olaparib, speculating with other DNA repair mechanisms that may make TNBC patients insensitive to PARP inhibitors alone (121). The combination of PARP inhibitors with chemotherapy is currently being evaluated in various clinical trials (112).

The proto-oncogene **cellular Src** (c-Src) has been also postulated as a possible TNBC target due to its overexpression in this breast cancer subtype (122). It consists of a non-receptor tyrosine kinase protein that plays a key role in embryonic development and cell growth and is associated with metastatic disease progression. The oral c-Src inhibitor dasatinib was proven to block basal-like breast cancer cell growth (122) and showed a clinical benefit when combined with or after chemotherapy treatment in TNBC (123, 124). At-present effort now focuses on the optimal use of c-Src inhibitors in clinical practice.

Increased activation of **mammalian target of rapamycin** (mTOR), an effector of the PI3K signaling pathway, is a common finding in TNBC (125). Hence, several mTOR inhibitors are under investigation in TNBC patients such as everolimus and temsirolimus, alone or in combination with chemotherapy drugs and TKIs (112, 126).

Expression of **androgen receptor** (AR) is positive in approximately 10-15% of TNBC cases (127) and preclinical studies demonstrated an androgen-dependent growth of some TNBC cells (128). AR is an intracellular receptor that is activated by binding any of the androgenic hormones, including testosterone and dihydrotestosterone. Once activated, it functions as a DNA-binding transcription factor that regulates gene expression. AR-positive TNBC patients could, therefore, benefit from antiandrogen treatment. TNBC clinical trials using bicalutamide or enzalutamide, two AR inhibitors, proved a 19-25% of clinical benefit rate (129, 130). However, clinical significance and functional role of AR in breast tumors are not well

characterized (131, 132). Hence, AR inhibition as a new targeted therapy for TNBC patients is expected to be further developed.

TNBC cells lack ER and PR expression, which makes them insensitive to endocrine therapy. However, Wang *et al.* identified a new estrogen receptor, **ER- α 36**, with distinct features than the commonly studied ER- α 66 (133). Interestingly, ER- α 36 can mediate signal transduction in both ER-positive and ER-negative breast cancer cells (134), and it is thought to have a positive feedback loop with EGFR (135). Therefore ER- α 36 might represent a potential target for TNBC treatment despite the lack of support from clinical trials.

Finally, cellular and molecular **immunotherapies** appear to be very promising approaches in TNBC. Tumor cells are able to evade recognition and destruction by the host immune surveillance through the immune checkpoint system. Some TNBC cells and tumor infiltrating immune cells express high levels of the programmed cell death-ligand 1 (PD-L1), a ligand that binds the programmed cell death protein 1 (PD-1) receptor which inactivates T cells. By upregulating ligands for PD-1, cancer cells hinder antitumor immune response in the tumor microenvironment. Thus, PD-1 and PD-L1 inhibitors, such as pembrolizumab and atezolizumab, respectively, can disrupt the ligand-receptor interaction and restore the T cell functions (136, 137). Although the clinical benefit rate of these inhibitors is relatively low, some patients show good prognosis and significantly increased overall survival rates (138, 139). For this reason, current efforts are focused on improving the response of TNBC patients to anti-PD-1/PD-L1 treatment and converting non-responders into responders. Other immunotherapeutic methods include specific chimeric antigen receptor T cell (CAR-T) therapy and the use of antibodies against cytotoxic T-lymphocyte-associated protein 4 (CTLA-4), which inhibits T cell activation (140, 141).

4 *Cancer stem cells*

Stem cells are, by definition, a rare cell population that have the ability to perpetuate themselves through self-renewal and to generate mature cells of a particular tissue through differentiation. In a similar way, tumors contain a small population of cells with indefinite proliferative potential that drive the formation and growth of tumors (142). They are so-called cancer stem cells (CSCs).

The existence of cancer cells with stem properties was first documented in 1937 by Furth and Kahn. Using serial transplantations and limiting dilutions, they transplanted derived-leukemia single cells into inbred mice. Approximately 5% of derived cells initiated leukemia and were able to recapitulate features of the original clinical tumor. Therefore, authors proved the existence of a small population within the tumor that exhibited tumorigenic properties and was capable of extensive proliferation (143). During the 1950s, solid tumor experimentation was further developed confirming that only few cancer cells were able to initiate a malignant tumor (144, 145) and, years later, more leukemia and multiple myeloma works corroborated this theory (146–149). However, two formal possibilities remained thus far: either all tumor cells had a low probability of proliferating extensively in these assays, or most tumor cells were unable to proliferate extensively and only a small, definable subset was consistently clonogenic. To decide between hypotheses, it was necessary to isolate different classes of tumor cells and demonstrate that one portion was highly enriched for clonogenic capacity and all other cell types were depleted for this capacity. Therefore, in 1997 Bonnet *et al.* were the first to identify and purify human acute myeloid leukemia (AML) CSCs from patient samples using the specific expression pattern of clusters of differentiation (CD) CD34⁺/CD38⁻. Cells with this expression pattern were the only ones capable of transferring AML from human patients to nonobese diabetic/severe combined immunodeficiency (NOD/SCID) mice,

although they represented a small proportion of AML cells (between 0.02-2% among patient samples) (150). Therefore, the second hypothesis was confirmed.

Before the identification of this malignant subpopulation, intrinsic **tumor heterogeneity** was explained by the classical model. This hypothesis explains that tumor cells display many different phenotypes, but most cells can proliferate extensively and form new tumors. However, cancer cells would have a low probability of exhibiting their potential in an assay of clonogenicity or tumorigenicity (**Figure 6A**). Once CSCs were described, the cancer stem cell-driven model was proposed. In this, tumor cells are heterogeneous and only the CSCs have the ability to proliferate extensively and form new tumors (**Figure 6B**). Existing therapeutic treatments have been based largely on the classical model. Failure of these therapies to cure most solid cancers may be due to the major accuracy of the second model.

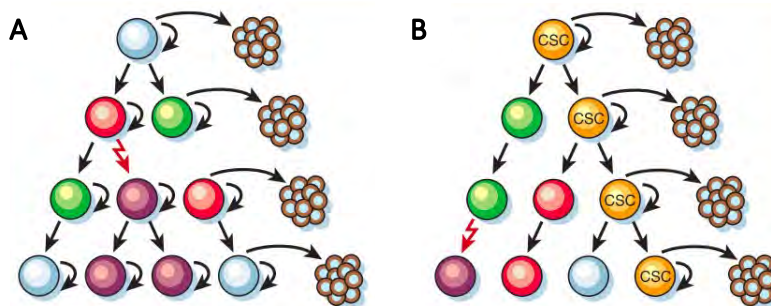


Figure 6. Two general models of heterogeneity in solid cancer cells. A Cancer cells of many different phenotypes have the potential to proliferate extensively, but any one cell would have a low probability of exhibiting this potential in an assay of clonogenicity or tumorigenicity. **B** Most cancer cells have only limited proliferative potential, but a subset of cancer cells (the cancer stem cells, CSCs) consistently proliferate extensively in clonogenic assays and can form new tumors on transplantation. Taken from Reya *et al.* 2001 (142).

4.1 Breast cancer stem cell identification

In 2003, Al-Hajj *et al.* identified the breast CSCs (BCSCs), the first in any solid tumor, based on the cell-surface markers expression $CD44^+/CD24^{low}$. Cells with this

expression pattern, whether obtained from a primary site or metastatic pleural effusions, had the ability to give rise to tumors when xenotransplanted into NOD/SCID mice. Interestingly, tumors generated contained both tumorigenic and non-tumorigenic cells and portrayed diverse expression patterns of CD44 and CD24, conserving the phenotypic heterogeneity of the initial tumor (151). More specifically, **CD44** is the hyaluronic acid (HA) receptor which consists of a multifunctional class I transmembrane glycoprotein. Its expression is significantly enhanced in stem-like cells from most tumors, where it possesses a key role in tumor initiation (152) and metastasis (153). CD44 is also expressed in normal cells and it is associated with cell adhesion, proliferation, migration, angiogenesis, and differentiation (154, 155). On the other hand, **CD24** is the small cell surface protein known as heat-stable antigen. Its function is related to cell interaction (156) and facilitates the adhesion to fibronectin, collagen, and laminin (157). As previously seen, CD24 was found to be less expressed in stem-like cells compared to differentiated cells (158). Overall, CD44⁺/CD24^{-/low} cells display a potent tumorigenic ability (151). It is worth noting that TNBC presents the highest percentage of CD44⁺/CD24^{-/low} stem cells among BC subtypes (159). Despite the fact of being the first described BCSCs markers, there are some contradictory data concerning the role of CD44 and CD24 in tumorigenesis, invasion, and metastasis (160–163). For instance, CD44 and CD24 expression levels show a high degree of variability among different cell lines, which is reflected in the great heterogeneity found in the established cell lines from the same tumor type (163, 164). Moreover, some works did not find a clear association of CD44⁺/CD24^{-/low} abundance and metastatic capacity (165–167). This fact, along with lack of CD44 and CD24 expression in some breast tumor types, empowers the need for the identification of new BCSC markers (162, 168).

Another marker used to identify not only BCSCs but stem-like cells from several tumors is the activity of the aldehyde dehydrogenase 1 (**ALDH1**). This detoxifying enzyme is the main responsible for the oxidation of retinol (vitamin A) to retinoic acid, which is essential for the early differentiation of stem cells (169). BCSCs with

high ALDH1 activity display self-renewal capacity, tumorigenesis, and are highly proliferative (170, 171). As seen with the CD44⁺/CD24^{-/low} expression pattern, ALDH1-positive cells are more abundant in TNBC compared with the other breast cancer subtypes (30).

Regarding this two major BCSCs markers, CD44⁺/CD24^{-/low} and ALDH1, there is little overlap between them, probably due to the presence of two distinct BCSC subpopulations. Besides, both markers are differently expressed among distinct subtypes of breast cancer.

More stemness-related molecules have been postulated as feasible BCSCs markers. Since BCSCs share some characteristics similar to mammary stem cells, BCSCs also express pluripotency, self-renewal, and **stemness markers** such as the sex determining region Y HMG-box 2 and 4 (SOX2 and SOX4), NANOG, octamer-binding transcription factor 3/4 (OCT3/4), CD49f, and CD133 (172). SOX2 is a transcription factor involved in pluripotency maintenance and self-renewal capacity (173). In tumoral tissues, it plays a key role in differentiation, invasion, metastasis, and drug resistance (174). SOX4 is another transcription factor related to the development processes and progression of cancer (175), and it is used as a CSC-specific marker (176). NANOG is a key transcription factor involved in self-renewal and pluripotency maintenance in embryonic stem cells. Moreover, it is thought to be regulated by the cooperative action of SOX2 and OCT3/4 (177). OCT3/4 is a transcription factor fundamental in the maintenance of pluripotency and self-renewal in embryonic stem cells and primordial germ cells (178). CD49f has been related to cell adhesion, poor prognosis, and reduced survival in BC (179). Moreover, CD49f was found to possess a key role in stemness maintenance through direct regulation of OCT3/4 and SOX2 (180). Finally, the transmembrane glycoprotein CD133 has been identified in stem-like cells of many tumors such as colon (181, 182), liver (183), pancreas (184), and endometrium (185) among others. There are some studies that identify CD133 as a good BCSC marker (186, 187) but, unfortunately, its prognostic role has not been well defined yet.

In vitro, BCSCs also have the ability to grow in non-adherent conditions forming **mammospheres** (188). Dontu *et al.* were the first to develop a methodology that allowed the *in vitro* propagation of human mammary epithelial cells in an undifferentiated state, based on their ability to proliferate in suspension. These cells were proven to be capable of growing in non-adherent conditions, forming mammospheres (188). Interestingly, this suspended population was enriched in stem cells since these cells were able to differentiate into distinct mammary lineages and form complex and functional three-dimensional (3D) structures. It is worth noting that not all cell lines are capable of forming mammospheres, and different shapes and ratios widely differ among them (189–191).

In vivo, the most common technique to identify BCSCs cells is determining the frequency of self-renewing cells with a **limiting dilution cell transplantation assay**. Briefly, tumor cells are transplanted into recipient animals at increasing doses and the proportion of animals that develop tumors is used to calculate the number of self-renewing cells within the original tumor sample (192, 193).

4.2 Breast cancer stem cells and chemoresistance

The application of standard cancer treatment, that acts on rapidly dividing cells, sometimes succeeds in reducing tumor volume and improves survival, but many patients suffer a disease relapse within few years. An explanation can be found in the tumor heterogeneity. While the majority of cells die because of treatment, cells enriched in stemness features survive chemotherapy exposure and contribute to disease progression or recurrence (**Figure 7**). In fact, several studies showed that resistance to chemotherapy and ionizing radiation can be achieved by BCSCs, both in established cell lines (167, 194–196) and xenografts models (194, 197, 198). For instance, higher mammosphere forming capacity and CD44⁺/CD24^{-/low} proportion were observed in tumor patients with chemotherapy compared to the untreated ones (197, 199). BCSCs usually remain most of the time in a quiescent state also

known as dormancy that may protect them from chemotherapy and/or radiation damage (200). Besides, BCSCs express high levels of adenosine triphosphate (ATP)-binding cassette (ABC) transporters (201, 202), which give them the ability to pump out chemotherapeutic agents (203). The relative BCSCs chemoresistance can also be explained by their increased ALDH1 activity, which is able to metabolically inactivate chemotherapeutic agents such as cyclophosphamide (204). In addition, BCSCs also possess a more efficient mechanism of DNA damage response (DDR) (205) and have the capacity to reduce intracellular reactive oxygen species (ROS) induced in ionizing radiation (194) which, collectively, lead to a decrease in apoptosis compared to other mammary cell types.

Since BCSCs are more aggressive, invasive, and prone to promote metastasis than the bulk cancer cells (206), targeting the BCSCs niche may lead to a better clinical outcome especially in the reduction of treatment resistance, metastasis, and tumor recurrence.

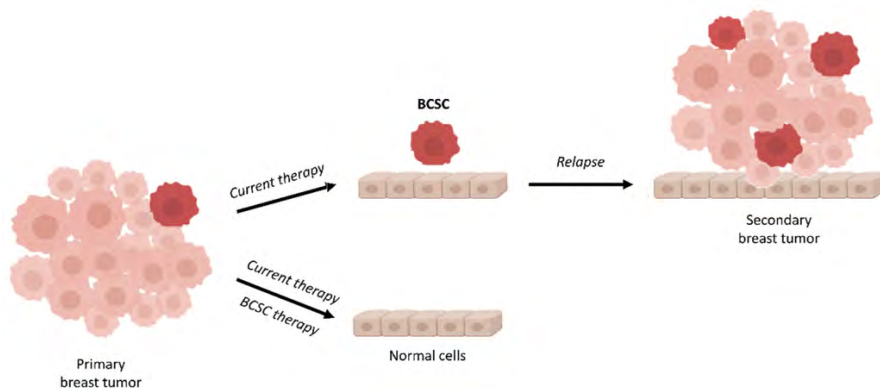


Figure 7. Schematic representation of tumor cell heterogeneity in an aggressive breast cancer. The primary tumor is formed of heterogeneous subpopulations of cells including breast cancer stem cells (BCSCs). Usually, a first-line therapy is chosen based on the histological subtype, stage of the tumor, presence of biomarkers, and other clinical data. If the first-line therapy does not target BCSCs, the tumor mass will be reduced but BCSCs will remain (mostly) unaffected. BCSCs present in the primary tumor can expand and give rise to a multi-drug resistant tumor (secondary breast tumor), leading to progression and metastasis of the tumor. Taken from Palomeras *et al.* 2018 (207).

4.3 Novel approaches against breast cancer stem cells

The relative resistance of BCSCs to standard therapies compared with bulk cancer cells highlights the need for novel therapies targeting the stem-like subpopulation. Therefore, BCSC properties, markers, and underlying mechanisms may be potential targets to design a more efficient therapy to use alone or in combination with current treatments. For instance, the **quiescent state** of BCSCs can be disrupted to force BCSCs to re-enter the cell cycle and increase the effect of current therapies which target proliferative cells. Quiescence-related proteins such as the cyclin-dependent kinase inhibitors p57KIP2, p27KIP1, and p18INK4c, and the subunit of the ubiquitin ligase complex Fbxw7 have shown a great potential to become targets in some studies (200, 208–210). Interestingly, Gasca *et al.* proved that forced expression of Fbxw7 restored paclitaxel sensitivity in resistant TNBC cells (211).

It has been shown that some **antibiotics** have antitumor ability and can affect CSC niche. Salinomycin is the most studied antibiotic, and it has been proven to selectively reduce BCSC subset by blocking the Wnt/ β -catenin pathway (212, 213). The combination of salinomycin targeting CSCs with current chemotherapeutic drugs have synergistically inhibited tumor growth (214–216). Recently, Lamb *et al.* tested several FDA-approved antibiotics that inhibit mitochondrial biogenesis, e.g., azithromycin, doxycycline, tigecycline, pyrvinium paomate, and chloramphenicol. Authors observed that antibiotics affected the cancer stem-like cells of hormone-positive and TNBC cells (217). Another example is thiostrepton, which is proved to possess a cytotoxic effect and cell cycle arrest against breast cancer cells (218). Yang *et al.* demonstrated that thiostrepton decreased mammosphere formation and CD44⁺/CD24^{-/low} population in TNBC cells by inhibiting SHH signaling pathway, which has an important role in BCSC self-renewal (219).

BCSC radioresistance may also constitute a novel approach to address a novel targeted regimen. After radiotherapy, BCSCs isolated from cell models and primary breast cancer culture showed high expression of **ataxia telangiectasia mutated** (ATM) genes, which constitute the DNA damage repair system. Treatment with an ATM inhibitor resensitized these cells to radiation (220). Hence, decreasing radiation resistance of BCSCs by targeting the ATM signaling could prevent relapse after conventional first-line therapy.

Since BCSCs display a larger **ALDH1 activity**, it may also be targeted to increase better outcome of BC patients. Croker *et al.* demonstrated that inhibition of ALDH1 activity by means of all-*trans* retinoic acid (ATRA) or the specific ALDH1 inhibitor diethylaminobenzaldehyde (DEAB) increases the effect of both chemotherapy and radiotherapy on TNBC models (221).

Lately, cancer research has started using nanotechnology to improve treatment efficacy and reduce toxicity. A good example is the use of **nanoparticles** to enhance cellular uptake and selectivity towards BCSCs. Li *et al.* developed salinomycin-loaded polymer-lipid hybrid nanoparticles conjugated with anti-HER2 antibodies. They affected both BCSCs and bulk tumor cells in hormone-positive and TNBC cells (222). The anti-alcoholism drug disulfiram was also encapsulated in a work by Liu *et al.* in order to improve the drug's half-life in the bloodstream. Interestingly, it showed cytotoxic activity against BCSCs and induced ROS activity in mammospheres from hormone-positive and TNBC cells (223). Besides, researchers have reported that the use of nanoparticles coated with HA, the primary CD44 binding molecule, improves cancer therapy efficacy owing to the delivery system enhancement (224–226). For instance, chemotherapy drug gemcitabine was loaded into HA-conjugated nanoparticles. The encapsulation process not only increased the inhibitory capacity of gemcitabine against BCSCs but also reduced the systemic toxicity of the drug alone on normal tissue (227).

Altogether, all these novel targeted therapies need to be further validated in clinical trials despite the promising results obtained in *in vitro* experimentation.

4.4 Epithelial-to-mesenchymal transition

Epithelial-to-mesenchymal transition (EMT) is an evolutionarily conserved developmental process that governs morphogenesis in multicellular organisms (228). By definition, epithelial cells can be seen as surface barrier cells with distinct apical versus basolateral polarity established by adherent and tight junctions. In contrast, mesenchymal cells serve scaffolding or anchoring functions and play a key role in tissue repair and wound healing. During embryonic development, differentiated epithelial cells can undergo profound morphogenetic changes, collectively referred to as EMT (**Figure 8**). This process, characterized by the dissolution of cell-cell junctions and loss of apico-basolateral polarity, leads to the formation of migratory mesenchymal cells with invasive properties (229). These mesenchymal cells are recruited to specific sites in the developing embryo where they can differentiate through the inverse process, known as mesenchymal-to-epithelial transition (MET). Overall, EMT is a multi-step process manifested by the following cellular and molecular changes:

- i. Loss of cell-cell adhesion and apical-basal polarity, involving E-cadherin, occludins, and claudins in cell-cell junctions
- ii. Downregulation of epithelial cytokeratins CK8, CK18, and CK19
- iii. Upregulation of mesenchymal proteins such as vimentin
- iv. Reorganization of the cytoskeleton to acquire more spindle-like morphology
- v. Increased motility and invasiveness
- vi. Resistance to apoptosis

The process of EMT involves the coordination of a **complex network**. A wide variety of extracellular signals and signaling pathways can trigger the EMT, such as Wnt/ β -catenin, Hedgehog, Notch, and some autocrine factors including the transforming growth factor beta (TGF- β) (230). Signal transduction of these pathways converges in the activation of one or several EMT-inducing transcription factors, for instance Snail (zinc finger protein SNAI1), Slug (zinc finger protein SNAI2), Zeb1 (zinc finger E-box-binding homeobox 1), Zeb2 (zinc finger E-box-binding homeobox 2), and Twist (class A basic helix-loop-helix protein 38). These transcription factors induce EMT through transcriptional repression of E-cadherin (231), as it is involved in the establishment of cell-cell adhesion (232). This fact is accompanied by the overexpression of the mesenchymal protein vimentin, which contributes to cytoskeleton organization and focal adhesion stability (233).

Apart from its paper in embryogenesis, EMT can be also activated in **pathological conditions** such as progression of carcinoma (234). Actually, EMT allows cancer cells to detach from primary tumor and metastasize to distant tissues (235). EMT-like tumor cells are usually seen at the invasive edge of primary tumors, where they eventually initiate the tumor metastasis cascade, including intravasation, extravasation, and formation of microscopic and macroscopic metastases in distant organs (236, 237). The role of EMT to promote tumor cell dissemination is well supported by studies on circulating tumor cells (CTCs), which exhibited EMT features (238–240) and express known EMT regulators (241). In metastatic conditions, EMT process should be suppressed once invasive cells reach the distant site. The reciprocal program MET is subsequently induced in order to return to the epithelial phenotype and to help disseminated tumor cells form sizable macro-metastatic colonies at distant organs. Such EMT/MET state transitions may serve as the underlying driving force of metastasis.

Cells undergoing EMT are demonstrated to acquire stem cells features, suggesting a key role of EMT in the **generation of BCSCs** and their maintenance (235). In fact, BCSCs exhibit an invasive gene signature which correlates with increased

metastasis, suggesting an association of BCSCs, EMT, and metastatic capacity (242). Induction of EMT in human mammary epithelial cells was proven to be sufficient to provoke the upregulation of several stem cell markers (243).

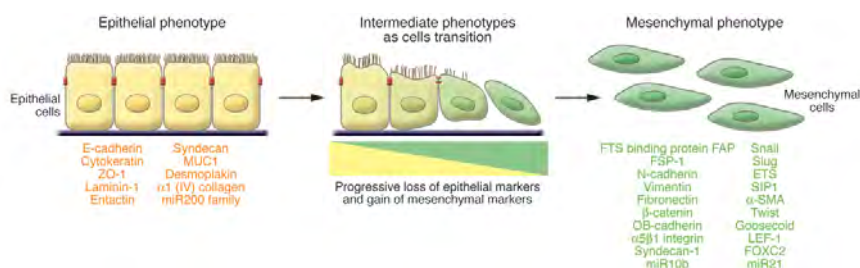


Figure 8. Epithelial-to-mesenchymal transition (EMT). An EMT involves a functional transition of polarized epithelial cells into mobile and extracellular matrix (ECM)-secreting mesenchymal cells. The epithelial and mesenchymal cell markers commonly used by EMT researchers are listed. Abbreviations: α -SMA (α -smooth muscle actin), ETS (v -ets erythroblastosis virus E26 oncogene homolog), FAP (fibroblast activation protein), FOXC2 (forkhead box C2), FSP-1 (fibroblast-specific protein 1), FTS (fused toes homolog), LEF-1 (lymphoid-enhancer-binding factor 1), miR200 (microRNA 200), MUC1 (mucin 1), SIP1 (survival of motor neuron protein interacting protein 1), ZO-1 (zona occludens 1). Taken from Kalluri *et al.* 2009 (236).

4.5 Breast cancer stem cell plasticity

As commented before, there is little overlap between $CD44^+/CD24^{-/low}$ and $ALDH1^+$ cells as both subpopulations identify distinct BCSCs within breast cancers (**Figure 9**). Both of these subsets display characteristics of BCSCs, but they also have properties unique to each particular type (244). Gene expression profiling indicates that $CD44^+/CD24^{-/low}$ cells have EMT signatures such as low expression of E-cadherin, high levels of vimentin, and tend to be relatively quiescent. This subpopulation was accordingly labeled as EMT-BCSCs. In contrast, $ALDH1^+$ cells display a more epithelial signature with high expression of E-cadherin, low levels of vimentin, and much more proliferative. Therefore, this subset was labeled as MET-BCSCs (171). Despite aforementioned differences, both BCSC niches display common features in terms of metastasis, treatment recurrence (170), enhanced

migration and invasion capacities (171, 245), intrinsic detoxifying abilities (246, 247), and increased DNA-damage repair responses (220, 248).

The EMT-BCSCs are usually located at the invasive edge of the tumor since their mesenchymal properties allow them to quickly move into the surrounding tissue. Once intravasated, they survive due to their intrinsic quiescence and resistance to anoikis, a programmed cell death associated with loss of adhesion. Oppositely, proliferative MET-BCSCs likely drive tumor cell growth in the tumor interior, being associated with self-renewal and macrometastasis generation due to their cycling profile. Interestingly, mounting data demonstrate the existence of a BCSC plasticity that enables them to transition between these two states (171). This transition dynamic is believed to have a great impact on tumor progression. Depending on the conditions and expansion of the tumor, BCSCs can change states and are able to rapidly switch the transcriptional machinery to undergo MET or EMT when needed.

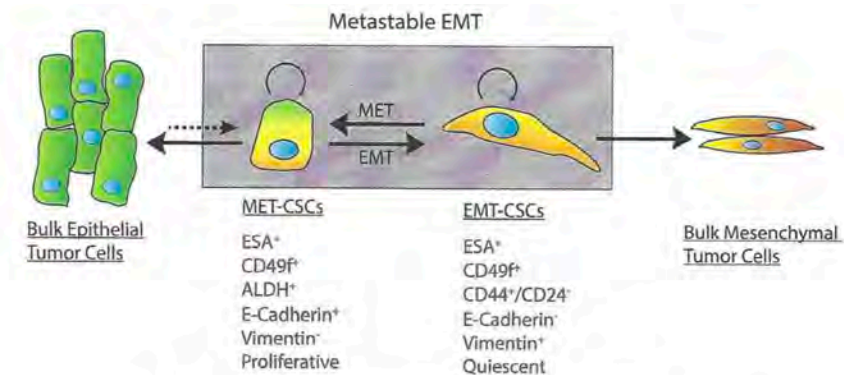


Figure 9. Model of epithelial-to-mesenchymal transition (EMT) and mesenchymal-to-epithelial transition (MET) in driving the plasticity of breast cancer stem cells (BCSCs). BCSCs can exist in two interconvertible states: MET-like (aldehyde dehydrogenase-positive; ALDH⁺) and EMT-like (CD44⁺/CD24^{-/low}). The reversible, metastable state change between BCSCs is induced by the tumor microenvironment. Permanent EMT processes induced by constitutive EMT inducing signals will promote differentiated mesenchymal-like tumor cells, leading to loss of BCSC properties. Similarly, permanent MET induced by constitutive MET inducing signals will promote luminal differentiation, leading to loss of BCSC properties. On the other hand, differentiated bulk epithelial tumor cells may undergo dedifferentiation (dashed arrow) and enter into the MET BCSC state. CSCs may be permanently locked into a proliferating mesenchymal state in mesenchymal-like tumors. Abbreviations: ESA (epithelial-specific antigen). Taken from Luo *et al.* 2015 (244).

4.6 Breast cancer stem cells and triple negative breast cancer

As previously seen in **Figure 5A**, the two main molecular subtypes represented in TNBC are the basal-like and mesenchymal-like (also known as claudin-low), in this order. Mesenchymal-like TNBC cells have specific characteristics including low expression of cell-cell adhesion proteins (claudin family of proteins) and enrichment with mesenchymal genes (vimentin, N-cadherin, and TWIST for instance), features associated to the induction of EMT (23) (**Figure 10**). Moreover, $CD44^+/CD24^{-/low}$ gene signature was mainly found in this TNBC subtype (249). Basal-like breast cancer displays a phenotype close to the BCSCs, with increased ALDH activity but higher epithelial markers expression.

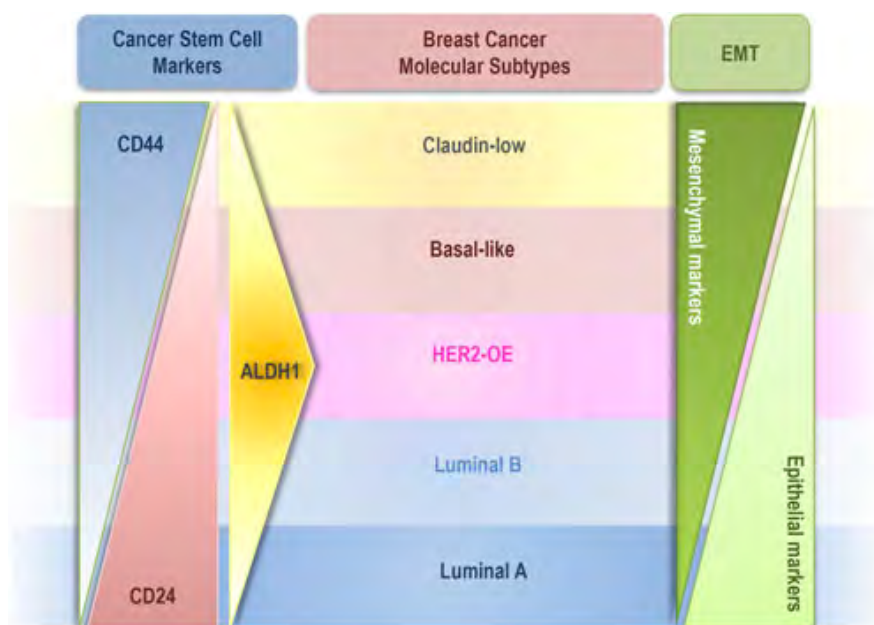


Figure 10. Representation of the putative association between breast cancer molecular subtypes and the expression pattern of breast cancer stem cell (BCSC) biomarkers. In this hypothesis, each molecular subtype is enriched in cancer cells with distinct levels of differentiation, being BCSCs more prevalent within the more undifferentiated molecular breast cancers, such as claudin-low (mesenchymal-like) tumors. **Abbreviations:** ALDH1 (aldehyde dehydrogenase 1), CD (cluster of differentiation), EMT (epithelial-to-mesenchymal transition), HER2-OE (human epidermal growth factor receptor 2 overexpressing). Taken from Schmitt *et al.* 2012 (250).

5 Fatty acid synthase

Alongside BCSC presence, it is known that cancer cells also suffer from metabolism deregulation to deal with the high demand of the uncontrolled cell growth. Perturbed metabolism allows cancer cells to accumulate metabolic intermediates as sources for building blocks and provide advantage in the tumor environment (251, 252). For example, long-chain fatty acids (FAs) are crucial elements of membrane lipids and are important substrates for cell energy metabolism as well. The most common saturated FA is the palmitate, which is the first one produced during fatty acid synthesis and is the precursor of longer FAs. Palmitate is synthesized *de novo* from acetyl-CoA and malonyl-CoA in a nicotinamide adenine dinucleotide phosphate hydrogen (NADPH) dependent manner by the multifunctional enzyme fatty acid synthase (FASN) (253). Interestingly, FASN has been found overexpressed and hyperactivated in several carcinomas including breast, prostate, lung, and colon among others (254–257). On the other hand, FASN is not expressed in normal tissue, except in lipogenic tissues such as liver (258), adipose tissue (259), and lactating mammary glands (260, 261), where diet regulates its expression. In normal tissue, fatty acid synthesis occurs when there is a caloric excess, and carbohydrates are stored as triglycerides. However, tumor cells are dependent on the generation of lipids to keep their demanding proliferation ratio. In cancer cells, most of the FAs are synthesized *de novo* by FASN (251), mainly as phospholipids which can act not only as structural pieces for membrane biosynthesis but also as signaling molecules (262–264).

5.1 Fatty acid synthase function

As depicted in **Figure 11**, cancer cells fervently consume glucose, which is processed and converted into pyruvate via the glycolytic pathway. Pyruvate is subsequently fed into the Krebs cycle in the mitochondria to yield ATP, releasing acetyl-CoA as one of the products of this reaction (265). A portion of acetyl-CoA is

carboxylated to malonyl-CoA by acetyl-CoA carboxylase (ACACA). Then, FASN performs the condensation of acetyl-CoA and malonyl-CoA to produce the 16-carbon saturated FA palmitate and other saturated long-chain FAs, which is dependent on NADPH. FAs can be further processed by elongases or desaturases to form more complex FAs, which are used for the synthesis of several cellular lipids such as phospholipids, triglycerides, and cholesterol esters, or for the acylation of proteins.

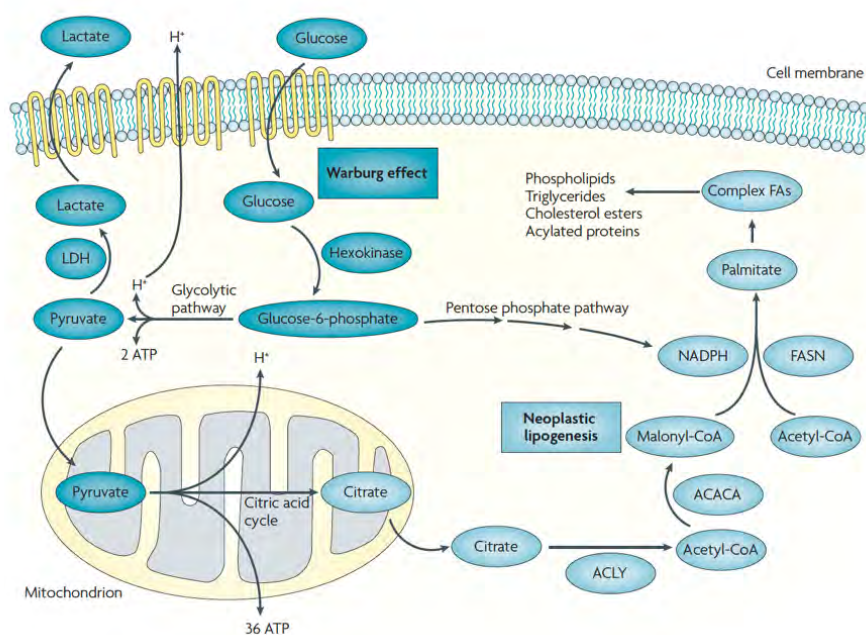


Figure 11. Connecting glucose metabolism and fatty acid (FA) biosynthesis pathways in tumor cells. About 25 enzymes are involved in the metabolism of glucose to FAs. The key elements of the main synthetic pathways and their connections are shown here. Abbreviations: ACACA (acetyl-CoA carboxylase), ACLY (adenosine triphosphate citrate lyase), ATP (adenosine triphosphate), FASN (fatty acid synthase), H⁺ (hydrogen), LDH (lactate dehydrogenase), NADPH (nicotinamide adenine dinucleotide phosphate hydrogen). Taken from Menendez *et al.* 2007 (268).

5.2 Fatty acid synthase regulation

In the majority of tissues, FASN is low expressed since cells preferably obtain all the FAs from exogenous supplies (266). There are some exceptions in physiological

conditions such as lipogenic tissues, hormone-sensitive tissues including endometrium during menstrual cycle, mammary gland during lactation, and hypothalamus (as a mechanism for food intake regulation), where *de novo* synthesis pathways are activated (258–261, 266, 267). In **normal tissues**, FASN expression can be regulated both metabolically and hormonally. Both signals converge, at least in part, on the PI3K/AKT/mTOR and MAPK pathways that modify the expression or maturation of transcription factors that regulates the expression of FASN (268). Some of these transcription factors that have cognate binding sites on the FASN gene promoter are stimulatory proteins 1 and 3 (Sp1 and Sp3), nuclear factor κ (NF- κ), upstream stimulatory factor (USF), and the sterol regulatory element binding protein 1 (SREBP1) (269). For instance, leptin (the hormone made by adipose cells that inhibits hunger) decreases SREBP1 gene expression, inhibiting the expression of lipogenic enzymes including FASN (270).

In **cancer**, FASN regulation changes from diet aspects to regulatory elements such as growth factors and their receptors (**Figure 12**). The HER family receptors have been linked with FASN overexpression in some cancers (271–273) since their signaling pathways result in the activation of the SREBP1 transcription factor. Therefore, deregulation in the HER-downstream pathways PI3K/AKT/mTOR and MAPK has been related to FASN expression (272, 274, 275). On the other hand, overactivation of hormonal pathways (ER, PR, and AR) also converges to PI3K/AKT/mTOR and MAPK activation, which stimulates FASN expression (276).

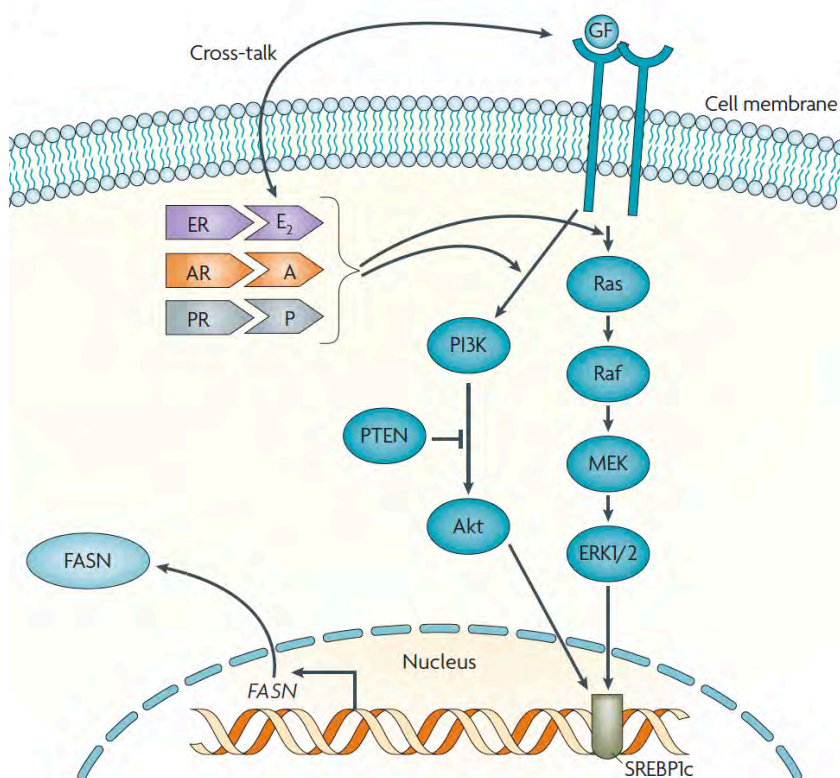


Figure 12. Regulation of fatty acid synthase (FASN) expression in cancer cells. Contrary to normal cells, cancer cells regulate FASN expression through membrane receptors (HER family as an example) and/or hormone receptors (estrogen receptor [ER], progesterone receptor [PR], and androgen receptor [AR]) that activate the phosphoinositide 3-kinase (PI3K)/ mammalian target of rapamycin (mTOR) or the mitogen activated protein kinase (MAPK) pathway. The activation of these pathways leads to the activation of the FASN transcription factor sterol regulatory element binding protein 1c (SREBP1c). **Abbreviations:** A (androgen), AKT (protein kinase B), E₂ (oestradiol), ERK1/2 (extracellular signal-regulated kinases 1 and 2), GF (growth factor), MEK (MAPK/ERK kinase), P (progestins), RAF (rapidly accelerated fibrosarcoma), RAS (rat sarcoma), PTEN (phosphatase and tensin homolog). Taken from Menendez *et al.* 2007 (268).

5.3 Fatty acid synthase inhibition and cancer

Due to the critical role of FASN in cancer cells, this enzyme has become a unique oncologic target. Its inhibition has been demonstrated to hinder tumor progression (277–279), block angiogenesis (280, 281), and overcome resistance to chemotherapeutic agents (282, 283). Besides, the combination of FASN inhibition

and common chemotherapy drugs such as taxanes or anthracyclines has been proved to be synergistic (284, 285). Several **mechanisms** that trigger the antitumoral effect of FASN inhibition are described hereinafter (262), also depicted in **Figure 13**.

- I. End-product starvation: highly proliferative tumor cells require FASN to produce the phospholipids that will form the newly synthesized membrane. Therefore, when FASN is inhibited, there is a lack of phospholipids that induces apoptosis in cancer cells (286, 287).
- II. Disturbance of membrane and protein localization function: in the cell membrane, there are some regions known as lipid rafts that contain high concentrations of lipids such as palmitate, cholesterol, and sphingosine, and are also rich in protein receptors such as the HER family (288, 289). A phospholipids shortage disrupts lipid raft assembling, impairing the correct localization or function of these receptors (263).
- III. Inhibition of DNA replication: phospholipids also play an important role in cell division. Hence, the lack of phospholipids blocks cell cycle before G1 and impedes cell division (290).
- IV. p53-regulated non-genotoxic metabolic stress: FASN inhibitors are proved to be more effective initiating cell death in non-functioning p53 tumor cells, whereas cells with intact p53 function tend to display cytostatic responses (291).
- V. Toxic accumulation of substrates: the inhibition of FASN leads to the toxic accumulation of its substrate malonyl-CoA. Malonyl-CoA hinders the activity of carnitine palmitoyltransferase 1 (CPT1), which in turn inhibits de β -oxidation promoting the accumulation of the sphingolipid ceramide. The accumulation of ceramide eventually causes the induction of proapoptotic genes involved in the ceramide-mediated apoptotic pathway (292).
- VI. Inhibition of proliferative pathways: FASN blockade results in the downregulation of AKT, which precedes the induction of tumor cell apoptosis (293, 294).

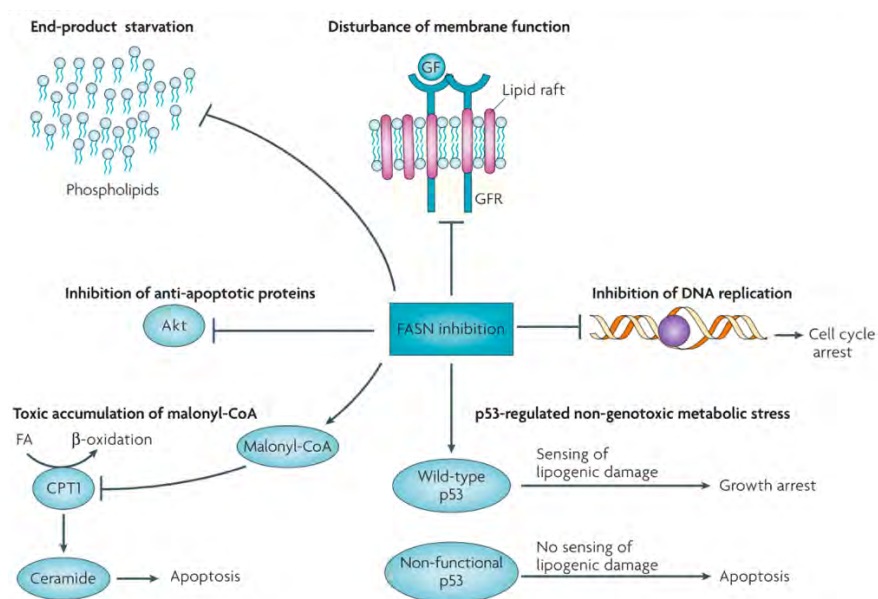


Figure 13. Fatty acid synthase (FASN) inhibition and cancer cell death. Several mechanisms have been proposed to explain the tumoricidal effects that occur after FASN blockade. **Abbreviations:** AKT (protein kinase B), CPT1 (carnitine palmitoyltransferase 1), GF (growth factor), GFR (growth factor receptor). Taken from Menendez *et al.* 2007 (262).

The inhibition of FASN was firstly described to be cytotoxic in cancer cells in 1960 and, since then, several **FASN inhibitors** have been developed. The first one to be identified was the antifungal antibiotic cerulenin (295, 296). However, its clinical application was limited due to the chemical instability caused by its very reactive epoxy group (297). To overcome this issue, the C75 cerulenin-derived molecule was designed removing the epoxy group. C75 displays tumor growth inhibition in xenograft prostate, breast, mesothelioma, lung, and ovarian cancer models (298–300). Despite initial good behavior in xenograft models, its clinical application is limited due to weight loss induction and food intake reduction (301). The following described FASN inhibitor is the (-)-epigallocatechin-3-gallate (EGCG), the main catechin found in green tea. It is described to be a powerful antioxidant and to possess anti-proliferative activity through the induction of apoptosis. EGCG targets multiple signaling pathways such as EGFR-HER2, MAPK, and PI3K/AKT/mTOR. Despite these off-targets effects, apoptosis after EGCG treatment occurs through

FASN inhibition (302, 303). The high concentrations needed and its poor oral bioavailability and stability in physiological conditions hinder its clinical application.

In short, the first generation of FASN inhibitors exhibited some limitations such as off-target toxicity, poor bioavailability, and little stability. Lately, a new generation of FASN inhibitors is in development, some of them based on the chemical structure of the above ones. For instance, the EGCG-derived G28UCM (in this thesis G28) displayed a strong 90% FASN activity inhibition and cancer cell cytotoxicity in a panel of human breast cancer cells, even in TNBC models (293, 304, 305). *In vivo*, G28 exhibited marked tumor volume reduction but with no sign of weight loss or anorexia (304). Interestingly, G28 also induced apoptosis and tumor reduction in both HER2+ breast cancer xenograft and in HER2+ resistant cell lines (306, 307).

6 Cancer cell culture

In the recent decades, *in vitro* cell culture has become an essential tool in the cell biology research field. At the end of the 19th century, scientists performed the first efforts to maintain living tissues and cells after organism death (308). Some years later, the establishment of the first human immortal cell line in 1951, the *HeLa* cells (309), promoted the use of *in vitro* cell culture supports. Therefore, there was an urgent need to develop a cell maintenance protocol in order to study *ex vivo* the cell behavior under established conditions.

In the first described attempts, cells were grown on flat surfaces made of glass and coated with collagen and other proteins to favor cell adhesion (310). Despite their applicability, researchers started to handle disposable plastic devices thanks to their ease of use and practicability. Since their establishment, polystyrene has been the most used polymer to manufacture single-use vessels (311). The main reasons are its optical clarity, good molding ability, and the possibility to be treated to modulate its hydrophilic features (312). It is therefore not surprising that, since the

'70s, treated polystyrene flasks have been used in worldwide laboratories due to their benefits (313). However, this flat plastic surface only allows the development of two-dimensional (2D) cell culture, leading to a monolayer cell culture. Cultured cells adopt a flattened morphology which clearly differs from the *in vivo* pattern (**Figure 14**). In physiological conditions cells are embedded in a 3D network composed by fibrous proteins and molecules, known as extracellular matrix (ECM), which plays a major role in cell regulation (314, 315). Therefore, *in vivo* cells interact with the ECM fibrous mesh and adjacent cells, thus adopting a more elongated and 3D morphology. The 2D shape caused by flat supports directly modifies membrane receptor polarity and cytoskeleton architecture, affecting gene expression and protein synthesis regulation (316, 317). Hence, experiments performed using 2D models can display a cell behavior different from the physiological one. More concretely, it has been proved that this key difference in cellular surroundings may influence CSC properties as well as their differentiation state (318, 319).

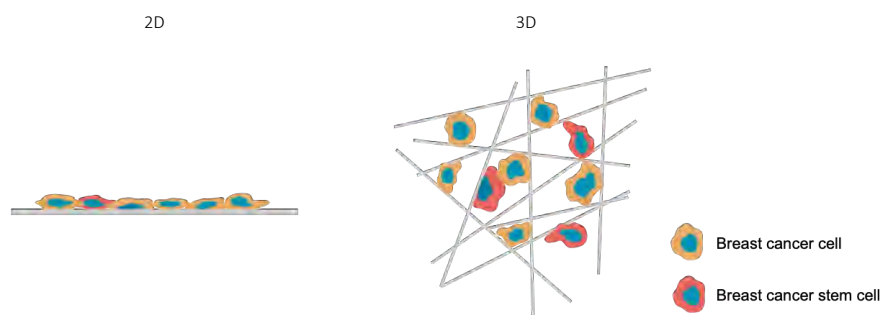


Figure 14. Schematic comparison between monolayer two-dimensional (2D) and three-dimensional (3D) breast cancer cell culture. In monolayer culture, cells show a flattened morphology accompanied by a low percentage of breast cancer stem cells (BCSCs), due to the inducing effect of 2D culture supports. In contrast, 3D cell culture allows cells to adopt a more elongated morphology, with a higher proportion of BCSCs. Own elaboration.

Aside from the lack of three-dimensionality, stiffness also stands for a significant difference between traditional *in vitro* cell culture supports and physiological surroundings. Mammalian cells are generally anchored to soft surfaces such as the ECM or another similar cell, in contrast with the rigidity found in 2D surfaces used

in laboratory studies (320). It has been reported that microenvironment stiffness can exert a great mechanical impact on the cell, acting on morphology, motility, proliferation, protein expression, and spreading (321, 322).

6.1 Three-dimensional cell culture supports


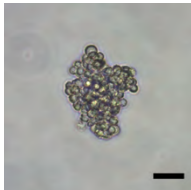
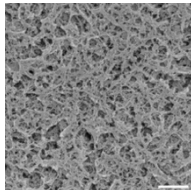
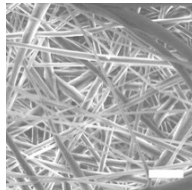
Due to the described gaps between monolayer culture and physiological surroundings, researchers have been focused their efforts on developing novel cell culture supports that resemble the 3D *in vivo* cell environment (**Table 2**). Firstly, it was discovered that neural cells could be grown in non-adherent surfaces, only allowing the growth of the cells that possessed the capacity to survive in suspension. Surviving cells displayed a rounded morphology and proliferated forming suspension **spheres**, composed by undifferentiated multipotent neural cells (323, 324). Since the discovery, spheres culture has become an assay to quantify stem cell activity in a wide range of cancers, including breast cancer (188, 325). However, their morphology does not mimic the *in vivo* shape and some cancer cells do not form compact spheres but loosely adhered clumps of cells.

Following efforts were, therefore, focused on the development of physical structures which mimic the ECM architecture. In 1960, Wichterle and Lim developed a matrix composed of a cross-linked network of polyhydroxyethylmethacrylate (pHEMA) with high water affinity. This biocompatible construct was designated as **hydrogel** (326). This initial prototype was subsequently modified to be used for 3D cell culture approaches. In current days, hydrogels are usually composed of biological materials such as agarose, fibrin, collagen, and hyaluronic acid, but maintaining the high water content (327). This hydrated structure makes them more similar to the architecture and mechanics of native ECM (328). The most well-known hydrogel is the gelatinous protein mixture Matrigel™, which is secreted by Engelbreth-Holm-Swarm mouse sarcoma cells (329). Their biological origin favors its biocompatibility, and they

intrinsically contain ECM proteins and growth factors. Despite the benefits, hydrogels also display some limitations including a possible non-optimal nutrient and oxygen diffusion, inaccurate composition, and variation among batches.

Finally, **scaffolds** have emerged as another 3D cell culture support in order to overcome the abovementioned issues. This model is based on a solid, physical support made by a network of filaments mostly made by synthetic materials such as polymers that simulate the ECM fibrous architecture (330). This 3D surrounding allows cells to interact with adjacent cells and also with polymeric fibers, so cells display an extended cytoplasm, close to the physiological morphology. For this reason, the cancer research field is taking advantage of the scaffold culture benefits. Hereinafter, this thesis will be focused on this last *in vitro* 3D cell culture support and its features will be disclosed in the following sections.

Table 2. Comparison of different cell culture supports used in worldwide laboratories. Abbreviations: 2D (two-dimensional), 3D (three-dimensional), CSC (cancer stem cell), ECM (extracellular matrix), PCL (poly(ϵ -caprolactone)). Taken from Rabionet *et al.* 2019 (311).

	2D		3D	
	Monolayer	Spheres	Hydrogels	Scaffolds
				
	MCF-7 cells in 2D adherent culture (scale bar= 50 μ m)	MDA-MB-231 cell sphere (scale bar= 50 μ m)	Scanning electron microscopy of Matrigel (scale bar= 1 μ m)	Scanning electron microscopy of PCL electrospinning scaffold (scale bar= 10 μ m)
Composition	Polystyrene adherent flat surfaces	Suspension culture in non-adherent surfaces	Biological material (water, agarose, fibrine, collagen, hyaluronic acid)	Biocompatible polymers

Continuation of **Table 2**.

	2D	3D		
	Monolayer	Spheres	Hydrogels	Scaffolds
Advantages	Cheap and fast technique	3D culture easy to perform	They mimic the ECM structure	They mimic the ECM structure
		Useful to quantify stem activity and to perform anticancer drug screening	They contain ECM proteins and growth factors	ECM proteins can be added
				Proved to enrich CSC subpopulation
Disadvantages	Environment differs from the physiological one	Sphere cells morphology does not mimic the <i>in vivo</i> shape	Non-optimal nutrient diffusion	Different cell lines may need different scaffold architecture
	Monolayer cells display less aggressiveness than <i>in vivo</i>	Some cancer cells do not form compact spheres but loosely adhered clumps of cells	Possible inaccurate composition	Trypsinization may be required
	2D culture leads to cancer stem cells differentiation			

6.2 Technologies to manufacture three-dimensional scaffolds

Several technologies are available for scaffold manufacture, as seen in **Table 3**. The **fused filament fabrication** (FFF) is an additive manufacturing (AM) technology widely used by 3D printers (331, 332). Briefly, the polymer is melted and deposited in successive layers to print the final construct, which can be previously designed. Due to its technical features, micrometric fibers can be easily manufactured but the production of smaller-diameter filaments is challenging. Hence, FFF scaffolds are usually used in tissue engineering (TE) studies thanks to their mechanical characteristics (331, 333–335). FFF allows investigators to design and customize

external profile and internal pattern depending on the tissue to be healed. Therefore, scaffolds can be directly customized from the patient. Despite its applicability, determining the optimal parameters for the production process is a mandatory and critical step (331, 332, 336). This procedure comprises the optimization of both design and fabrication parameters, which are related to the chosen polymer and the scaffold application (337). Indeed, architecture features including porosity, pore size, pore shape, and mechanical strength among others, need to be appropriate to achieve suitable cell growth and matrix formation (338). 3D printers using FFF technique represent one of the most accessible options to manufacture scaffolds (332). They usually are open-source and low-cost apparatus that can be easily modified to improve the quality of the printing (339). For example, 3D printing was integrated in a fully automated bench-top manufacturing system for TE applications called *BioCell Printing*. This bioprinting system integrates the production stage, sterilization, cell seeding, and *in vitro* culture in different zones (333, 340).

Another of the most used techniques for scaffold manufacture is **electrospinning** (ES). In this technology, the polymer is dissolved and placed into a syringe connected to a metallic needle. A high voltage is applied so the polymer fluid becomes charged, forming a cone-shaped protuberance called Taylor cone. When the electric force surpasses the surface tension, a stream of liquid is ejected from this formation. This stream travels from the needle to the ground collector while solvent is evaporating. Consequently, polymer fibers are randomly formed in the collector. This technology is capable of producing fibers with small diameters even close to the collagen fibers size, the main component of ECM (341). Therefore, electrospun scaffolds have a great potential in terms of mimicking the structure of native ECM. As in the case of FFF, ES is highly influenced by fabrication parameters including polymer concentration, chosen solvent, applied voltage, and polymer solution flow rate. These parameters, among others, determine the correct operation of the system and the final architecture of the meshes.

Table 3. Comparison of different technologies used to manufacture scaffolds for three-dimensional (3D) cell culture. Abbreviations: FFF (fused filament fabrication), PCL (poly(ϵ -caprolactone)). Taken from Rabionet *et al.* 2019 (311).

	Fused Filament Fabrication	Electrospinning
Scheme	<p>Extracted from www.reprap.org</p>	<p>Own elaboration</p>
Machinery	<p>RepRap BCN3D+ printer from BCN3D technologies (Barcelona, Spain)</p>	<p>Electrospinning apparatus from Spraybase® (Dublin, Ireland)</p>
Manufactured scaffolds	<p style="writing-mode: vertical-rl; transform: rotate(180deg);">Macroscopic view</p> <p>PCL scaffold manufactured by a 3D printer (scale bar= 4 mm)</p>	<p>PCL scaffold manufactured by an electrospinning apparatus (scale bar= 4 mm)</p>
	<p style="writing-mode: vertical-rl; transform: rotate(180deg);">Microscopic view</p> <p>Optical Microscopy micrograph of a FFF PCL scaffold (scale bar= 4 mm)</p>	<p>Scanning Electron Microscopy micrograph of an electrospun PCL scaffold (scale bar= 10 μm)</p>

6.3 Available biomaterials for scaffold manufacture

Overall, all cell types possess different morphological characteristics which may lead to distinct cell culture support requirements. These specific requests will determine the technology and biomaterial to be used, as well as the structure features of the scaffold. In fact, the chosen biomaterials, which are defined as materials that interface with biological entities (342), play a relevant role since they dictate some scaffold **critical features**. For instance, scaffold must be biocompatible, in other words, materials should interact positively with the host environment (either *in vitro* cell culture or *in vivo* organism) without eliciting adverse responses. Moreover, some meshes need to possess some degree of biodegradability, mainly scaffolds related to medical devices. These models need to degrade into non-toxic products with a controlled degradation rate that matches the regeneration rate of the native tissue (343). Currently, four classes of **biomaterials** are used:

- Acellular tissue matrices: known as biological scaffolds since they are composed of an extracellular matrix (ECM). They are not processed through the technologies here described, but through a decellularization process that include physical, chemical, and enzymatic methods to remove cell bodies from the remaining ECM (344, 345).
- Metals and their alloys: major metals used in medical applications include commercially pure titanium and its alloys, cobalt-based alloys, and stainless steel (346). Although some works have used metallic scaffolds for cell culture (347, 348), these materials are most used for load-bearing implants due to their mechanical reliability, strength, and impact resistance (349). However, metals can suffer from corrosion in physiological environments, thus releasing ions, which may reduce biocompatibility and put at risk the use of implants.
- Ceramic materials: ceramics are inorganic materials with high compressive strength and biological inertness (350–352). The most commonly used are

metallic oxides, calcium phosphate such as hydroxyapatite, and glass ceramics (e.g., Bioglass) (353, 354). They have been used for hard tissue replacement such as bone and teeth since ceramics exhibit similar chemical characteristics. For instance, several *in vitro* and *in vivo* works have shown that calcium phosphates support the adhesion, differentiation, and proliferation of osteogenesis-related genes, besides inducing gene expression in bone cells (355–358). Besides, some ceramics are usually coated onto a metal core or incorporated into polymers as composites (349, 359).

- Polymers: they are defined as materials consisting of macromolecules composed of many repeating subunits. Polymers stand for the main group in the scaffold manufacturing scenario, and can be naturally derived or synthetic, the latter of which can be bioinert or biodegradable. Natural polymers include albumin, collagen, cellulose, hyaluronic acid, starch, chitosan, dextran, silk, and heparin (354, 360). On the other hand, some examples of bioinert synthetic polymers are polyvinyl chloride, polyethylene, polypropylene, polystyrene, polyesters, polyamides, polyurethanes, and polysiloxanes (silicone) (354, 360). Lastly, biodegradable synthetic polymers include poly(glycolic acid), poly(lactic acid), poly(ϵ -caprolactone), and their copolymers. This last group has been widely used in a number of clinical applications, such as resorbable sutures, drug delivery systems, orthopedic fixation devices, and scaffolds for tissue engineering and *in vitro* cell culture (349).

One of the most relevant polymers in scaffolds production is the **poly(ϵ -caprolactone)** (PCL). PCL is a biodegradable and biocompatible polyester widely used for 3D cell culture applications. This plastic exhibits a slow degradation rate and a low melting point of 60°C due to its lower hydrogen bonding and polarity. In fact, a previous study revealed that FFF PCL scaffolds maintained in aqueous medium for 6 months exhibited an insignificant weight loss, maintaining their structure and mechanical properties almost intact (361). PCL can be processed with many technologies and it is soluble in several solvents such as chloroform,

dichloromethane, benzene, acetone, and dimethylformamide (362). PCL does not present any isomers, therefore, melting temperature and biological degradation remain stable. Its use is exponentially increasing in tissue engineering, drug delivery, and cell cultures (176, 336, 362–365). In order to achieve a specific biomechanical behavior, PCL can also be used in combination with other polyesters or even with other molecules including chitosan and gelatin (362, 366). Besides, biological profile of scaffolds can also be modulated by the addition of ECM components which act as biochemical agents, such as collagen (367), proteoglycans (368), hyaluran (369), and tropoelastin (370).

6.4 Breast cancer stem cell population in three-dimensional culture

As explained before, BCSCs account for a low percentage within the tumor (151) or cell line (371). Additionally, traditional 2D *in vitro* cell culture has been proved to induce BCSC differentiation process, which results in the loss of their stem features and their transformation into non-stem cancer cells (372). These two major handicaps make the *in vitro* study of BCSCs very challenging. Therefore, it comes as no surprise that current efforts are focused on the development of a 3D cell culture protocol to maintain the multipotential state of BCSCs.

In this scenario, multiple investigations have revealed that the use of scaffolds as a 3D cell culture tool increases the BCSC subpopulation (176, 364, 373). For instance, in 2012 Saha *et al.* cultured MCF-7 breast carcinoma cells on ES PCL scaffolds with an average fiber diameter of 2 μm . Cells displayed elongated and stellar morphology within 3D surroundings, in contrast with the flat shape found in monolayer cultures. Besides, authors proved that scaffold culture induced EMT in the breast cancer cells, attributing them with stem features including malignancy and invasion (373). One year later, Feng *et al.* also cultured several breast cancer

cell lines in ES PCL filaments which showed an average diameter of 1.6 μm . Interestingly, in this work the mesenchymal-like TNBC cell line MDA-MB-231 was used, among other hormone- and HER2-positive breast cancer cell models. All cell lines exhibited increased stem and EMT markers expression when cultured in PCL scaffolds, alongside a more invasive phenotype. In this case, ALDH1 activity and mammosphere-forming capacity were also determined to be upregulated within 3D surroundings (176). In 2014, more efforts were done in the work published by Sims-Mourtada *et al.* Breast cancer cells were seeded into even smaller hybrid PCL-chitosan nanofibers, with an average diameter of 430 nm. Scaffold culture led to an increase percentage of $\text{CD44}^+/\text{CD24}^{-/\text{low}}$ cells, altogether with improved mammosphere-forming ability and higher resistance to the chemotherapeutic agents docetaxel and doxorubicin. Authors proved that BCSC expansion was due to an inhibition of their differentiation rather than a proliferation increase of the stem-like cell subset (364).

On balance, scaffolds can represent a novel tool to culture and properly study the malignant BCSC subpopulation. Research on scaffold fabrication process and architecture is crucial to develop optimal 3D supports for the proliferation and enrichment of BCSC niche of every cell type.

CHAPTER 2 Hypothesis and Objectives

Hypothesis

Three-dimensional (3D) cell culture has been proven to maintain the stemness features of the sample. Therefore, the manufacture and use of biocompatible scaffolds for triple negative breast cancer (TNBC) cell culture may facilitate the study of the breast cancer stem cell (BCSC) subpopulation. The proper characterization of this malignant niche can enable the development of targeted therapies against cancer stem-like cells, which represent an interesting approach for tumors that only have systemic treatments such as TNBC.

Objectives

The main objective of this thesis was to develop an *in vitro* 3D cell culture protocol to properly expand and characterize the BCSC subpopulation of TNBC cell models. In order to fulfill the main objective, four specific objectives were pursued:

- I. **Use and optimization of fused filament fabrication (FFF) technology to manufacture polycaprolactone (PCL) scaffolds for 3D cell culture and stemness expansion**
 - a. Develop a sequential flowchart of process parameters optimization for open-source 3D printers to manufacture scaffolds
 - b. Test 3D cell culture adequacy of FFF PCL scaffolds with the reference models MCF-7 breast cancer (BC) cells and NIH/3T3 murine fibroblasts
 - c. Determine the optimal scaffold design and culture variables for cell growth using the reference MCF-7 BC model
 - d. Evaluate a possible MCF-7 BCSC enrichment in FFF PCL scaffold culture by the mammosphere forming assay

- II. **Use and optimization of electrospinning (ES) technology to manufacture PCL scaffolds for 3D cell culture and stemness expansion**
 - a. Optimize the ES process parameters in order to manufacture nanofiber PCL scaffolds
 - b. Develop a macroscopic characterization of produced ES PCL scaffolds
 - c. Test 3D cell culture adequacy of ES PCL scaffolds with the reference model MCF-7 BC cells
 - d. Evaluate a possible MCF-7 BCSC enrichment in ES PCL scaffold culture by the mammosphere forming assay

- III. **Evaluation of BCSC and fatty acid synthase (FASN) role in chemosensitive and chemoresistant MDA-MB-231 TNBC cells**
 - a. Determine BCSC features and FASN expression in the parental cell line MDA-MB-231 and its derivatives resistant to doxorubicin (231DXR) and paclitaxel (231PTR)
 - b. Evaluate epithelial-to-mesenchymal (EMT) profile in chemoresistance models
 - c. Study the impact of FASN inhibition in the parental and chemoresistant cell models

- IV. **Enrichment of BCSCs in the TNBC cell models MDA-MB-231 (mesenchymal-like) and MDA-MB-468 (basal-like) within 3D ES PCL scaffold culture**
 - a. Manufacture the previously optimized ES PCL scaffolds and develop a microscopic and mechanical characterization
 - b. Analyze MDA-MB-231 and MDA-MB-468 cell proliferation and morphology within 3D surroundings by MTT and fluorescence microscopy, respectively
 - c. Evaluate a possible BCSC enrichment in ES PCL scaffold culture by several approaches (mammosphere forming assay, ALDEFLUOR assay, chemoresistance, and stemness markers expression)

- d. Study the EMT profile and signaling pathways modulation on 3D-cultured cells
- e. Study FASN expression and inhibition implication in the BCSCs-enriched population of scaffolds-cultured TNBC cells

CHAPTER 3 Results I

Use and optimization of fused filament fabrication technology to manufacture PCL scaffolds for 3D cell culture and stemness expansion

This chapter is based on the following publications:

Title Design of a scaffold parameter selection system with additive manufacturing for a biomedical cell culture

Authors Marc Rabionet, Emma Polonio-Alcalá, Antonio J. Guerra, Jessica Martin, Teresa Puig*, Joaquim Ciurana*

Journal Materials

Publication year 2018

Impact Factor ²⁰¹⁸ 2.972 (Q2 in Materials Science, Multidisciplinary; position 102 of 293)

DOI 10.3390/ma11081427

Title Optimization of poly(ϵ -caprolactone) scaffolds suitable for 3D cancer cell culture (Proceeding)

Authors Ariadna Giró-Perafita, Marc Rabionet, Teresa Puig*, Joaquim Ciurana*

Journal Procedia CIRP

Publication year 2016

CiteScore ²⁰¹⁶ 1.8 (65th percentile in Industrial and Manufacturing Engineering; position 106 of 304)

DOI 10.1016/j.procir.2015.07.031

Title Breast cancer stem cell culture and enrichment using poly(ϵ -caprolactone) scaffolds

Authors Sònia Palomeras[†], Marc Rabionet[†], Inés Ferrer, Ariadna Sarrats, Maria Luisa Garcia-Romeu, Teresa Puig*, Joaquim Ciurana*

Journal Molecules

Publication year 2016

Impact Factor ²⁰¹⁶ 2.861 (Q2 in Chemistry, Organic; position 17 of 59)

DOI 10.3390/molecules21040537

_ Paper to be considered for compendium of publications format

* Corresponding author

[†] These authors contributed equally to this manuscript

Abstract

In most cases, the use of fused filament fabrication (FFF; also known as fused deposition modeling or FDM) machines for biomedical purposes needs an optimization step to properly select both manufacturing process parameters and scaffold design features.

Chapter 3 aims to explore the feasibility of a FFF open-source low-cost 3D printer to produce poly(ϵ -caprolactone) (PCL) scaffolds for 3D cell culture applications and stemness maintenance. In order to achieve a correct scaffold printing, several fabrication and design parameters were tested, such as extruder and bed temperature, deposition velocity, layer height, filament diameter, distance between filaments, and deposition angle. Then, the suitability of produced scaffolds for 3D cell growth was evaluated with the reference models MCF-7 breast cancer (BC) cells and NIH/3T3 murine fibroblasts, widely used in the related literature. Cell proliferation within distinct scaffold designs was evaluated by the trypan blue exclusion assay. Afterwards, the impact of FFF scaffold culture was further analyzed on the MCF-7 cells. The effect of different cell culture variables was tested, such as microplate adherence features and a previous medium addition to the scaffold. Lastly, MCF-7 BCSC niche was quantified in monolayer and in 3D culture through the mammospheres forming assay.



As a result, a novel sequential flowchart was developed as a scaffold parameter selection system for 3D printers. Temperature values of 85°C and 35°C were found to be optimal for the 3D printer extruder and bed, respectively. PCL scaffolds were manufactured with a filament diameter of 0.3 mm and a distance between filaments of 0.7 mm, which allowed a correct printing process. Three different scaffold designs were produced, displaying a different deposition angle between layers: 90°, 45°, and 60°. Results showed that a higher cell proliferation value was obtained in the 60° scaffolds when using MCF-7 cells, and 90° version in the case

Chapter 3

of NIH/3T3 model. Finally, MCF-7 cells were proven to show a higher cell growth kinetics when using non-adherent microplates, regardless of a prior medium addition. Interestingly, MCF-7 cells cultured on FFF PCL 60° scaffolds exhibited a greater mammosphere forming capacity than monolayer cells, indicating a possible BCSC enrichment.

Article

Design of a Scaffold Parameter Selection System with Additive Manufacturing for a Biomedical Cell Culture

Marc Rabionet ^{1,2}, Emma Polonio ^{1,2}, Antonio J. Guerra ² , Jessica Martin ¹, Teresa Puig ^{1,*} and Joaquim Ciurana ^{2,*} 

¹ Oncology Unit (TargetsLab), Department of Medical Sciences, Faculty of Medicine, University of Girona, Emili Grahit 77, 17003 Girona, Spain; m.rabionet@udg.edu (M.R.); emma.polonio@udg.edu (E.P.); jessica.martin@udg.edu (J.M.)

² Department of Mechanical Engineering and Industrial Construction, University of Girona, Maria Aurèlia Capmany 61, 17003 Girona, Spain; antonio.guerra@udg.edu

* Correspondence: teresa.puig@udg.edu (T.P.); quim.ciurana@udg.edu (J.C.)

Received: 10 July 2018; Accepted: 10 August 2018; Published: 14 August 2018



Abstract: Open-source 3D printers mean objects can be quickly and efficiently produced. However, design and fabrication parameters need to be optimized to set up the correct printing procedure; a procedure in which the characteristics of the printing materials selected for use can also influence the process. This work focuses on optimizing the printing process of the open-source 3D extruder machine RepRap, which is used to manufacture poly(ϵ -caprolactone) (PCL) scaffolds for cell culture applications. PCL is a biocompatible polymer that is free of toxic dye and has been used to fabricate scaffolds, i.e., solid structures suitable for 3D cancer cell cultures. Scaffold cell culture has been described as enhancing cancer stem cell (CSC) populations related to tumor chemoresistance and/or their recurrence after chemotherapy. A RepRap BCN3D+ printer and 3 mm PCL wire were used to fabricate circular scaffolds. Design and fabrication parameters were first determined with SolidWorks and Slic3r software and subsequently optimized following a novel sequential flowchart. In the flowchart described here, the parameters were gradually optimized step by step, by taking several measurable variables of the resulting scaffolds into consideration to guarantee high-quality printing. Three deposition angles (45°, 60° and 90°) were fabricated and tested. MCF-7 breast carcinoma cells and NIH/3T3 murine fibroblasts were used to assess scaffold adequacy for 3D cell cultures. The 60° scaffolds were found to be suitable for the purpose. Therefore, PCL scaffolds fabricated via the flowchart optimization with a RepRap 3D printer could be used for 3D cell cultures and may boost CSCs to study new therapeutic treatments for this malignant population. Moreover, the flowchart defined here could represent a standard procedure for non-engineers (i.e., mainly physicians) when manufacturing new culture systems is required.

Keywords: scaffold; PCL; RepRap; fused filament fabrication; three-dimensional; cell culture

1. Introduction

Scaffolds are solid structures usually made of a polymeric material that is used for a wide range of applications. They provide a necessary support for three-dimensional (3D) cell growth, thanks to their biocompatibility and biodegradability [1], and are extremely useful in *in vitro* 3D cell cultures. Traditional cell culture is applied to two-dimensional (2D) models on flat surfaces, but this methodology is not representative of the cells' physiological environment and usually confers them with less malignancy. The literature has reported that 3D cell culture with scaffolds can increase the cancer stem cell (CSC) population [2–4]. CSCs correspond to a small population within the tumor which is resistant to chemotherapy and capable of dividing to form the tumor again after treatment

(this is known as recurrence or metastasis) [5,6]. Since this malignant subpopulation represents a small percentage within the tumor, the population expansion and enrichment described would help in their study and promote further development of therapeutic strategies.

Additive manufacturing (AM) technologies have arisen as a novel set of tools with which to fabricate scaffolds [5,7]. In particular, 3D printers based on fused filament fabrication (FFF) technology are one of the most accessible and simplest options [8]. They are open-source, low-cost machines which usually use thermoplastic materials [9,10] and can easily be modified to improve the quality of the printed 3D products [11]. A variety of biocompatible polymers can be used for scaffold production with FFF. Poly-L-lactic acid (PLA) is a biodegradable thermoplastic aliphatic polyester that has great potential in clinics thanks to its biocompatibility and restorability. Consequently, it is widely used in tissue engineering [12]. Poly(ϵ -caprolactone) (PCL; Figure 1) is also a biodegradable polyester proven to be biocompatible and toxic-dye-free, but it has a slower degradation rate and different mechanical and physical features. For instance, PCL has a lower melting point (60 °C), reflecting its lower hydrogen bonding and polarity which determine its chemical and molecular behavior. Moreover, PCL does not have any isomers so there are no variances in the melting temperature and biological degradation. Due to these characteristics, its use in tissue engineering, drug delivery, and cell cultures is increasing [2,3,6,13,14]. PCL can be also used as copolymers, such as PCL-collagen and PCL-gelatin, and in combination with other polymers, for example PLA or PEG [13,15].

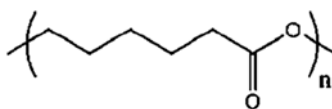


Figure 1. Poly(ϵ -caprolactone) chemical structure.

As scaffold production with 3D printers is a new area, greater effort should be made to determine the optimal parameters for the process [1,6,9]. The processing parameters in question are closely related to the properties of the polymer chosen and the subsequent application intended for the scaffold(s). First, the design parameters determine the architecture of the scaffold and can comprise the filament diameter, the distance between filaments, and the deposition angle [16]. They can also be modified depending on the desired design and application of the scaffold. Second, fabrication parameters control the printing process. These parameters include the extruder and bed temperature, deposition velocity, and layer height, and are closely linked to the material of the polymer and the environment [9,17].

When scaffolds are produced for tissue engineering or regenerative medicine, controlling features, such as pore size, pore shape, or mechanical strength, is mandatory [9,18]. Although there are some studies into the 3D printing of scaffolds based on fused deposition modeling (FDM) [19,20] very few analyze the effects the architecture of the scaffold may have on cell proliferation, and none develop schematic procedures or methods aimed at retaining any knowledge gained. Grémare et al., [21] studied the physicochemical and biological properties of PLA scaffolds produced by 3D printing (FFF). The authors studied four different square pore sizes (0, 150, 200, and 250 μ m). Results showed that scaffold pore size had negligible effects on their mechanical properties. After three and seven days of human bone marrow stromal cell (HBMSC) culture being applied, the scaffolds exhibited excellent viability and homogeneous distribution regardless of the pore size. Hutmancher et al. [22] studied the mechanical and cell culture response of PCL scaffolds using $61 \pm 1\%$ porosity and two matrix architectures. Results showed that five-angle scaffolds had significantly lower stiffness under compression loading than those with a three-angle pattern. Data also revealed that in terms of cell proliferation, while a scaffold with a 0/60/120° lay-down pattern had a higher proliferation rate in the first 2 weeks, the scaffolds with a 0/72/144/36/108° lay-down overtook the three-angle matrix architecture in Weeks 3 and 4. Recently, Rabionet et al. [23] analyzed the effects of tubular scaffold

architecture on cell proliferation for vascular applications. Results showed the strong influence the 3D process parameters have on the scaffold architecture and, subsequently, cell proliferation. Narrow pores produced lower cell proliferation due to the lower oxygen and nutrient exchange.

As the literature has reported, cell proliferation onto a scaffold depends on the material, the architecture, and cell kinetics. Whenever physicians need to work with cells, they require the best scaffolding features to obtain ideal cell culture results. In fact, the main problem was that scaffolds did not provide the same results for different lines of cells when the cells are cultured. When working with cells, physicians have different purposes and goals. For instance, they may want to enrich or treat the cells or to determine the impact a drug is having/has had on the cells. While identical scaffold features do not provide the same results, the cell line does. In fact, each cell line works better with different scaffold features. For this reason, this work aims to optimize the design features and the selection of the manufacturing process parameters when the open-source 3D extruder machine RepRap is utilized. This methodology focuses on manufacturing PCL scaffolds suitable for 3D cancer cell cultures and CSCs expansion as a first step before expanding to other cell lines. Both design and fabrication parameters have been optimized by following a specific flowchart step by step, and checking a measurable variable. In addition, preliminary in vitro experiments were performed to study the impact the scaffold design and fabrication have on the efficiency physicians require from the 3D cell culture and the scaffolds produced. Therefore, a sample application for the mass production of PCL scaffolds using a low-cost machine could be used to improve cancer stem cell research. The flowchart developed here provides a novel methodology to adjust process parameters to print micrometric scaffolds suitable for three-dimensional cell culture because, as is demonstrated, each cell line required different scaffold features. Hence, an optimization diagram could represent a common procedure which could be used by non-engineering professionals when a 3D cell culture protocol has to be established de novo. Physicians working with 3D cell cultures usually need some kind of rules or guidelines to follow to set up the cell culture. This paper's contribution is the methodology required to set up the 3D printing technology for a new line of cell culture by first defining the design characteristics and then the parameter selection for the manufacturing process. This paper does not contribute to the knowledge about PCLs or the 3D printing machine itself, but instead provides a methodology for physicians. The contribution is the method and steps to follow when scaffolds need to be manufactured for a new cell line.

2. Experimental Setup

2.1. Material

A 3 mm poly(ϵ -caprolactone) (PCL) wire (Perstorp, Malmö, Sweden) with a density of 1145 Kg/m³ and a molecular weight of 80,000 g/mol, was used to fabricate circular scaffolds 19 mm in diameter (Corning Life Sciences, New York, NY, USA). PCL is a biodegradable polyester with a low melting point (60 °C) and a glass transition of about -60 °C.

2.2. Three-Dimensional Printer Machine

An open-source and modular RepRap BCN 3D+ printer (CIM, Barcelona, Spain) was used to produce three-dimensional scaffolds (Figure 2). This printer was selected because of its capacity to allow a user to optimize its parameters as they see fit. It uses fused filament fabrication (FFF). First, the filament was unwound from a roll of wire and supplied to the extruder. Then, the material was extruded through the nozzle using different temperatures depending on the value being tested. Finally, the printed filament was deposited onto a heated platform (also known as a bed).

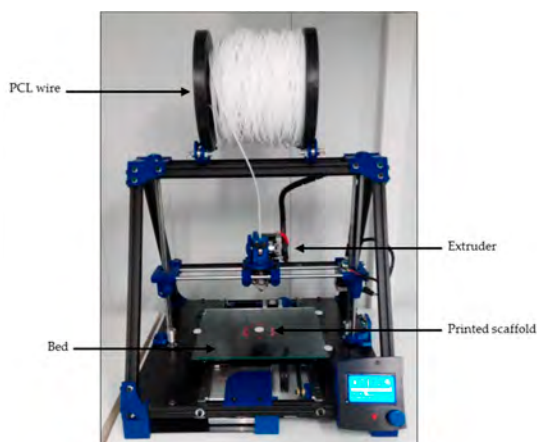


Figure 2. RepRap BCN 3D+ printer with a 3 mm PCL wire.

2.3. Scaffold Design and Additive Manufacturing

SolidWorks (Waltham, Massachusetts, Estatics Units) was the computer-aided design (CAD) software chosen for the scaffolds' design. The stereolithography (STL) file formats the designs that were transferred to the computer-aided manufacturing (CAM) software Slic3r to establish the fabrication parameters. This software, while maintaining the SolidWorks design, generated G-code files which can control and regulate the machine to obtain the correctly-printed scaffolds. Scaffold design features were selected based on other research work focused on tissue engineering which had similar goals to this work, i.e., cell enrichment or treatment, or drug delivery applicability. The features are described in Table 1. Previous screening experiments were carried out to adjust the range of the scaffold design features.

Table 1. Process parameters used for PCL scaffold printing.

	Parameters	Tested Values	Measurable Variable
Fabrication parameters	Extruder temperature	65, 70, 75, 80, 85, and 90 °C	Printed filament diameter
	Bed temperature	25, 30, 33, 35, and 37 °C	1-Material adhesion (Y/N)
	Deposition velocity	10, 20, and 30 mm/s	2-First layer height
	Layer height	0.28 and 0.3 mm	Printed filament diameter Printing quality (absence of blobs)
Design parameters	Filament diameter	0.175, 0.3, and 0.5 mm	1-Adhesion of contiguous filaments (Y/N)
	Distance between filaments	0.5, 0.7, and 1 mm	2-Printed filament diameter
	Deposition angle	90°, 45°, and 60°	1-Real distance between filaments 2-Smallest pore option Pore angles

2.4. Process Parameter Optimization

The fabrication parameters and design feature values used for the experimental setup are shown in Table 1. A wide range of characteristics and parameter values were selected from the literature as the screening values with which to start. A wide range of processing parameters were selected based on the research work focused on tissue engineering with similar goals to ours, i.e., the enrichment or treatment of cells of the applicability for drug delivery. Thus, previous screening experiments

were carried out to adjust the range of the processing parameters for the scaffolds. By following a sequential flowchart (Figure 3), the optimal tested value to be selected for each parameter was determined. Optimization was first performed using a generic geometrical form. A fixed circular scaffold design was used as the control pattern: 0.4 mm in diameter and layer height extruded filament, 1 mm distance between filaments, 90° deposition angle, 19 mm in diameter scaffold, and eight scaffold layers. As optimization progressed, design feature values were replaced by the optimal ones, resulting in a final scaffold design suitable for three-dimensional cancer cell culture. Furthermore, the cancer cell culture is now more like real physiological conditions, including an enrichment of the CSCs' subpopulation. Each step on the flowchart presented in Figure 3 included parameter testing and a physical scaffold variable measurement to assess the quality of the printing. Thus, optimal parameter values were sequentially determined and considering the final application as the optimal function to be reached. Physical variables, such as printed filament diameter, first layer height, and real distance between filaments, were measured using an inverted optical microscope (Nikon, Tokyo, Japan). Printed structures, as well as a nanometric ruler, were placed on the stage. Binomial variables (material adhesion, adhesion of contiguous filaments, printing quality such as the absence of blobs etc.) were assessed by sight. Finally, the cell efficiency of the different deposition angles was evaluated through a three-dimensional breast cancer cell culture to validate the parameters selected. Breast CSCs were used because their expansion would represent a new opportunity to develop new treatments against cancer stem features related to cancer relapse and metastasis.

2.5. Cell Line

MCF-7 breast carcinoma cells (ATCC® HTB-22™) and NIH/3T3 murine fibroblasts cell lines (ATCC® CRL-1658™) were obtained from the American Type Culture Collection (ATCC, Rockville, MD, USA). MCF-7 and NIH/3T3 cells were cultured in DMEM (Dulbecco's Modified Eagle's Medium) (Gibco, Waltham, MA, USA) supplemented with 10% fetal bovine serum, 1% L-glutamine (which means 2 mM L-glutamine), 1% sodium pyruvate (which means 1 mM sodium pyruvate), 50 U/mL penicillin and 50 µg/mL streptomycin (HyClone, Logan, UT, USA). Cells were maintained at 37 °C and in a 5% CO₂ atmosphere.

2.6. Scaffold Sterilization

Scaffolds were sterilized following a previously-described methodology [2,24]. Meshes were submerged in a 70% ethanol/water solution overnight, washed with PBS (Gibco, Waltham, MA, USA), and finally exposed to UV light for 30 min. Only the top side was irradiated because PCL has a semi-transparent behavior when exposed to UV wavelengths [25]. This sterilization method was followed to avoid any changes in the stents' final properties [18].

2.7. Three-Dimensional Cell Culture in Scaffolds

Scaffolds were designed by considering their subsequent use in regular 12-well cell culture microplates. First, cells were detached from the original cell culture microplate and counted using the trypan blue dye method. As viable cells possess an intact membrane, trypan blue cannot penetrate them, but as dead cells have an altered membrane the dye can penetrate them. Therefore, trypan blue was added in a cell sample and cell viability was counted using a Neubauer Chamber (Marienfeld-Superior, Lauda-Königshofen, Germany) and an inverted optical microscope. A total of 100,000 cells (MCF-7) or 40,000 (NIH/3T3) in 250 µL cell suspension were placed onto the center of the scaffolds' surface to allow cell attachment. After 3 h of incubation, 1.5 mL of fresh medium was added to cover the scaffold and the cells were incubated for 72 h. Then, the scaffold was placed in a new well to quantify only the cells attached. It was washed with PBS and 1 mL of trypsin was added. After incubation, 2.5 mL of fresh medium was added, and the cell suspension was collected and centrifuged at 1500 rpm for 5 min. Finally, the supernatant was discarded, and the cells were re-suspended and counted.

2.8. Statistical Analysis

Results were collected from at least six independent experiments. All data are expressed as mean \pm standard error (SE). Data were analyzed by Student's *t* test.

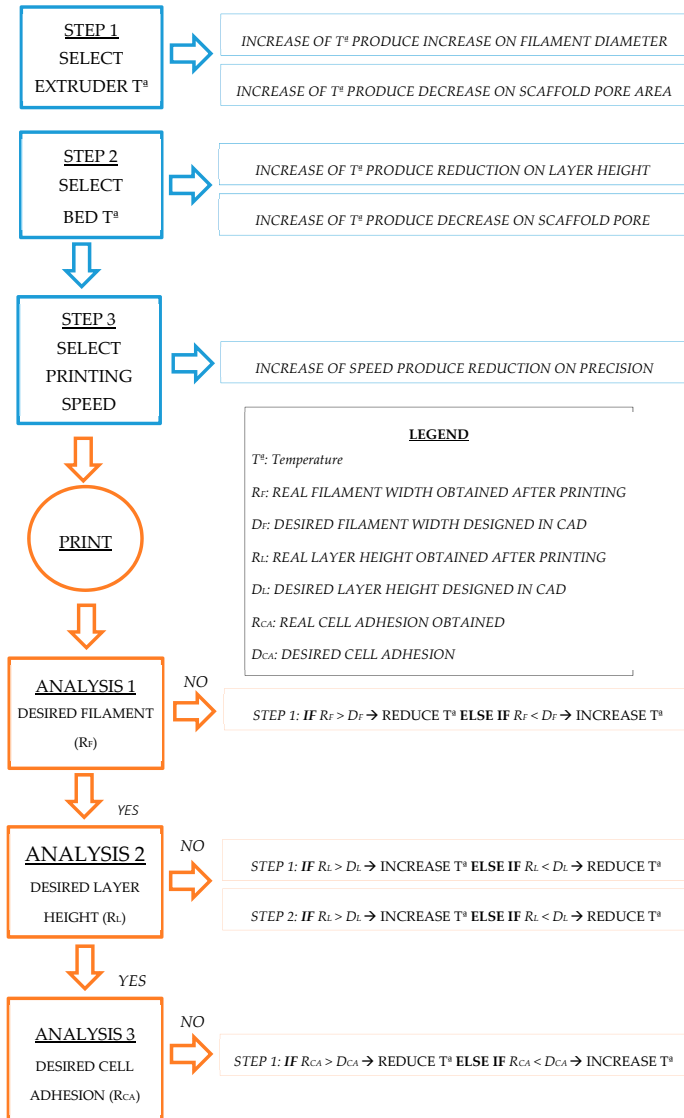


Figure 3. Flowchart of process parameter optimization. Every parameter consists of the values tested and, on the right, the corresponding measurable variable for new cell cultures. Fabrication parameters are in the left column and design parameters in the right.

3. Results: Scaffolds Production

Following the method developed, experimental work was first carried out to find the best way to produce scaffolds which can sustain cell cultures. Sequential work was done to set scaffold design features and manufacturing process parameters.

3.1. Optimization of Process Parameters

Processing parameters were optimized to achieve high quality scaffold printing for cell culture application. Thus, different physical scaffold variables were measured to ensure the correct fit between the computer design and the printed scaffold. The processing parameters included both fabrication and design parameters as shown in the “Experimental Setup” section (Table 1). Processing parameters were chosen according to the literature and the state-of-art [9,11,16,17]. However, the process optimization methodology explained here, based on a sequential flowchart (Figure 3), is both innovative and unique.

Experiments were initially carried out with a generic scaffold design (see Section 2.4 “Methods”) to set the fabrication parameters and then adjusted to the design parameters required to produce the scaffolds.

Fabrication parameters (extruder and bed temperature, deposition velocity, and layer height) were introduced with Slic3r software. These parameters are related to the characteristics of the polymeric material (mainly PCL) and the printing process. However, different values were tested for the parameters (by checking the measurable variable mentioned in Table 1) in order to meet scaffold manufacturing requirements.

Once the polymeric material and its fabrication parameters had been characterized and set, design features were subsequently established using the SolidWorks 3D software. Parameters, such as filament diameter, distance between filaments, and deposition angle, were tested. These are related to the three-dimensional design of the scaffold and the effect they have on the cancer cell culture.

First, to determine the optimal fabrication parameters, a fixed scaffold design was established as a control pattern: 90° deposition angle, 0.4 mm in diameter filament and 1 mm distance between filaments. This enabled us to do printings with the same design, but different fabrication parameters, to find the optimal ones. Later, as the design parameters were optimized, they were replaced.

Following the flowchart defined in Figure 3, all the parameters were characterized and selected sequentially to obtain the appropriate setup for producing 3D-printed scaffolds. The optimization of each process parameter is described in the following sections.

3.2. Extruder Temperature

Poly(ϵ -caprolactone) was chosen as the polymer to work with because of its compatibility with cell cultures. PCL has a low melting point (60 °C). To achieve enough malleability and considering there is some heat dissipation, higher temperatures were also tested to find the optimal value (Table 1). A fixed scaffold design described in the Methods section was printed. Then, *the printed filament diameter* was measured as a physical variable. Low extruder temperatures (65–80 °C) could not melt the material enough, thus the amount of the extruded material was low. As a consequence, the printed filament diameter was smaller than the one designed (0.4 mm). High temperatures (90 °C) melt the polymer excessively and also increase the diameter of the filament due to flattening and some blobs being produced. Therefore, the optimal extruder temperature was established at 85 °C. The printed filament diameter was 0.39 ± 0.05 mm.

3.3. Bed Temperature

To set the optimal bed temperature, a generic geometrical scaffold design was printed, and two different measurable variables were evaluated. Material adhesion was assessed as a binomial variable (yes/no), firstly testing the lowest temperature (25 °C, Table 1). If the printed material had not adhered enough to the surface (no), another printing was performed, this time with a higher bed

temperature. Once the material had adhered to the surface (yes), the first layer height was then measured. Bed temperatures ranging from 25 to 33 °C gave a non-adherent first layer scaffold. In addition, much higher temperatures (37 °C) melt the material excessively, flattening the filament and decreasing the height of the first layer (lower than the 0.4 mm designed one). A 35 °C bed temperature was considered optimal as this allowed first layer adhesion and the filaments were not flattened. Their first layer height was 0.37 ± 0.07 mm.

3.4. Deposition Velocity

The goal with this parameter was to find a high deposition velocity without forgetting the quality of the printed scaffold. The printed filament diameter was chosen as the tangible variable with which to analyze the impact this parameter has on the scaffold. The optimal deposition velocity was established as being 10 mm/s. The filament diameter was 0.42 ± 0.05 mm. When the speed was faster (20 and 30 mm/s) the material did not have enough time to deposit itself on the surface, resulting in smaller filament diameter or sometimes even discontinuous filament production.

3.5. Filament Diameter

At this point, the diameter of the printed filament deposited on the collector was analyzed. Extrusion and deposition velocity can exert a direct influence on fiber morphology. Therefore, once the manufacturing velocity had been fixed, the diameter of the extruded filament was evaluated next. Three different design filament diameters were tested: 0.175, 0.3, and 0.5 mm. To ensure the filaments remained tangent along the vertical axis, the printer's layer height was adjusted to each design filament diameter. Diameters that were too large caused the adhesion of two contiguous filaments, favored by their proximity and elevated temperature. For this reason, the first variable studied was the possible adhesion of contiguous filaments, such as a binomial variable (yes/no). Thus, only the values that did not cause the adhesion of two filaments in the same layer were selected to continue the analysis (0.175 and 0.3 mm). The second measured variable was the printed filament diameter. A design diameter of 0.175 mm caused erratic printing because the amount of material was too low to form a linear filament. The final value tested, 0.3 mm, was found to be optimal as it gave a printed filament diameter of 0.31 ± 0.02 mm. The established filament diameter value also determined the thickness of each layer. The scaffolds were manufactured with eight layers, so the final thickness of the scaffolds was 2.4 mm.

3.6. Layer Height

Layer height is defined as the distance between two connected layers along the Z axis. Since all layers are designed and printed on top of each other, this parameter was determined by the printed filament diameter. For this reason, the filament diameter, although being a design parameter, was established before finishing, optimizing the fabrication parameters (Figure 3). In some cases, the deposited material tends to flatten out and so the printed height is lower. At that point, two different values were analyzed: 0.3 mm (the whole filament diameter) and 0.28 mm (because of a certain flattening) and the quality of the printing recorded (absence of blobs). In this case, 0.3 mm was found to be the optimal layer height for our design as flattening, due to high temperatures, did not occur. When evaluating smaller established heights, the printing process produced blobs.

The absence of filament flattening may be attributed to the relatively low extruder temperature used, (85 °C, see Section 2.1) which can be considered low compared with other biocompatible polymers used in 3D printing, such as PLA [9,12].

3.7. Distance between Filaments

This is a key parameter because it affects the pore size of the scaffold [9]. This design parameter consists of the shortest distance between the axis of two filaments located within the same layer. We were interested in achieving small pore sizes, thus, we focused on the testing small distances (0.5,

0.7, 1 mm). Nevertheless, small distances between filaments may be problematic if two contiguous filaments join. For this reason, the real distance between filaments was measured to take into account whether this value matched that of the one expected (designed).

Distances of 0.7 and 1 mm gave no filament joining, so real distances were higher than 0. Within these values, the smallest value was chosen (0.7 mm). Taking into account this parameter and the optimal filament diameter previously established, the distance between the outer parts of two contiguous filaments was, consequently, 0.4 mm (Figure 4).

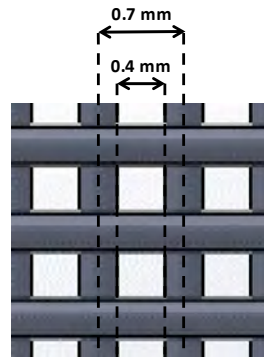


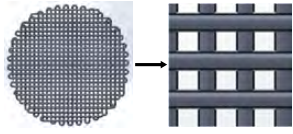
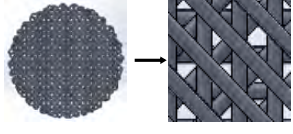
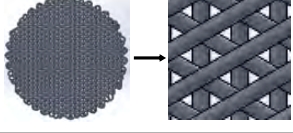
Figure 4. Distances between two contiguous filaments. Axis (0.7 mm) and outer distance (0.4 mm) are represented. Filament diameter was fixed at 0.3 mm.

3.8. Deposition Angle

Once all previous parameters were optimized, three different scaffolds with different deposition angles were designed and manufactured, thus obtaining different pore characteristics, which may influence cell attachment and growth (Table 2). As high-quality printings for all three designs were achieved, it was agreed to test the adequacy for 3D cell culture with all three designs.

An MCF-7 breast carcinoma cell line was used to preliminarily evaluate scaffold ability in terms of three-dimensional cell culture. MCF-7 cells were seeded onto scaffolds and cultivated for 72 h. Then, attached cells were trypsinized and counted. No cells were counted on the 90° scaffolds. Under an optical microscope, no cells were observed on the filament, but rather attached at the bottom of the microplate well (Figure 5a), which is in agreement with cell counting. Scaffolds of 45° showed a subtle cell adhesion of $3.52 \pm 1.16\%$ when compared with the 2D control. We subsequently tested 60° scaffolds, which showed an increased cell adhesion of $26.50 \pm 10.98\%$. In both cases, cells were previously observed at the well bottom and attached to the scaffold filaments, with the last ones indicated by white arrows (Figure 5b,c, respectively).

Table 2. Scaffold designs with different deposition angles: 90°, 45°, and 60°.

Deposition Angles	Pore Shape	Area	Plan View
90°	Square	0.16 mm ²	
45°	Six variable forms (triangles and irregular polygons)	1.98 × 10 ⁻⁴ to 0.13 mm ²	
60°	Equilateral triangle	0.1256 mm ²	

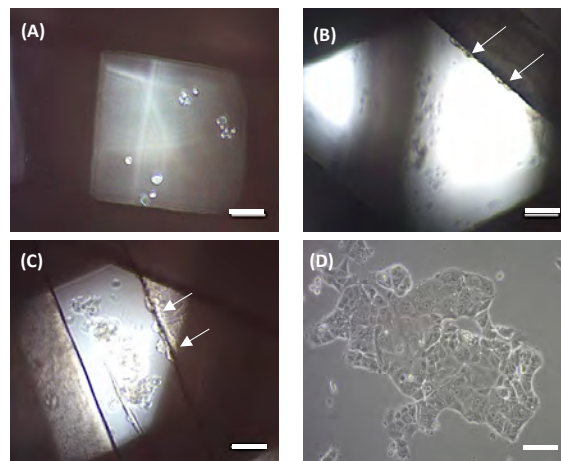


Figure 5. Optical microscope images of MCF-7 cells seeded on the scaffolds. In 90° scaffolds, cells were attached at the bottom of the well (A). In 45° and 60° scaffolds, cells were attached both on the scaffold and at the well (B,C, respectively). (D) MCF-7 cells in 2D culture. White arrows on the images indicate cells adhered to PCL filaments. Scale bars represent 100 μ m.

Then, scaffolds were also evaluated through fibroblast cell cultures. Murine NIH/3T3 fibroblasts were seeded onto the three designs during 72 h and cell proliferation was assessed. In this case, fibroblasts adhered to all three scaffold models (Figure 6), with the highest cell proliferation value being found on the 90° design ($56.30 \pm 5.03\%$ compared to the 2D control). The other two architectures exhibited slightly smaller values. For instance, 60° scaffolds presented a $49.52 \pm 5.62\%$ cell growth and 45° models, $39.11 \pm 8.12\%$, compared to the monolayer culture.

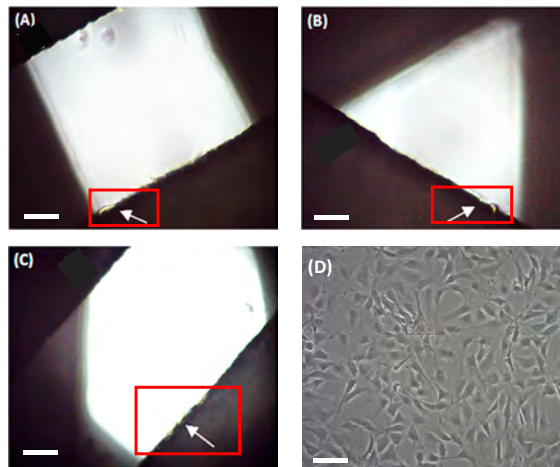


Figure 6. Optical microscope images of NIH/3T3 cells seeded on the scaffolds. Cells were attached on scaffolds of 90° (A), 60° (B), and 45° (C). (D) NIH/3T3 cells in a 2D culture. White arrows on the images indicate cells adhered to PCL filaments. Scale bars represent 100 μm .

3.9. Optimal Process Parameters Values

After the optimization experiments and basic cell culture tests had been completed, the optimal processing parameters for PCL scaffold printing were established (see Table 3) once the methodology had been applied to set each optimal parameter for cell cultures and for future experiments with CSCs culture enrichment using PCL scaffolds.

Table 3. Optimal processing parameter values to be used for PCL scaffold printing.

Title	Parameters	Optimal Values
Manufacturing parameters	Extruder temperature	85 °C
	Bed temperature	35 °C
	Deposition velocity	10 mm/s
	Layer height	0.3 mm
Design parameters	Filament diameter	0.3 mm
	Distance between filaments	0.7 mm
	Deposition angle	60° (MCF-7 breast cancer cells) 90° (NIH/3T3 murine fibroblasts)

4. Discussion

In this work, a methodology to optimize the processing parameters for PCL scaffold production using a RepRap 3D printer has been developed. By using an optimization flowchart, PCL scaffolds suitable for cell culture were manufactured (Figure 3). The optimal processing parameters determined are closely related to those defined in other studies using the same technology and material. Domingos et al., (2013) set up an 80 °C printing temperature, 10 mm/s velocity, an approximately 0.3 mm filament diameter and a layer height of 0.28 mm [15]. A previous study by the same research group used an extrusion temperature of 70 °C and a speed of 8 mm/s [1]. These small variations support the idea of using a single, common methodology (Figure 3) to optimize the processing parameters. Compared with previous work in the literature, the flowchart provided here makes it

easier to adjust scaffold design features and processing parameters according to cell line characteristics. Several case studies were run to validate the flowchart depicted in Figure 3. Results show how cell culture is improved by using scaffolds which allow cell cultures to be created in 3D conditions and optimized based on the cells' features. In addition, process parameters were also evaluated using cell culture experiments. All scaffold culture experiments presented sterility resulting from the sterilization procedure described here. Both 60° and 45° scaffolds showed adequate design parameters for the MCF-7 cell cultures. In particular, the 60° scaffold design displayed the highest percentage of cell attachment, and exhibited good biocompatibility for the MCF-7 breast cancer cells. In contrast, the NIH/3T3 fibroblast cells presented a more homogeneous growth along the three scaffold designs. However, the 90° scaffold showed the highest cell proliferation value. Therefore, different kinds of cells may prefer different scaffold architectures, further demonstrating the need of a common procedure to find the optimal values. Moreover, a tumor and a non-tumor cell line were tested, showing the flexibility of the flowchart described here.

Three-dimensional cell culture on scaffolds may also be improved by other fabrication-independent parameters such as polarity of cell culture plates, culture media and time [26], as well as different cell culture types, including a dynamic model [27]. This optimization will be the focus of further studies as we attempt to improve cell attachment percentages. Furthermore, CSC population enrichment by cell culture on scaffolds will be evaluated using different approaches.

To date, most of the work related to scaffold production focuses on optimizing design features and forgets about improving fabrication parameters [1,9,16]. In this work, a flowchart to optimize the parameters of the whole process has been proposed (Figure 3) to help with their selection. In addition, this methodology may be further used to set up scaffold manufacturing (both the design features and the fabrication parameters) when using a RepRap 3D printer or any other AM technologies and/or materials.

5. Conclusions

In this work, the design features and fabrication parameters of scaffolds and the RepRap 3D printer were optimized to produce PCL scaffolds suitable for three-dimensional cell cultures. The optimization was performed following a detailed and unidirectional flowchart, thus providing some procedural guidelines with great potential for other popular manufacturing technologies and materials. The contribution of this paper is for scaffolds made with PCL materials. However, this experiment was only carried out to validate the methodology developed as a valuable method for future cell cultures. Often, physicians work with 2D cell cultures, but, as seen here, 3D cell cultures appear to be good method of improving cell culture enrichment. Furthermore, as the design features and manufacturing parameters need to be set for the different cell lines used each time, this methodology will help physicians and other operators to do just that.

Moreover, the scaffolds produced were proven to allow cell attachment and cell growth. The 60° scaffold design mainly worked for the MCF-7 cells and the 90° for the NIH/3T3 fibroblasts. Three-dimensional cell cultures with PCL scaffolds fabricated with a 3D printer offer both researchers and clinics a set of novel applications for the future. The flowchart developed represents a new tool with which to quickly manufacture scaffolds for a wide range of applications, including cell cultures and tissue engineering. For instance, the use of 3D cell cultures can boost CSC populations to study new therapeutic treatment.

Author Contributions: Conceptualization, J.C. and T.P.; Methodology, J.C.; Validation, A.J.G. and M.R.; Formal Analysis, M.R., J.M. and E.P.; Writing-Original Draft Preparation, J.C.; Writing-Review & Editing, M.R., E.P. and A.J.G.; Supervision, T.P. and J.C.

Funding: This research was funded by Spanish Grants: Fundación Ramón Areces, Instituto de Salud Carlos III (PI1400329) and Ministerio de Economía y Competitividad (DPI2016-77156-R), and through the support of the Catalan Government (2014SGR00868) and the University of Girona (MPCUdG2016/036).

Conflicts of Interest: The authors declare no conflicts of interest. The sponsors had no role in the design of the study, in the collection, analyses, or interpretation of data, in the writing of the manuscript, or in the decision to publish the results.

References

- Domingos, M.; Dinucci, D.; Cometa, S.; Alderighi, M.; Bártolo, P.J.; Chiellini, F. Polycaprolactone Scaffolds Fabricated via Bioextrusion for Tissue Engineering Applications. *Int. J. Biomater.* **2009**, *2009*, 23964. [[CrossRef](#)] [[PubMed](#)]
- Feng, S.; Duan, X.; Lo, P.-K.; Liu, S.; Liu, X.; Chen, H.; Wang, Q. Expansion of breast cancer stem cells with fibrous scaffolds. *Integr. Biol.* **2013**, *5*, 768–777. [[CrossRef](#)] [[PubMed](#)]
- Sims-Mourtada, J.; Niamat, R.A.; Samuel, S.; Eskridge, C.; Kmiec, E.B. Enrichment of breast cancer stem-like cells by growth on electrospun polycaprolactone-chitosan nanofiber scaffolds. *Int. J. Nanomed.* **2014**, *9*, 995–1003. [[CrossRef](#)] [[PubMed](#)]
- Saha, S.; Duan, X.; Wu, L.; Lo, P.-K.; Chen, H.; Wang, Q. Electrospun fibrous scaffolds promote breast cancer cell alignment and epithelial-mesenchymal transition. *Langmuir* **2012**, *28*, 2028–2034. [[CrossRef](#)] [[PubMed](#)]
- Khalil, S.; Sun, W. Bioprinting endothelial cells with alginate for 3D tissue constructs. *J. Biomech. Eng.* **2009**, *131*, 111002. [[CrossRef](#)] [[PubMed](#)]
- Gu, G.X.; Su, L.; Sharma, S.; Voros, J.L.; Qin, Z.; Buehler, M.J. Three-Dimensional-Printing of Bio-Inspired Composites. *J. Biomech. Eng.* **2016**, *138*, 021006. [[CrossRef](#)] [[PubMed](#)]
- Giró-Perafita, A.; Rabionet, M.; Puig, T.; Ciurana, J. Optimization of Poli(ϵ -caprolactone) scaffolds suitable for 3D cancer cell culture. *Procedia CIRP* **2016**, *49*, 61–66.
- De Ciurana, J.; Serenó, L.; Vallès, È. Selecting process parameters in RepRap additive manufacturing system for PLA scaffolds manufacture. *Procedia CIRP* **2013**, *5*, 152–157. [[CrossRef](#)]
- Milionis, A.; Noyes, C.; Loth, E.; Bayer, I.S.; Lichtenberger, A.W.; Stathopoulos, V.N.; Vourdas, N. Water-Repellent Approaches for 3-D Printed Internal Passages. *Mater. Manuf. Process.* **2016**, *31*, 1162–1170. [[CrossRef](#)]
- Mohamed, O.A.; Masood, S.H.; Bhowmik, J.L. Experimental Investigations of Process Parameters Influence on Rheological Behavior and Dynamic Mechanical Properties of FDM Manufactured Parts. *Mater. Manuf. Process.* **2016**, *31*, 1983–1991. [[CrossRef](#)]
- Gupta, B.; Revagade, N.; Hilborn, J. Poly(lactic acid) fiber: An overview. *Prog. Polym. Sci.* **2007**, *32*, 455–482. [[CrossRef](#)]
- Duling, R.R.; Dupaix, R.B.; Katsube, N.; Lannutti, J. Mechanical characterization of electrospun polycaprolactone (PCL): A potential scaffold for tissue engineering. *J. Biomech. Eng.* **2008**, *130*, 011006. [[CrossRef](#)] [[PubMed](#)]
- Baker, B.M.; Nerurkar, N.L.; Burdick, J.A.; Elliott, D.M.; Mauck, R.L. Fabrication and modeling of dynamic multipolymer nanofibrous scaffolds. *J. Biomech. Eng.* **2009**, *131*, 101012. [[CrossRef](#)] [[PubMed](#)]
- Lange, B.L.; Brendel, T.; Hüttmann, G. Temperature dependence of light absorption in water at holmium and thulium laser wavelengths. *Appl. Opt.* **2002**, *41*, 5797–5803. [[CrossRef](#)] [[PubMed](#)]
- Domingos, M.; Intranuovo, F.; Russo, T.; De Santis, R.; Gloria, A.; Ambrosio, L.; Ciurana, J.; Bartolo, P. The first systematic analysis of 3D rapid prototyped poly(ϵ -caprolactone) scaffolds manufactured through BioCell printing: the effect of pore size and geometry on compressive mechanical behaviour and in vitro hMSC viability. *Biofabrication* **2013**, *5*, 045004. [[CrossRef](#)] [[PubMed](#)]
- Bartolo, P.; Domingos, M.; Gloria, A.; Ciurana, J. BioCell Printing: Integrated automated assembly system for tissue engineering constructs. *CIRP Ann-Manuf. Technol.* **2011**, *60*, 271–274. [[CrossRef](#)]
- Sultana, N.; Mokhtar, M.; Hassan, M.I.; Jin, R.M.; Roozbahani, F.; Khan, T.H. Chitosan-Based Nanocomposite Scaffolds for Tissue Engineering Applications. *Mater. Manuf. Process.* **2015**, *30*, 273–278. [[CrossRef](#)]
- Zein, I.; Huttmacher, D.W.; Tan, K.C.; Teoh, S.H. Fused deposition modeling of novel scaffold architectures for tissue engineering applications. *Biomaterials* **2002**, *23*, 1169–1185. [[CrossRef](#)]
- Hsu, S.-H.; Yen, H.-J.; Tseng, C.-S.; Cheng, C.-S.; Tsai, C.-L. Evaluation of the growth of chondrocytes and osteoblasts seeded into precision scaffolds fabricated by fused deposition manufacturing. *J. Biomed. Mater. Res.* **2007**, *80*, 519–527. [[CrossRef](#)] [[PubMed](#)]

20. Yen, H.-J.; Tseng, C.-S.; Hsu, S.-H.; Tsai, C.-L. Evaluation of chondrocyte growth in the highly porous scaffolds made by fused deposition manufacturing (FDM) filled with type II collagen. *Biomed. Microdevices* **2009**, *11*, 615–624. [[CrossRef](#)] [[PubMed](#)]
21. Grémare, A.; Guduric, V.; Bareille, R.; Heroguez, V.; Latour, S.; L'heureux, N.; Fricain, J.C.; Catros, S.; Nihouannen, D.L. Characterization of printed PLA scaffolds for bone tissue engineering. *J. Biomed. Mater. Res. Part A* **2018**, *106*, 887–894. [[CrossRef](#)] [[PubMed](#)]
22. Hutmacher, D.W.; Schantz, T.; Zein, I.; Ng, K.W.; Teoh, S.H.; Tan, K.C. Mechanical properties and cell cultural response of polycaprolactone scaffolds designed and fabricated via fused deposition modeling. *J. Biomed. Mater. Res.* **2001**, *55*, 203–216. [[CrossRef](#)]
23. Rabionet, M.; Guerra, A.J.; Puig, T.; Ciurana, J. 3D-printed Tubular Scaffolds for Vascular Tissue Engineering. *Procedia CIRP* **2018**, *68*, 352–357. [[CrossRef](#)]
24. Rabionet, M.; Yeste, M.; Puig, T.; Ciurana, J. Electrospinning PCL Scaffolds Manufacture for Three-Dimensional Breast Cancer Cell Culture. *Polymers* **2017**, *9*, 328. [[CrossRef](#)]
25. Guerra, A.J.; Cano, P.; Rabionet, M.; Puig, T.; Ciurana, J. Effects of different sterilization processes on the properties of a novel 3D-printed polycaprolactone stent. *Polym. Adv. Technol.* **2018**, *29*, 2327–2335. [[CrossRef](#)]
26. Chen, M.; Michaud, H.; Bhowmick, S. Controlled Vacuum Seeding as a Means of Generating Uniform Cellular Distribution in Electrospun Polycaprolactone (PCL) Scaffolds. *J. Biomech. Eng.* **2009**, *131*, 1–8. [[CrossRef](#)] [[PubMed](#)]
27. Ferlin, K.M.; Prendergast, M.E.; Miller, M.L.; Nguyen, B.N.B.; Kaplan, D.S.; Fisher, J.P. Development of a Dynamic Stem Cell Culture Platform for Mesenchymal Stem Cell Adhesion and Evaluation. *Mol. Pharm.* **2014**, *11*, 2172–2181. [[CrossRef](#)] [[PubMed](#)]



© 2018 by the authors. Licensee MDPI, Basel, Switzerland. This article is an open access article distributed under the terms and conditions of the Creative Commons Attribution (CC BY) license (<http://creativecommons.org/licenses/by/4.0/>).



The Second CIRP Conference on Biomanufacturing

Optimization of Poli(ϵ -caprolactone) scaffolds suitable for 3D cancer cell cultureGiró-Perafita Ariadna^a, Rabionet Marc^a, Puig Teresa^{a*} and Ciurana Joaquim^{b*}

^a Oncology Unit (TargetsLab), Department of Medical Sciences - Faculty of Medicine - University of Girona, Emili Grahit 77, 17077 Girona, Spain
^b Department of Mechanical Engineering and Industrial Construction - University of Girona, Maria Aurèlia Capmany 61, 17071 Girona, Spain

* Corresponding authors. Tel.: +34-972-41-8265 ; fax: +34-972-41-9098. E-mail address: quim.ciurana@udg.edu
 Tel.: +34-972-41-9628 E-mail address: teresa.puig@udg.edu

Abstract

Fused Deposition Model (FDM) as Additive manufacturing (AM) technologies may offer a viable and simpler alternative to manufacture scaffolds for different purposes such as tissue engineering and cells culture. Existing commercial FDM machines are currently being modified to improve their accuracy, capabilities and use. However, for biocompatible and/or bioimplantable materials such as Poli (ϵ -caprolactone) PCL there is still a lot of work to do to set up process parameters. Cells culture had been carried on 2D without being a proper and real midst. In fact cells do not grow only in two flat directions but in all directions making strong net. Since cells responses to proteins or drugs is important for knowing proliferation or enrichment more real culture in 3D is needed. This work focuses on the study and optimization of open-source 3D printer machine, called RepRap, employed to manufacture biocompatible scaffolds for 3D cells culture of Triple-Negative Breast Cancer (TNBC). It has been shown that scaffolds culture can enhance the Cancer Stem Cell (CSC) population, responsible in part for tumour recurrence after chemotherapy. Mammosphere Forming Index (MFI) was defined in all cell lines to evaluate this population in TNBC cell lines sensible and resistant to chemotherapy. Enriching TNBC cells with CSC after scaffold culture will help to study new therapeutic treatments directed to this population. Several process parameters are tested to manufacture scaffolds and cells culture had been carried out in order to validate the results. Results show that porosity plays an important role in scaffolds manufacture having low cells adhesion and growth. Lower porosity values should be tested to further evaluate MFI index after scaffold culture as cell growth and enrichment indication.

© 2015 The Authors. Published by Elsevier B.V. This is an open access article under the CC BY-NC-ND license (<http://creativecommons.org/licenses/by-nc-nd/4.0/>).

Peer-review under responsibility of the scientific committee of The Second CIRP Conference on Biomanufacturing

Keywords: PCL; Scaffold; Additive Manufacturing; Fused deposition model; Cancer Cells; 3D Cell-Culture; Stem Cells

1. Introduction

Cell culture is a technique widely used in cancer research laboratories, for instance to the study of cancer biology and the development of new therapeutic strategies. Nowadays, 2D cell culture is the most frequent technique used. Although interest for 3D cell culture is emerging because cell architecture and interactions simulates better the biology of a tissue compared to the flat-growing 2D systems [1].

The development of accurate constructs made of a matrix or scaffold and living cells to repair and regenerate damaged tissue is a current challenge in the tissue engineering field [2]. Taking advantage of this, scaffold fabrication for 3D cell-culture has emerged using technologies already developed for this purpose. One of these techniques is the additive manufacturing technology, which enables the fabrication of

customized scaffolds directly from the patient. For this purpose, existing additive manufacturing machines are currently being modified to improve their accuracy and capabilities. The optimization of process parameters is a major challenge to obtain adequate scaffold morphology and biomechanical behavior, which are to improve cell adhesion and proliferation. Indeed, appropriate porosity, pore size, pore shape, and mechanical strength are required to achieve cell growth and matrix formation [3]. Open source extruders, like the RepRap machine, allow a thorough study of several process parameters involved in the fabrication of scaffolds such as deposition speed, layer thickness, filament distance, deposition pattern, extrusion and bed temperatures and speed movement. Therefore, a precise control over this manufacturing process is required.

Triple-Negative Breast Cancer (TNBC) is a type of breast cancer which runs an aggressive course and has a poor prognosis. It shows the highest recurrence rate compared to other breast cancer types [4]. TNBC lacks of validated directed therapy, and patients are treated mainly with chemotherapy (anthracyclines and taxans). Even though TNBC shows a good response to these therapies, recurrence at 5 years following diagnosis is about 30% of the cases [5,6].

Recent studies showed that chemoresistance can be achieved by a unique and rare cell niche with stemness features, the so-called Cancer Stem Cells (CSC) [7,8]. These cells, capable of tumor initiation, are not only responsible for tumor recurrence, but also metastasis [9]. Interestingly, scaffolds not only allow cells to interact in a 3D way improving the in-vitro 2D system, but also it has been described that 3D cultures can enhance the CSC population [10,11].

In this study it had been investigated the optimization of the open source and low-cost 3D extruder machine RepRap, employed to fabricate PCL scaffolds suitable for 3D cell culture. Design and manufacturing parameters were determined to ensure the best performance. In addition, this work focuses in 3D scaffolds ability to enrich the CSC population for developing new therapeutic strategies to target this population.

2. Materials and Methods

2.1. Material

A 3mm Poli(ϵ -caprolactone) (PCL) wire (Perstorp, Malmö, Sweden) was used to manufacture the scaffolds. PCL is biodegradable polyester proven to be biocompatible and free of toxic dye.

2.2. 3D printer machine and software

Printer machine RepRap BCN 3D+ was used to produce three-dimensional scaffolds. It is an open source and modular 3D printer designed by RepRap BCN. This printer uses the Fused Filament Fabrication (FFF) technology so called Fused Deposition Model (FDM). The filament unwound from a coil is supplied to the extruder. Then, at certain temperature and pressure, exerted by a gear, causes the extrusion of the material through the nozzle, which is finally deposited onto a heated computer-controlled Cartesian platform.

The scaffold's design was carry out with the computer-aided design (CAD) software SolidWorks. The designs were saved in STL file formats, which are transferred to a computer-aided manufacturing (CAM) software called Slic3r. This program was used for establishing the printing parameters. It generates G-code files able to command and control the machine in order to obtain the scaffolds printed.

Table 1 shows the process parameters utilized for the experimental set up. Design parameters, such as shape, layer thickness, diameter of filament and distance between filaments, were studied and analysed. Deposition angle between layers was fixed at 0-90°. Shape refers to the basic feature of the scaffold produced. Thickness is the total height of the scaffold and the distance between filaments is the

shortest distance between two filaments located within the same layer.

Table 1. Scaffold parameters and levels tested in order to obtain the optimal printing

	Parameters	Levels
DESIGN PARAMETERS	Deposition angle (°)	0-90
	Shape	square, round
	Thickness (mm)	1.8, 3.6
	Diameter of filament (mm)	0.175, 0.30, 0.50
	Distance between filaments (mm)	0.5, 0.7, 1
MANUFACTURING PARAMETERS	Deposition speed (mm/s)	10, 20, 30, 50
	Layer height (mm)	0.15, 0.20, 0.25, 0.28, 0.30, 0.35
	Extrusion temperature (°C)	65, 75, 80, 85, 90, 95, 105, 110, 115, 120, 130, 150, 155, 160, 180, 200
	Bed temperature (°C)	25, 30, 33, 35, 37

Other parameters were set, like deposition speed, layer height and temperatures. The deposition speed was defined as the speed for printing movements of the extruder. Layer height is the distance between two connected layers along the Z axis. Finally, temperatures of the extruder and the glass platform were set up as well.

2.3. Cell Culture

MCF-7, MDA-MB-231 and HCC1806 breast carcinoma cells were obtained from the American Type Culture Collection (ATCC, Rockville, MD, USA). MDA-MB-231 and HCC1806 are cell lines established from patients with TNBC. MCF-7 are a HER2 positive cell line, (a type of breast cancer that overexpresses the Human Epidermal Growth Factor Receptor 2), used for scaffold validation. Doxorubicin (chemotherapeutic drug) was used to create resistant models from MDA-MB-231 (231D $\mathbf{X}\mathbf{R}$) and HCC1806 (HCCD $\mathbf{X}\mathbf{R}$) in our laboratory by treating cells at increasing doses of doxorubicin for 48 hours periods until 6 months.

MCF-7, and MDA-MB-231 and 231D $\mathbf{X}\mathbf{R}$ cells were cultured in DMEM (Dulbecco's Modified Eagle's Medium) (Gibco, Waltham, MA, USA) supplemented with 10% fetal bovine serum, 1% L-glutamine, 1% sodium pyruvate, 50U/mL penicillin and 50µg/mL streptomycin (HyClone, Logan, UT, USA). HCC1806 and HCCD $\mathbf{X}\mathbf{R}$ cells were cultured in RPMI (Roswell Park Memorial Institute) (Gibco, Waltham, MA, USA) and supplemented as above. All cells were maintained at 37°C and 5% CO₂ atmosphere.

2.4. Mammosphere-forming assay

In order to evaluate CSC population, the mammosphere-forming technique was performed (Figure 1). Cells from 2D or PCL scaffolds were removed by trypsinization. Then cells were counted, and seeded into a 6-well cell culture microplate coated with pHEMA using DMEM/F12 medium supplemented with B27, EGF and FGF (20ng/mL), 1% L-glutamine, 1% sodium pyruvate and 25U/mL penicillin and

25µg/mL streptomycin . Finally, cells were incubated for 5 or 7 days and mammospheres bigger than 50µm were counted using an inverted optical microscope. Mammosphere Forming Index (MFI) was calculated using the formula described below:

$$MFI = \frac{N^{\circ} \text{ mammosphere}}{N^{\circ} \text{ cells plated}} \cdot 100$$

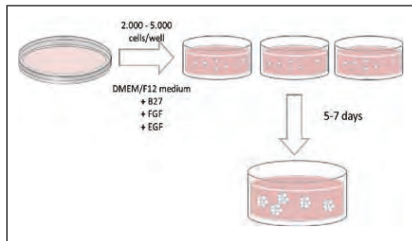


Figure 1. Mammosphere-forming assay protocol

For the mammosphere treatment experiments, doxorubicin was added in the seeding process. Mammosphere Forming Inhibition (MFI_{in}) was calculated, as shown in the formula below:

$$MFI_{in} = 100 - \frac{N^{\circ} \text{ mammospheres}_{\text{treatment}}}{N^{\circ} \text{ mammospheres}_{\text{control}}} \cdot 100$$

2.5. Growth inhibition assay

MDA-MB-231, HCC1806, 231DXR and HCCDXR were plated out at a density of 5×10^3 cells/2mL/well in 6-well plates. Posterior overnight cell adherence, fresh medium along with the corresponding doxorubicin concentration was added to the cultures. Following treatment, media was replaced by drug-free medium (1mL/well) containing MTT (3,4,5-dimethylthiazol-2-yl-2,5-diphenyltetraolium bromide, Sigma) solution, and incubation was prolonged for 2 hours at 37°C. Formazan crystals formed by metabolically viable cells were dissolved in DMSO (300µL/well) and absorbance was determined at 570nm in a multi-well plate reader (Model Anthos Labtec 2010 1.7). Using control OD values (C) and test OD values (T), % of Cell Proliferation Inhibition (CPI) was calculated from the equation below:

$$CPI = 100 - \frac{T}{C} \cdot 100$$

Data presented are from two separate wells per assay and the assay was performed at least three times.

2.6. Scaffold sterilization

Scaffolds were sterilized with 70% ethanol/water solution overnight, washed with PBS (Gibco, Waltham, MA, USA) and finally exposed to UV light for 90 minutes.

2.7. Cell culture in scaffolds

Scaffolds were placed into a 12-well cell culture microplate. First, 250µL of cell suspension (10.000-100.000 cells) were placed onto the centre of its surface to allow cells attach on the scaffold. After 1 hour incubation period, 1.5mL of fresh medium was added to cover the scaffold. Cells were incubated for 72 hours and then counted. (Figure 2).

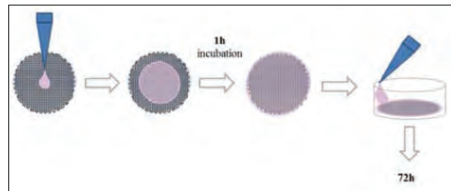


Figure 2. Cell seeding protocol on PCL scaffolds.

To quantify the cells attached, the scaffold was placed in a new well, washed with PBS and 1mL of trypsin was added. After incubation, 2.5mL of fresh medium were added and the cell suspension was collected and centrifuged at 1500rpm for 5 min. Finally, the supernatant was discarded and cells were counted using a Neubauer Chamber and an inverted optical microscope. The same procedure was done to obtain the cells attached at the well where the scaffold was placed.

2.8. Statistical analysis

All data are expressed as mean \pm standard error (SE). Data were analyzed by Student t test. Statistical significant levels were $p < 0.05$ (denoted as *), $p < 0.01$ (denoted as **) and $p < 0.001$ (denoted as ***). p -value is shown in results when significance is reached ($p < 0.05$).

3. Results

3.1. Scaffolds design and manufacturing

Scaffolds were designed with a round shape, with the size of 19mm diameter to allow their use in regular cell culture plate-dishes of 12 wells. The final designs had 1.8mm of thickness, composed of 6 different layers of polymeric material, being 0.3mm of thickness each layer. The distance between filaments was 0.7mm and the deposition angle was established at 0-90° (Table 2).

Scaffolds manufacturing parameters were optimized by screening experiments to print the scaffolds efficiently and properly for cells culture (Table 3).

The deposition speed took a small value to optimize the material's deposition. The nozzle tip size was fixed at 0.35mm. The printed filaments had a diameter of 0.30mm. With visual screening, it was proved that the optimal extrusion temperature was 85°C (Figure 3). Finally, scaffolds were fabricated with a bed temperature of 35°C, to guarantee their adhesion to the printing platform.

Table 2. Scaffold design parameters.

Parameters	
Diameter	19mm
Shape	Round
Thickness	1.8mm
Number of layers	6
Distance between filaments	0.7mm
Deposition angle	0-90°
Diameter of filament	0.30mm

Table 3. Scaffold manufacturing parameters

Parameters	
Deposition velocity	10mm/s
Layer height	0.30mm
Nozzle tip size	0.35mm
Extrusion temperature	85°C
Bed temperature	35°C

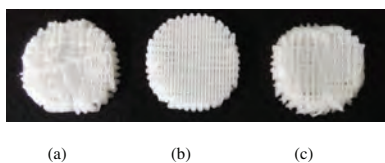


Figure 3. Scaffold manufacturing at different extrusion temperature (a) 80°C, (b) 85°C, (c) 90°C.

3.2. Cancer Stem Cells population characterization

Cancer Stem Cells are a very rare population within the tumor. These cells have been demonstrated to have the ability to survive and propagate in a non-adherent way, forming spheres called mammospheres [7,12,13].

To determine CSC population, the mammosphere-forming assay was performed in cell lines MCF-7, MDA-MB-231, HCC1806, and resistant models 231DXR and HCCDXR (Figure 4). MFI was then calculated (Table 4).

CSC represents a small population in all cell lines, with values ranging from 0.67% to 2.47% of MFI. When comparing the ability to form mammosphere between parental and resistant cells to doxorubicin, no increase of MFI was observed in the two models.

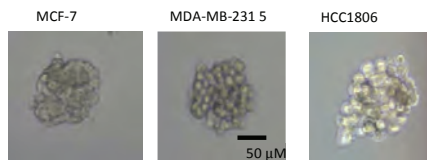


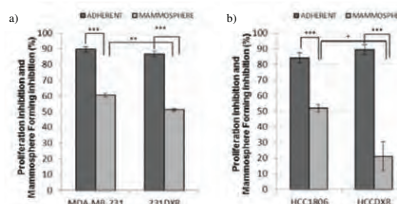
Figure 4. Mammospheres under optic microscope for MCF-7, MDA-MB-231 and HCC1806.

Table 4. Mammosphere Forming Index (MFI).

Cell Line	Cells seeded (cells/well)	Days	MFI (%)
MCF-7	2.000	7	2.47±0.26
MDA-MB-231	5.000	5	1.78±0.24
HCC1806	5.000	5	0.92±0.17
231DXR	5.000	5	1.75±0.27
HCCDXR	5.000	5	0.67±0.04

Data are shown as mean ±SEM.

As cell plasticity plays an important role in tumor biology and drug resistance, it was checked the ability to form mammospheres under doxorubicin pressure [14-16]. To do so, the experiments were repeated in presence of doxorubicin in both sensible and resistant cell lines and MFI was calculated for each model. The same experiment was performed in adherent conditions using the MTT assay as described in Material and Methods section. Intrinsic resistance of CSC to doxorubicin was observed in all models (Figure 4). In adherent conditions, cell lines proliferation inhibition (% CPI) ranged from 84.2% to 89.5%. Otherwise, MFI values showed significant lower inhibition in all cell lines, ranging from 20.6% to 60.7% (p -values < 0.001).

Figure 5. Proliferation inhibition and Mammosphere forming inhibition (MFI) under doxorubicin treatment for 5 days. (a) MDA-MB-231 and 231DXR with doxorubicin (70nM). (b) HCC1806 and HCCDXR with doxorubicin (140nM). Experiments were performed at least three times in duplicate. *($p < 0.05$), **($p < 0.01$) and ***($p < 0.001$) indicate levels of statistical significance.

The cytotoxic effect of doxorubicin was then evaluated in CSC population comparing parental and resistant models (Figure 4). MDA-MB-231 and 231DXR showed an MFI of 60.66% and 51.29% (*p* value: 0.005) respectively. HCC1806 MFI was 51.97% and 20.61% for HCCDXR (*p* value: 0.036). CSC population from resistant models HCCDXR and 231DXR showed significance resistant to doxorubicin, maybe due to an enrichment of this population in this models [8].

3.3. Scaffolds and cell culture

The scaffold with deposition angles of 0-90° (Figure 2a) was printed and tested for cell culture (Figure 5).

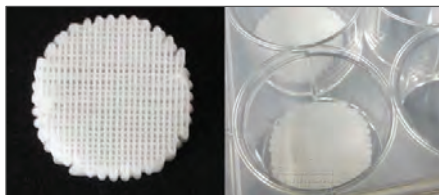


Figure 5. Scaffold fabricated with RepRap Machine a) 19mm diameter, 1.8mm thick, and deposition angles of 0-90° b) the scaffold plated in a 12 well-plate.

Before its use, scaffolds were sterilized as mentioned in Material and Methods section. Then MCF-7 cells were seeded at different densities (10,000, 50,000 and 100,000 cells/well) during 72 hours. Attached and non-attached cells were counted.

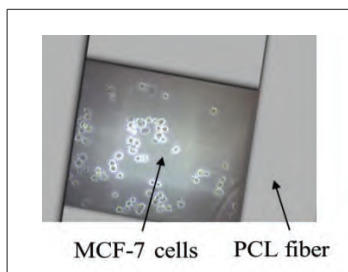


Figure 6. Optical microscope images of MCF-7 cells attached at the bottom of the well. Scaffold fiber has been drawn on the top.

In this first attempt, no cells were attached to the scaffold. As it was described and then observed under the microscope, this scaffold has large pores. The fibers of the different layers have the same disposition angle and, for that reason, cells can easily fall to the bottom of the well before they can get attached to PCL fibers (Figure 6).

As PCL fibers have already been tested in cell culture [10], new goal is set up focusing on designing and testing new

scaffolds with different deposition angles between layers to achieve different and smaller pore sizes.

Two more designs have been performed, where the deposition angles were variable, taking the values of 0-60-120° and 0-45-90-135° (Figure 7). The variation of the angle deposition between layers results in a different pore size and shapes between the scaffolds (Table 5).

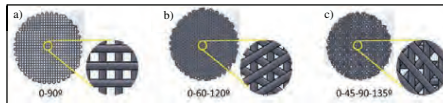


Figure 7. Scaffolds designs with different deposition angles: (a) 0-90°, (b) 0-60-120°, (c) 0-45-90-135°.

Table 5. Pore characteristics depending on the deposition angle

Deposition angles	Pores shape	Area
0-90°	Square	0.15mm ²
0-60-120°	Equilateral triangle	0.1256mm ²
0-45-90-135°	6 variable forms (triangles and irregular polygons)	1.98x10 ⁻⁴ to 0.13mm ²

4. Conclusions

In this study, the parameters of the open source RepRap 3D printer have been optimized to fabricate scaffolds of PCL suitable for cell culture.

Parameters, like deposition speed, diameter of the filament and extrusion and bed temperatures have been determined to obtain an optimal manufacture.

Design parameters, such as round shape, diameter and thickness were thought to allow its use in regular 12 well-cell culture plates. Three different designs have been performed, with different angles between layers, obtaining different pores sizes in all designs.

MCF-7 and TNBC cell lines had the ability to form mammospheres with low values of MFI, showing that CSC represents a very small population in these cell lines. CSC enriched population showed also intrinsic resistance to chemotherapy when compared to adherent culture. On the other hand, CSC population in resistant cell models developed in our lab (HCCDXR and 231DXR) showed increased ability to form mammospheres compared to the parental models under doxorubicin treatment.

MCF-7 cell line was used to test the scaffolds printed with deposition angles of 0-90°. Because of the same distribution of the fibers between layers and the large pores size of this design, cells drifted at the bottom of the well without attaching the scaffold. The other two designs, with smallest pore size will be tested in further studies.

Acknowledgements

This work was supported in part by Spanish Grants: Fundación Ramón Areces (TP), Instituto de Salud Carlos III (PI1400329, TP), Ministerio de Economía i Competitividad

(DPI2013-45201-P), and the support of Catalonian Government (2014SGR00868).
 Marc Rabionet is the recipient of a Departmental Collaboration Grant from the Ministerio de Educación Cultura y Deportes of Spain for the academic years 2014-2015.

References

- [1] D. Antoni, H. Burckel, E. Josset, G. Noel, Three-Dimensional Cell Culture: A Breakthrough in Vivo, *Int. J. Mol. Sci.* 16 (2015) 5517–5527. doi:10.3390/ijms16035517.
- [2] B. Bártolo, P.J., Almeida, H.A., Rezende, R.A., Laoui, T., Bidanda, Advanced Processes to Fabricate Scaffolds for Tissue Engineering, in: P.B. Bopaya Bidanda (Ed.), *Virtual Prototyp. Bio Manuf. Med. Appl.*, Springer, 2008: pp. 149–170.
- [3] T.J. Hollister S.J., Maddox RD., Optimal Design and Fabrication of Scaffolds to Mimic Tissue Properties and Satisfy Biological Constraints, *Biomaterials.* (2002) 4095–4103.
- [4] L.A. Carey, C.M. Perou, C.A. Livasy, L.G. Dressler, D. Cowan, K. Conway, et al., Race , Breast Cancer Subtypes , and Survival in the Carolina Breast Cancer Study, *JAMA.* 295 (2006) 2492–2502.
- [5] O. Metzger-Filho, A. Tutt, E. De Azambuja, K.S. Saini, G. Viale, S. Loi, et al., Dissecting the heterogeneity of triple-negative breast cancer, *J. Clin. Oncol.* 30 (2012) 1879–1887. doi:10.1200/JCO.2011.38.2010.
- [6] R. Dent, M. Trudeau, K.I. Pritchard, W.M. Hanna, H.K. Kahn, C. a Sawka, et al., Triple-negative breast cancer: clinical features and patterns of recurrence., *Clin. Cancer Res.* 13 (2007) 4429–34. doi:10.1158/1078-0432.CCR-06-3045.
- [7] G. Dontu, W.M. Abdallah, J.M. Foley, K.W. Jackson, M.F. Clarke, M.J. Kawamura, et al., In vitro propagation and transcriptional profiling of human mammary stem / progenitor cells, *Genes Dev.* 17 (2003) 1253–1270. doi:10.1101/gad.1061803.potential.
- [8] C.J. Creighton, X. Li, M. Landis, J.M. Dixon, V.M. Neumeister, A. Sjolund, et al., Residual breast cancers after conventional therapy display mesenchymal as well as tumor-initiating features., *Proc. Natl. Acad. Sci. U. S. A.* 106 (2009) 13820–13825.
- [9] B.K. Abraham, P. Fritz, M. McClellan, P. Hauptvogel, M. Athelou, H. Brauch, Prevalence of CD44 + / CD24 – / low Cells in Breast Cancer May Not Be Associated with Clinical Outcome but May Favor Distant Metastasis, *Clin. Cancer Res.* (2005) 1154–1159.
- [10] S. Feng, X. Duan, P.-K. Lo, S. Liu, X. Liu, H. Chen, et al., Expansion of breast cancer stem cells with fibrous scaffolds., *Integr. Biol. (Camb).* 5 (2013) 768–77. doi:10.1039/c3ib20255k.
- [11] S. Saha, P.-K. Lo, X. Duan, H. Chen, Q. Wang, Breast tumour initiating cell fate is regulated by microenvironmental cues from an extracellular matrix, *Integr. Biol.* 4 (2012) 897. doi:10.1039/c2ib20034a.
- [12] F.L. Shaw, H. Harrison, K. Spence, M.P. Ablett, B.M. Simões, G. Farnie, et al., A detailed mammosphere assay protocol for the quantification of breast stem cell activity., *J. Mammary Gland Biol. Neoplasia.* 17 (2012) 111–7. doi:10.1007/s10911-012-9255-3.
- [13] T. Pereira, G. Ivanova, A.R. Caseiro, P.P. Barbosa, P.J. Bartolo, J.D. Santos, A.L. Luis, A.C. Mauricio. MSCs conditioned media and umbilical cord blood plasma metabolomics and composition. *PLOS ONE.* 9 (2014) (11): e113769
- [14] N.D. Marjanovic, R. a. Weinberg, C.L. Chaffer, Cell plasticity and heterogeneity in cancer, *Clin. Chem.* 59 (2013) 168–179. doi:10.1373/clinchem.2012.184655
- [15] T. Pereira, P.A.S. Armanda-da-Silva, I. Amorim, A. Rema, A.R. Caseiro, A. Gartner, M. Rodrigues, M. Lopes, P.J. Bartolo, J.D. Santos, A.L. Luis, A.C. Mauricio. Effects of human mesenchymal stem cells (HMSCs) isolated from the Whorton's jelly of the umbilical cord and conditioned media (CM) on skeletal muscle regeneration using myectomy model. *Stem Cells International*, (2014) Article ID 376918
- [16] T. Pereira, A. Gartner, I. Amorim, A. Almeida, A.R. Caseiro, P.A. Armanda-da-Silva, S. Amado, F. Fregnan, A.S. Varejão, J.D. Santos, P.J. Bartolo, S. Geuna, A.L. Luis, A.C. Mauricio. Promoting nerve regeneration in a neurotmesis rat model using poly(DL-lactide-ε-caprolactone) membranes and mesenchymal stem cells from the Wharton's jelly: in vitro and in vivo analysis. *BioMed Research International.* (2014) Article ID 302659, 2014

Article

Breast Cancer Stem Cell Culture and Enrichment Using Poly(ϵ -Caprolactone) Scaffolds

Sònia Palomeras ^{1,†}, Marc Rabionet ^{1,2,†}, Inés Ferrer ², Ariadna Sarrats ^{1,2},
 Maria Luisa Garcia-Romeu ², Teresa Puig ^{1,*} and Joaquim Ciurana ^{2,*}

¹ New Therapeutic Targets Laboratory (TargetsLab)—Oncology Unit, Department of Medical Sciences, Faculty of Medicine, University of Girona, Girona 17071, Spain; sonia.palomeras@udg.edu (S.P.); m.rabionet@udg.edu (M.R.); ariadna.sarrats@udg.edu (A.S.)

² Product, Process and Production Engineering Research Group (GREP), Department of Mechanical Engineering and Industrial Construction, University of Girona, Girona 17071, Spain; ines.iferrer@udg.edu (I.F.); mluisa.gromeu@udg.edu (M.L.G.-R.)

* Correspondence: teresa.puig@udg.edu (T.P.); quim.ciurana@udg.edu (J.C.); Tel.: +34-972-419628 (T.P.); +34-972-418265 (J.C.)

† These authors contributed equally to this work.

Academic Editors: Chee Kai Chua and Wai Yee Yeong

Received: 14 March 2016; Accepted: 20 April 2016; Published: 23 April 2016

Abstract: The cancer stem cell (CSC) population displays self-renewal capabilities, resistance to conventional therapies, and a tendency to post-treatment recurrence. Increasing knowledge about CSCs' phenotype and functions is needed to investigate new therapeutic strategies against the CSC population. Here, poly(ϵ -caprolactone) (PCL), a biocompatible polymer free of toxic dye, has been used to fabricate scaffolds, solid structures suitable for 3D cancer cell culture. It has been reported that scaffold cell culture enhances the CSCs population. A RepRap BCN3D+ printer and 3 mm PCL wire were used to fabricate circular scaffolds. PCL design and fabrication parameters were first determined and then optimized considering several measurable variables of the resulting scaffolds. MCF7 breast carcinoma cell line was used to assess scaffolds adequacy for 3D cell culture. To evaluate CSC enrichment, the Mammosphere Forming Index (MFI) was performed in 2D and 3D MCF7 cultures. Results showed that the 60° scaffolds were more suitable for 3D culture than the 45° and 90° ones. Moreover, 3D culture experiments, in adherent and non-adherent conditions, showed a significant increase in MFI compared to 2D cultures (control). Thus, 3D cell culture with PCL scaffolds could be useful to improve cancer cell culture and enrich the CSCs population.

Keywords: breast cancer; cancer stem cell; scaffold; PCL; RepRap; tridimensional cell culture; mammospheres

1. Introduction

Breast cancer (BC) is the second most common cause of cancer-related death in women. Recent research has focused on a small population of the heterogeneous tumor cells that are responsible for tumor initiation and subsequent progression, the so-called Cancer Stem Cells (CSCs) [1]. Different studies revealed that these cells possess several characteristics similar to mammary stem cells [2], including radio- [3] and chemoresistance [4]. These properties favor breast cancer's tumor recurrence. CSCs have the ability to undergo self-renewal and a potential to differentiate into non-stem breast cancer cells, generating cells with a variety of phenotypes within tumors [5]. The expression pattern of cells' surface markers such as CD44 and CD24 has been used to isolate and enrich breast CSCs from the tumors [1,6]. Furthermore, these cells are able to grow and survive as non-adherent spheres, termed "mammospheres", which enables their expansion in culture [7,8]. The study of

CSC has been limited by the inability to propagate these cells without inducing differentiation, thus losing their stem-related features. The traditional two-dimensional (2D) cell culture systems are adequate to study cancer cells *in vitro*, but cannot completely simulate the *in vivo* cellular environment. This important difference in the cellular surroundings [9] may influence CSC properties and prevent their differentiation [10].

In recent years, three-dimensional (3D) cell culture has been developed to mimic the architecture of the extracellular matrix and the tissue environment, which can afford CSC culture without induction of differentiation. Scaffolds are one of the 3D culture systems, which are three-dimensional structures mostly made of polymeric materials. The use of biodegradable biopolymers as a structural 3D support material has emerged from using technologies already developed for this purpose, such as the Fused Filament Fabrication (FFF), widely used by 3D printers [11]. One of the most used biopolymers is poly(ϵ -caprolactone) (PCL), which exhibits suitable properties for tissue engineering, good mechanical characteristics, and relatively long-term biodegradability; it has also been proven to be biocompatible and free of toxic dyes [12]. Several studies have improved different mechanical, structural, and fabrication aspects of PCL tissue engineering scaffolds [13–15], but few studies have focused on cell attachment efficiency, proliferation, and differentiation within this 3D structure. Our previous studies investigated the optimization of the open-source and low-cost 3D extruder machine RepRap, employed to fabricate PCL scaffolds suitable for three-dimensional cell culture.

Cancer Stem Cells (CSCs) only represent a small population (10%–25%) of a tumor sample or cell line. CSCs are difficult to culture in 2D systems without inducing cell differentiation. To avoid this issue, this work focused on optimizing a three-dimensional culture protocol with a well-known breast cancer cell line (MCF7 cells). Scaffold cultures have been shown to provide a more physiological environment than monolayers (2D). Therefore, CSCs can grow with undifferentiated properties, while the rest of the sample cells remain differentiated. Consequently, a 3D culture can produce CSC enrichment compared to a 2D cell culture. Three-dimensional cell culture does not select or isolate CSCs, so an additional technique is necessary to quantify this population, the mammosphere-forming assay. Culture and medium conditions only allow the growth and proliferation of cells with CSC properties, forming spheres.

The present study has focused on the effect of different culture properties to improve scaffolds' adequacy for breast cancer cells. In addition, the final objective of this work is to evaluate the CSCs' enrichment due to scaffolds' cell culture. Three-dimensional cell culture can be a useful way to enrich and isolate CSCs for further investigation targeted to this malignant subpopulation. According to this hypothesis, a higher cell proliferation could lead to a higher absolute number of CSCs.

2. Results

2.1. Scaffold Design and Manufacturing

In previous studies, design and manufacturing parameters were optimized to achieve high-quality scaffold printing, following a specific flowchart. All parameters have been modified considering the biopolymeric material characteristics and the printing process in order to optimize the porosity for cell culture.

Scaffolds were designed with a 19 mm diameter and a round shape to allow their use in regular cell culture plate dishes of 12 wells. Different design parameters were studied and analyzed, such as filament diameter, distance between filaments, and deposition angle (Table 1). The final designs had 2.4 mm of thickness, composed of eight different layers of polymeric material, each 0.3 mm thick.

The optimized fabrication parameters were extruder and bed temperature, deposition velocity, and layer height. These manufacturing parameters allowed accurate printing of the established designs.

The process parameters are shown in Table 1.

Table 1. Optimal process parameters values used for PCL scaffold printing.

	Parameters	Optimal Values
Design Parameters	Filament diameter	0.3 mm
	Distance between filaments	0.7 mm
	Deposition angle	90°, 60° and 45°
Fabrication Parameters	Extruder temperature	85 °C
	Bed temperature	35 °C
	Deposition velocity	10 mm/s
	Layer height	0.3 mm

2.2. Scaffold Angle Design Evaluation

Control size, geometry, interconnectivity, and spatial distribution of pores are critical parameters of scaffold designs [13]. Furthermore, pore parameters can influence the ability of cells to attach PCL filaments and fill the voids to create a 3D mass of cells. For these reasons, different pore designs were performed, selecting three deposition angles: 90°, 45°, and 60° (Figure 1).

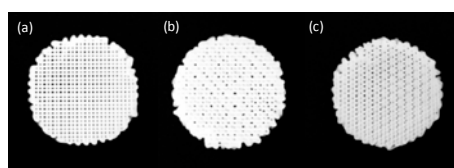


Figure 1. Three deposition angle designs fabricated with RepRap Machine. (a) 90° scaffold; (b) 45° scaffold; and (c) 60° scaffold.

MCF7 cells were seeded on the scaffolds and cultivated for 72 h in adherent culture plates. Cells were observed using an inverted optical microscopy (Figure 2a) and the attached ones were counted (Figure 2b). In 90° scaffolds, cells were only observed at the bottom of the well and non-attached cells were counted. Big pores may mean that cells can easily fall down to the bottom of the well before they can attach to PCL filaments. Attached cells were observed on the fibers of 45° and 60° designs, perhaps due to the smaller pore size. The cellular adhesion was higher in 60° ($24.40\% \pm 1.16\%$) than in 45° ($3.52\% \pm 3.96\%$) scaffolds.

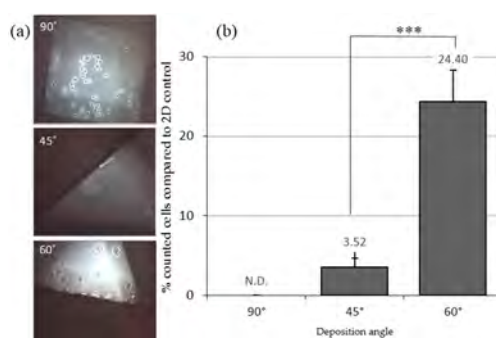


Figure 2. Cells cultured in 3D conditions with adherent well plates. (a) Inverted optical microscopy images of MCF7 cells seeded on different scaffold designs; (b) cells counted (%) three days after seeding in different deposition angle designed scaffolds. Results are shown as mean \pm standard error. *** ($p < 0.001$) indicates levels of statistically significance.

The 45° and 60° scaffolds show adequacy for cell culture. In particular, the 60° design presented the highest percentage of cell attachment. For this reason, we utilized 45° and 60° scaffolds to study the ability of cells to attach to PCL filaments and discarded the 90° scaffold design.

2.3. Adherent and Non-Adherent Conditions for Scaffold Cell Adhesion

Nowadays, biocompatibility studies for *in vitro* assessment of scaffolds are very important. It is necessary to know the effects of tissue culture plate surface properties on cell adhesion to PCL filaments. To evaluate surface characteristics on seeding efficiency and cell growth in 3D culture, studies with adherent and non-adherent (pHEMA) wells were assayed. The same conditions were used in the 2D culture as in the control. There were no differences in cell morphology for those on scaffolds grown in both treated and non-treated well plates for the three days of the experiment.

The attached cells were observed using an inverted optical microscopy. For both scaffold designs (45° and 60°), in adherent and non-adherent surface conditions, two types of cells were observed in the culture. In adherent conditions there were cells attached on the PCL filaments and cells attached at the bottom of the well (Figure 3a,b). Similarly, in non-adherent conditions cells were attached on PCL filaments and cells also formed suspension aggregates between the pores (Figure 3c,d). In both conditions cells were trypsinized and counted.

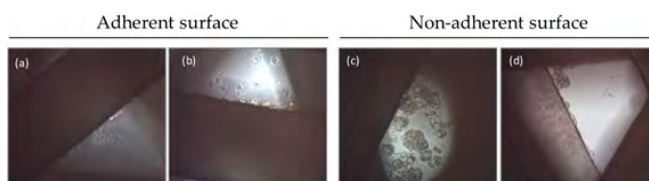


Figure 3. Inverted optical microscopy images of MCF7 cells seeded on scaffolds with adherent and non-adherent wells. (a) 45° and (b) 60° scaffolds in adherent conditions. Cells were attached both at scaffolds and at the surface; (c) 45° and (d) 60° scaffolds in non-adherent conditions. Cells were attached at the scaffolds and also formed suspension aggregates between the PCL filaments.

A higher percentage of counted cells with respect to the 2D control was seen in 60° scaffolds as compared to 45° scaffolds (Figure 4). In adherent conditions this difference was not significant ($p = 0.28$). In non-adherent conditions the percentage of cells in 60° scaffolds was significantly higher ($p = 0.0006$) in contrast to the 45° scaffolds.

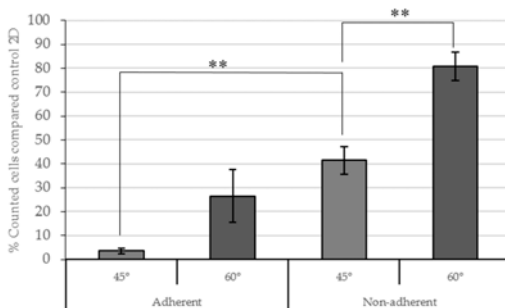


Figure 4. Counted cells (%) in 3D conditions compared to 2D control conditions three days after seeding. Adherent and non-adherent wells were assayed. Results are shown as mean \pm standard error. ** ($p < 0.01$) indicates levels of statistical significance.

Increased cell adhesion was observed on the scaffolds placed on a non-adherent surface compared to the scaffolds in adherent plates after 72 h seeding. The 60° scaffolds showed major cell adhesion in non-adherent conditions. However, the 45° scaffolds had significant differences ($p = 0.006$) between adherent and non-adherent conditions (Figure 4).

The number of cells attached at the bottom of the well in adherent conditions was then evaluated in both designs and compared to the 2D control. For 60° scaffolds, the percentage of cells was $9.04\% \pm 1.47\%$ and for 45° scaffolds it was a little higher ($11.78\% \pm 4.75\%$).

Based on the results, non-adherent conditions showed the highest cell attachment for both designs (45° and 60°). Some authors described a previous medium addition into the scaffold before cell seeding to facilitate cell attachment [15–17]. The medium addition was assayed to optimize cell adhesion in PCL filaments in non-adherent wells (Figure 5). Medium was placed on the center of scaffolds 30 min before cell seeding. A control without previous medium addition was also used.

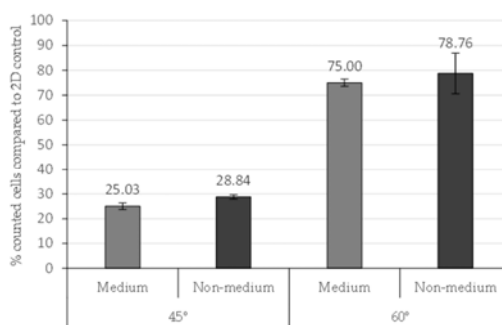


Figure 5. Counted cells in 45° and 60° scaffolds with previous medium or non-medium addition in the scaffold structure. Results are shown as mean \pm standard error.

This experiment enhances the previous results, showing an increased percentage of cells in 60° scaffolds compared to 45°. The medium addition did not modify the cell attachment in 45° and 60° scaffolds, with p -values of 0.082 and 0.691, respectively. In consequence, the previous medium addition was not established in the seeding scaffold protocol.

These results showed an optimal cell seeding efficiency and proliferation of 60° scaffolds.

2.4. Culturing MCF7 Cells on PCL Scaffolds Induces the Expansion of the CSC Subpopulation

Previous research reported that mammary epithelial stem and progenitor cells are able to survive and propagate in an attachment-independent manner and form floating spherical colonies, which are termed mammospheres [7]. Therefore, the number of spheres is often used to identify CSCs. To confirm whether the PCL fibrous scaffold culture system increases the CSCs population, we measured the Mammosphere Formation Index (MFI) of MCF7 cells previously cultured in 2D and 3D cultures with adherent and non-adherent conditions. Based on the results obtained in 3D culture studies, the deposition angle was fixed at 60°, because a 60° angle was the featured scaffold design with the highest proliferation rate.

Previous to the present study, an experimental procedure was performed to characterize the CSC population in the MCF7 line. It has been verified that the cell line of study was capable of forming mammospheres, with an MFI of $2.24\% \pm 0.23\%$.

We found that the MCF7 cells from PCL fibrous scaffolds have increased the MFI compared with the control cells from a polystyrene surface ($p = 0.003$ for adherent conditions and $p = 0.001$ for non-adherent; Figure 6). There was no evidence of statistically different MFI in adherent and non-adherent conditions. Those data suggest that CSCs expanded in this mammary cancer cell line

when cultured in scaffolds and a higher MFI is not related to the chemical characteristics of the surface well plate.

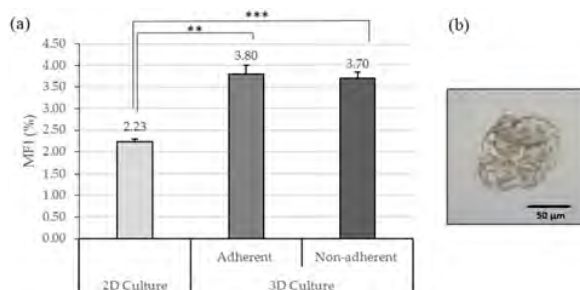


Figure 6. CSCs population analysis. (a) Mammospheres Forming Index (MFI; %) of 2D culture and all 3D conditions. Results are shown as mean \pm standard error. (b) Inverted optical microscopy images of a MCF7 mammosphere. ** ($p < 0.01$) and *** ($p < 0.001$) indicate levels of statistically significance.

2.5. Flow Cytometry Optimization Analysis

Al-Hajj *et al.* reported the first phenotypic description of breast CSCs based on a high expression of CD44 and absent or low expression of CD24 on the cell surface (CD44⁺/CD24⁻/low phenotype) [1]. To determine the CSCs' population enrichment in the 3D scaffold's culture, flow cytometry assay was performed using antibodies against CD44-FITC and CD24-PE surface markers and using 7-AAD to assess cell viability. To achieve this aim, the flow cytometry protocol was optimized in MCF7 with a 2D culture.

To analyze the efficiency of antibodies against MCF7 cells, fluorochromes conjugated with the antibodies were tested. Cells were observed with a confocal microscope (Figure 7a). Positive cells for CD44 were green due to the emission spectrum peak wavelength of FITC (519 nm). CD24 positive cells, conjugated with PE, were red with an emission peak wavelength of 573 nm. In this preliminary analysis of MCF7, the purity of the CD44⁺/CD24⁻/low cell population in 2D culture was 58.76% (Figure 7b).

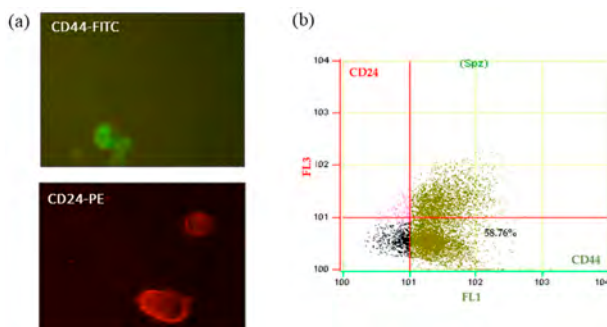


Figure 7. Expression of CD44 and CD24 cell surface markers on MCF7 2D cultured cells. (a) Confocal microscopy images of MCF7 cells marked with antibody CD24 and CD44 (Green: CD44-FITC; Red: CD24-PE); (b) flow cytometric analysis of CD24 and CD44 surface markers in MCF-7 cells from 2D culture system. Abbreviations: FITC, fluorescein isothiocyanate; PE, phycoerythrin.

These preliminary results in 2D culture conditions might be useful in future studies characterizing the CSC subpopulation (CD44⁺/CD24⁻/low phenotype) generated in 3D scaffolds. Based on our literature review, we expect to observe an increase in CD44⁺/CD24⁻/low cells in breast cancer cells cultured in PCL scaffolds.

3. Discussion

CSCs have one of the most important roles in cancer and, for this reason, they must be specifically removed for a successful therapy. It has been reported that their frequency in primary tumors is correlated with the extent of tumor invasion and metastasis and, in turn, patients' prognosis [1,2,18,19]. Therefore, their study has acquired great importance in recent years but it has been limited by the lack of physiologically relevant culture methods. Two-dimensional *in vitro* cell culture has been used in cancer research for many years. This monolayer culture can produce alterations in cell morphology and gene expression compared with those grown *in vivo* [10]. Tridimensional cell culture gives a more accurate morphological representation of tumor development and physiological environment.

PCL scaffolds have been manufactured to test the cell adhesion efficiency of an MCF7 breast cancer cell line. The fabrication parameters used for PCL scaffold production show similar values to other studies. Domingos *et al.* set up a printing temperature of 80 °C, 10 mm/s velocity, and a layer height of 0.28 mm [20]. This combination of parameters generated meshes similar to the scaffolds used in this study. Furthermore, the effect of design parameter was evaluated through breast cancer cell culture in the current work.

MCF7 culture in scaffolds showed the importance of the deposition angle in cell attachment and cell growth. The two scaffold designs with greater efficiency for cell culture, 45° and 60°, had smaller pore size and different pore shape compared with the 90° one. These results can be compared to those of Domingos *et al.*, who cultured a subtype of CSCs, the hMSCs (human Mesenchymal Stem Cells), in PCL scaffolds with different angle designs of 90°, 45°, and 60°. Their results showed more attached cells in 60° scaffolds than 45°, confirming the own results. However, they presented the 90° scaffold as optimal for cell culture with the highest values of cell adhesion. They showed that a higher deposition angle provides more space for cells to attach and proliferate [20]. The difference with the results obtained in the present assay may be due to the cell line studied. Specific cells require a different pore size for optimal attachment, growth, and motility [21]. Cell attachment is a complex process, affected by numerous aspects such as cell behavior, material surface properties, and environmental factors.

In the current study, the efficiency of cell adhesion to the scaffolds has been evaluated based on the use of adherent and non-adherent wells. Polystyrene of the cell culture microplate was specifically treated to facilitate cell attachment. For non-adherent wells a commonly utilized polymer named poly(2-hydroxyethyl methacrylate) (pHEMA) has been used [22]. Once dried in the bottom of the well, it has neutral charge and is highly hydrophobic, avoiding cell attachment. Higher cell adhesion was observed on the scaffolds placed on non-adherent surfaces compared to the scaffolds on adherent plates. Blocking polystyrene treatment from adding pHEMA increased cell attachment in the PCL scaffolds. In consequence, cells only had the possibility of attaching to the PCL filaments of the scaffolds.

Tridimensional PCL fibrous scaffolds may offer an attractive alternative to culturing and propagating CSCs *in vitro*. In this study, it has been shown that tumor cells cultured in a 3D system displayed a significantly higher capacity to form mammospheres compared to the 2D control, revealing CSCs enrichment. The use of adherent and non-adherent wells did not affect the MFI. This variable has only altered the cells' attachment to the scaffold rather than their ability to form mammospheres. Sims-Mourtada *et al.* and Feng *et al.* also showed a significant increase in the mammospheres formation index after scaffolds' culture. In both works, the MFI after 3D culture was double the value obtained in 2D conditions. Sims-Mourtada *et al.* published that the MFI increase in a 3D culture was due to the differentiation inhibition of CSCs, since they did not observe an increase of the rate proliferation [23]. The second author suggested that CSCs' enrichment was on account of the epithelial–mesenchymal transition (EMT), which can trigger the transformation of cancer cells to CSCs [15]. Others studies

indicated that the malignant phenotype of cancer cells was also dramatically reduced when cells were transferred from *in vivo* conditions to 2D cell culture plates [24,25].

An important feature of breast cancer stem cells is the expression of the surface markers CD44 and CD24. Flow cytometry can be a powerful methodology to discriminate between populations and, therefore, determine the percentage of the CD44⁺/CD24⁻/low cells. The CSCs' expansion due to tridimensional scaffold culture can be monitored in this way. At this point, staining and flow cytometry protocols for MCF7 cells have been developed.

Taken together, the presented results suggest that a 3D PCL scaffold culture spurred MCF7 cells to generate a cell population with CSC properties. Nevertheless, additional experiments are being developed with flow cytometry to determine the percentage of phenotype CD44⁺/CD24⁻/low as well as the analysis of the expression of genes related to epithelial–mesenchymal transition (EMT) expression. All of these assays are mandatory to characterize the population cells enriched in 3D PCL scaffolds, to study CSC properties, and to screen for new therapeutic agents targeting cancer stem cell populations.

4. Materials and Methods

4.1. Design and Manufacture of Scaffolds

4.1.1. Filament

A 3 mm poly(ϵ -caprolactone) (PCL) wire (Perstorp, Malmö, Sweden) was used to manufacture the scaffolds. PCL has properties for tissue engineering with good mechanical characteristics, established biocompatibility, and relatively long-term biodegradability; it is also free of toxic dyes [12].

4.1.2. 3D Printer Machine and Software

A three-dimensional RepRap BCN3D+ printer (Barcelona, Spain) was chosen to produce 3D scaffolds due to its open-source and modular related features. The machine has the capability to be modified and optimized by the user. This characteristic enable to print accurate geometric structures and reproducible scaffolds designs [11,26]. This printer used the Fused Filament Fabrication (FFF) technology, or so-called Fused Deposition Modeling (FDM), consisting of the deposition of the fused material in successive layers.

The designs of the scaffolds were performed with the computer-aided design (CAD) modeling software SolidWorks. The constructions were saved in STL file formats and transferred to Slic3r, computer-aided manufacturing (CAM) software, to establish the manufacturing parameters. Finally, this program generates G-code files capable of controlling the printer's movements.

Design and manufacturing parameters were optimized for PCL and RepRap BCN3D+. Design parameters were established considering the scaffolds' use in cell culture microplates with 12 wells (Table 2). Manufacturing parameters were determined in order to print the scaffolds efficiently and suitably for cell culture (Table 3). Both parameters were optimized by following a sequential flowchart.

Table 2. Design parameters and the corresponding optimized values.

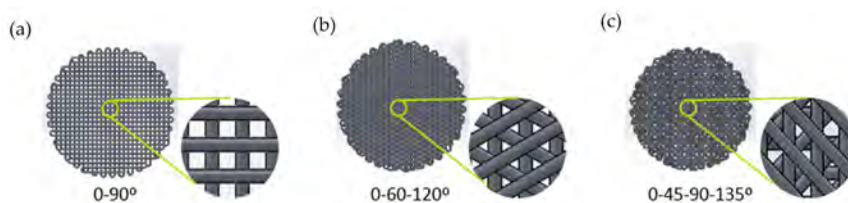
Design Parameters	Optimal Values
Diameter	19 mm
Shape	Round
Number of layers	8
Distance between filaments	0.7 mm
Gap distance	0.4 mm
Deposition angle	90°, 45°, 60°
Filament diameter	0.30 mm

Table 3. Manufacturing parameters and the corresponding optimized values.

Manufacturing Parameters	Optimal Values
Deposition velocity	10 mm/s
Layer height	0.30 mm
Extrusion temperature	85 °C
Bed temperature	35 °C

4.1.3. Deposition Angle Designs

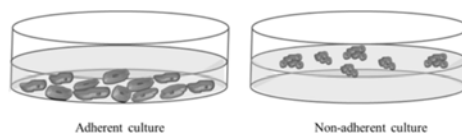
Three different scaffold designs have been performed with variable deposition angles, taking the values of 90°, 45°, and 60° (Figure 8). The variation of the angle of deposition between layers results in a different pore size and shape between the scaffolds (Table 4), which makes cell culture suitable or not.

**Figure 8.** Scaffolds designs with different deposition angles: (a) 90°; (b) 60°; (c) 45°.**Table 4.** Pore characteristics depending on the deposition angle.

Deposition Angles	Pores Shape	Area
90°	Square	0.15 mm ²
45°	Six variable forms (triangles and irregular polygons)	1.98×10^{-4} to 0.13 mm ²
60°	Equilateral triangle	0.1256 mm ²

4.2. Adherent and Non-Adherent Cultures

To study the effects of the well plate's surface conditions (adherent *versus* non-adherent) on cell seeding efficiency and the subsequent enrichment of cancer stem cells in 3D PCL scaffolds, 12 multi-well surface plates were tested. The adherent surface conditions were tested in standard 12-well culture microplates. Non-adherent conditions were assayed with 12-well cell culture microplates treated with a hydrophobic and neutral charge polymer, poly(2-hydroxyethyl methacrylate) (pHEMA; Sigma Aldrich Co. LLC., St. Louis, MO, USA) (Figure 9). Non-adherent microplates covered with pHEMA were dried at 45 °C overnight and exposed to UV light for 20 min. The PCL scaffolds were divided in two groups and placed into the individual wells of adherent and non-adherent plates.

**Figure 9.** Schematic representation of adherent and non-adherent culture.

4.3. Cell Culture

MCF-7 breast carcinoma cells (Figure 10) were obtained from the American Type Culture Collection (ATCC, Rockville, MD, USA). MCF-7, is a HER2-positive cell line—a type of breast cancer that overexpresses Human Epidermal Growth Factor Receptor 2. Previous studies evaluated the biocompatibility of the scaffold with an MCF7 cell line [15,23].

Cells were cultured in Dulbecco's Modified Eagle's Medium (Gibco, Waltham, MA, USA) supplemented with 10% fetal bovine serum, 1% L-glutamine, 1% sodium pyruvate, 50 U/mL penicillin, and 50 µg/mL streptomycin (HyClone, Logan, UT, USA). Cells were maintained at 37 °C and 5% CO₂ atmosphere.

Conventional cell culture was performed to study the cell proliferation in the different scaffold designs. For this reason, the medium was supplemented with nutrients and metabolites needed for the growth and proliferation of a vast majority of cancer cells, including MCF7.



Figure 10. MCF7 cell line in 2D adherent culture.

4.4. Cell Culture in Scaffolds

4.4.1. Scaffold Sterilization

Scaffolds were sterilized with 70% ethanol/water solution overnight, washed with PBS (Gibco, Waltham, MA, USA), and finally exposed to UV light for 90 min.

4.4.2. Cell Culture in Scaffolds

Scaffolds were placed into a 12-well cell culture microplate. First, 250 µL of cell suspension containing 100,000 cells were placed in the middle of its surface to allow cells to attach to the scaffold. After a 3 h incubation period, 1.5 mL of fresh medium were added to cover the scaffold (Figure 11). Cells were incubated for 72 h and then counted.

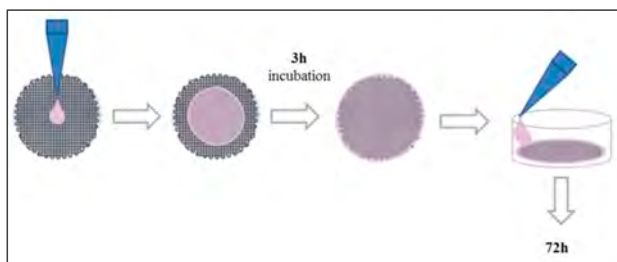


Figure 11. Cell seeding protocol on PCL scaffolds.

4.4.3. Trypsinization and Cell Counting

The culture medium was removed with a micropipette. Then scaffolds were placed in new wells to quantify only the attached cells; they were washed with PBS and 1 mL of trypsin was added. After incubation, 2.5 mL of fresh medium were added and cell suspension was collected and centrifuged at 1500 rpm for 5 min. Finally, cells from the pellet were counted. The same procedure was done to obtain the number of cells attached at the bottom of the well. Cells were counted using a Neubauer Chamber (Marienfeld-Superior, Lauda-Königshofen, Germany) and an inverted optical microscope. Trypan blue solution was used to assess cell viability. This test measured the amount of viable cells, based on the concept that viable cells have an intact membrane and trypan blue cannot be incorporated. Dead cells have an altered membrane and take up the dye.

4.5. Mammosphere-Forming Assay

In order to evaluate CSC population, the mammosphere-forming technique was performed (Figure 12) as previously described [8]. Cells from 2D culture or 3D scaffolds were removed and re-suspended with DMEM/F12 medium supplemented with B27, EGF, and FGF (20 ng/mL), 1% L-glutamine, 1% sodium pyruvate, 25 U/mL penicillin, and 25 µM/mL streptomycin. Re-suspended cells were seeded into a six-well Cell Culture Microplate (Corning Life Sciences, New York, NY, USA) coated with pHEMA (Sigma Aldrich Co. LLC.) at a density of 2000 cells/well. Finally, cells were incubated for seven days and mammospheres bigger than 50 µm were counted using an inverted optical microscopy. The Mammosphere Forming Index (MFI) was calculated using the formula described below:

$$MFI = \frac{N^{\circ} \text{ mammospheres}}{N^{\circ} \text{ seeded cells}} \times 100 \quad (1)$$

It is necessary to evaluate a subpopulation (CSCs) of a heterogeneous cell sample. This subpopulation is composed of undifferentiated cells with self-renewal characteristics. They are related to tumor initiation and they are capable of growth in suspension. For that reason, we used different medium supplements such as B27 (contains critical factors for cell survival and growth, excluding the use of serum), EGF, and FGF (growth factors). These are the culture conditions appropriate for allowing the growth and self-renewal of the CSCs.

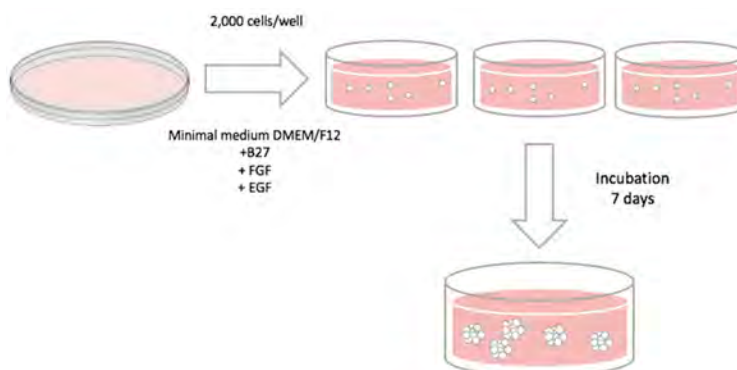


Figure 12. Mammosphere-forming assay protocol.

4.6. Flow Cytometry Analysis

MCF7 cell growth on the polystyrene dishes was trypsinized as described above. Cells were re-suspended at a density of 1×10^5 cells/mL in 25 µL of phosphate-buffer saline containing 2% of

fetal bovine serum and blocked with human blocking reagent (Milteny Biotec, Bergisch Gladbach, Germany) for 10 min at 4 °C. Cells were stained with phycoerythrin-conjugated CD44 and fluorescein isothiocyanate-conjugated CD24 (BD Pharmingen, Franklin Lakes, NJ, USA) for 30 min at 4 °C in dark. After washing, cells were re-suspended in a phosphate buffer containing 2% FBS and stained with 7AAD (BD Pharmingen) for 10 min at 4 °C. Samples were analyzed on a fluorescence-activated cell sorting Cell Laboratory QuantaSCTM cytometer (Beckman Coulter, Fullerton, CA, USA). Compensation was performed with single-stained cells to decrease overlaps of fluorophore emission spectrums.

4.7. Statistical Analysis

All data are expressed as mean \pm standard error (SE). Data were analyzed by Student *t* test. Statistical significant levels were $p < 0.05$.

5. Conclusions

In the present study, different scaffold designs and culture parameters were tested on a breast cancer MCF7 cell line. Design of 60° and non-adherent conditions showed the highest cell counting after treatment with trypsin. CSC population was enriched in a tridimensional cell culture with 60° PCL scaffolds compared to the 2D culture control, increasing their MFI. The development of the flow cytometry analysis provides the basis for further studies to investigate CSC properties, as well as to screen new therapeutic agents targeting cancer stem cell populations. Using 3D culture, the total cell number will increase significantly and so will the CSC subpopulation. Then, we will perform cellular and molecular experiments to characterize the CSC population in order to find new therapeutic strategies against stem cells.

PCL scaffolds built with 3D printing machines revealed good results for cell cultures. Optimization of scaffolds' porosity has been the key to cell growth and enrichment. This study suggests new criteria for enhancing bioprinting machines based on layer deposition.

Acknowledgments: This work was supported partially by Spanish grants from Fundación Ramón Areces, Instituto de Salud Carlos III (PI1400329) and Ministerio de Economía Y Competitividad (DPI2013-45201-P), and the support of the Catalanian government (2014SGR00868). The authors are grateful for the financial support from the University of Girona (MPCUdG2016/036). We are grateful to TechnoSperm from University of Girona (Girona, Spain) for their support in the flow cytometry analysis.

Author Contributions: Joaquim Ciurana and Teresa Puig conceived and designed the experiments; Sònia Palomeras and Marc Rabionet performed the experiments; Inés Ferrer, Ariadna Sarrats, and Maria Luisa Garcia-Romeu analyzed the data; Joaquim Ciurana and Teresa Puig contributed reagents/materials/analysis tools; Sònia Palomeras, Marc Rabionet, Joaquim Ciurana, and Teresa Puig wrote the paper.

Conflicts of Interest: The authors declare no conflict of interest. The founding sponsors had no role in the design of the study; in the collection, analyses, or interpretation of data; in the writing of the manuscript, and in the decision to publish the results.

Abbreviations

The following abbreviations are used in this manuscript:

2D	Two-dimensional
3D	Three-dimensional
7-AAD	7-AminoActinoMycin D
B27	B27 supplement
BC	Breast Cancer
CAD	Computer-Aided Design
CAM	Computer-Aided Manufacturing
CD24	Cluster of Differentiation 24
CD44	Cluster of Differentiation 44

CSCs	Cancer Stem Cells
DMEM	Dulbecco's Modified Eagle's Medium
DMEM/F12	Dulbecco's Modified Eagle's Medium Nutrient Mixture F-12
EGF	Epidermal Growth Factor
EMT	Epithelial–Mesenchymal Transition
FDM	Fused Deposition Modeling
FFF	Fused Filament Fabrication
FGF	Fibroblast Growth Factor
FITC	Fluorescein IsoThioCyanate
HER2	Human Epidermal growth Factor Receptor 2
hMSCs	Human Mesenchymal Stem Cells
MFC7	Michigan Cancer Foundation-7
MFI	Mammosphere Forming Index
PBS	Phosphate-Buffered Saline
PCL	Poly(ϵ -caprolactone)
PE	Phycocyanin
pHEMA	poly(2-HydroxyEthyl Methacrylate)

References

- Al-Hajj, M.; Wicha, M.S.; Benito-Hernandez, A.; Morrison, S.J.; Clarke, M.F. Prospective identification of tumorigenic breast cancer cells. *Proc. Natl. Acad. Sci. USA* **2003**, *100*, 3983–3988. [[CrossRef](#)] [[PubMed](#)]
- Velasco-Velázquez, M.A.; Homsí, N.; De La Fuente, M.; Pestell, R.G. Breast cancer stem cells. *Int. J. Biochem. Cell Biol.* **2012**, *44*, 573–577. [[CrossRef](#)] [[PubMed](#)]
- Diehn, M.; Cho, R.W.; Lobo, N.A.; Kalisky, T.; Dorie, M.J.; Kulp, A.N.; Qian, D.; Lam, J.S.; Ailles, L.E.; Wong, M.; *et al.* Association of reactive oxygen species levels and radioresistance in cancer stem cells. *Nature* **2009**, *458*, 780–783. [[CrossRef](#)] [[PubMed](#)]
- Li, X.; Lewis, M.T.; Huang, J.; Gutierrez, C.; Osborne, C.K.; Wu, M.F.; Hilsenbeck, S.G.; Pavlick, A.; Zhang, X.; Chamness, G.C.; *et al.* Intrinsic resistance of tumorigenic breast cancer cells to chemotherapy. *J. Natl. Cancer Inst.* **2008**, *100*, 672–679. [[CrossRef](#)] [[PubMed](#)]
- Reya, T.; Morrison, S.J.; Clarke, M.F.; Weissman, I.L. Stem cells, cancer, and cancer stem cells. *Nature* **2001**, *414*, 105–111. [[CrossRef](#)] [[PubMed](#)]
- Al-Hajj, M.; Clarke, M.F. Self-renewal and solid tumor stem cells. *Oncogene* **2004**, *23*, 7274–7282. [[CrossRef](#)] [[PubMed](#)]
- Dontu, G.; Abdallah, W.M.; Foley, J.M.; Jackson, K.W.; Clarke, M.F.; Kawamura, M.J.; Wicha, M.S. *In vitro* propagation and transcriptional profiling of human mammary stem/progenitor cells. *Genes Dev.* **2003**, *17*, 1253–1270. [[CrossRef](#)] [[PubMed](#)]
- Shaw, F.L.; Harrison, H.; Spence, K.; Ablett, M.P.; Simões, B.M.; Farnie, G.; Clarke, R.B. A detailed mammosphere assay protocol for the quantification of breast stem cell activity. *J. Mammary Gland Biol. Neoplas.* **2012**, *17*, 111–117. [[CrossRef](#)] [[PubMed](#)]
- Xu, F.; Burg, K.J.L. Three-dimensional polymeric systems for cancer cell studies. *Cytotechnology* **2007**, *54*, 135–143. [[CrossRef](#)] [[PubMed](#)]
- Hale, J.S.; Li, M.; Lathia, J.D. The malignant social network: Cell-cell adhesion and communication in cancer stem cells. *Cell Adhes. Migr.* **2012**, *6*, 346–355. [[CrossRef](#)] [[PubMed](#)]
- De Ciarana, J.; Serenó, L.; Vallès, È. Selecting process parameters in RepRap additive manufacturing system for PLA scaffolds manufacture. *Procedia CIRP* **2013**, *5*, 152–157. [[CrossRef](#)]
- Woodruff, M.A.; Huttmacher, D.W. The return of a forgotten polymer—Polycaprolactone in the 21st century. *Prog. Polym. Sci.* **2010**, *35*, 1217–1256. [[CrossRef](#)]
- Zhu, N.; Chen, X. Biofabrication of Tissue Scaffolds. In *Advances in Biomaterials Science and Biomedical Applications*; Pignatello, R., Ed.; InTech: Rijeka, Croatia, 2013.

14. Wang, H.; Vijayavenkataraman, S.; Wu, Y.; Shu, Z.; Sun, J.; Fuh Ying Hsi, J. Investigation of process parameters of electrohydro-dynamic jetting for 3D printed PCL fibrous scaffolds with complex geometries. *Int. J. Bioprint.* **2016**, *2*. [[CrossRef](#)]
15. Feng, S.; Duan, X.; Lo, P.-K.; Liu, S.; Liu, X.; Chen, H.; Wang, Q. Expansion of breast cancer stem cells with fibrous scaffolds. *Integr. Biol.* **2013**, *5*, 768–777. [[CrossRef](#)] [[PubMed](#)]
16. Chen, M.; Patra, P.K.; Warner, S.B.; Bhowmick, S. Role of fiber diameter in adhesion and proliferation of NIH 3T3 fibroblast on electrospun polycaprolactonecaffolds. *Tissue Eng.* **2007**, *13*, 579–587. [[CrossRef](#)] [[PubMed](#)]
17. Chen, M.; Michaud, H. Controlled vacuum seeding as a means of generating uniform cellular distribution in electrospun polycaprolactone (PCL) scaffolds. *J. Biomech. Eng.* **2016**, *131*, 1–8. [[CrossRef](#)] [[PubMed](#)]
18. Liu, H.; Patel, M.R.; Prescher, J.A.; Patsialou, A.; Qian, D.; Lin, J.; Wen, S.; Chang, Y.F.; Bachmann, M.H.; Shimono, Y.; *et al.* Cancerstem cells from human breast tumors are involved in spontaneous metastases in orthotopic mouse models. *Proc. Natl. Acad. Sci. USA* **2010**, *107*, 18115–18120. [[CrossRef](#)] [[PubMed](#)]
19. Velasco-velázquez, M.A.; Popov, V.M.; Lisanti, M.P.; Pestell, R.G. The role of breast cancer stem cells in metastasis and therapeutic implications. *Am. J. Pathol.* **2011**, *179*, 2–11. [[CrossRef](#)] [[PubMed](#)]
20. Domingos, M.; Intranuovo, F.; Russo, T.; De Santis, R.; Gloria, A.; Ambrosio, L.; Ciurana, J.; Bartolo, P. The first systematic analysis of 3D rapid prototyped poly(ϵ -caprolactone)caffolds manufactured through BioCell printing: the effect of poreize and geometry on compressive mechanical behaviour and *in vitro* hMSC viability. *Biofabrication* **2013**, *5*. [[CrossRef](#)] [[PubMed](#)]
21. Ranucci, C.S.; Kumar, A.; Batra, S.P.; Moghe P, V. Control of hepatocyte function on collagen foams: Sizing matrix pores toward elective induction of 2-D and 3-D cellular morphogenesis. *Biomaterials* **2000**, *21*, 783–793. [[CrossRef](#)]
22. Re, F.; Zanetti, A.; Sironi, M.; Polentarutti, N.; Lanfranccone, L.; Dejana, E.; Colotta, F. Inhibition of anchorage-dependent cell spreading triggers apoptosis in cultured human endothelial cells. *J. Cell Biol.* **1994**, *127*, 537–546. [[CrossRef](#)] [[PubMed](#)]
23. Sims-Mourtada, J.; Niamat, R.A.; Samuel, S.; Eskridge, C.; Kmiec, E.B. Enrichment of breast cancerstem-like cells by growth on electrospun polycaprolactone-chitosan nanofibercaffolds. *Int. J. Nanomed.* **2014**, *9*, 995–1003. [[CrossRef](#)] [[PubMed](#)]
24. Kim, J.B. Three-dimensional tissue culture models in cancer biology. *Semin. Cancer Biol.* **2005**, *15*, 365–377. [[CrossRef](#)] [[PubMed](#)]
25. Griffith, L.G.; Swartz, M.A. Capturing complex 3D tissue physiology *in vitro*. *Nat. Rev. Mol. Cell Biol.* **2006**, *7*, 211–225. [[CrossRef](#)] [[PubMed](#)]
26. Cruz Sanchez, F.A.; Boudaoud, H.; Muller, L.; Camargo, M. Towards a standard experimental protocol for open source additive manufacturing. *Virtual Phys. Prototyp.* **2014**, *9*, 151–167. [[CrossRef](#)]

Sample Availability: Samples of the compounds are not available from the authors.



© 2016 by the authors; licensee MDPI, Basel, Switzerland. This article is an open access article distributed under the terms and conditions of the Creative Commons Attribution (CC-BY) license (<http://creativecommons.org/licenses/by/4.0/>).

CHAPTER 4 Results II

Use and optimization of electrospinning technology to manufacture PCL scaffolds for 3D cell culture and stemness expansion

This chapter is based on the following publication:

Title	Electrospinning parameters selection to manufacture polycaprolactone scaffolds for three-dimensional breast cancer cell culture and enrichment (Proceeding)
Authors	Marc Rabionet, Teresa Puig*, Joaquim Ciurana*
Journal	Procedia CIRP
Publication year	2017
CiteScore <small>2017</small>	2.4 (74 th percentile in Industrial and Manufacturing Engineering; position 85 of 328)
DOI	10.1016/j.procir.2017.03.341

* Corresponding author

Abstract

Despite the suitability of fused filament fabrication (FFF) scaffolds for breast cancer 3D culture and stemness maintenance, more efforts are done to create structures with more resemblance to the physiological surroundings. In these settings, electrospinning (ES) technology has emerged in the field due to its capability of producing nanofilaments, similar to the native fibrous proteins present in the extracellular matrix (ECM).

Chapter 4 aims to explore the feasibility of an ES apparatus to produce poly(ϵ -caprolactone) (PCL) ECM-like scaffolds for 3D cell culture applications and stemness maintenance. Therefore, a solution of PCL and acetone was electrospun and various fabrication parameters were analyzed, including polymer solution flow rate and applied voltage. Several emitter tip images were captured to monitor and evaluate the electrospinning process. Two different ES scaffolds were produced varying the initial PCL concentration, being 7.5 and 15% w/v the two values chosen. Produced scaffolds were cultured with the breast cancer reference model MCF-7. Cell proliferation within the two scaffold models were analyzed through MTT assay. Lastly, a mammosphere forming assay was performed to study the effect of ES scaffold culture on the breast cancer stem cell (BCSC) subpopulation.

Results showed that a voltage of 7 kV and a flow rate of 6 mL/h enabled a stable and continuous production of electrospun nanofibers. The production of the two scaffold models was achieved. Meshes from 7.5% PCL solution displayed lower cell proliferation compared with 15% scaffolds. Interestingly, MCF-7 cells cultured in both models presented a higher mammosphere forming index compared with 2D control, thus indicating a BCSC expansion.



3rd CIRP Conference on BioManufacturing

Electrospinning parameters selection to manufacture polycaprolactone scaffolds for three-dimensional breast cancer cell culture and enrichment

Marc Rabionet^{a,b}, Teresa Puig^{a*}, Joaquim Ciurana^{b*}

^aOncology Unit (TargetsLab), Department of Medical Sciences - Faculty of Medicine - University of Girona, Emili Grahit 77, 17003 Girona, Spain

^bDepartment of Mechanical Engineering and Industrial Construction - University of Girona, Maria Aurèlia Capmany 61, 17003 Girona, Spain

* Corresponding author. Tel.: +34 972418265; fax: +34 972418098. E-mail address: teresa.puig@udg.edu, quim.ciurana@udg.edu

Abstract

Only a small cell population of a breast tumour presents stem cell characteristics, thus so-called breast cancer stem cells (BCSCs). BCSCs are tumour-initiating cells and chemoresistant and they can grow in non-adherent conditions as mammospheres. Study of BCSCs is a challenge due to their low representation and the inability to propagate them without inducing differentiation. Previous studies have demonstrated that three-dimensional (3D) cell culture models such as scaffolds enhance the BCSCs population.

In this project, scaffolds were fabricated by electrospinning technology. Specific values of voltage and flow rate were fixed to electrospun 7.5 and 15% poly(ϵ -caprolactone) (PCL) solutions according to process stability. Both scaffolds were seeded with MCF-7 breast cancer cells and 7.5% meshes displayed lower cell proliferation compared with 15% scaffolds. Cells cultured in both scaffolds presented a significant Mammosphere Forming Index (MFI) increase, thus indicating a BCSCs enrichment.

Results show that three-dimensional cell culture with electrospun 15% PCL scaffolds could be useful to expand BCSCs population facilitating the future development of new therapeutic strategies against this tumour subpopulation.

© 2016 The Authors. Published by Elsevier B.V. This is an open access article under the CC BY-NC-ND license (<http://creativecommons.org/licenses/by-nc-nd/4.0/>).

Peer-review under responsibility of the scientific committee of the 3rd CIRP Conference on BioManufacturing 2017

Keywords: Electrospinning; process parameters; PCL; scaffolds; cell culture

1. Introduction

Breast cancer is the most common tumour diagnosed among women excluding skin cancer. It has been estimated to account for the 28.3% of all new female carcinomas and the 16.8% of female cancer deaths in Europe during 2012 [1]. In addition, tumour relapse occurs in 30% of early-stage breast cancer [2] and it stands for the main cause of deaths related to mammary tumours [3].

Different studies have focused on understanding the heterogeneous nature of tumours, such as breast cancer. It is demonstrated that a small cell population is responsible for tumour initiation and progression. These cells possess several characteristics similar to mammary stem cells, thus termed Breast Cancer Stem Cells (BCSCs) [4,5]. This subpopulation has the ability to undergo self-renewal and differentiate into non-stem breast cancer cells. Furthermore, they are capable of

growing in suspension and surviving as non-adherent spheres, termed mammospheres [6,7]. BCSCs can be identified and isolated due to their expression pattern of cells' surface markers such as CD44 and CD24 [5], and their increased activity of the aldehyde dehydrogenase (ALDH) enzyme [8]. Different investigations revealed their radio- [9] and chemoresistance [10] favouring tumour recurrence and metastasis [11]. Thereby, their study is essential to identify new therapeutic targets against cancer stem cell population. However, it has been limited by the inability to propagate them without inducing their differentiation [12] and their low representation within the tumour [5] or cell line [13].

Traditionally, cancer cell culture is performed within two-dimensional (2D) surroundings, providing a quick and cheap way to study their properties *in vitro*. In contrast, 2D systems differ from the *in vivo* environment and cells can only grow in monolayer. Cytoskeleton remodelling caused by cell

flattening modifies the gene expression and protein [14,15]. Therefore, experiments performed in 2D can not be representative of the physiological cell behaviour leading to, for example, CSCs differentiation [16]. Three-dimensional (3D) cell models simulate the extracellular matrix and maintain the tissue organization. One of the 3D culture systems are the scaffolds, three-dimensional structures mostly made of biopolymeric material such as poly(ϵ -caprolactone) (PCL). Cells can establish interactions with polymeric filaments and with adjacent cells, maintaining their *in vivo* function and increasing their intracellular signalling. Previous studies demonstrated that 3D culture with scaffolds produced a BCSCs increase [17–19].

Different methodologies are used to produce scaffolds. The Fused Filament Fabrication (FFF) offers a simple and viable way to manufacture these structures. This additive manufacturing technology, widely used by 3D printers [20] and prototypes [21,22], consists on the deposition of the fused material in successive layers. With this procedure, micrometric filaments can be achieved but production of thinner fibres is problematic. Electrospinning is a technology capable of producing nanometric filaments, also used as drug delivery systems [23]. In this technique, polymer is dissolved and placed in a syringe connected to a metallic needle. A high voltage is applied to the biopolymer fluid so the solution droplet becomes charged. When the electric force overcomes the surface tension, a stream of liquid is ejected. This charged structure, called Taylor cone, enables de continuous production of polymer filaments from the needle to the ground collector. When this process is done, the solvent evaporates and nanofibres are randomly formed in the collector.

A preceding study of our research group showed a BCSCs expansion after 3D culture with FFF scaffolds [24–26] and other groups demonstrated this enrichment using electrospun scaffolds [17–19]. The present study has focused on the characterization of electrospinning process and produced PCL scaffolds. Different scaffolds and culture conditions have been tested to improve three-dimensional breast cancer cell proliferation. The final objective of this work is to evaluate the impact of 3D cell culture on BCSCs population. According to the background, three-dimensional cell culture with electrospun scaffolds can be a useful way to enrich BCSCs for developing new therapeutic strategies to target this malignant population.

2. Materials and Methods

2.1. Scaffolds Manufacture

Poly(ϵ -caprolactone) (PCL; Sigma-Aldrich, St. Louis, MO, USA) was dissolved in acetone (PanReac AppliChem, Gatersleben, Germany) to obtain 7.5 and 15% w/v PCL concentrations. An electrospinning apparatus (Spraybase, Dublin, Ireland) connected to a 18G needle was used to produce scaffolds. PCL solution was supplied to the emitter with a flow rate controlled by the Syringe Pump Pro software (New Era Pump Systems, Farmingdale, NY, USA) and different voltages were applied. Distance between emitter and collector was fixed at 15 cm. Room relative humidity and

temperature were fixed at 55–60% and 20°C, respectively, to avoid solvent evaporation. Emitter tip images were captured with a Chamaleon camera (Point Grey Research, Richmond, BC, Canada). Process was stopped when 5 mL of solution were ejected. Then scaffolds were cut into squares of 16 mm to allow their use in 12-wells cell culture microplates.

2.2. Scaffolds Characterization

Scaffolds weight and thickness were measured with an analytical balance (Sartorius, Göttingen, Germany) and a digital micrometer (Mahr GmbH, Göttingen, Germany), respectively. Six specimens from three different batches were evaluated to calculate the average value.

2.3. Cell Line

MCF-7 breast cancer cell line was obtained from the American Type Culture Collection (ATCC; Rockville, MD, USA). Cells were cultured in Dulbecco's Modified Eagle's Medium (DMEM; Gibco, Waltham, MA, USA) supplemented with 10% fetal bovine serum, 1% L-glutamine, 1% sodium pyruvate, 50 U/mL penicillin, and 50 μ g/mL streptomycin (HyClone, Logan, UT, USA). Cells were maintained in a 5% CO₂ humidified incubator at 37°C.

2.4. Three-Dimensional Cell Culture

Scaffolds were sterilized with 70% ethanol/water solution overnight, washed with PBS (Gibco) and exposed to UV light for 30 min. Then scaffolds were placed in 12-well non-adherent cell culture microplates (Sartstedt, Nümbrecht, Germany). Cell densities of 50 000, 100 000 and 300 000 cells/well were prepared in 50 μ L volume. Cell suspension was pipetted onto the scaffold centre. After 3 hours' incubation, 1.5 mL of medium was added. Two-dimensional controls with same cell densities were performed.

2.5. Cell Proliferation Assay

The (3-(4,5-dimethylthiazolyl-2)-2,5-diphenyltetrazolium bromide) (MTT) assay was used to test cell proliferation. MTT is a yellow tetrazolium salt which can be reduced by metabolically active cells resulting in water-insoluble purple crystals of formazan. The formazan crystals can be solubilized by dimethyl sulfoxide (DMSO) into a colored solution. Therefore, the absorbance of formazan solution is directly related to the initial cell amount.

Thus, scaffolds were washed with PBS and put into new wells. They were incubated with 1 mL medium and 100 μ L MTT (Sigma-Aldrich) for 2 h 30 min. Formazan crystals were dissolved with 1 mL DMSO. Four 100 μ L aliquots from each well were pipetted into a 96-well plate and placed into a microplate reader (Bio-Rad, Hercules, CA, USA). Absorbance was measured at 570 nm.

2.6. Mammosphere-Forming Assay

Cells from 2D culture and scaffolds were trypsinized and suspended with DMEM/F12 medium (HyClone) supplemented with B27 (Gibco), EGF and FGF (20 ng/mL; Miltenyi Biotec, Bergisch Gladbach, Germany), 1% L-glutamine and 1% sodium pyruvate. Suspended cells were seeded into a 6-well non-adherent cell culture microplate (Sarstedt) at a density of 2000 cells/well. Cells were incubated for 7 days and mammospheres bigger than 50 μ m were counted. Mammosphere Forming Index (MFI) was calculated using the formula described below (1).

$$MFI (\%) = \frac{n^{\circ} \text{mammospheres}}{n^{\circ} \text{seeded cells}} \times 100 \quad (1)$$

2.7. Statistical Analysis

All data are expressed as mean \pm standard error (SE). Data were analysed by Student t test. Statistical significant levels were $p < 0.05$ (denoted as *), $p < 0.01$ (**) and $p < 0.001$ (***)

3. Results

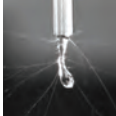


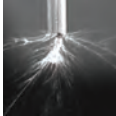
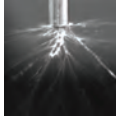







Electrospinning is a technology highly influenced by fabrication parameters such as polymer concentration, applied voltage and polymer solution flow rate. Literature shows a wide range of electrospun specifications [17–19,27–29]. Therefore, different parameters values were tested to reach a stable Taylor cone and a steady stream (Figure 1).

Poly(ϵ -caprolactone) (PCL) and acetone were chosen as biopolymer and non-toxic solvent, respectively. Two different concentrations of 7.5 and 15% PCL were produced and voltages of 7 and 15 kV were applied to analyse Taylor cone formation. Polymer fluid was supplied with flow rates of 1, 3 and 6 mL/h. Images from needle tip were taken 90 seconds after process beginning, shown in Table 1.

In all conditions, the polymeric solution droplet solidified once exposed to air, producing a stalactite-like form. These structures were also produced with different room humidity (50–60%) and temperature values (19–25°C) (data not shown). Only the stream located at the end of this structure was functional. The other ones, produced by the voltage, remained as solidified PCL filaments. Voltage of 15 kV produced unstable Taylor cones and a higher number of non-functional streams in all tested parameters instead of 7 kV. Flow rate was also related to droplet morphology. Higher speeds exhibited thicker structures with few non-functional streams, remaining the Taylor cone stable. Both polymer concentrations presented a similar trend during screening. However, 15% PCL solution showed thicker stalactite-like structures in response to the high amount of polymer.

As the main aim is to obtain a stable Taylor cone and produce continuous filaments, voltage of 7 kV and flow rate of 6 mL/h were selected to produce scaffolds suitable for 3D cell culture. Both PCL concentrations (7.5 and 15%) were chosen to test different scaffolds. Considering electrospinning background, polymer concentration is directly related to fibre morphology [30]. Hence, two different meshes can be evaluated through 3D cell culture and BCSCs enrichment.

Table 1. Taylor cone formation of PCL-acetone solutions under different electrospinning parameters (PCL concentration, flow rate and applied voltage). Emitter tip images were taken 90 seconds after electrospinning start.

[PCL]	7.5% w/v		
	1 mL/h	3 mL/h	6 mL/h
7 kV			
15 kV			
[PCL]	15% w/v		
	1 mL/h	3 mL/h	6 mL/h
7 kV			
15 kV			

A 5 mL PCL solution volume was processed with electrospinning thus a membrane made of filaments was obtained. The PCL film was cut with squares shapes of 16 mm to obtain final scaffolds (Figure 1). Specimens weight and thickness were measured to perform a macroscopic characterization. Weight and thickness values from different electrospinning processes did not statistically differ, with p -values ranging from 0.16 to 0.98 (data not shown). Grouped data is presented in Table 2. Scaffolds of 7.5% PCL solution were less heavy ($p = 8.86 \times 10^{-28}$) and thinner ($p = 3.94 \times 10^{-7}$) than 15% ones, in agreement with the PCL amount in each solution.

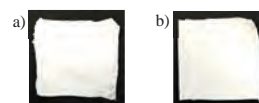


Figure 1. Electrospun scaffolds cut into squares of 16 mm side from 7.5% (a) and 15% w/v PCL solution (b).

Table 2. Macroscopic characterization of 7.5 and 15% electrospun PCL scaffolds (7 kV, 6 mL/h) after cutting them into 16 mm squares. Values are expressed as mean \pm standard error.

	7.5% PCL	15% PCL
Weight (mg)	6.71 \pm 0.17	14.11 \pm 0.30
Thickness (μ m)	147.22 \pm 5.00	196 \pm 4.65

Scaffolds were tested with 3D culture of MCF-7 breast cancer cells. Sterilized scaffolds were placed in non-adherent 12-well microplates. Meshes were seeded with three different cell densities (50 000, 100 000 and 300 000 cells) and incubated during 3 days. After incubation, MTT cell proliferation assay was carried out (Figure 2). In all culture conditions, 15% scaffolds showed a significant increase in cell proliferation compared with 7.5% specimens. Scaffolds exhibited major cell efficiency when seeded with low cell density (50 000 cells) compared with 2D control. Both scaffolds seeded with 100 000 cells showed significant reductions in normalized cell proliferation ($p=5.48 \times 10^{-3}$ for 7.5% specimens and $p=5.90 \times 10^{-3}$ for 15%) compared with 50 000 cells. Scaffolds from 15% PCL solution incubated with 300 000 cells also exhibited significant decreased efficiency ($p=5.11 \times 10^{-3}$) compared with low cell density.

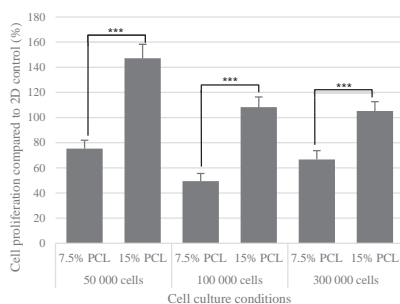


Figure 2. Cell proliferation analysis after 3 culture days of 7.5 and 15% PCL scaffolds seeded with three different cell densities. Adherent 2D control was also performed with same culture conditions. Statistical significant level was $p < 0.001$ (***)

Mammosphere forming assay was performed to study the effect of 3D cell culture on BCSCs population (Figure 3). BCSCs can survive and proliferate in non-adherent surfaces, forming spherical colonies called mammospheres. Therefore, mammospheres number is a correlate of BCSCs abundance in the sample [6,7]. Cells previously cultured in 2D and 3D models were seeded in non-adherent microplates. After 7 days' incubation, mammospheres were visualized and counted. Mammospheres from cells cultured in 2D and 3D did not display different morphology (Figure 3a-c). Regarding mammospheres number, 3D cultured cells showed a significant higher Mammosphere Forming Index (MFI) compared with 2D cultured ones (Figure 3d), indicating a BCSCs enrichment. Both scaffolds exhibited similar MFI values, with a 3-fold increase compared with the control.

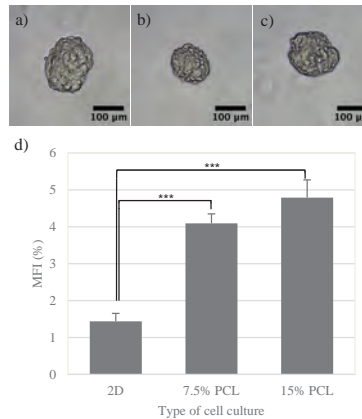


Figure 3. Mammosphere forming assay. (a-c) Mammosphere images from 2D cultured cells (a), 3D cultured with 7.5% PCL scaffolds (b) and 3D cultured with 15% PCL scaffolds (c). (d) Mammosphere Forming Index (MFI) of MCF-7 cells after 2D and 3D culture. Statistical significant level was $p < 0.001$ (***)

4. Discussion

Voltage, flow rate and PCL concentration values were tested to achieve a stable Taylor cone (Table 1). In all screening tests, PCL solution partially solidified producing a stalactite-like form. Apparently, acetone was evaporated due to its high volatility producing this lengthened formation at the needle tip. Some authors electrospun PCL-acetone solution, but solvent evaporation in the emitter tip was not mentioned as Taylor cone structure was not studied [27–29, 31]. Low voltage of 7 kV and high flow rate of 6 mL/h produced a more stable Taylor cone. Relation between applied electric field and droplet morphology was superficially studied by Zong et al. using polylactic acid (PLA) dissolved in dimethyl formamide (DMF). They assumed that high voltage removed quickly the solution droplet from the tip. Thus, the droplet became smaller and the Taylor cone oscillated due to the high voltage. The same authors indicated the existence of a minimum solution volume available in the needle tip to reach a steady Taylor cone [32]. However, fewer differences were observed in droplet morphology varying flow rate parameter compared with voltage.

Scaffolds weight and thickness were presented in Table 2. Values of scaffolds from different electrospinning processes did not present significant differences demonstrating reproducibility between batches in regard to physical characterization. Furthermore, macroscopic characterization results were in agreement with PCL amount in each solution, being the 7.5% scaffold weight the half than 15% specimen.

Scaffolds from 15% PCL solution displayed a significant cell proliferation increase in all cell densities compared with

7.5% meshes (Figure 2). In summary, cells showed higher growth kinetics in scaffolds from higher PCL concentration. Opposed to these results, a human cancer cell study asserted that higher cell proliferations can be obtained with small fibres diameters from low biopolymer concentration scaffolds [33]. Cell proliferation differences can be attributed to filament framework characteristics. It was demonstrated that low PCL concentration resulted in meshes with spherical structures made by non-filamented polymer, called beads. The presence of beads led to fibroblast proliferation decrease [28, 31]. Moreover, other variables such as porosity and morphology could directly affect cell adhesion and proliferation. Regarding cell density, both scaffolds presented higher normalized cell efficiency at 50 000 seeded cells (Figure 2). Cell viability in scaffolds was proven to be influenced by initial cell amount [34]. Proliferating cells narrow the pores space, decreasing oxygen and nutrient diffusivity [35]. Thus, cell densities of 100 000 and 300 000 cells appeared slightly larger to allow a perfect mass exchange.

Cells cultured in 7.5 and 15% scaffolds exhibited a 3-fold increased MFI compared with cells cultured in monolayer (Figure 3). Both meshes showed similar MFI values while 15% PCL scaffolds presented a significant increased cell proliferation. As mentioned above, differences on their structure can explain the contrast of cell proliferation. Although these characteristics, both scaffolds provide a three-dimensional environment. This fact allows the cell to establish interactions with filaments in different plans of the space, enabling the cytoskeleton reorganization and gene expression regulation.

Regarding CSCs expansion, Feng et al. published a 2-fold MFI increase with MCF-7 cells cultured in electrospun PCL scaffolds [17]. These authors also noticed that 3D culture enhanced EMT markers expression and cell invasion. Relation between scaffolds culture and EMT was previously reported by Saha et al. H605 mouse mammary tumour cells showed higher expression of EMT markers when cultured in electrospun PCL fibers. Authors established that H605 cells cultured in scaffolds underwent EMT-like transitions [18]. In addition, Sims-Mourtada et al. described BCSCs enrichment since MCF-7 cells cultured in scaffolds showed a double MFI than 2D cultured cells. The authors suggested that enrichment was on account of an inhibition of BCSCs differentiation [19]. The same work described that 3D cultured cells exhibited increased chemoresistance. Consequently, three-dimensional cell culture could be an alternative to perform cytotoxicity experiments to obtain more reliable and physiological results.

Taking into account all data, this work proved that electrospinning is a potent technology useful in diverse fields. Controlling process parameters allowed the production of different meshes, demonstrating its potential for nanotechnology research. Produced scaffolds have been proven to allow cell adhesion and proliferation. Scaffolds mimic the extracellular matrix, allowing the cells to adopt a more *in vivo* morphology and behaviour. Finally, cell culture with electrospun PCL scaffolds has proven to expand BCSCs population. Therefore, 3D cell culture could facilitate the

development of new therapeutic strategies against this malignant subpopulation.

Acknowledgements

This work was funded partially by Spanish grants from Fundación Ramón Areces, Instituto de Salud Carlos III (PII400329) and by European Regional Development Fund (FEDER) and Ministerio de Economía y Competitividad (DPI2013-45201-P) and the support of the Catalanian government (2014SGR00868). The authors are grateful for the financial support from the University of Girona (MPCUdG2016/036).

References

- [1] Ferlay J, Soerjomataram I, Dikshit R, Eser S, Mathers C, Rebelo M, et al. Cancer incidence and mortality worldwide: Sources, methods and major patterns in GLOBOCAN 2012. *Int J Cancer*. 2015;136(5):E359–86.
- [2] Tudoran OM, Balacescu O, Berindan-Neagoe I. Breast cancer stem-like cells: clinical implications and therapeutic strategies. *Clujul Med*. 2016;89(2):193–8.
- [3] Jones RA, Campbell CI, Wood GA, Petrik JJ, Moorehead RA. Reversibility and recurrence of IGF-IR-induced mammary tumors. *Oncogene*. Macmillan Publishers Limited; 2009;28(21):2152–62.
- [4] Velasco-Velázquez M a., Homsí N, De La Fuente M, Pestiell RG. Breast cancer stem cells. *Int J Biochem Cell Biol*. Elsevier Ltd; 2012;44(4):573–7.
- [5] Al-Hajj M, Wicha MS, Benito-Hernandez A, Morrison SJ, Clarke MF. Prospective identification of tumorigenic breast cancer cells. *Proc Natl Acad Sci U S A*. 2003;100(7):3983–8.
- [6] Dontu G, Abdallah WM, Foley JM, Jackson KW, Clarke MF, Kawamura MJ, et al. In vitro propagation and transcriptional profiling of human mammary stem / progenitor cells. *genes Dev*. 2003;17:1253–70.
- [7] Shaw FL, Harrison H, Spence K, Ablett MP, Simoes BM, Farnie G, et al. A detailed mammosphere assay protocol for the quantification of breast stem cell activity. *J Mammary Gland Biol Neoplasia*. 2012;17(2):111–7.
- [8] Ginestier C, Hur MH, Charafe-Jauffret E, Monville F, Dutcher J, Brown M, et al. ALDH1 is a marker of normal and malignant human mammary stem cells and a predictor of poor clinical outcome. *Cell Stem Cell*. NIH Public Access; 2007;1(5):555–67.
- [9] Diehn M, Cho RW, Lobo NA, Kalisky T, Dorie MJ, Kulp AN, et al. Association of reactive oxygen species levels and radioresistance in cancer stem cells. *Nature*. 2009;458(7239):780–3.
- [10] Li X, Lewis MT, Huang J, Gutierrez C, Osborne CK, Wu M-F, et al. Intrinsic Resistance of Tumorigenic Breast Cancer Cells to Chemotherapy. *JNCI J Natl Cancer Inst*. 2008;100(9):672–9.
- [11] Abraham BK, Fritz P, McClellan M, Hauptvogel P, Athelogou M, Brauch H. Prevalence of CD44+CD24-low cells in breast cancer may not be associated with clinical outcome but may favor distant metastasis. *Clin Cancer Res*. 2005;11(3):1154–9.
- [12] Tsuyada A, Chow A, Wu J, Somlo G, Chu P, Loera S, et al. CCL2 mediates cross-talk between cancer cells and stromal fibroblasts that regulates breast cancer stem cells. *Cancer Res*. 2012;72(11):2768–79.
- [13] Charafe-Jauffret E, Ginestier C, Iovino F, Wicinski J, Cervera N, Finetti P, et al. Breast cancer cell lines contain functional cancer stem cells with metastatic capacity and a distinct molecular signature. *Cancer Res*. 2009;69(4):1302–13.
- [14] Thomas CH, Collier JH, Sfeir CS, Healy KE. Engineering gene expression and protein synthesis by modulation of nuclear shape. *Proc Natl Acad Sci U S A*. 2002;99(4):1972–7.
- [15] Vergani L, Grattarola M, Nicolini C. Modifications of chromatin structure and gene expression following induced alterations of cellular shape. *Int J Biochem Cell Biol*. 2004;36(8):1447–61.

- [16] Hale JS, Li M, Lathia JD. The malignant social network: Cell-cell adhesion and communication in cancer stem cells. *Cell Adh Migr.* 2012;6(4):346–55.
- [17] Feng S, Duan X, Lo P-K, Liu S, Liu X, Chen H, et al. Expansion of breast cancer stem cells with fibrous scaffolds. *Integr Biol (Camb).* 2013;5(5):768–77.
- [18] Saha S, Duan X, Wu L, Lo P-K, Chen H, Wang Q. Electrospun fibrous scaffolds promote breast cancer cell alignment and epithelial-mesenchymal transition. *Langmuir.* 2012;28(4):2028–34.
- [19] Sims-Mourtada J, Niamat R a., Samuel S, Eskridge C, Kmiec EB. Enrichment of breast cancer stem-like cells by growth on electrospun polycaprolactone-chitosan nanofiber scaffolds. *Int J Nanomedicine.* 2014;9(1):995–1003.
- [20] De Ciurana J, Serenó L, Vallès E. Selecting process parameters in RepRap additive manufacturing system for PLA scaffolds manufacture. In: *Procedia CIRP.* 2013. p. 152–7.
- [21] Bartolo P, Domingos M, Gloria a., Ciurana J. BioCell Printing: Integrated automated assembly system for tissue engineering constructs. *CIRP Ann - Manuf Technol.* 2011;60(1):271–4.
- [22] Domingos M, Intranuovo F, Russo T, De Santis R, Gloria a, Ambrosio L, et al. The first systematic analysis of 3D rapid prototyped poly(ϵ -caprolactone) scaffolds manufactured through BioCell printing: the effect of pore size and geometry on compressive mechanical behaviour and in vitro hMSC viability. *Biofabrication.* 2013;5(4):45004.
- [23] Ciurana J, Rodríguez CA. Trends in nanomaterials and processing for drug delivery of polyphenols for cancer and other treatments. *Curr Drug Targets.* 2015.
- [24] Palomerás S, Rabionet M, Ferrer I, Sarrats A, Garcia-Romeu ML, Puig T, et al. Breast Cancer Stem Cell Culture and Enrichment Using Poly(ϵ -Caprolactone) Scaffolds. *Molecules.* Multidisciplinary Digital Publishing Institute; 2016;21(4):537.
- [25] Giró-Perafita A, Rabionet M, Puig T, Ciurana J. Optimization of Poly(ϵ -caprolactone) scaffolds suitable for 3D cancer cell culture. *Procedia CIRP.* 2016;49(The Second CIRP Conference on Biomufacturing):61–6.
- [26] Sarrats A, Rabionet M, Puig T, Ciurana J. Selection of process parameters to fabricate poly(ϵ -caprolactone) scaffolds suitable for 3D cell culture. *J Biomech Eng.* 2016;
- [27] Bosworth LA, Downes S. Acetone, a Sustainable Solvent for Electrospinning Poly(ϵ -Caprolactone) Fibres: Effect of Varying Parameters and Solution Concentrations on Fibre Diameter. *J Polym Environ.* 2012;20(3):879–86.
- [28] Chen M, Patra PK, Warner SB, Bhowmick S. Role of fiber diameter in adhesion and proliferation of NIH 3T3 fibroblast on electrospun polycaprolactone scaffolds. *Tissue Eng.* 2007;13(3):579–87.
- [29] Chen M, Michaud H, Bhowmick S. Controlled Vacuum Seeding as a Means of Generating Uniform Cellular Distribution in Electrospun Polycaprolactone (PCL) Scaffolds.
- [30] Deitzel J., Kleinmeyer J, Harris D, Beck Tan N. The effect of processing variables on the morphology of electrospun nanofibers and textiles. *Polymer (Guildf).* 2001;42(1):261–72.
- [31] Chen M, Patra PK, Warner SB, Bhowmick S. Optimization of electrospinning process parameters for tissue engineering scaffolds. *Biophys Rev Lett.* 2006;1(2):153–78.
- [32] Zong X, Kim K, Fang D, Ran S, Hsiao BS, Chu B. Structure and process relationship of electrospun bioabsorbable nanofiber membranes. *Polymer (Guildf).* 2002;43(16):4403–12.
- [33] Sztot CS, Buchanan CF, Gatenholm P, Rylander MN, Freeman JW. Investigation of cancer cell behavior on nanofibrous scaffolds. *Mater Sci Eng C.* 2011;31(1):37–42.
- [34] Galban CJ, Locke BR. Analysis of cell growth kinetics and substrate diffusion in a polymer scaffold. *Biotechnol Bioeng.* John Wiley & Sons, Inc.; 1999;65(2):121–32.
- [35] Makhaniok A, Haranava Y, Goranov V, Panseri S, Semerikhina S, Russo A, et al. In silico prediction of the cell proliferation in porous scaffold using model of effective pore. *Biosystems.* 2013;114(3):227–37.

CHAPTER 5 Results III

Evaluation of BCSC and FASN role in chemosensitive and chemoresistant MDA-MB-231 TNBC cells

This chapter is based on the following publication:

Title	<u>EGCG-derivative G28 shows high efficacy inhibiting the mammosphere-forming capacity of sensitive and resistant TNBC models</u>
Authors	Ariadna Giró-Perafita [†] , Marc Rabionet [†] , Marta Planas, Lidia Feliu, Joaquim Ciurana, Santiago Ruiz-Martínez*, Teresa Puig*
Journal	Molecules
Publication year	2019
Impact Factor ₂₀₁₉	3.267 (Q2 in Chemistry, Multidisciplinary; position 70 of 177)
DOI	10.3390/molecules24061027

_ Paper to be considered for compendium of publications format

* Corresponding author

[†] These authors contributed equally to this manuscript

Abstract

Apart from the importance of the microenvironment in the stemness maintenance, different approaches can be performed in order to study the breast cancer stem cells (BCSCs). For instance, an enrichment of BCSC features is usually found in tumors that progressed after chemotherapy. Moreover, the lipogenic enzyme fatty acid synthase (FASN) also plays an important role in drug resistance and stemness preservation. Therefore, evaluation of FASN and BCSC role in chemoresistance acquisition may elucidate the relationship behind all these elements. This investigation can describe the potential of FASN and its pharmacological blocking as a novel approach for BCSC niche.






Chapter 5 aims to explore the role of FASN and BCSCs in a parental triple negative breast cancer (TNBC) cell model and its chemoresistant derivatives. Therefore, the study was carried out with the mesenchymal-like TNBC cell model MDA-MB-231, sensitive and resistant to the chemotherapeutic agent doxorubicin (231DXR) and paclitaxel (231PTR). FASN expression was assessed in all cell models through Western blot analysis, with and without the presence of the drugs. Similarly, the mammosphere forming and ALDH assays were performed to determine BCSC subpopulation in all samples, alongside RT-PCR to evaluate the expression of some epithelial-to-mesenchymal (EMT)-related genes. Ultimately, the impact of FASN blocking was tested in the BCSC-enriched mammosphere culture, through the addition of the FASN inhibitors C75, EGCG, G28, G56, and G37.

Results showed an increased proportion of BCSCs in the doxorubicin-resistant model, as well as the existence of an EMT process after the addition of the chemotherapeutic drugs. Among the tested FASN inhibitors, G28 exhibited a greater antiproliferative effect in monolayer culture and, interestingly, a high mammosphere-forming inhibition capacity in all cell models. Therefore, results highlight the importance of FASN inhibition for the treatment of TNBC patients,

especially those who progress after chemotherapy and possess greater stemness features.

Article

EGCG-Derivative G28 Shows High Efficacy Inhibiting the Mammosphere-Forming Capacity of Sensitive and Resistant TNBC Models

Ariadna Giró-Perafita ^{1,2,†} , Marc Rabionet ^{2,3,†} , Marta Planas ⁴ , Lidia Feliu ⁴ ,
Joaquim Ciurana ³ , Santiago Ruiz-Martínez ^{2,*} and Teresa Puig ^{2,*}

¹ Perlmutter Cancer Center, NYU School of Medicine, 522 First Avenue, Smilow Research Building, Room 1104, New York, NY 10016, USA; ariadna.giroporafita@nyulangone.org

² New Therapeutic Targets Laboratory (TargetsLab)-Oncology Unit, Department of Medical Sciences, Faculty of Medicine, University of Girona, Emili Grahit 77, 17003 Girona, Spain; m.rabionet@udg.edu

³ Product, Process and Production Engineering Research Group (GREP), Department of Mechanical Engineering and Industrial Construction, University of Girona, Maria Aurèlia Capmany 61, 17003 Girona, Spain; quim.ciurana@udg.edu

⁴ Laboratori d'Innovació en Processos i Productes de Síntesi Orgànica (LIPPSO), Department of Chemistry, University of Girona, Maria Aurèlia Capmany 69, 17003 Girona, Spain; marta.planas@udg.edu (M.P.); lidia.feliu@udg.edu (L.F.)

* Correspondence: santiago.ruiz@udg.edu (S.R.-M.); teresa.puig@udg.edu (T.P.);
Tel.: +34-972-419-548 (S.R.-M.); +34-972-419-628 (T.P.)

† These authors contributed equally to this work.

Academic Editors: Margarida Castell Escuer and Mariona Camps-Bossacoma
Received: 15 January 2019; Accepted: 12 March 2019; Published: 15 March 2019



Abstract: Recent studies showed that Fatty Acid Synthase (FASN), a lipogenic enzyme overexpressed in several carcinomas, plays an important role in drug resistance. Furthermore, the enrichment of Breast Cancer Stem Cell (BCSC) features has been found in breast tumors that progressed after chemotherapy. Hence, we used the triple negative breast cancer (TNBC) cell line MDA-MB-231 (231) to evaluate the FASN and BCSC population role in resistance acquisition to chemotherapy. For this reason, parental cell line (231) and its derivatives resistant to doxorubicin (231DXXR) and paclitaxel (231PTR) were used. The Mammosphere-Forming Assay and aldehyde dehydrogenase (ALDH) enzyme activity assay showed an increase in BCSCs in the doxorubicin-resistant model. Moreover, the expression of some transcription factors involved in epithelial-mesenchymal transition (EMT), a process that confers BCSC characteristics, was upregulated after chemotherapy treatment. FASN inhibitors C75, (–)-Epigallocatechin 3-gallate (EGCG), and its synthetic derivatives G28, G56 and G37 were used to evaluate the effect of FASN inhibition on the BCSC-enriched population in our cell lines. G28 showed a noticeable antiproliferative effect in adherent conditions and, interestingly, a high mammosphere-forming inhibition capacity in all cell models. Our preliminary results highlight the importance of studying FASN inhibitors for the treatment of TNBC patients, especially those who progress after chemotherapy.

Keywords: FASN inhibition; triple-negative breast cancer; cancer stem cells; EGCG; G28; polyphenolic compound; fatty acid metabolism

1. Introduction

Breast cancer is the most common cancer among women worldwide with approximately 2.1 million diagnoses estimated in 2018 according to the International Agency for Research on Cancer [1]. Triple negative breast cancer (TNBC) represents approximately 15–20% of patients with breast

carcinomas and is characterized by the lack of expression of estrogen and progesterone receptors (ER/PR) and neither expression nor amplification of the HER2 oncogene [2]. The absence of these three biomarkers prevents the use of currently available targeted therapies for breast cancer [3,4], and leaves systemic cytotoxic chemotherapy as the sole treatment option [5]. Despite a good initial response to chemotherapy in neoadjuvant settings, only 30% of patients will exhibit a survival of more than five years following diagnosis [6–8]. Compared to other BC subtypes, TNBC presents the highest recurrence rate along with the shortest time, which is associated with a significantly poorer overall survival [2,7]. Two major molecular subtypes are represented in TNBC, basal-like (80%) and claudin-low (CL) or mesenchymal-like (ML; 20%), this last one being enriched in cells with stem features [9]. Current therapies failure and resistance may be explained in part by the presence of a small population of cells that display stem properties within breast tumors known as breast cancer stem cells (BCSCs). In vitro, BCSC-enriched populations display specific features: cell-surface specific marker pattern (CD44^{high}/CD24^{low}), the ability to form mammospheres when growing in non-adherent conditions, aldehyde dehydrogenase 1 (ALDH1) enzyme activation, and enhanced resistance to chemotherapy [10]. Additionally, the induction of epithelial-mesenchymal transition (EMT) through *E-cadherin* expression decrease and upregulation of mesenchymal proteins, such as *vimentin* or *N-cadherin*, results in stem properties [11]. Some transcription factors involved in EMT regulation are *slug*, *zeb1*, *zeb2*, *twist* and *snail* [12,13].

Moreover, it has recently been demonstrated that the regulation of lipid metabolism promotes BCSCs and cancer chemoresistance [14]. Back in 1924, Warburg made evident metabolism deregulation in cancer cells [15,16], becoming many years later a hallmark of cancer [17]. Cell membranes are formed by long-chain fatty acids, being also important substrates for energy cell metabolism. The Fatty Acid Synthase (FASN) is the enzyme responsible for the de novo synthesis of palmitate, the most abundant fatty acid [18]. Several carcinomas such as breast, colon, lung, prostate, among others, overexpress FASN [19–22], suggesting it as a unique onco target. Blocking FASN activity causes in vitro and in vivo anticancer activity by inhibiting tumor progression [23–28], hindering angiogenesis [29,30], overcoming drug-resistance [31,32], and synergistically increasing the efficacy of chemotherapy [26,33,34]. A recent study showed that FASN was expressed in 92% of tumor tissue samples coming from a cohort of 100 TNBC patients and its association with positive node status made evident its role as a possible predictive biomarker in this aggressive BC subtype [35].

(–)-Epigallocatechin 3-gallate (EGCG) is a powerful antioxidant and the most abundant catechin in green tea. Its apoptotic effect leads to antiproliferative activity [36–39]. Although EGCG targets HER1-HER2, MAPK, and AKT signaling pathways among others, it has been described that its apoptosis-inducing effect occurs through FASN inhibition [28,40,41]. Several studies have demonstrated a weak effect of EGCG in 20 different human cancer stem cell populations when used alone but synergistically increased in combination with different anticancer drugs [42]. We have produced a battery of new polyphenolic derivatives structurally related to EGCG, from which G28, G56, and G37 proved to possess enhanced FASN inhibitory activity [43–45]. These compounds also showed cancer cell cytotoxicity in a set of human breast cancer cells. G28 displayed a potent tumor volume reduction in vivo with no weight loss or anorexia, the main side-effects of other FASN inhibitors like the cerulenin-derived compound C75 [28,41,43]. G28 also showed apoptosis induction in HER2+ resistant cell lines and tumor diminishment in HER2+ breast cancer xenografts [26,46].

In the present study, we evaluated FASN and BCSC characteristics, i.e., mammosphere-forming capacity and ALDH1 activity, in the acquisition of chemoresistance in the TNBC model MDA-MB-231 (231). Moreover, we used the natural FASN inhibitor EGCG and its synthetic derivatives G28, G56, and G37 in comparison to C75 (Figure 1) to target FASN through these BCSC features from these TNBC models resistant to doxorubicin (231DXR) and paclitaxel (231PTR), the most common drugs currently used in this BC subtype devoid of a validated targeted therapy.

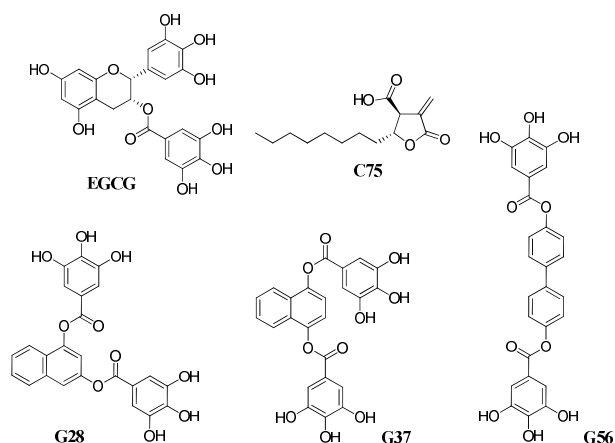


Figure 1. Structure of compounds EGCG, C75, G28, G37, and G56.

2. Results

2.1. FASN Expression in MDA-MB-231 Derived Chemoresistant Cell Lines

FASN activity has demonstrated to play an important role in drug resistance through new phospholipid synthesis for membrane renovation and plasticity. It also decreases ceramide levels, inhibiting apoptosis via PARP activation [32,47–50].

To assess the role of FASN in chemoresistance acquisition in TNBC, we developed MDA-MB-231 (231) cells resistant to doxorubicin (231DXR) [34] and paclitaxel (231PTR) (Supplementary Figure S1). It has been described that doxorubicin-resistant cell lines become sensitive through the inhibition of FASN [34,51]. Therefore, we studied how FASN protein levels were modified after drug treatment of sensitive and chemoresistant TNBC cells. Our results showed that 231DXR FASN levels experienced a 2-fold increase after 24 h of doxorubicin treatment (Figure 2A), while such effect was not observed in parental cells. On the other hand, paclitaxel did not show any effect on FASN protein levels neither in 231 nor in 231PTR (Figure 2B). PARP cleavage, a marker for apoptosis, is increased in parental cell lines compared to its resistant counterparts for both drugs, making evident their chemoresistance (Figure 2).

2.2. BCSC-Enriched Population in Sensitive and Resistant Cell Lines

Despite the fact that BCSCs are a very low-represented population within tumors, selection or enrichment of these cells after chemotherapy treatment can result in a tumor relapse due to their intrinsic chemoresistance and their tumorigenic ability [52–54]. Here, we aim at the evaluation of the BCSC population in our sensitive and resistant models by means of two of these techniques, i.e., mammospheres-forming capacity and ALDH1 activity. The influence of doxorubicin and paclitaxel treatment was also evaluated.

To determine whether there was an enrichment of this population in our resistant models, we used the Mammosphere-Forming Assay (MFA; Figure 3A) in 231 parental cell line and in the chemoresistant derivatives 231DXR and 231PTR (Figure 3B). 231 and 231DXR displayed similar Mammosphere-Forming Index (MFI), comparable to those of 231 and 231PTR. Likewise, no morphological differences were found among the three cell models (data not shown). Since one of the BCSC population characteristics is its inherent chemoresistance [55], we carried out doxorubicin and paclitaxel treatments in adherent and mammosphere cell culture, in both sensitive and resistant

cell models. Cell density, chemotherapy drug dosage (concentration that inhibited 30% (IC₃₀) of cell viability for doxorubicin (70 nM) or paclitaxel (5 nM) at 48 h), and treatment duration were performed equally in both approaches. The 3-(4,5-dimethylthiazol-2-yl)-2,5-diphenyltetrazolium bromide (MTT) assay was carried out in adherent conditions to determine cell viability, whereas, in non-adherent culture, the Mammosphere-Forming Inhibition (MFI_n) was used. The BCSC-enriched population showed inherent doxorubicin resistance when compared to adherent conditions for both sensitive and resistant cell lines (Figure 3C). In adherent settings, the inhibition of viability ranged from 89.81% ± 1.65 (231) to 86.7% ± 1.85 (231DXR). Nevertheless, MFI_n values exhibited lower inhibition in both cell lines treated with doxorubicin. Furthermore, in non-adherent culture, a doxorubicin cytotoxic effect was significantly higher in parental cells (60.66% ± 1.17) compared to the resistant model (51.29% ± 0.58, $p < 0.01$). Similar results were found with paclitaxel treatment (Figure 3D). The reduction in viability in adherent condition was significantly higher in sensitive cells (90.47% ± 1.40) compared with paclitaxel-resistant model (72.61% ± 0.94) with $p < 0.001$. Additionally, BCSC-enriched population in mammospheres assay showed paclitaxel intrinsic resistance, with MFI_n values of 47.82% ± 3.17 (231) and 31.24% ± 5.59 (231PTR).

We next measured the ALDH1 activity using the ALDEFLUOR™ assay. Obtained data revealed a significant increase of ALDH1 activity in the resistant counterpart 231DXR (26.52% ± 1.81) compared to parental (10.81% ± 5.74; $p < 0.05$) (Figure 3E). Interestingly, ALDH-bright (ALDH^{br}) cells from both sensitive and resistant cell lines were also increased, with no significance, after 12 and 24 h of doxorubicin treatment, reaching values of 42.15% ± 10.53 and 38.10% ± 6.71, respectively. 231DXR cells exhibited a non-significant increase of ALDH1 activity in comparison with 231 cells after 12 h treatment (36.87% ± 3.56 vs. 17.28% ± 5.68), showing similar levels at 24 h after treatment.

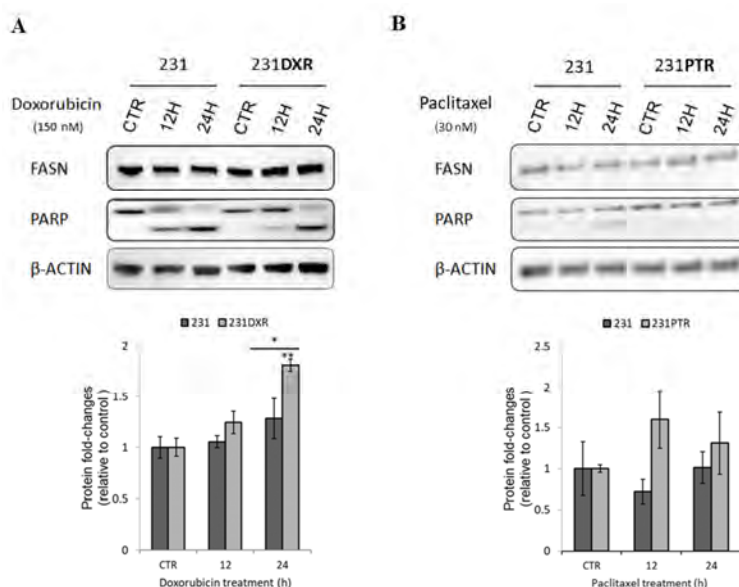


Figure 2. FASN protein expression after doxorubicin or paclitaxel treatment in 231, 231DXR or 231PTR cell lines. Western blot analysis of FASN, and PARP expression after 12 h or 24 h of (A) doxorubicin (150 nM) or (B) paclitaxel (30 nM) treatment. FASN levels are normalized by β -actin and expressed as fold-changes relative to control at each time point. Experiments were performed four times. * ($p < 0.05$) and ** ($p < 0.01$) indicate levels of statistical significance.

Regarding an ALDH^{br} population in paclitaxel-resistant 231 cell line, no significant differences were found between sensitive and resistant cell models (Figure 3F). Paclitaxel treatment decreased ALDH^{br} population after 24 h of treatment in sensitive cells ($p < 0.01$), whereas ALDH^{br} population in 231PTR cells remained similar during treatment.

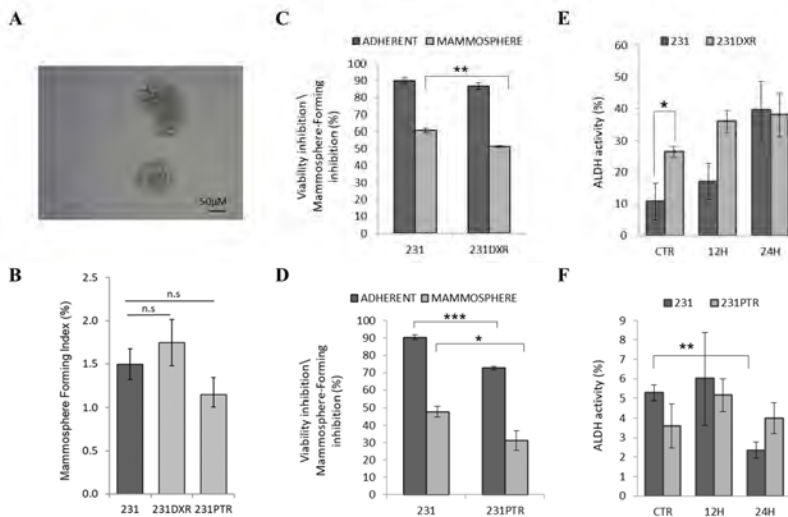


Figure 3. Mammosphere-Forming Assay and ALDH activity assay in resistant cells. (A) Representative image of mammospheres from 231 (parental) cell line at day 5; (B) Mammosphere-Forming Index (MFI) for 231, 231DXR and 231PTR. Cell viability inhibition and Mammosphere-Forming Inhibition (MFI) for (C) doxorubicin (70 nM) in 231 and 231DXR or (D) paclitaxel treatment (5 nM) in 231 and 231PTR for five days. In the same conditions, ALDH activity quantification (%) for (E) 231DXR and (F) 231PTR compared to 231. Results are expressed as mean \pm SEM. * ($p < 0.05$), ** ($p < 0.01$) and *** ($p < 0.001$) indicate levels of statistical significance or n.s. when no significance was found.

2.3. Evaluation of EMT in Drug-Resistant TNBC Models

Cell plasticity is a key process in the development of drug resistance [56]. It has been described that induction of EMT can lead to cell dedifferentiation, acquiring BCSC features such as chemoresistance [11,39]. We wondered if the development of this phenotype was due to EMT process triggered by chemotherapy treatment. To that purpose, RNA expression of the EMT-related transcription factors *snail*, *slug*, *twist*, *zeb1* and *zeb2* was evaluated after doxorubicin or paclitaxel treatment. The basal levels of *snail* were 2-fold higher in 231DXR compared to 231 ($p < 0.05$). When doxorubicin was added, interestingly, a significant increase of *snail* was observed in the 231 cell line, while such a strong effect was not observed in 231DXR (Figure 4A). *Vimentin* gene expression levels were analyzed since it is an intermediate filament protein related to the mesenchymal phenotype. After 12 h of doxorubicin treatment, *vimentin* expression was significantly increased in both cell lines with a higher growth in 231DXR (Figure 4A).

Concerning paclitaxel resistant cells, *slug* transcription factor was upregulated in 231PTR compared with sensitive 231 cells ($p < 0.05$) but opposite results were observed in *vimentin* levels at the same time points (Figure 4B).

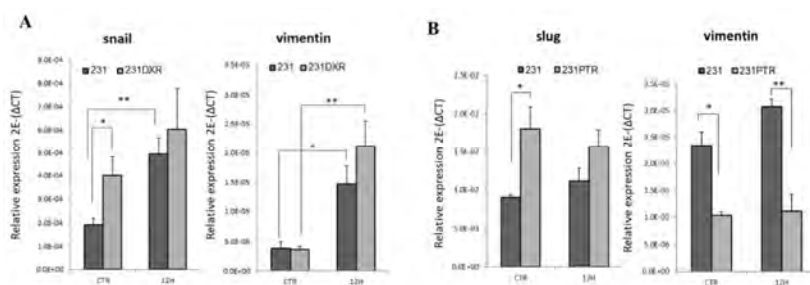


Figure 4. EMT-related genes expression after chemotherapy agents' treatment. (A) *snail* and *vimentin* gene expression in 231 and 231DXR cells after 12 h of doxorubicin treatment (150 nM); (B) *slug* and *vimentin* gene expression in 231 and 231PTR after 12 h of paclitaxel treatment (30 nM). Experiments were performed at least three times. * ($p < 0.05$), ** ($p < 0.01$) and *** ($p < 0.001$) indicate levels of statistical significance.

2.4. C75, EGCG and Its Derivatives G28, G56, and G37 Effect in BCSC-Enriched Populations

MFI was performed in 231, 231DXR, and 231PTR cell lines in order to study the impact of FASN inhibition in the BCSC-enriched population.

Five different FASN inhibitors i.e., C75, EGCG, and its synthetic derivatives G28, G56, and G37 [45], were used to evaluate their efficacy in reducing mammosphere-forming capability. The concentration that inhibited 30% (IC₃₀) of cell viability at 48 h was used (Supplementary Figure S2) [34]. Then, adherent and non-adherent cell cultures were treated with IC₃₀ of each compound (Figure 5).

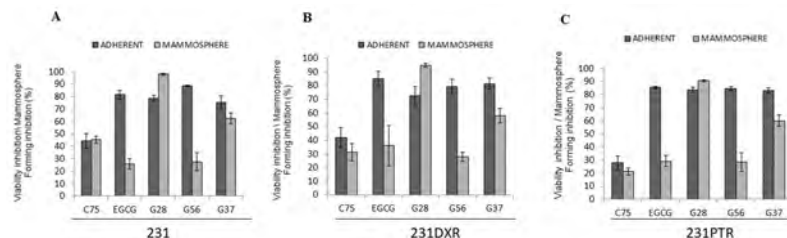


Figure 5. Cell viability inhibition vs. Mammosphere-Forming Inhibition (MFI) for FASN inhibitors EGCG, C75, G28, G56 and G37. (A) 231, (B) 231DXR, and (C) 231PTR were treated for five days with C75 (30 μ M), EGCG (120 μ M), G28 (50 μ M), G56 (50 μ M), and G37 (50 μ M). Experiments were performed at least three times in duplicate.

No differences were found with C75 treatment in adherent and non-adherent conditions in 231 or both resistant cell models (231DXR and 231PTR), with values ranging from $45.26\% \pm 2.94$ to $21.24\% \pm 5.18$. EGCG cytotoxic effect was significantly diminished in non-adherent settings in all cell lines. EGCG reduced viability in adherent cells with percentages ranging from $81.54\% \pm 3.38$ (231) to $85.43\% \pm 0.99$ in 231PTR. Instead, MFI values laid between $25.71\% \pm 4.42$ (231) and $36\% \pm 14.70$ in 231DXR.

G28 displayed a noticeable cytotoxic effect in both adherent and suspension conditions. Although the reduction in viability ranged from $78.70\% \pm 2.50$ (231) to $72.66\% \pm 6.76$ (231DXR) and $83.50\% \pm 2.08$ (231PTR) in adherent conditions, the same dose of G28 exhibited a significantly cytotoxic effect in suspension, with values of $98.10\% \pm 0.72$ for 231, $94.70\% \pm 1.55$ for 231DXR and $90.67\% \pm 1.60$ for 231PTR.

Regarding G56 and G37 compounds, both exhibited a strong effect in adherent conditions in all cell models. For instance, cells treated with G56 showed a reduction in viability of $88.56\% \pm 0.57$ (231), $79.31\% \pm 5.18$ (231DXR) and $84.66\% \pm 1.63$ (231PTR). As a counterpart, G37 treatment resulted in similar values, concretely $75.24\% \pm 5.32$ for sensitive 231 cells, $81.33\% \pm 4.04$ for doxorubicin-resistant cells and $83.07\% \pm 1.93$ for 231PTR cells. On the other hand, both compounds showed lower MFIn effect, especially G56, which exhibits decreased values of $27.56\% \pm 7.20$ (231), $28.01\% \pm 3.42$ (231DXR), and $28.47\% \pm 6.86$ (231PTR), similar to those found in EGCG treatment.

3. Discussion

The two major molecular subtypes within TNBCs are the CL and ML. The last one accounts for 20% of TNBCs (the second in incidence after basal-like in TNBC [9]), and exhibits an enrichment of the EMT features, showing BCSC properties, and having a poor prognosis [9,57]. Furthermore, the enrichment of CSC features has been found in tumors that progressed after therapy [52,53]. In the present study, an ML subtype cell line MDA-MB-231 (231) and its resistant derivatives 231DXR and 231PTR were used to evaluate the BCSC population in chemotherapy resistance acquirement.

BCSCs are a low-represented population within tumors, primary and established cell lines; therefore, different methodologies have been settled to study the BCSC-enriched population with these cells in vitro. The 231 cell line is known to form vague mammospheres that can be passaged for several generations that can be passed on for several generations [58–61]. While no differences were found regarding the index formation between the three cell lines assayed, significant differences were observed using this methodology under drug treatment. Both 231DXR and 231PTR showed increased ability to form mammospheres under drug treatment compared to 231 showing both, drug resistance and anchorage-independent growth. The ALDEFLUORTM assay indicated that ALDH^{br} cell population was significantly increased in the 231DXR cell line, whereas ALDH^{br} 231PTR cell percentage remained similar to that in the parental. Interestingly, the number of ALDH^{br} cells significantly increased in the parental cell line after doxorubicin treatment. Taken together, these results suggest that 231DXR cell line shows an increase in BCSC features, and that these features can be induced after doxorubicin treatment. On the other hand, despite the fact that we did not observe an obvious enrichment in BCSC characteristics in 231PTR compared to parental cells, the intrinsic BCSC features of this ML cell line were maintained.

Cell plasticity plays a key role in tumor progression, and the plastic CSC concept defines that bidirectional conversions between non-CSCs and CSCs may exist. Thus, the activation of the EMT process may lead to the CSC phenotype [11,38,39]. 231DXR and 231PTR cell lines showed higher resistance to their respective chemotherapeutic agent in comparison with 231 in adherent or suspension condition. Additionally, and as expected, doxorubicin and paclitaxel showed more cytotoxic effects in adherent conditions compared to non-adherent ones. Interestingly, the ALDH1 activity was enhanced after doxorubicin treatment in both sensitive and resistant 231DXR cell models. This phenotype is associated with chemoresistance in patients [62]. Remarkably, basal expression of *snail*, an EMT inducer directly associated with tumor development and relapse [63–65], significantly increased in 231DXR compared to sensitive cells. Regarding paclitaxel resistance, no differences were observed in the ALDH^{br} population. The EMT-related transcription factor *slug*, linked to cancer progression and BCSC activity [66], was upregulated in 231PTR cells compared to 231 cell model with no changes in *vimentin* levels.

Although doxorubicin counts with undeniable advantages as an antitumor drug, it has been shown to promote stemness in murine cell lines [67–69]. Recent evidence showed that doxorubicin treatment increased stem cell-related signaling pathways, explaining the inherent chemoresistance of MDA-MB-231 (compared to another ML cell line, Hs578T) [70]. Previous studies showed the ability of paclitaxel to increase the BCSC subpopulation in 231 TNBC cell lines [71]; however, non-obvious enrichment was observed in our hands, but a maintenance of the intrinsic stem features of this ML subtype.

FASN overexpression confers many advantages to tumor cells such as the ability to preserve a high proliferation rate, and it also plays a key role in drug resistance acquisition [32,47,49]. We have proven that FASN inhibition overcame doxorubicin resistance in chemoresistant cell lines [34], and FASN protein levels significantly increased in the 231DXR cell model when treated with doxorubicin. It has been previously described in breast cancer that FASN protein levels increase as a mechanism to become resistant [72]. Gonzalez-Guerrico and coworkers showed that the inhibition of FASN led to the conversion of the ML phenotype to a non-malignant one by downregulating EMT markers in a breast cancer model [73]. Additionally, the FASN inhibitor metformin blocked lipogenesis, leading to a switch from basal- to luminal-like sphere morphologies [73]. Likewise, resveratrol, another FASN inhibitor, precluded the growth of the CSC population both in vitro and in vivo using a breast cancer xenograft model [74]. FASN expression has also been shown to be important in stemness preservation in glioma [75]. In this work, we evaluated the effect of the inhibition of FASN in an CSC population through the ability to hinder mammosphere-formation capacity compared to the cytotoxic effect in adherent culture. No differences were found using C75 in adherent or suspension conditions. G28 displayed a noticeably better inhibitory effect in non-adherent conditions in both sensitive and resistant cell lines. Interestingly, this outcome was not found when using any of the chemotherapeutical agents (doxorubicin or paclitaxel). These results set up the basis for further investigation using FASN inhibitors in combination with chemotherapy to target BCSCs as well as the bulk of the tumor to improve the outcome of patients with TNBC.

In conclusion, the results presented in this work suggest that chemoresistance of 231DXR and 231PTR (ML cell models) is not only a static drug-selected state, but also an acquired reversible phenotype that can be triggered during treatment. 231DXR presented a larger BCSC population compared to the doxorubicin sensitive 231 cell line, which was also enhanced with the presence of the chemotherapeutical agent. This might be explained by the activation of EMT induced through *snail*. Despite the preliminary nature of the obtained results, they provide a rationale to suppress FASN as a potential strategy for a highly proliferative neoplasia such as TNBC.

4. Materials and Methods

4.1. Cell Culture and Development of Doxorubicin- and Paclitaxel-Resistant TNBC Cells

MDA-MB-231 cell line was obtained from the American Type Culture Collection (ATCC) and was routinely grown in DMEM (Gibco, Thermo Fisher Scientific, Waltham, MA, USA) supplemented with 10% FBS (HyClone Laboratories, GE Healthcare, Chicago, IL, USA), 1% L-glutamine (Gibco), and 1% sodium pyruvate (Gibco), 50 U/mL Pen/Strep (Linus). Cells were kept at 37 °C and 5% CO₂ atmosphere. Doxorubicin-resistant cells MDA-MB-231 (231DXR) and paclitaxel-resistant cells (231PTR) were developed using a stepwise selection method. Increasing doses of doxorubicin (TEDEC-Meiji Farma, Alcalá de Henares, Spain) and paclitaxel (Accord Healthcare Ltd., Thaltej, India) were added until their corresponding IC₅₀ was reached. Briefly, cells were initially treated with a concentration of 0.1xIC₅₀ of each drug. After 48 h, treatment medium was replaced for fresh medium. When the cells were capable of growing and reached appropriate confluence, they were treated with double the previous concentration for 48 h. The stepwise selection method was subsequently performed until the final concentration of drug was that of the parental IC₅₀. It took around six months for each cell line. Resistance was confirmed by cell viability assay.

4.2. Western Blot Analysis of Cell Lysates

Cell lines were treated during 12 or 24 h with half the concentration of doxorubicin that inhibited 50% (0.5xIC₅₀) of the MDA-MB-231 parental cells' viability previously determined with MTT assay after 48 h [34]. A final concentration of 3xIC₅₀ of paclitaxel was used (Supplementary Figure S1). After treatment, parental and resistant TNBC cells were lysed in ice-cold lysis buffer (Cell Signaling Technology Inc., Danvers, MA, USA) with 100 µg/mL phenylmethylsulfonyl fluoride (PMSF) by

vortexing every 5 min for 30 min. Equal amounts of protein were heated in an lithium dodecyl sulfate (LDS) Sample Buffer with Sample Reducing Agent (Invitrogen, Carlsbad, CA, USA) for 10 min at 70 °C, electrophoresed on SDS-polyacrylamide gel (SDS-PAGE), and transferred onto nitrocellulose membranes. Blots were incubated for 1 h in blocking buffer (5% powdered-skim milk in Phosphate-buffered saline 0.05% Tween (PBS-T)) and incubated overnight at 4 °C with the appropriate antibodies diluted in blocking buffer (Table 1). Specific horseradish peroxidase (HRP)-conjugated secondary antibodies were incubated for 1 h at room temperature. The immune complexes were detected using a chemiluminescent HRP substrate (Super Signal West Femto (Thermo Scientific Inc.) or Immobilon Western (Merck Millipore, Burlington, MA, USA)). β -actin (Santa Cruz Biotechnology Inc., Dallas, TX, USA) was used as a control of protein loading. Western blot analyses were repeated at least four times and representative results are shown. Quantification analyses of Western blot data were performed using a computer-assisted densitometer. The results are expressed as ratio of protein levels vs. β -actin levels.

Table 1. Antibody description.

Antibody	Reference	Supplier	Dilution	Source
FASN	ADI-905-069-100	EnzoLife Sciences	1:1500	rabbit
PARP	9542	Cell Signaling Technology	1:1000	rabbit
β -actin	Sc-47778	Santa Cruz Inc.	1:1000	mouse

4.3. Cell Viability Assays

To elucidate inhibitory effects of chemotherapy drugs and FASN inhibitors, 231 and resistant counterparts were seeded in 96-well microplates at a cell density of 4×10^3 cells/well in their corresponding growth medium. After 24 h, culture medium was removed and 100 μ L of fresh medium with increasing doses of paclitaxel, or FASN inhibitors (EGCG (Sigma-Aldrich, St. Louis, MO, USA; dissolved in PBS 5% DMSO), C75 (Sigma), EGCG-derivatives G28, G56 or G37 (dissolved in DMSO)) were added to each well. The synthesis of FASN inhibitors G28, G56, and G37 was performed as previously described [45]. Following 48 h treatment, a colorimetric MTT assay was used to measure cell viability as previously described [27]. Graph plots were performed in order to elucidate paclitaxel resistance and inhibitory concentrations.

On the other hand, cell viability inhibition experiments were performed seeding 5000 cells in adherent 6-well cell culture microplates with DMEM. Cells were incubated for 24 h to allow cell attachment and then chemotherapy drugs (doxorubicin or paclitaxel) or FASN inhibitors were added at a unique specific concentration (IC_{30} of parental cells calculated at 48 h) for five days. Finally, cell viability was also measured using a colorimetric MTT assay.

4.4. Mammosphere-Forming Assay

The mammosphere-forming procedure was used to evaluate an CSC population, following previously described protocols [55,56]. After cell detachment, 2000 cells were seeded into a non-adherent 6-well cell culture microplate. Cells were cultured with DMEM/F12 medium supplemented with B27, hEGF (20 ng/mL), 1% L-glutamine, and 1% sodium pyruvate. Microplates were incubated for 5 days and mammospheres bigger than 50 μ m were counted using an inverted optical microscope. Different parameters were calculated using the formulas described above: (A) the Mammosphere-Forming Index (MFI) and (B) Mammosphere-Forming Inhibition (MFI_n). For MFI_n analysis, compounds were added at the moment of seeding. An IC_{30} of chemotherapy drugs and FASN inhibitors calculated at 48 h on MDA-MB-231 parental cells was used.

Formula:

$$A \quad MFI = \frac{N^{\circ} \text{ mammosphere}}{N^{\circ} \text{ cells plated}} \cdot 100 \quad B \quad MFI_n = 100 - \frac{N^{\circ} \text{ mammospheres}_{\text{treatment}}}{N^{\circ} \text{ mammospheres}_{\text{control}}} \cdot 100$$

4.5. Quantitative Real-Time PCR Analysis

Cells were treated with a concentration of doxorubicin or paclitaxel equal to the $0.5 \times IC_{50}$ and $3 \times IC_{50}$, respectively, obtained after 48 h of treatment. After 12 or 24 h treatment, cells were washed with PBS, and then Qiazol (Qiagen, Hilden, Germany) was added. RNeasy mini kit (Qiagen) was used to isolate total RNA according to manufacturer instructions. RNA was reverse-transcribed into complementary DNA (cDNA) using High Capacity cDNA Archive Kit (Applied Biosystems, Foster City, CA, USA). Different gene expression levels were determined using LightCycler[®] 480 Real-time PCR System (Roche, Basel, Switzerland) with LightCycler[®] 480 SYBR Green I Master (Roche), following manufacturer instructions. Primers used are shown in Table 2. RT-PCR analyses were performed at least three times and each gene was run in triplicate. Gene expression levels were quantified using the standard formula $2^{-\Delta CT}$ and normalized to the housekeeping gene β -actin ($2^{-\Delta\Delta CT}$).

Table 2. Primer design.

FASN	Forward	CAGGCACACACGATGGAC
	Reverse	CGGAGTGAATCTGGGTGAT
Snail	Forward	GCTGCAGGACTCTAATCCAGA
	Reverse	ATCTCCGGAGGTGGGATG
Vimentin	Forward	TGGTCTAACGGTTTCCCCTA
	Reverse	GACCTCGGAGCGAGAGTG
β -actin	Forward	ATTGGCAATGAGCGGTTT
	Reverse	CGTGGATGCCACAGGACT

4.6. Aldefluor Assay

Aldefluor[™] kit (STEMCELL Technologies) was used to determine ALDH enzyme activity, following company guidelines. Briefly, ALDH reagent (BAAA) freely diffuses into viable cells and ALDH enzyme catalyzes its conversion to BAA, which is negatively charged and retained into cells. Intracellular BAA increases fluorescence which can be analyzed through flow cytometry. As seen before for 12 and 24 h treatments, $0.5 \times IC_{50}$ and $3 \times IC_{50}$ (calculate at 48 h on parental cells) for doxorubicin and paclitaxel, respectively, were used. After treatment, cells were detached and 2×10^5 cells per sample were collected. After washing with PBS, 500 μ L of the kit buffer was added to each condition. Afterwards, 2.5 μ L of the ALDH reagent was added and 250 μ L of the suspension was immediately transferred to a new Eppendorf with 2.5 μ L of the ALDH inhibitor *N,N*-diethylaminobenzaldehyde (DEAB), in order to consider background fluorescence (Supplementary Figure S3). All samples were incubated at 37 °C for 40 min. Cells were then centrifuged and washed and samples were prepared to be analyzed through cytometry (FACSCalibur II, BD Bioscience). Images were obtained with FlowJo software (Flow Jo LLC, Ashland, OR, USA).

5. Conclusions

The study of the BCSC-enriched population in an ML TNBC cell line (MDA-MB-231) and its doxorubicin-resistant derivative (231DXR) showed increased BCSC features in both sensitive and resistant cell models after chemotherapy treatment. We have previously recognized FASN as a possible co-target to resensitize chemoresistant cells to doxorubicin [34]. Moreover, its implication in drug

resistance acquisition in breast cancer has already been identified [72]. Results derived from the present paper showed that the newly developed FASN inhibitor EGCG-derived G28 had a strong inhibitory effect on the mammosphere-formation capacity (a stem feature) in sensitive and both drug-resistant models, 231DXR and 231PTR. However, these outcomes are still in initial states and more approaches should be performed. According to recent published research, FASN would not only play an important role in a highly proliferative neoplasia such as TNBC, but also in drug resistance acquisition and in sustaining malignancy in cancer [73–75], being a promising (co)target for patients with TNBC that progress to current treatments.

Supplementary Materials: The following are available online at <http://www.mdpi.com/1420-3049/24/6/1027/s1>, Figure S1: Viability assays for 231 and 231PTR at increasing doses of paclitaxel for 48 h; Figure S2: Viability assays for 231, 231DXR, and 231PTR at increasing doses of FASN inhibitors for 48 h; Figure S3: ALDEFLUOR plots for 231 and 231DXR after doxorubicin treatment.

Author Contributions: Conceptualization, T.P., A.G.-P. and S.R.-M.; methodology, A.G.-P., M.R., M.P. and L.F.; validation, A.G.-P., M.R. and S.R.-M.; resources, T.P., J.C., M.P., and L.F.; writing—original draft preparation, A.G.-P., M.R. and S.R.-M.; writing—review and editing A.G.-P., M.R., L.F., M.P., J.C., S.R.-M. and T.P.; supervision, T.P.; funding acquisition, T.P.

Funding: M.R. acknowledges University of Girona for the pre-doctoral grant (IFUdG2017/62). The authors thank University of Girona (MPCUdG2016/036) and the Catalanian Government (2017SGR00385) for the support. This work was partially supported by Spanish grants from Fundación Ramón Areces and Instituto de Salud Carlos III (ISCIII) (PI11/00692 and PI14/00329), Fundació Oncolliga and RadikalSwim (OncoSwim).

Acknowledgments: We are grateful to Marc Yeste from TechnoSperm (University of Girona) for his support in the flow cytometry analyses.

Conflicts of Interest: The authors declare no conflict of interest.

References

1. Ferlay, J.; Colombet, M.; Soerjomataram, I.; Mathers, C.; Parkin, D.M.; Piñeros, M.; Znaor, A.; Bray, F. Estimating the global cancer incidence and mortality in 2018: GLOBOCAN sources and methods. *Int. J. Cancer* **2018**. [[CrossRef](#)] [[PubMed](#)]
2. Bianchini, G.; Balko, J.M.; Mayer, I.A.; Sanders, M.E.; Gianni, L. Triple-negative breast cancer: challenges and opportunities of a heterogeneous disease. *Nat. Rev. Clin. Oncol.* **2016**, *13*, 674–690. [[CrossRef](#)] [[PubMed](#)]
3. Dalmáu, E.; Armengol-Alonso, A.; Muñoz, M.; Seguí-Palmer, M.Á. Current status of hormone therapy in patients with hormone receptor positive (HR+) advanced breast cancer. *Breast* **2014**, *23*, 710–720. [[CrossRef](#)] [[PubMed](#)]
4. Nixon, N.A.; Hannouf, M.B.; Verma, S. A review of the value of human epidermal growth factor receptor 2 (HER2)-targeted therapies in breast cancer. *Eur. J. Cancer* **2018**, *89*, 72–81. [[CrossRef](#)] [[PubMed](#)]
5. Griffiths, C.L.; Olin, J.L. Triple negative breast cancer: A brief review of its characteristics and treatment options. *J. Pharm. Pract.* **2012**, *25*, 319–323. [[CrossRef](#)] [[PubMed](#)]
6. Anders, C.K.; Carey, L.A. Biology, Metastatic Patterns, and Treatment of Patients with Triple-Negative Breast Cancer. *Clin. Breast Cancer* **2009**, *9*, S73–S81. [[CrossRef](#)] [[PubMed](#)]
7. Guarneri, V.; Dieci, M.V.; Conte, P. Relapsed Triple-Negative Breast Cancer: Challenges and Treatment Strategies. *Drugs* **2013**, *73*, 1257–1265. [[CrossRef](#)] [[PubMed](#)]
8. Massihnia, D.; Galvano, A.; Fanale, D.; Perez, A.; Castiglia, M.; Incorvaia, L.; Listì, A.; Rizzo, S.; Cicero, G.; Bazan, V.; et al. Triple negative breast cancer: Shedding light onto the role of pi3k/akt/mtor pathway. *Oncotarget* **2016**, *7*, 60712–60722. [[CrossRef](#)] [[PubMed](#)]
9. Prat, A.; Parker, J.S.; Karginova, O.; Fan, C.; Livasy, C.; Herschkowitz, J.I.; He, X.; Perou, C.M. Phenotypic and molecular characterization of the claudin-low intrinsic subtype of breast cancer. *Breast Cancer Res.* **2010**, *12*. [[CrossRef](#)]
10. Palomeras, S.; Ruiz-Martínez, S.; Puig, T. Targeting Breast Cancer Stem Cells to Overcome Treatment Resistance. *Molecules* **2018**, *23*, 2193. [[CrossRef](#)]
11. Mani, S.A.; Guo, W.; Liao, M.-J.; Eaton, E.N.; Ayyanan, A.; Zhou, A.Y.; Brooks, M.; Reinhard, F.; Zhang, C.C.; Shiptsin, M.; et al. The Epithelial-Mesenchymal Transition Generates Cells with Properties of Stem Cells. *Cell* **2008**, *133*, 704–715. [[CrossRef](#)]

12. Kotiyal, S.; Bhattacharya, S. Breast cancer stem cells, EMT and therapeutic targets. *Biochem. Biophys. Res. Commun.* **2014**, *453*, 112–116. [[CrossRef](#)]
13. Grzegorzolka, J.; Biala, M.; Wojtyra, P.; Kobierzycki, C.; Olbromski, M.; Gomulkiewicz, A.; Piotrowska, A.; Rys, J.; Podhorska-Okolow, M.; Dziegiel, P. Expression of EMT Markers SLUG and TWIST in Breast Cancer. *Anticancer Res.* **2015**, *35*, 3961–3968.
14. Wang, T.; Fahrman, J.F.; Lee, H.; Li, Y.J.; Tripathi, S.C.; Yue, C.; Zhang, C.; Lifshitz, V.; Song, J.; Yuan, Y.; et al. JAK/STAT3-Regulated Fatty Acid β -Oxidation Is Critical for Breast Cancer Stem Cell Self-Renewal and Chemoresistance. *Cell Metab.* **2017**, 1–15. [[CrossRef](#)]
15. Warburg, O. On the origin of cancer Cells. *Science* **1956**, *123*, 309–314. [[CrossRef](#)]
16. Devic, S. Warburg Effect—A Consequence or the Cause of Carcinogenesis? *J. Cancer* **2016**, *7*, 817–822. [[CrossRef](#)]
17. Hanahan, D.; Weinberg, R.A. Hallmarks of cancer: the next generation. *Cell* **2011**, *144*, 646–674. [[CrossRef](#)]
18. Wakil, S.J. Fatty Acid Synthase, A Proficient Multifunctional Enzyme. *Biochemistry* **1989**, *28*, 4523–4530. [[CrossRef](#)]
19. Zaytseva, Y.Y.; Harris, J.W.; Mitov, M.I.; Kim, J.T.; Butterfield, D.A.; Lee, E.Y.; Weiss, H.L.; Gao, T.; Evers, B.M. Increased expression of fatty acid synthase provides a survival advantage to colorectal cancer cells via upregulation of cellular respiration. *Oncotarget* **2015**, *6*, 18891–18904. [[CrossRef](#)]
20. Witkiewicz, A.K.; Nguyen, K.H.; Dasgupta, A.; Kennedy, E.P.; Yeo, C.J.; Lisanti, M.P.; Brody, J.R. Co-expression of fatty acid synthase and caveolin-1 in pancreatic ductal adenocarcinoma: Implications for tumor progression and clinical outcome. *Cell Cycle* **2008**, *7*, 3021–3025. [[CrossRef](#)]
21. Shah, U.S.; Dhir, R.; Gollin, S.M.; Chandran, U.R.; Lewis, D.; Acquafondata, M.; Pflug, B.R. Fatty acid synthase gene overexpression and copy number gain in prostate adenocarcinoma. *Hum. Pathol.* **2006**, *37*, 401–409. [[CrossRef](#)] [[PubMed](#)]
22. Veigel, D.; Wagner, R.; Stübiger, G.; Wuczkowski, M.; Filipits, M.; Horvat, R.; Benhamú, B.; López-Rodríguez, M.L.; Leisser, A.; Valent, P.; et al. Fatty acid synthase is a metabolic marker of cell proliferation rather than malignancy in ovarian cancer and its precursor cells. *Int. J. Cancer* **2015**, *136*, 2078–2090. [[CrossRef](#)]
23. Pizer, E.S.; Wood, F.D.; Heine, H.S.; Romantsev, F.E.; Pasternack, G.R.; Kuhajda, F.P. Inhibition of fatty acid synthesis delays disease progression in a xenograft model of ovarian cancer. *Cancer Res.* **1996**, *56*, 1189–1193. [[PubMed](#)]
24. Li, J.N.; Gorospe, M.; Chrest, F.J.; Kumaravel, T.S.; Evans, M.K.; Han, W.F.; Pizer, E.S. Pharmacological inhibition of fatty acid synthase activity produces both cytostatic and cytotoxic effects modulated by p53. *Cancer Res.* **2001**, *61*, 1493–1499. [[PubMed](#)]
25. Puig, T.; Porta, R.; Colomer, R. Fatty acid synthase: a new anti-tumor target. *Med. Clin. (Barc.)* **2009**, *132*, 359–363. [[CrossRef](#)] [[PubMed](#)]
26. Blancafort, A.; Giró-Perafita, A.; Oliveras, G.; Palomeras, S.; Turrado, C.; Campuzano, Ò.; Carrión-Salip, D.; Massaguer, A.; Brugada, R.; Palafox, M.; Gómez-Miragaya, J.; González-Suárez, E.; Puig, T. Dual fatty acid synthase and HER2 signaling blockade shows marked antitumor activity against breast cancer models resistant to anti-HER2 drugs. *PLoS ONE* **2015**, *10*, e0131241. [[CrossRef](#)] [[PubMed](#)]
27. Bandyopadhyay, S.; Zhan, R.; Wang, Y.; Pai, S.K.; Hirota, S.; Hosobe, S.; Takano, Y.; Saito, K.; Furuta, E.; Iiizumi, M.; et al. Mechanism of apoptosis induced by the inhibition of fatty acid synthase in breast cancer cells. *Cancer Res.* **2006**, *66*, 5934–5940. [[CrossRef](#)] [[PubMed](#)]
28. Puig, T.; Vázquez-Martín, A.; Relat, J.; Pétriz, J.; Menéndez, J.A.; Porta, R.; Casals, G.; Marrero, P.F.; Haro, D.; Brunet, J.; Colomer, R. Fatty acid metabolism in breast cancer cells: Differential inhibitory effects of epigallocatechin gallate (EGCG) and C75. *Breast Cancer Res. Treat.* **2008**, *109*, 471–479. [[CrossRef](#)]
29. Seguin, F.; Carvalho, M.A.; Bastos, D.C.; Agostini, M.; Zecchin, K.G.; Alvarez-Flores, M.P.; Chudzinski-Tavassi, A.M.; Coletta, R.D.; Graner, E. The fatty acid synthase inhibitor orlistat reduces experimental metastases and angiogenesis in B16-F10 melanomas. *Br. J. Cancer* **2012**, *107*, 977–987. [[CrossRef](#)] [[PubMed](#)]
30. Browne, C.D.; Hindmarsh, E.J.; Smith, J.W. Inhibition of endothelial cell proliferation and angiogenesis by orlistat, a fatty acid synthase inhibitor. *FASEB J.* **2006**, *20*, 2027–2035. [[CrossRef](#)] [[PubMed](#)]
31. Meena, A.S.; Sharma, A.; Kumari, R.; Mohammad, N.; Singh, S.V.; Bhat, M.K. Inherent and acquired resistance to paclitaxel in hepatocellular carcinoma: molecular events involved. *PLoS ONE* **2013**, *8*, e61524. [[CrossRef](#)] [[PubMed](#)]

32. Rysman, E.; Brusselmans, K.; Scheys, K.; Timmermans, L.; Derua, R.; Munck, S.; Van Veldhoven, P.P.; Waltregny, D.; Daniels, V.W.; Machiels, J.; et al. De novo lipogenesis protects cancer cells from free radicals and chemotherapeutics by promoting membrane lipid saturation. *Cancer Res.* **2010**, *70*, 8117–8126. [[CrossRef](#)] [[PubMed](#)]
33. Menendez, J.A.; Vellon, L.; Colomer, R.; Lupu, R. Pharmacological and small interference RNA-mediated inhibition of breast cancer-associated fatty acid synthase (oncogenic antigen-519) synergistically enhances Taxol (paclitaxel)-induced cytotoxicity. *Int. J. Cancer* **2005**, *115*, 19–35. [[CrossRef](#)]
34. Giró-Perafita, A.; Palomeras, S.; Lum, D.H.; Blancafort, A.; Viñas, G.; Oliveras, G.; Pérez-Bueno, F.; Sarrats, A.; Welm, A.L.; Puig, T. Preclinical Evaluation of Fatty Acid Synthase and EGFR Inhibition in Triple Negative Breast Cancer. *Clin. Cancer Res.* **2016**, *22*, 4687–4697. [[CrossRef](#)] [[PubMed](#)]
35. Giró-Perafita, A.; Sarrats, A.; Pérez-Bueno, F.; Oliveras, G.; Buxó, M.; Brunet, J.; Viñas, G.; Puig Miquel, T. Fatty acid synthase expression and its association with clinico-histopathological features in triple-negative breast cancer. *Oncotarget* **2017**, *8*, 74391–74405. [[CrossRef](#)] [[PubMed](#)]
36. Scheel, C.; Weinberg, R.A. Cancer stem cells and epithelial-mesenchymal transition: Concepts and molecular links. *Semin. Cancer Biol.* **2012**, *22*, 396–403. [[CrossRef](#)] [[PubMed](#)]
37. Huber, M.A.; Kraut, N.; Beug, H. Molecular requirements for epithelial-mesenchymal transition during tumor progression. *Curr. Opin. Cell Biol.* **2005**, *17*, 548–558. [[CrossRef](#)] [[PubMed](#)]
38. Marjanovic, N.D.; Weinberg, R.A.; Chaffer, C.L. Cell plasticity and heterogeneity in cancer. *Clin. Chem.* **2013**, *59*, 168–179. [[CrossRef](#)]
39. Morel, A.-P.; Lièvre, M.; Thomas, C.; Hinkal, G.; Ansieau, S.; Puisieux, A. Generation of breast cancer stem cells through epithelial-mesenchymal transition. *PLoS ONE* **2008**, *3*. [[CrossRef](#)] [[PubMed](#)]
40. Chen, D.; Wan, S.B.; Yang, H.; Yuan, J.; Chan, T.H.; Dou, Q.P. EGCG, green tea polyphenols and their synthetic analogs and prodrugs for human cancer prevention and treatment. *Adv. Clin. Chem.* **2011**, *53*, 155–177.
41. Puig, T.; Relat, J.; Marrero, P.F.; Haro, D.; Brunet, J.; Colomer, R. Green tea catechin inhibits fatty acid synthase without stimulating carnitine palmitoyltransferase-1 or inducing weight loss in experimental animals. *Anticancer Res.* **2008**, *28*, 3671–3676. [[PubMed](#)]
42. Fujiki, H.; Sueoka, E.; Rawangkan, A.; Suganuma, M. Human cancer stem cells are a target for cancer prevention using (–)-epigallocatechin gallate. *J. Cancer Res. Clin. Oncol.* **2017**, *143*, 1–12. [[CrossRef](#)]
43. Oliveras, G.; Blancafort, A.; Urruticochea, A.; Campuzano, O.; Gómez-Cabello, D.; Brugada, R.; López-Rodríguez, M.L.; Colomer, R.; Puig, T. Novel anti-fatty acid synthase compounds with anti-cancer activity in HER2+ breast cancer. *Ann. N. Y. Acad. Sci.* **2010**, *1210*, 86–92. [[CrossRef](#)] [[PubMed](#)]
44. Turrado, C.; Puig, T.; García-Cárceles, J.; Artola, M.; Benhamú, B.; Ortega-Gutiérrez, S.; Relat, J.; Oliveras, G.; Blancafort, A.; Haro, D.; et al. New synthetic inhibitors of fatty acid synthase with anticancer activity. *J. Med. Chem.* **2012**, *55*, 5013–5023. [[CrossRef](#)] [[PubMed](#)]
45. Crous-Masó, J.; Palomeras, S.; Relat, J.; Camó, C.; Martínez-Garza, Ú.; Planas, M.; Feliu, L.; Puig, T. (–)-Epigallocatechin 3-gallate synthetic analogues inhibit fatty acid synthase and show anticancer activity in triple negative breast cancer. *Molecules* **2018**, *23*, 1160. [[CrossRef](#)] [[PubMed](#)]
46. Puig, T.; Aguilar, H.; Cufí, S.; Oliveras, G.; Turrado, C.; Ortega-Gutiérrez, S.; Benhamú, B.; López-Rodríguez, M.L.; Urruticochea, A.; Colomer, R. A novel inhibitor of fatty acid synthase shows activity against HER2+ breast cancer xenografts and is active in anti-HER2 drug-resistant cell lines. *Breast Cancer Res.* **2011**, *13*, R131. [[CrossRef](#)] [[PubMed](#)]
47. Liu, H.; Wu, X.; Dong, Z.; Luo, Z.; Zhao, Z.; Xu, Y.; Zhang, J.-T. Fatty acid synthase causes drug resistance by inhibiting TNF- α and ceramide production. *J. Lipid Res.* **2013**, *54*, 776–785. [[CrossRef](#)] [[PubMed](#)]
48. Zeng, L.; Wu, G.-Z.; Goh, K.J.; Lee, Y.M.; Ng, C.C.; You, A.B.; Wang, J.; Jia, D.; Hao, A.; Yu, Q.; et al. Saturated fatty acids modulate cell response to DNA damage: implication for their role in tumorigenesis. *PLoS ONE* **2008**, *3*, e2329. [[CrossRef](#)] [[PubMed](#)]
49. Wu, X.; Qin, L.; Fako, V.; Zhang, J.-T. Molecular mechanisms of fatty acid synthase (FASN)-mediated resistance to anti-cancer treatments. *Adv. Biol. Regul.* **2014**, *54*, 214–221. [[CrossRef](#)] [[PubMed](#)]
50. Talebi, A.; Dehairs, J.; Swinnen, J.V. De novo lipogenesis and membrane remodeling in cancer. *Biomed. Res. India* **2012**, *23*, 49–53.

51. Bauerschlag, D.O.; Maass, N.; Leonhardt, P.; Verburg, F.A.; Pecks, U.; Zeppernick, F.; Morgenroth, A.; Mottaghy, F.M.; Tolba, R.; Meinhold-Heerlein, I.; et al. Fatty acid synthase overexpression: target for therapy and reversal of chemoresistance in ovarian cancer. *J. Transl. Med.* **2015**, *13*, 1–12. [[CrossRef](#)]
52. Creighton, C.J.; Li, X.; Landis, M.; Dixon, J.M.; Neumeister, V.M.; Sjolund, A.; Rimm, D.L.; Wong, H.; Rodriguez, A.; Herschkowitz, J.I.; et al. Residual breast cancers after conventional therapy display mesenchymal as well as tumor-initiating features. *Proc. Natl. Acad. Sci. USA* **2009**, *106*, 13820–13825. [[CrossRef](#)]
53. Vidal, S.J.; Rodriguez-Bravo, V.; Galsky, M.; Cordon-Cardo, C.; Domingo-Domenech, J. Targeting cancer stem cells to suppress acquired chemotherapy resistance. *Oncogene* **2013**, *1–13*. [[CrossRef](#)]
54. Domingo-Domenech, J.; Vidal, S.J.; Rodriguez-Bravo, V.; Castillo-Martin, M.; Quinn, S.A.; Rodriguez-Barrueco, R.; Bonal, D.M.; Charytonowicz, E.; Gladoun, N.; de la Iglesia-Vicente, J.; et al. Suppression of Acquired Docetaxel Resistance in Prostate Cancer through Depletion of Notch- and Hedgehog-Dependent Tumor-Initiating Cells. *Cancer Cell* **2012**, *22*, 373–388. [[CrossRef](#)]
55. Dean, M.; Fojo, T.; Bates, S. Tumour stem cells and drug resistance. *Nat Rev Cancer* **2005**, *5*, 275–284. [[CrossRef](#)]
56. Thiery, J.P. Epithelial-mesenchymal transitions in tumour progression. *Nat. Rev. Cancer* **2002**, *2*, 442–454. [[CrossRef](#)]
57. Prat, A.; Perou, C.M. Deconstructing the molecular portraits of breast cancer. *Mol. Oncol.* **2011**, *5*, 5–23. [[CrossRef](#)]
58. Shaw, F.L.; Harrison, H.; Spence, K.; Ablett, M.P.; Simoes, B.M.; Farnie, G.; Clarke, R.B. A detailed mammosphere assay protocol for the quantification of breast stem cell activity. *J. Mammary Gland Biol. Neoplasia* **2012**, *17*, 111–117. [[CrossRef](#)]
59. Prud'Homme, G.J.; Glinka, Y.; Toulina, A.; Ace, O.; Subramaniam, V.; Jothy, S. Breast cancer stem-like cells are inhibited by a non-toxic aryl hydrocarbon receptor agonist. *PLoS ONE* **2010**, *5*. [[CrossRef](#)]
60. Grimshaw, M.J.; Cooper, L.; Papazisis, K.; Coleman, J.A.; Bohnenkamp, H.R.; Chiapero-Stanke, L.; Taylor-Papadimitriou, J.; Burchell, J.M. Mammosphere culture of metastatic breast cancer cells enriches for tumorigenic breast cancer cells. *Breast Cancer Res.* **2008**, *10*, R52. [[CrossRef](#)]
61. Wang, R.; Lv, Q.; Meng, W.; Tan, Q.; Zhang, S.; Mo, X.; Yang, X. Comparison of mammosphere formation from breast cancer cell lines and primary breast tumors. *J. Thorac. Dis.* **2014**, *6*, 829–837. [[CrossRef](#)]
62. Tanei, T.; Morimoto, K.; Shimazu, K.; Seung, J.K.; Tanji, Y.; Taguchi, T.; Tamaki, Y.; Noguchi, S. Association of breast cancer stem cells identified by aldehyde dehydrogenase 1 expression with resistance to sequential paclitaxel and epirubicin-based chemotherapy for breast cancers. *Clin. Cancer Res.* **2009**, *15*, 4234–4241. [[CrossRef](#)]
63. Moody, S.E.; Perez, D.; Pan, T.C.; Sarkisian, C.J.; Portocarrero, C.P.; Sterner, C.J.; Notorfrancesco, K.L.; Cardiff, R.D.; Chodosh, L.A. The transcriptional repressor Snail promotes mammary tumor recurrence. *Cancer Cell* **2005**, *8*, 197–209. [[CrossRef](#)]
64. Tran, H.D.; Luitel, K.; Kim, M.; Zhang, K.; Longmore, G.D.; Tran, D.D. Transient SNAIL1 expression is necessary for metastatic competence in breast cancer. *Cancer Res.* **2014**, *74*, 6330–6340. [[CrossRef](#)]
65. Ye, X.; Tam, W.L.; Shibue, T.; Kaygusuz, Y.; Reinhardt, F.; Ng Eaton, E.; Weinberg, R.A. Distinct EMT programs control normal mammary stem cells and tumour-initiating cells. *Nature* **2015**, *525*, 256–260. [[CrossRef](#)]
66. Phillips, S.; Kuperwasser, C. SLUG: Critical regulator of epithelial cell identity in breast development and cancer. *Cell Adhes. Migr.* **2014**, *8*, 578–587. [[CrossRef](#)]
67. Zhuang, X.; Zhang, W.; Chen, Y.; Han, X.; Li, J.; Zhang, Y.Y.; Zhang, S.; Liu, B. Doxorubicin-enriched, ALDH(br) mouse breast cancer stem cells are treatable to oncolytic herpes simplex virus type 1. *BMC Cancer* **2012**, *12*, 549. [[CrossRef](#)]
68. Kruger, J.A.; Kaplan, C.D.; Luo, Y.; Zhou, H.; Markowitz, D.; Xiang, R.; Reisfeld, R.A. Characterization of stem cell-like cancer cells in immune-competent mice. *Blood* **2006**, *108*, 3906–3912. [[CrossRef](#)]
69. Bandyopadhyay, A.; Wang, L.; Agyin, J.; Tang, Y.; Lin, S.; Yeh, I.T.; De, K.; Sun, L.Z. Doxorubicin in combination with a small TGF β inhibitor: A potential novel therapy for metastatic breast cancer in mouse models. *PLoS ONE* **2010**, *5*. [[CrossRef](#)]
70. Tudoran, O.; Soritau, O.; Balacescu, L.; Visan, S.; Barbos, O.; Cojocneanu-Petric, R.; Balacescu, O.; Berindan-Neagoe, I. Regulation of stem cells-related signaling pathways in response to doxorubicin treatment in Hs578T triple-negative breast cancer cells. *Mol. Cell. Biochem.* **2015**, *409*, 163–176. [[CrossRef](#)]

71. Silva Galbiatti-Dias, A.L.; Fernandes, G.M.M.; Castanhole-Nunes, M.M.U.; Hidalgo, L.F.; Nascimento Filho, C.H.V.; Kawasaki-Oyama, R.S.; Ferreira, L.A.M.; Biselli-Chicote, P.M.; Pavarino, É.C.; Goloni-Bertollo, E.M. Relationship between CD44(high)/CD133(high)/CD117(high) cancer stem cells phenotype and Cetuximab and Paclitaxel treatment response in head and neck cancer cell lines. *Am. J. Cancer Res.* **2018**, *8*, 1633–1641.
72. Liu, H.; Liu, Y.; Zhang, J.-T. A new mechanism of drug resistance in breast cancer cells: fatty acid synthase overexpression-mediated palmitate overproduction. *Mol. Cancer Ther.* **2008**, *7*, 263–270. [[CrossRef](#)]
73. Gonzalez-Guerrico, A.M.; Espinoza, I.; Schroeder, B.; Park, C.H.; KVP, C.M.; Khurana, A.; Corominas-Faja, B.; Cuyàs, E.; Alarcón, T.; Kleer, C.; et al. Suppression of endogenous lipogenesis induces reversion of the malignant phenotype and normalized differentiation in breast cancer. *Oncotarget* **2016**, *7*, 71151–71168. [[CrossRef](#)]
74. Pandey, P.R.; Okuda, H.; Watabe, M.; Pai, S.K.; Liu, W.; Kobayashi, A.; Xing, F.; Fukuda, K.; Hirota, S.; Sugai, T.; et al. Resveratrol suppresses growth of cancer stem-like cells by inhibiting fatty acid synthase. *Breast Cancer Res. Treat.* **2011**, *130*, 387–398. [[CrossRef](#)]
75. Yasumoto, Y.; Miyazaki, H.; Vaidyan, L.K.; Kagawa, Y.; Ebrahimi, M.; Yamamoto, Y.; Ogata, M.; Katsuyama, Y.; Sadahiro, H.; Suzuki, M.; et al. Inhibition of fatty acid synthase decreases expression of stemness markers in glioma stem cells. *PLoS ONE* **2016**, *11*, 1–14. [[CrossRef](#)]

Sample Availability: Samples of the compounds are not available from the authors.



© 2019 by the authors. Licensee MDPI, Basel, Switzerland. This article is an open access article distributed under the terms and conditions of the Creative Commons Attribution (CC BY) license (<http://creativecommons.org/licenses/by/4.0/>).

CHAPTER 6 Results IV

Enrichment of BCSCs in the TNBC models MDA-MB-231 (mesenchymal-like) and MDA-MB-468 (basal-like) within 3D electrospun PCL scaffold culture

This chapter is based on the following publications:

Title Manufacture of PCL scaffolds through electrospinning technology to accommodate triple negative breast cancer cells culture (Proceeding)

Authors Marc Rabionet, Teresa Puig*, Joaquim Ciurana*

Journal Procedia CIRP

Publication year 2020

CiteScore ₂₀₂₀ 3.3 (68th percentile in Industrial and Manufacturing Engineering; position 107 of 336)

DOI 10.1016/j.procir.2020.05.124

Title Electrospinning PCL scaffolds manufacture for three-dimensional breast cancer cell culture

Authors Marc Rabionet, Marc Yeste, Teresa Puig*, Joaquim Ciurana*

Journal Polymers

Publication year 2017

Impact Factor ₂₀₁₇ 2.935 (Q1 in Polymer Science; position 19 of 87)

DOI 10.3390/polym9080328

Title Fatty acid synthase as a novel biomarker for triple negative breast cancer stem cell subpopulation cultured on electrospun scaffolds

Authors Marc Rabionet, Emma Polonio-Alcalá, Joana Relat, Marc Yeste, Jennifer Sims-Mourtada, April M. Kloxin, Marta Planas, Lidia Feliu, Joaquim Ciurana*, Teresa Puig*

Journal Under review on Materials Today Bio

Publication year -

Impact Factor ₂₀₂₀ 7.348 (Q1 in Materials Science, Biomaterials; position 6 of 40)

DOI -

_ Paper to be considered for compendium of publications format

* Corresponding author

Abstract

In a previous chapter, the suitability of ES PCL scaffolds for 3D culture and stemness expansion has been confirmed using a reference breast cancer cell model. Moreover, preceding section has explored the potential of FASN as a target for BCSC-enriched TNBC samples.

Chapter 6 aims to use ES PCL scaffolds as a tool to enrich the BCSC niche of TNBC cell models. Hence, this malignant subpopulation can be properly studied, as well as the role of some underlying elements such as FASN. Therefore, previously optimized ES PCL scaffolds were manufactured and characterized through scanning electron microscopy (SEM), differential scanning calorimetry (DSC), thermal gravimetric analysis (TGA), and dynamic mechanic analysis (DMA). The TNBC cell lines MDA-MB-231 (mesenchymal-like molecular subtype) and MDA-MB-468 (basal-like) were used in this work with the aim to have the whole molecular representation of the TNBC disease. Both cell lines were cultured on scaffolds and cell morphology and proliferation kinetics were examined along time, by fluorescence microscopy and MTT assay, respectively. To quantify BCSC subpopulation in monolayer and scaffold culture several assays were performed, including mammospheres, ALDH, CD44⁺/CD24^{-/low}, and chemoresistance. RT-PCR and Western blot techniques were used to assess the expression of stemness- and EMT-related markers altogether with proteins involved in the main cell signaling pathways. Lastly, FASN expression was determined in 2D and 3D cultures using a radioactivity assay. To determine the impact of FASN blockade in BCSC-enriched samples, the inhibitors EGCG and G28 were added before performing a mammosphere forming assay.

Results showed that ES PCL scaffolds offered a soft physical support formed by a network of nanofilaments. When cultured on scaffolds, TNBC cells displayed a more elongated cytoplasm, which was accompanied by a slower cell proliferation

kinetics. Interestingly, several BCSC markers were found to be upregulated in scaffolds, confirming a BCSC expansion due to 3D culture. Other than that, scaffold-cultured cells display a shift from MAPK to PI3K/AKT/mTOR signaling pathways, alongside an enhanced EGFR and HER2 activation. Ultimately, FASN was found hyperactivated in BCSC-enriched samples and its pharmacological inhibition led to stemness diminishment, overcoming the stemness expansion achieved in 3D culture.

Available online at www.sciencedirect.com

ScienceDirect

Procedia CIRP 89 (2020) 98–103

www.elsevier.com/locate/procedia

CIRP BioManufacturing Conference 2019

Manufacture of PCL scaffolds through electrospinning technology to accommodate Triple Negative Breast Cancer cells culture

Marc Rabionet^{a,b}, Teresa Puig^{b*}, Joaquim Ciurana^{a*}

^aProduct, Process and Production Engineering Research Group (GREP), Department of Mechanical Engineering and Industrial Construction, University of Girona, Maria Aurèlia Capmany 61, 17003 Girona, Spain

^bNew Therapeutic Targets Laboratory (TargetsLab), Department of Medical Sciences, University of Girona, Emili Grahit 77, 17003 Girona, Spain

* Corresponding author. Tel.: 34-972-418-265 / 419-618. E-mail address: quim.ciurana@udg.edu (Joaquim Ciurana) / teresa.puig@udg.edu (Teresa Puig)

Abstract

Two-dimensional (2D) cell culture structures are demonstrated to differ from the *in vivo* environment. Therefore, cells adopt a flattened morphology that may lead to a non-physiological behaviour. For instance, 2D culture induces the differentiation of the cancer stem cells (CSCs), a tumorigenic cell niche whose study is crucial in tumors with a high relapse rate such as the triple negative breast cancer (TNBC). As an alternative, electrospun scaffolds which mimic the native extracellular matrix structure have emerged as a three-dimensional culture support. In this work, two different meshes of 7.5 and 15% of poly(ϵ -caprolactone) (PCL) were fabricated, differentiating in their microstructure. Scaffolds exhibited similar DSC and TGA curves compared with raw PCL, indicating their purity. TNBC MDA-MB-468 cells were seeded on scaffolds and adopted a more elongated morphology when cultured on 15% PCL meshes. Hence, electrospinning PCL scaffolds may become a suitable tool to culture TNBC cells in a more physiological manner.

© 2020 The Authors. Published by Elsevier B.V.

This is an open access article under the CC BY-NC-ND license (<http://creativecommons.org/licenses/by-nc-nd/4.0/>)

Peer-review under responsibility of the scientific committee of the CIRP BioManufacturing Conference 2019.

Keywords: polycaprolactone; scaffolds; electrospinning; three-dimensional cell culture; triple negative breast cancer

1. Introduction

Since some decades ago, disposable polystyrene vessels have been used for cell culture applications due to their practicability [1]. These flat plastic supports enable the foundation of a two-dimensional (2D) cell culture which represents an easy and cheap way to maintain cell division. However, 2D surfaces are clearly in conflict with the physiological surrounding that cells found in the organism. Inside the body, cells are naturally embedded by a three-dimensional (3D) network constituted by fibrous proteins and molecules known as extracellular matrix (ECM) [2]. Actually, the most abundant element is the collagen, a structural protein which is set up in the form of nanofilaments [3]. In this manner, ECM offers a physical support for cells to attach and grow, apart from its role in cell regulation [2], [4]. Cells tend

to adopt an elongated pattern in *in vivo* conditions as they are able to attach different filaments as well as adjacent cells. Nevertheless, in 2D surfaces cells can only proliferate forming a monolayer and they normally adopt a flattened morphology. Cell flatness directly modifies the membrane receptor polarity as well as the cytoskeleton organization, affecting the gene expression and protein synthesis [5].

As an alternative, research has been focused on the development of 3D supports for cell culture purposes, including scaffolds among others. Scaffolds consist on a network of biopolymeric filaments, mimicking the EMC structure [6]. Therefore, they provide a physical structure which enable cells to adopt a more *in vivo* morphology. Lastly, electrospinning process has gained importance in the scaffolds manufacturing field. The main reasons are its potential

2212-8271 © 2020 The Authors. Published by Elsevier B.V.

This is an open access article under the CC BY-NC-ND license (<http://creativecommons.org/licenses/by-nc-nd/4.0/>)

Peer-review under responsibility of the scientific committee of the CIRP BioManufacturing Conference 2019.

10.1016/j.procir.2020.05.124

regarding the fabrication of small diameters fibers and its customizability [7], [8]. A wide range of polymers can be electrospun to manufacture fibrous meshes, including the poly(ϵ -caprolactone) (PCL), an FDA approved polyester characterized by its viscoelastic and rheological properties [9].

Cancer research field is taking advantage of the development of 3D structures for cell culture applications. It is demonstrated that cancer cells cultured on 3D structures including scaffolds exhibited a more elongated shape in discordance with monolayer cultured cells [10], [11]. The closeness of 3D-cultured cells morphology to the *in vivo* one makes scaffolds an ideal alternative to study physiological cell behavior. For instance, scaffolds were proved to maintain the differentiation state of cancer cells [10], [12]. Since some decades ago, cancers have been studied as a heterogeneous mixture of different cell types: normal cancer cells and a rare subpopulation of cancer stem cells (CSCs) [13]. CSCs display a key role in cancer development and tumor relapse [14], [15]. Lately, 3D culture supports are used to maintain stemness capacity since monolayer culture induces CSCs differentiation [10], [11], [16], [17].

The main goal of this work is to assess scaffolds potential for three-dimensional breast cancer cell culture applications. For this reason, two different PCL solutions were electrospun since polymer concentration is proved to exert a strong influence on scaffolds structure [8], [18]. Produced meshes were characterized and seeded with a triple negative breast cancer (TNBC) cell line considering that this subtype display the highest proportion of cancer recurrence with a value of 34% [19], an issue directly related to CSCs presence. Cell proliferation and morphology were determined on monolayer culture and 3D scaffolds. Obtained results suggest the suitability of electrospun PCL meshes as a novel tool for 3D breast cancer cell culture. Further studies must be focused on CSC population experimentation with the aim of developing a novel targeted therapy against this malignant niche, useful for TNBC patients.

2. Materials and Methods

2.1. Scaffolds manufacture

Poly(ϵ -caprolactone) (PCL; 80,000 g/mol; Sigma-Aldrich, St. Louis, MO, USA) was dissolved in acetone (PanReac AppliChem, Gatersleben, Germany). Two different solutions of 7.5 and 15% w/v PCL were produced under 45°C and agitation. Scaffolds were manufactured with an electrospinning machine (Spraybase, Dublin, Ireland) and an 18 G needle emitter (inner diameter of 0.8 mm) located 15 cm above the stationary collector. A voltage of 7 kV was applied and the flow rate was determined at 6 mL/h by the Syringe Pump Pro software (New Era Pump Systems, Farmingdale, NY, USA). Electrospinning process was finished when 10 or 5 mL of PCL-acetone solution were ejected, for 7.5 and 15% PCL concentrations, respectively. Once electrospinning process was finished, resulting scaffolds were cut into squares with a scalpel.

2.2. Scanning Electron Microscopy (SEM) analysis

Microscopic architecture of both scaffolds models was observed through scanning electron microscopy (SEM; Zeiss, Oberkochen, Germany) after carbon coating. Captured images were analyzed with Image J software (National Institutes of Health, Bethesda, MD, USA).

2.3. Differential Scanning Calorimetry (DSC) analysis

Differential scanning calorimetry (DSC; TA Instruments Q2000 V24.4, Newcastle, DE, USA) was carried out on commercial PCL pellets (as received) and on scaffolds from 7.5 and 15% PCL solution. About 5 mg of each sample were placed in aluminum pans. Experiments were conducted from 30°C to 100°C at a rate of 10°C/min. To prevent oxidative degradation, analyses were performed in nitrogen with a flow rate of 50 mL/min.

2.4. Thermal Gravimetric Analysis (TGA)

The thermal degradation of samples was studied through a Thermal Gravimetric Analysis (TGA) using a Mettler Toledo TGA 1 (Columbus, OH, USA). Around 10 mg of non-processed PCL and scaffolds from 7.5 and 15% PCL solution were analyzed. Measurements were performed with a temperature ranging from 30°C to 700°C with a ratio of 10°C/min.

2.5. Cell line

MDA-MB-468 triple negative breast cancer cell line was obtained from the American Type Culture Collection (ATCC; Rockville, MD, USA). MDA-MB-468 cells were routinely grown in Dulbecco's Modified Eagle's Medium (DMEM; Gibco, Waltham, MA, USA) supplemented with 10% fetal bovine serum, 1% L-glutamine, 1% sodium pyruvate, 50 U/mL penicillin, and 50 μ g/mL streptomycin (HyClone, Logan, UT, USA). Cells were maintained in a 5% CO₂ humidified incubator at 37°C and culture medium was changed every 3 days.

2.6. Three-dimensional cell culture

Electrospun meshes were first sterilized with 70% ethanol/water solution overnight, washed with PBS (Gibco) and exposed to UV light for 30 min. Then, scaffolds were placed in a 12-well non-adherent cell culture microplate (Sartstedt, Nümbrecht, Germany). Cell suspension was prepared in a volume of 50 μ L and pipetted onto the scaffold center. After an incubation period of 3 hours, 1 mL of medium per well was added. Two-dimensional controls were also performed. For cell proliferation assay, 2 500 cells/well were seeded. In contrast, for cell morphology analysis, the following cell densities were performed (see Table 1). Thus, similar cell confluence was reached among different cell culture supports and culture days.

Table 1. Cell densities performed for cell morphology analysis.

		Cell culture support	
		2D	3D
Cell culture days	3 days	60 000	60 000
	6 days	20 000	30 000
	12 days	4 000	6 000

2.7. Cell proliferation assay

The MTT assay was used to test cell proliferation on the different cell culture supports. After the culture period, medium was removed and scaffolds were put into new wells. They were incubated with 1 mL of medium and 100 μ L of MTT (Sigma-Aldrich) for 2 h and 30 min. Resulting formazan crystals were dissolved with 1 mL of dimethyl sulfoxide (DMSO; Sigma-Aldrich). Four aliquots of 100 μ L from each sample were transferred into a 96-well plated and placed into a microplate reader (Bio-Rad, Hercules, CA, USA). Monolayer culture samples were equally processed and absorbance was measured at 570 nm.

2.8. Cell morphology analysis

MDA-MB-468 cells were seeded on adherent coverslips (Sarstedt) and 7.5% and 15% PCL scaffolds. After incubation, cells were washed with PBS and fixed with 4% paraformaldehyde (PFA; Sigma-Aldrich) for 20 min. Then, samples were washed and incubated with 0.2% Triton X-100 (Sigma-Aldrich) for 10 min to permeabilize the cells. Blocking buffer (PBS with 3% bovine serum albumin [BSA; Sigma-Aldrich]) was added for 20 min. Later, cells were incubated for 20 min with rhodamine-phalloidin (Cytoskeleton Inc., Denver, CO, USA) (1:250) to stain actin cytoskeleton and then with 4,6-diamidino-2-phenylindole (DAPI; BD Pharmingen, Franklin Lakes, NJ, USA) (1:1000) for 10 min to stain nuclei. All incubations were performed at room temperature. Fluorescent samples were imaged with a confocal microscope (Nikon A1R, Nikon, Tokyo, Japan). Camera settings (illumination intensity, quality, resolution and colour) were standardized for all photographs. Rhodamine-phalloidin and DAPI, for red and blue fluorescence respectively, were captured and merged with Image J software (National Institutes of Health). This software was also used to determine nuclear and cytoplasmic elongation factors. Briefly, five cells of ten different pictures were randomly selected and their length and width of the nucleus and cytoplasm were measured. Finally, the following formula was used:

$$\text{Nuclear/Cytoplasmic Elongation Factor} = \frac{\text{length nucleus/cytoplasm}}{\text{width nucleus/cytoplasm}}$$

2.9. Statistics analysis

All data are expressed as mean \pm standard error (SE). Data were analyzed using IBM SPSS (Version 21.0; SPSS Inc., Chicago, IL, USA) through ANOVA and post hoc tests. Statistical significant levels were $p < 0.05$ (denoted as *), $p <$

0.01 (**), and $p < 0.001$ (***). All observations were confirmed by at least three independent experiments.

3. Results and discussion

3.1. Electrospun PCL scaffolds characterization

Once scaffolds were produced, they were characterized through several approaches. Meshes from 7.5 and 15% PCL-acetone solution were observed under a scanning electron microscopy (Fig. 1).

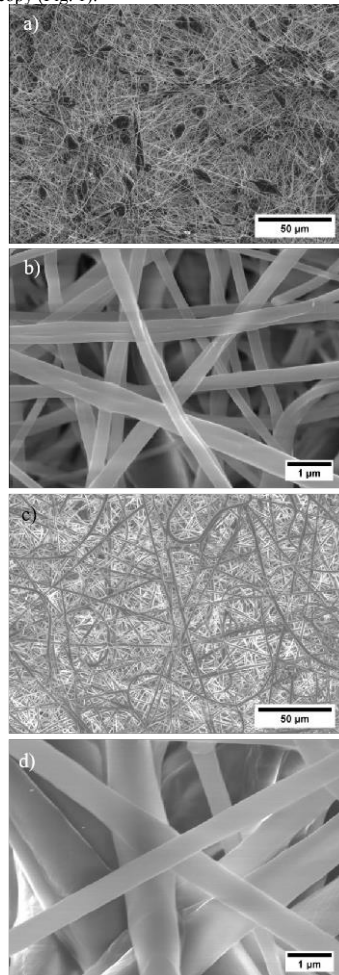


Fig. 1. Microscopic characterization of 7.5 (a and b) and 15% PCL (c and d) electrospun scaffolds. Specimens were imaged at 500 X (a and c) and 15000 X magnifications (b and d).

As previously described, both models exhibited similar surface porosity whereas 15% PCL specimens showed larger pores compared with 7.5% PCL scaffolds [11]. A previous study determined the fiber diameter of the different specimens, with an average value of 295.12 ± 148.45 nm and 701.13 ± 401.89 nm for 7.5 and 15% PCL scaffolds, respectively [11]. Interestingly, meshes from 7.5% PCL solution presented spherical structures made by non-filamentous polymer, apart from the nanofibers (Fig. 1A). These formations, called beads, are related with low polymer concentrations [20].

A Differential Scanning Calorimetry (DSC) analysis was later performed with the electrospun scaffolds in order to study their thermal behavior (see Fig. 2.).

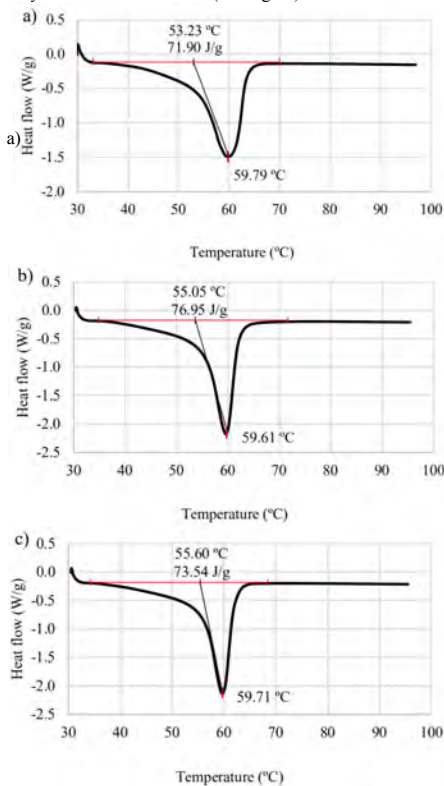


Fig. 2. DSC curves of PCL pellets (a) and 3D scaffolds from 7.5% (b) and 15% PCL solution (c).

The plots presented the typical DSC curves of a partially crystalline polymer with no impurities. The endothermic peak indicates the melting temperature, which displayed no differences among samples ranging from 59.61 to 59.79 °C. According to the obtained results, the melting temperature of pure PCL was reported to be around 60°C [21], [22]. These facts indicated the absence of impurities and, therefore, that manufacturing process did not affect the integrity of the

biopolymer. The onset melting temperature of raw PCL pellets was 53.23°C whereas both scaffold models displayed slightly higher values between 55.05 and 55.60 °C. Non-processed PCL exhibited a melting enthalpy of 71.90 J/g. Manufactured PCL scaffolds displayed moderately greater values of 76.95 and 73.54 J/g for 7.5 and 15% PCL meshes respectively, in agreement with previous analyses [23].

Then, thermal degradation of samples was studied through a Thermal Gravimetric Analysis (TGA). TGA curves of non-processed PCL pellet and electrospun 7.5 and 15% PCL scaffolds are presented in Fig. 3. All specimens exhibited a single step curve, indicating a stable degradation in a simple process. No differences were observed among pristine PCL and manufactured PCL scaffolds since their TGA curves appeared overlapped (Fig. 3). Moreover, degradation process of raw PCL and PCL meshes started around 350°C, as reported by the literature [24], [25]. These data support the hypothesis that electrospinning manufacturing process did not affect the integrity of PCL on resulting scaffolds and no impurities were detected.

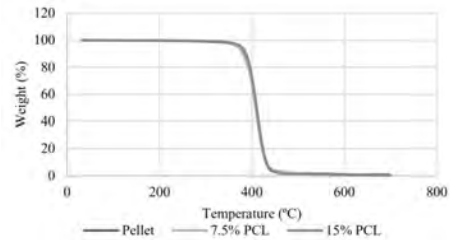


Fig. 3. TGA thermographs of PCL pellets and 3D scaffolds from 7.5% and 15% PCL solution.

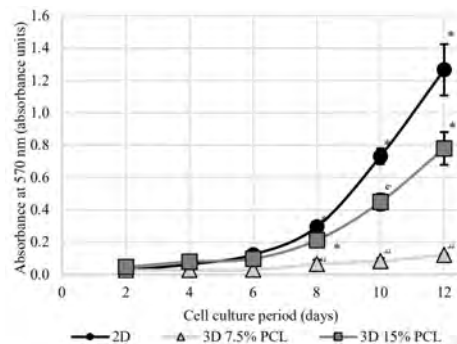


Fig. 4. Cell proliferation analysis for MDA-MB-468 triple negative breast cancer cells cultured on two-dimensional surfaces (2D) and on 7.5% and 15% PCL scaffolds (3D). (*), (#), and (\$) symbols represent significant ($p < 0.05$) differences among groups.

3.2. Breast cancer cell proliferation

Electrospun PCL scaffolds could become a suitable physical support for 3D cell culture. Indeed, scaffold

microarchitecture exert a high influence on cell adhesion and growth [11], [26], [27]. For this reason, adherent 2D surfaces and 7.5 and 15% PCL meshes were seeded with MDA-MB-468 breast cancer cells in order to evaluate cell efficiency (Fig. 4). Differences among cell culture models were found from 8 days of culture, when cell growth rate on 2D control and 15% PCL scaffolds adopted higher values compared to 7.5% PCL samples. Meshes from 7.5% PCL displayed the significantly lowest cell proliferation rate with almost a linear trend. In contrast, 15% PCL model served as the optimal support, with high absorbance values close to the monolayer ones.

3.3. Breast cancer cell morphology

Three-dimensional scaffolds provide a physical support which mimics the extracellular matrix structure. Therefore, cells can establish interactions with adjacent cells and with polymeric filaments, adopting a more *in vivo* morphology. For this reason, MDA-MB-468 cells morphology among different culture supports was studied through fluorescence microscopy during 3, 6 and 12 culture days. As can be seen in Fig. 5, MDA-MB-468 cells seeded on 2D surfaces exhibited a rounded shape since their cytoplasm remained flattened. Cells on 7.5% PCL scaffolds displayed a morphology similar to the aforementioned, with a globular appearance. In contrast, a fraction of cells cultured on 15% PCL meshes showed a higher number of cytoplasmic prolongations, adopting as a result a more elongated shape compared with the other culture supports. Regarding nuclear appearance, no qualitative differences were observed among conditions.

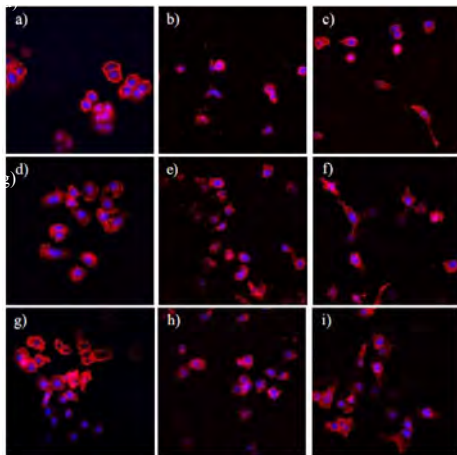


Fig. 5. Fluorescence images of MDA-MB-468 cells cultured during 3 (a-c), 6 (d-f), and 12 days (g-i). Cells were cultured on two-dimensional (2D) adherent coverslips (a, d, and g), or on three-dimensional scaffolds from 7.5% PCL solution (b, e, and h) and 15% PCL solution (c, f, and i). Actin cytoskeleton was stained with rhodamine-phalloidin (red) and nucleus was stained with 4,6-diamidino-2-phenylindole (DAPI; blue). Pictures were captured at a magnification of 400X.

In order to analyze possible quantitative differences concerning morphology, nuclear and cytoplasmic elongation factor were calculated (Fig. 6). As previously seen, no differences were observed on nuclear elongation. However, statistically significant differences were detected on cytoplasmic elongation analysis in agreement with previous observations. MDA-MB-468 cells when cultured on 15% PCL scaffolds adopted a more elongated cytoplasm along time in dealing with the other conditions (Fig. 6B).

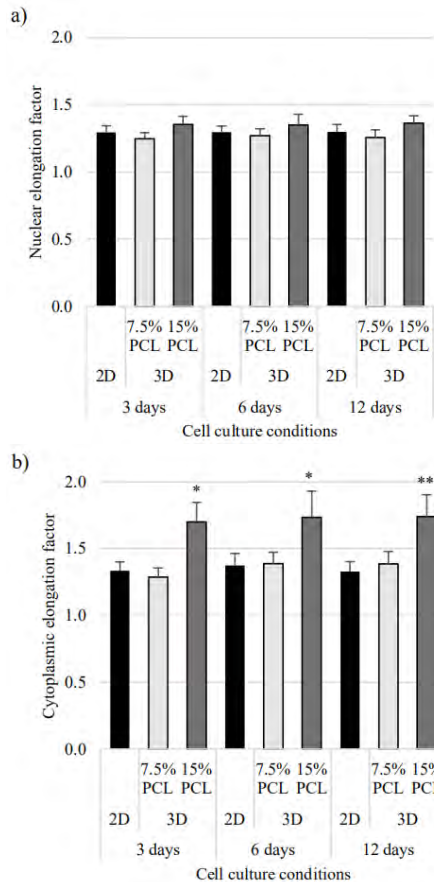


Fig. 6. MDA-MB-468 cell morphology analysis cultured on bidimensional surfaces (2D) and on 7.5% and 15% PCL scaffolds. Nuclear (a) and cytoplasmic elongation (b) were measured. Elongation values from scaffolds were compared with monolayer values and levels of statistically significance were indicated as * ($p < 0.05$) and ** ($p < 0.01$).

4. Conclusion

In this work, electrospun PCL scaffolds are presented as an alternative to monolayer culture regarding CSCs study. Presented data verify the capability of electrospinning as a scaffolds manufacturing process for cell culture applications. DSC and TGA curves of scaffolds almost overlap raw PCL data, indicating the absence of material modification neither contamination. Meshes from 7.5% PCL solution exhibited smaller fiber diameters and the presence of beads. In contrast, 15% PCL scaffolds exhibited greater filament diameters and beads absence. These discrepancies were reflected on cell proliferation analysis. MDA-MB-468 cells presented a higher cell growth rate when cultured on 15% PCL meshes compared with the 7.5% PCL model, as well as a strongest cytoplasmic elongation. Taking all into account, electrospun PCL scaffolds were able to accommodate TNBC cells culture. Therefore, cancer research could take benefit from 3D scaffolds for culture and stemness studies.

Acknowledgements

This work was supported by Spanish grants from Fundación Ramón Areces and Instituto de Salud Carlos III (PI1400329). The authors are grateful to the pre-doctoral grant (IFUdG2017/62), the support of the Catalan Government (2017SGR00385) and RadikalSwim (OncoSwim). The authors also thank Dr. Marc Yeste (Department of Biology, University of Girona) and the Research Technical Services from the University of Girona.

References

- [1] J. A. Ryhan, "Evolution of Cell Culture Surfaces," *Biofiles*, vol. 3, no. 8, pp. 21–24, 2008.
- [2] A. D. Theocharis, S. S. Skandalis, C. Gialeli, and N. K. Karamanos, "Extracellular matrix structure," *Adv. Drug Deliv. Rev.*, vol. 97, pp. 4–27, Feb. 2016.
- [3] S. P. Barton and R. Marks, "Measurement of collagen-fibre diameter in human skin," *J. Cutan. Pathol.*, vol. 11, no. 1, pp. 18–26, Feb. 1984.
- [4] C. Frantz, K. M. Stewart, and V. M. Weaver, "The extracellular matrix at a glance," *J. Cell Sci.*, vol. 123, no. 24, pp. 4195–4200, Dec. 2010.
- [5] L. Vergani, M. Grattarola, and C. Nicolini, "Modifications of chromatin structure and gene expression following induced alterations of cellular shape," *Int. J. Biochem. Cell Biol.*, vol. 36, no. 8, pp. 1447–61, Aug. 2004.
- [6] E. Knight and S. Przyborski, "Advances in 3D cell culture technologies enabling tissue-like structures to be created in vitro," *J. Anat.*, pp. 1–11, 2014.
- [7] M. Chen, P. K. Patra, S. B. Warner, and S. Bhowmick, "Optimization of electrospinning process parameters for tissue engineering scaffolds," *Biophys. Rev. Lett.*, vol. 01, no. 02, pp. 153–178, Apr. 2006.
- [8] L. A. Bosworth and S. Downes, "Acetone, a Sustainable Solvent for Electrospinning Poly(ϵ -Caprolactone) Fibres: Effect of Varying Parameters and Solution Concentrations on Fibre Diameter," *J. Polym. Environ.*, vol. 20, no. 3, pp. 879–886, Apr. 2012.
- [9] M. A. Woodruff and D. W. Hutmacher, "The return of a forgotten polymer - Polycaprolactone in the 21st century," *Prog. Polym. Sci.*, vol. 35, no. 10, pp. 1217–1256, 2010.
- [10] J. Sims-Mourtada, R. a. Niamat, S. Samuel, C. Esckridge, and E. B. Kmiec, "Enrichment of breast cancer stem-like cells by growth on electrospun polycaprolactone-chitosan nanofiber scaffolds," *Int. J. Nanomedicine*, vol. 9, no. 1, pp. 995–1003, 2014.
- [11] M. Rabionet, M. Yeste, T. Puig, and J. C. Curana, "Electrospinning PCL Scaffolds Manufacture for Three-Dimensional Breast Cancer Cell Culture," *Polymers (Basel)*, vol. 9, no. 8, p. 328, Aug. 2017.
- [12] S. Saha, X. Duan, L. Wu, P.-K. Lo, H. Chen, and Q. Wang, "Electrospun fibrous scaffolds promote breast cancer cell alignment and epithelial-mesenchymal transition," *Langmuir*, vol. 28, no. 4, pp. 2028–34, Jan. 2012.
- [13] M. Al-Hajj, M. S. Wicha, A. Benito-Hernandez, S. J. Morrison, and M. F. Clarke, "Prospective identification of tumorigenic breast cancer cells," *Proc. Natl. Acad. Sci.*, vol. 100, no. 7, pp. 3983–3988, Apr. 2003.
- [14] B. K. Abraham, P. Fritz, M. McLellan, P. Hauptvogel, M. Athelgou, and H. Brauch, "Prevalence of CD44+/CD24-/low cells in breast cancer may not be associated with clinical outcome but may favor distant metastasis," *Clin. Cancer Res.*, vol. 11, no. 3, pp. 1154–9, Feb. 2005.
- [15] X. Li et al., "Intrinsic Resistance of Tumorigenic Breast Cancer Cells to Chemotherapy," *JNCI J. Natl. Cancer Inst.*, vol. 100, no. 9, pp. 672–679, Apr. 2008.
- [16] S. Feng et al., "Expansion of breast cancer stem cells with fibrous scaffolds," *Integr. Biol. (Camb)*, vol. 5, no. 5, pp. 768–77, 2013.
- [17] S. Palomeras et al., "Breast cancer stem cell culture and enrichment using poly(ϵ -caprolactone) scaffolds," *Molecules*, 2016.
- [18] J. Dias and P. Bártolo, "Morphological Characteristics of Electrospun PCL Meshes – The Influence of Solvent Type and Concentration," *Procedia CIRP*, vol. 5, pp. 216–221, 2013.
- [19] R. Dent et al., "Triple-Negative Breast Cancer: Clinical Features and Patterns of Recurrence," *Clin. Cancer Res.*, vol. 13, no. 15, 2007.
- [20] H. Fong, I. Chun, and D. Reneker, "Beaded nanofibers formed during electrospinning," *Polymer (Guildf)*, vol. 40, no. 16, pp. 4585–4592, Jul. 1999.
- [21] O. Coulembier, P. Degée, J. L. Hedrick, and P. Dubois, "From controlled ring-opening polymerization to biodegradable aliphatic polyester: Especially poly(β -malic acid) derivatives," *Prog. Polym. Sci.*, vol. 31, no. 8, pp. 723–747, Aug. 2006.
- [22] Z. X. Meng, W. Zheng, L. Li, and Y. F. Zheng, "Fabrication and characterization of three-dimensional nanofiber membrane of PCL-MWCNTs by electrospinning," *Mater. Sci. Eng. C*, vol. 30, no. 7, pp. 1014–1021, 2010.
- [23] K. Assaf, C. V. Leal, M. S. Derami, E. A. de Rezende Duek, H. J. Ceragioli, and A. L. R. de Oliveira, "Sciatic nerve repair using poly(ϵ -caprolactone) tubular prosthesis associated with nanoparticles of carbon and graphene," *Brain Behav.*, vol. 7, no. 8, pp. 1–12, 2017.
- [24] J. M. Lee et al., "Three dimensional poly(ϵ -caprolactone) and silk fibroin nanocomposite fibrous matrix for artificial dermis," *Mater. Sci. Eng. C*, vol. 68, no. June, pp. 758–767, 2016.
- [25] B. Huang, G. Caetano, C. Vyas, J. J. Blaker, C. Diver, and P. Bártolo, "Polymer-ceramic composite scaffolds: The effect of hydroxyapatite and β -tri-calcium phosphate," *Materials (Basel)*, vol. 11, no. 1, 2018.
- [26] M. Chen, P. K. Patra, S. B. Warner, and S. Bhowmick, "Role of fiber diameter in adhesion and proliferation of NIH 3T3 fibroblast on electrospun polycaprolactone scaffolds," *Tissue Eng.*, vol. 13, no. 3, pp. 579–87, Mar. 2007.
- [27] C. S. Szot, C. F. Buchanan, P. Gatenholm, M. N. Rylander, and J. W. Freeman, "Investigation of cancer cell behavior on nanofibrous scaffolds," *Mater. Sci. Eng. C*, vol. 31, no. 1, pp. 37–42, Jan. 2011.

Article

Electrospinning PCL Scaffolds Manufacture for Three-Dimensional Breast Cancer Cell Culture

 Marc Rabionet ^{1,2}, Marc Yeste ³ , Teresa Puig ^{1,*} and Joaquim Ciurana ^{2,*} 

¹ New Therapeutic Targets Laboratory (TargetsLab)—Oncology Unit, Department of Medical Sciences, Faculty of Medicine, University of Girona, Emili Grahit 77, 17003 Girona, Spain; m.rabionet@udg.edu

² Product, Process and Production Engineering Research Group (GREP), Department of Mechanical Engineering and Industrial Construction, University of Girona, Maria Aurèlia Capmany 61, 17003 Girona, Spain

³ Biotechnology of Animal and Human Reproduction (TechnoSperm), Department of Biology, Institute of Food and Agricultural Technology, University of Girona, Pic de Peguera 15, 17003 Girona, Spain; marc.yeste@udg.edu

* Correspondence: teresa.puig@udg.edu (T.P.); quim.ciurana@udg.edu (J.C.);
Tel.: +34-972-419628 (T.P.); +34-972-418265 (J.C.)

Received: 27 June 2017; Accepted: 27 July 2017; Published: 1 August 2017

Abstract: In vitro cell culture is traditionally performed within two-dimensional (2D) environments, providing a quick and cheap way to study cell properties in a laboratory. However, 2D systems differ from the in vivo environment and may not mimic the physiological cell behavior realistically. For instance, 2D culture models are thought to induce cancer stem cells (CSCs) differentiation, a rare cancer cell subpopulation responsible for tumor initiation and relapse. This fact hinders the development of therapeutic strategies for tumors with a high relapse percentage, such as triple negative breast cancer (TNBC). Thus, three-dimensional (3D) scaffolds have emerged as an attractive alternative to monolayer culture, simulating the extracellular matrix structure and maintaining the differentiation state of cells. In this work, scaffolds were fabricated through electrospinning different poly(ϵ -caprolactone)-acetone solutions. Poly(ϵ -caprolactone) (PCL) meshes were seeded with triple negative breast cancer (TNBC) cells and 15% PCL scaffolds displayed significantly ($p < 0.05$) higher cell proliferation and elongation than the other culture systems. Moreover, cells cultured on PCL scaffolds exhibited higher mammosphere forming capacity and aldehyde dehydrogenase activity than 2D-cultured cells, indicating a breast CSCs enrichment. These results prove the powerful capability of electrospinning technology in terms of poly(ϵ -caprolactone) nanofibers fabrication. In addition, this study has demonstrated that electrospun 15% PCL scaffolds are suitable tools to culture breast cancer cells in a more physiological way and to expand the niche of breast CSCs. In conclusion, three-dimensional cell culture using PCL scaffolds could be useful to study cancer stem cell behavior and may also trigger the development of new specific targets against such malignant subpopulation.

Keywords: poly(ϵ -caprolactone); electrospinning; scaffolds; three-dimensional cell culture; triple negative breast cancer; breast cancer stem cells; mammospheres; aldehyde dehydrogenase

1. Introduction

Presently, in vitro cell culture represents a crucial tool to study cell behavior outside the organism. Most cell cultures are performed with a two-dimensional (2D) environment providing cheap and easy cell maintenance. A flat plastic surface is treated, obtaining adherent features to enable cell adhesion and proliferation. Therefore, these cells can only grow forming a monolayer, establishing interactions with surface and contiguous cells. Cells adopt a flattened morphology, which results in a modified membrane receptor polarity and cytoskeleton architecture. Different studies demonstrated

that cell shape variations interfere with gene expression and protein synthesis regulation [1,2]. Consequently, the 2D cell culture model described differs from the physiological environment of living organisms. Body cells are embedded in the extracellular matrix (ECM), a three-dimensional (3D) complex constituted by fibrous proteins and molecules. This network structure provides a physical support for cell growth as well as playing a major role in cell regulation [3,4]. Cells can establish connections with their adjacent counterparts and with ECM fibrous mesh, thereby tending to adopt a more elongated morphology. This clear 3D physiological architecture contrasts with the lack of structure of two-dimensional cell culture. Hence, conclusions from *in vitro* monolayer cell culture experiments could be not applicable in terms of *in vivo* cell behavior, empowering the requirement of 3D models for cell culture.

Over recent years, various three-dimensional cell culture systems have emerged, differing in their composition, arrangement and final application. The models based on a solid, physical support are called scaffolds and are made up of a network of filaments mostly made by synthetic materials [5]. This 3D product can be manufactured by electrospinning technology using a high electric field. The polymer is dissolved and the solution is charged at high voltage. When electric force overcomes the surface tension, the polymer solution is pulled onto the target plate and the solvent is evaporated, collecting nanofibers which intersect each other [6]. The resultant architecture mimics the ECM fibrous assemblage and cultured cells are able to adopt a more *in vivo* shape. Obviously, all cell types possess distinct morphological characteristics which may lead to different cell culture support requirements. In this regard, it is worth noting that scaffold manufacturing techniques allow product customization, so that different process parameters, such as scaffold porosity, fiber diameter and microstructure, may be modified on the basis of the final application [7–9]. Poly(ϵ -caprolactone) (PCL) is a synthetic polymer that has been widely used to fabricate scaffolds, due to its viscoelastic and malleable properties, absence of isomers and low cost [10]. PCL may be processed with many technologies since it presents a low melting point around 60 °C and it is soluble in several solvents, such as chloroform, dichloromethane, benzene, acetone and dimethylformamide [11]. Moreover, PCL shows biocompatible properties, long-term biodegradability but bioresorbable [12], all these features making it a good candidate for biomedical and cell culture applications.

As previously explained, polymeric filaments offer physical support to cells to adhere and proliferate into the 3D structure. This fact enables cells to acquire a more elongated shape, close to physiological morphology, in contrast with the flatness adopted in monolayer cultures. Hence, the cancer research field is taking advantage of the three-dimensional cell culture model's benefits. Over the last two decades, cancers have not been studied as an abnormal growth of a single cell type, as cells with distinct characteristics, such as normal cancer cells and, in minor proportion, cancer stem cells (CSCs) are found in a given tumor. While the CSCs subpopulation only represents a small percentage of tumor cells, they have been demonstrated to drive cell growth in a wide variety of cancer types including leukemia [13], brain [14,15], myeloma [16] and breast [17]. Therefore, CSCs possess tumorigenic features, among other specific characteristics, useful for their identification and isolation. This subset is capable of undergoing self-renewal and differentiating into non-stem cancer cells due to their stem properties. Moreover, CSCs are able to grow in suspension and proliferate forming spheres [14,18], and can be isolated due to an enhanced activity of the aldehyde dehydrogenase (ALDH) enzyme [19]. As expected, this subpopulation with stem characteristics plays a key role in cancer development and prognosis. A link between CSCs and tumor relapse after treatment and metastasis is proven [20] since they show relative high radio- [21] and chemoresistance [22]. This fact becomes relevant in some specific cancer types with an appreciable recurrence percentage, such as breast cancer. Concretely, triple negative breast cancer (TNBC) presents the highest proportion of tumor relapse with a value around 34% and the lowest mean time to local and distant recurrence when compared with other breast cancer types [23]. TNBC is characterized by the absence of breast cancer molecular biomarker amplification, so therapeutic targets against TNBC do not exist and patients are treated with general chemotherapy [24].

Breast cancer stem cells (BCSCs) could become a potential target for future treatments against TNBC. However, BCSCs *in vitro* culture encounters a number of difficulties. Cancer stem subpopulation represents a low percentage within the tumor [17,25] and two-dimensional cell culture induces its differentiation losing stem features [26]. Previous investigations demonstrated that three-dimensional cell culture maintained and expanded BCSCs subset when compared with 2D culture samples [27–30]. Therefore, the present sought to test the suitability of fabricated electrospun PCL scaffolds to provide a more suitable niche for BCSCs to grow. Scaffolds from two different polymer concentrations were tested to evaluate 3D culture suitability with triple negative breast cancer cells. Cell proliferation and morphology were evaluated on different culture days and finally, BCSCs were quantified to discern the scaffold's culture effect. In agreement with literature, PCL scaffolds could be a useful tool to culture breast cancer cells in a more physiological way and expand the BCSCs subpopulation. Customizable methodologies such as electrospinning enable the production of distinct three-dimensional meshes concerning the cell of interest requests. Moreover, the BCSCs' enrichment could facilitate their study and the development of specific treatments against this malignant subpopulation. BCSCs targeted treatments could replace aggressive procedures like chemotherapy and attack the highly recurrent tumors such as triple negative breast cancer.

2. Materials and Methods

2.1. Scaffolds Fabrication

Poly(ϵ -caprolactone) (PCL) and acetone were chosen as biopolymer and non-toxic solvent respectively, to manufacture the scaffolds. PCL 3 mm pellets with an average molecular weight of 80,000 g/mol (Sigma-Aldrich, St. Louis, MO, USA) were dissolved in acetone (PanReac AppliChem, Gatersleben, Germany). Two different concentrations of 7.5 and 15% *w/v* PCL were achieved under 40 °C and agitation using a magnetic stirrer. Scaffolds were fabricated with an electrospinning instrument (Spraybase, Dublin, Ireland). PCL solution was placed in a plastic syringe (BD Plastipak, Franklin Lakes, NJ, USA) connected to an 18 G needle emitter with an inner diameter of 0.8 mm. A fixed voltage of 7 kV was applied and a flow rate of 6 mL/h was established by the Syringe Pump Pro software (New Era Pump Systems, Farmingdale, NY, USA). The distance between the emitter and stationary collector was 15 cm. The electrospinning process was stopped when 10 or 5 mL of solution were ejected, for 7.5 and 15% PCL concentrations respectively. The meshes were then cut into squares with a scalpel.

2.2. Scanning Electron Microscopy Analysis

Microscopic characterization was performed through scanning electron microscopy (SEM; Zeiss, Oberkochen, Germany) after carbon coating. Scaffolds were imaged on the top and bottom to confirm fibre uniformity and Image J software (National Institutes of Health, Bethesda, MD, USA) was used for image analysis. Fibre diameter, surface porosity and pore area were calculated from the top and bottom sides to calculate the average value.

2.3. Cell Line

MDA-MB-231 triple negative breast cancer cell line was obtained from the American Type Culture Collection (ATCC; Rockville, MD, USA). Cells were routinely grown in Dulbecco's Modified Eagle's Medium (DMEM; Gibco, Waltham, MA, USA) supplemented with 10% fetal bovine serum (FBS), 1% L-glutamine, 1% sodium pyruvate, 50 U/mL penicillin/streptomycin (HyClone, Logan, UT, USA). Cells were kept at 37 °C and 5% CO₂ atmosphere and culture medium was changed every 3 days.

2.4. Three-Dimensional Cell Seeding

PCL meshes were sterilized by immersion into 70% ethanol/water solution overnight, washed three times with PBS (Gibco, Waltham, MA, USA) and finally exposed to UV light for 30 min. Sterilized

scaffolds were placed in non-adherent cell culture microplates (Sartstedt, Nümbrecht, Germany) and soaked in culture medium for 30 min at 37 °C before cell seeding to facilitate cell attachment. Corresponding cell density was prepared in a small volume of medium (50–100 µL). Cell suspension was pipetted drop by drop onto the scaffold centre. Then scaffolds were incubated for three hours at 37 °C and 5% CO₂ atmosphere to allow cell attachment and after that incubation period, culture medium was added.

2.5. Cell Proliferation Assay

A suspension of 100 MDA–MB–231 cells per cm² were seeded on adherent microplate wells (Sartstedt), 7.5% and 15% PCL scaffolds. Cell culture was maintained for 12 days. Every two days, samples were collected and 3-(4,5-dimethylthiazolyl-2)-2,5-diphenyltetrazolium bromide (MTT) assay was performed to quantify cell viability. Briefly, adherent wells and scaffolds were washed with PBS and meshes were put into new wells. Volumes of 1 mL DMEM and 100 µL MTT (Sigma-Aldrich, St. Louis, MO, USA) were added and samples were incubated for 150 min. In this test, only viable cells retain the ability of transforming yellow MTT into purple formazan crystals. After incubation, formazan crystals were dissolved with 1 mL DMSO (Sigma-Aldrich, St. Louis, MO, USA) under shaking. Four 100 µL aliquots from each well were pipetted into a 96-well plate and placed into a microplate reader (Bio-Rad, Hercules, CA, USA). Absorbance was measured at 570 nm. Culture medium of remaining samples was changed every two days.

2.6. Three-Dimensional Cell Culture

In order to evaluate the amount of BCSCs, MDA–MB–231 cells were cultured for 3, 6 and 12 days on scaffolds without passaging, changing the culture medium every three days. Considering cell growth kinetics of MDA–MD–231 cell line, 20,000, 8000 and 400 cells/cm² were seeded for 3, 6 and 12 days of culture respectively, achieving a similar cell confluence at the end of each culturing period. Since cell confluence affects cell behaviour and metabolism, the final cell amount was fixed to avoid variations due to this effect. In the case of 2D samples, cells were cultured on monolayer for 3 days at a cell seeding density of 20,000 cells/cm² in the same way as the scaffolds. Prior to the present work, cell line was grown routinely on two-dimensional plastics, thus only 3 days culture time was performed. Preceding experiments showed no differences in reference of cell behaviour between 2D cultured cells during 3, 6 and 12 days using the aforementioned initial cell densities (20,000, 8000 and 400 cells/cm² respectively; data not shown).

2.7. Fluorescence Microscopy Analysis

Triple negative MDA–MB–231 cells were cultured on adherent coverslips (Sarstedt) and 7.5 and 15% PCL meshes, for 2D and 3D culture respectively. After the culture period, cells were washed with PBS and fixed with 4% paraformaldehyde (PFA; Sigma, St. Louis, MO, USA) for 20 min. To permeabilize the cells, coverslips and scaffolds were washed and 0.2% Triton X-100 (Sigma) was added for 10 min. Then samples were blocked with PBS containing 3% bovine serum albumin (BSA; Sigma) as a blocking buffer for 20 min. Cells were subsequently incubated at room temperature for 20 min with rhodamine-phalloidin (Cytoskeleton Inc., Denver, CO, USA) (1:200) to stain actin cytoskeleton and then with 4,6-diamidino-2-phenylindole (DAPI; BD Pharmingen, Franklin Lakes, NJ, USA) (1:1000) also at room temperature for 10 min to stain nuclei. Fluorescence was observed under a fluorescent microscope (Zeiss Axio Imager Microscope, Carl Zeiss, Göttingen, Germany) and a Nikon DS-Ri1 coupled camera (Nikon, Tokyo, Japan) was used to acquire all images. Camera settings (illumination intensity, quality, resolution and colour) were standardised for all photographs. Rhodamine-phalloidin (red) and DAPI (blue) fluorescence were captured and merged with Image J software (National Institutes of Health, Bethesda, MD, USA). This software was also used to calculate nuclear and cytoplasmic elongation factors. In brief, five cells of ten different images were

randomly selected to measure the length and width of the nucleus and cytoplasm as shown in the following formula:

$$\text{Nuclear/Cytoplasmic Elongation Factor} = \frac{\text{length nucleus/cytoplasm}}{\text{width nucleus/cytoplasm}} \geq 1$$

2.8. Mammosphere-Forming Assay

Scaffolds were washed with PBS and put into new wells to collect only those cells attached to PCL filaments. Cells from 2D culture and scaffolds were detached with trypsin-EDTA (Cultek, Madrid, Spain) at 37 °C and 5% CO₂ atmosphere. Afterwards, trypsinization cells were resuspended with DMEM/F12 medium (HyClon) containing the following supplements: B27 (Gibco, Waltham, MA, USA), EGF and FGF (20 ng/mL; Milteny Biotec, Bergisch Gladbach, Germany), 1% L-glutamine and 1% sodium pyruvate. A suspension of 2000 cells/well was seeded onto a 6-well, non-adherent cell culture microplate (Sarstedt) and incubated for 7 days at 37 °C and 5% CO₂. After this period, spherical mammospheres bigger than 50 µm were counted. The equation described below was used to calculate the Mammosphere Forming Index (MFI) of each culture condition:

$$\text{MFI (\%)} = \frac{\text{no mammospheres}}{\text{no seeded cells}} \times 100$$

2.9. ALDEFLUOR Assay

To analyze the aldehyde dehydrogenase (ALDH) activity, an ALDEFLUOR™ kit (Stem Cell Technologies, Durham, NC, USA) was used following the manufacturer indications. Cells were detached from the culture plastic (2D samples) and PCL scaffolds (3D) as explained in Section 2.8, washed with PBS and subsequently resuspended in ALDEFLUOR™ assay buffer at a concentration of 400,000 cells/mL. ALDEFLUOR™ Reagent (BODIPY-aminoacetaldehyde; BAAA) was added to each cell suspension. In order for the background fluorescence to be considered, a negative control for every sample was set by adding ALDEFLUOR™ diethylaminobenzaldehyde (DEAB), an ALDH inhibitor, to each cell suspension prior to adding BAAA in ALDEFLUOR assay buffer. All samples were incubated for 45 min at 37 °C in the dark.

Incubated samples were analyzed with a Cell Lab Quanta flow cytometer (Beckman Coulter Inc., Miami, FL, USA) to quantify the ALDH-positive cell population. The argon ion laser (488 nm) was used as a light source set at a power of 22 mW. Green fluorescence was detected with fluorescent channel 1 (FL1) optical filter (dichroic/splitter, dichroic long-pass: 550 nm, band-pass filter: 525 nm, detection width 505 to 545 nm). Information of a minimum of 10,000 events was recorded in List-mode Data files (LMD) and analyzed using FlowJo 10.2 software (FlowJo LLC, Ashland, OR, USA). Data were not compensated.

First, side-scatter (SS) and electronic volume (EV; equivalent to forward scatter) dot plots were performed and only single cells were selected, excluding debris and cells aggregates (less than 5%). Then, SS and log FL1 dot plots from DEAB samples were created to establish background fluorescence. The ALDH-positive cells' gate was traced, delimiting the rightmost area and including only the 0.5% of total cell population. BAAA samples were equally processed and ALDH-positive cells gates of respective controls were used to discern the sample percentage of cells with high ALDH activity.

2.10. Statistical Analysis

All data are expressed as mean ± standard error of the mean (SEM). Data were analyzed using IBM SPSS (Version 21.0; SPSS Inc., Chicago, IL, USA). First, normality and homoscedasticity were evaluated using Shapiro-Wilks and Levene tests, respectively. As for cell proliferation and mammosphere forming assays, data were found to present a normal distribution and variances were homogeneous, a general linear model followed by post-hoc Sidak test was run. Factors were the treatment (i.e., 2D, 3D with 7.5% PCL, and 3D with 15% PCL and the culturing time). As far as the ALDEFLUOR assay,

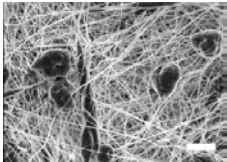
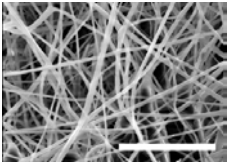
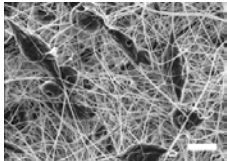
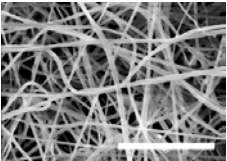
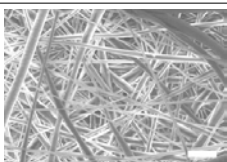
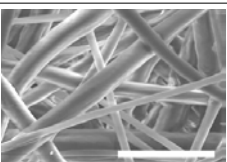
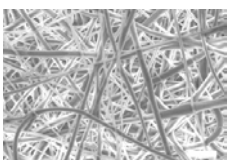
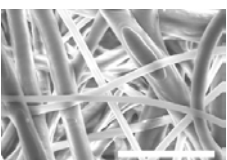
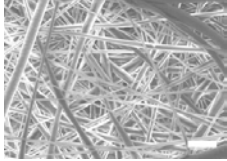
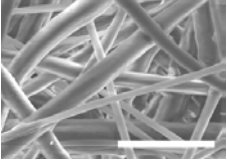
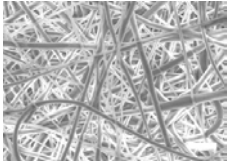
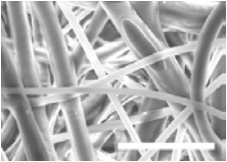
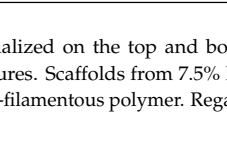
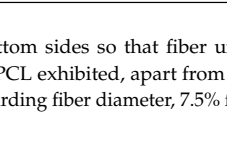


the same tests were run following transformation of data with arcsine square root ($\arcsin\sqrt{x}$), as this was required for correcting the heteroscedasticity. Finally, as ratios between nuclear and cytoplasmic elongation factors (Fluorescence Microscopy Analysis in Section 3.3), did not fulfil with parametric assumptions, even when transformed, they were tested with Kruskal-Wallis and Mann-Whitney tests. The level of significance was set at $p < 0.05$. All observations were confirmed by at least three independent experiments.

3. Results

3.1. Electrospun Scaffolds Characterization

Once the polymer solution was electrospun, 7.5% PCL meshes showed an average thickness of $147.22 \pm 5.00 \mu\text{m}$, whereas 15% scaffolds' depth was $196.00 \pm 4.65 \mu\text{m}$. To study microscopic scaffold architecture, both specimens were imaged by Scanning Electron Microscopy (SEM; Table 1).

Table 1. Microscopic characterization of 7.5% and 15% electrospun poly (ϵ -caprolactone) (PCL) scaffolds (7 kV, 6 mL/h). Top and bottom sides were visualized through scanning electron microscopy micrographs at different magnifications. Both sides were used to calculate fiber diameter, surface porosity and pore area. (Scale bars: 10 μm).

	Side	Magnification		
		1500 \times	5000 \times	
7.5% PCL	Top			Fibre diameter $295.12 \pm 148.45 \text{ nm}$ Surface porosity $28.39\% \pm 4.53\%$ Pore area $0.24 \pm 0.42 \mu\text{m}^2$
				
	Bottom			
				
15% PCL	Top			Fibre diameter $701.13 \pm 401.89 \text{ nm}$ Surface porosity $22.48\% \pm 7.57\%$ Pore area $0.84 \pm 1.82 \mu\text{m}^2$
				
	Bottom			
				

Meshes were visualized on the top and bottom sides so that fiber uniformity was certified, presenting similar features. Scaffolds from 7.5% PCL exhibited, apart from the filaments, spherical structures made by non-filamentous polymer. Regarding fiber diameter, 7.5% films showed an average

diameter close to 300 nm, whereas the diameter of those containing 15% PCL increased up to 700 nm. Both scaffolds presented similar surface porosity, but they differed in the average pore area. Scaffolds from 15% PCL solution exhibited larger pores compared with 7.5% meshes.

3.2. Cell Proliferation

As aforementioned, scaffolds could provide a three-dimensional environment for cancer cell culture. Architecture and porosity of filaments directly interfered with cell adhesion and growth. As seen in the previous section, 7.5% and 15% PCL scaffolds were proven to exhibit distinct microscopic structures. To evaluate the influence of scaffold microenvironment on cell growth, MDA-MB-231 cells were cultured on 2D adherent surfaces and on 7.5% and 15% meshes. Cell viability was evaluated through MTT assay on successive culture days, presented in Figure 1.

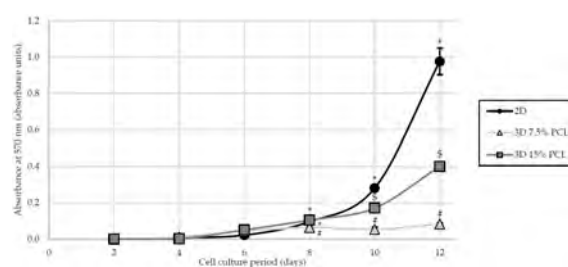


Figure 1. Cell proliferation analysis for MDA-MB-231 cells cultured on two-dimensional surfaces (2D) and on 7.5% and 15% PCL scaffolds (3D). (*), (#) and (\$) symbols represent significant ($p < 0.05$) differences between groups.

On the first assay days, few differences were observed regarding cell proliferation between different culture models. Variations between cell culture supports took place when a minimum cell confluence was reached, starting from day 8. MDA-MB-231 cells cultured on 2D adherent microplates presented a higher cell proliferation ratio compared to three-dimensional scaffolds, adopting strongly exponential kinetics. Scaffolds fabricated with 15% PCL solution also showed an exponential cell growth, but with a smaller slope. In contrast, 7.5% PCL meshes exhibited the lowest cell proliferation with a fairly linear trend. Since day 8, cell proliferation of 7.5% PCL scaffolds was significantly reduced when compared with monolayer culture (p -values ranging from <0.001 to 0.014) and 15% PCL meshes (p -values ranging from 0.002 to 0.040).

3.3. Cell Morphology

MDA-MB-231 cells were cultured on adherent two-dimensional coverslips (2D) and three-dimensional PCL scaffolds (3D). Three different cell culture times (3, 6 and 12 days) were tested to evaluate whether morphology differences existed. Actin cytoskeleton and nucleus were stained to analyze possible changes in cell morphology between culture systems. MDA-MB-231 cells were routinely cultured on plastic cell culture dishes, establishing a cell monolayer where cells appeared to have a flattened structure. MDA-MB-231 cell line was also characterized to adopt a relatively lengthened cytoplasm. Fluorescent microscopy images confirmed the morphology described in 2D models (Figure 2). Some cells presented cytoplasmic prolongations, while others had a round shape and nucleus aspect was predominantly ellipsoidal. Then, MDA-MB-231 cells displayed different morphology when the two scaffold types, 7.5% and 15% PCL, were compared. Cells cultured on 7.5% PCL meshes (Figure 3a–c) exhibited similar aspects to 2D cultured ones, including nucleus and cytoplasm architecture. This trend was observed along the different days of cell culture with no noticeable differences. In contrast, a high number of MDA-MB-231 cells showed lengthened

morphology when cultured on 15% PCL scaffolds (Figure 3d–f). Cytoplasm prolongations were longer than the ones from 2D and 3D 7.5% PCL cultures. When cell culture days increased, prolongations seemed to be even more extended. Moreover, some cells appeared to be unfocused on 15% PCL meshes pictures, indicating that cell culture occurred on different scaffold depth. No qualitative differences were observed concerning nuclear shape.

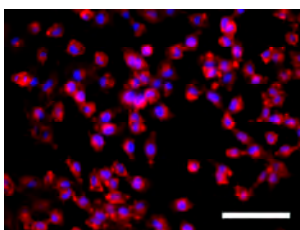


Figure 2. MDA–MB–231 cells grown in two-dimensional (2D) adherent coverslips. Actin cytoskeleton was stained with rhodamine-phalloidin (red) and nucleus was stained with 4,6-diamidino-2-phenylindole (DAPI; blue). Fluorescence microscopy images were captured at a magnification of 200 \times (Scale bar: 100 μ m).

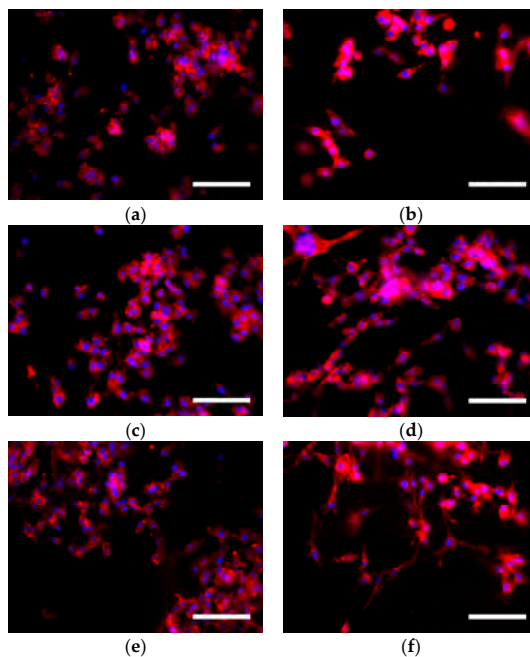


Figure 3. MDA–MB–231 cells grown in three-dimensional (3D) PCL scaffolds. Cells were seeded on 7.5% PCL (a,c,e) and 15% PCL meshes (b,d,f). Cells were cultured for 3 (a,b), 6 (c,d) and 12 days (e,f) without passage. Actin cytoskeleton was stained with rhodamine-phalloidin (red) and nucleus was stained with DAPI (blue). Fluorescence microscopy images were captured at a magnification of 200 \times (Scale bars: 100 μ m).

To quantitatively evaluate cell morphology in 2D and 3D cultures, nuclear and cytoplasmic elongation were measured as described in Section 2.7. No significant changes in nucleus elongation were observed between 2D and 3D cultures (Figure 4a), which agreed with the aforementioned descriptive microscopic observation. The nuclear elongation factor of 2D cultured cells was 1.60 ± 0.12 , pointing out to the ellipsoidal form of the nucleus. All 3D cultured cells factors were similar or slightly lower, between 1.47 ± 0.07 and 1.60 ± 0.08 . Cytoplasm pattern was also studied (Figure 4b) and, whereas MDA–MB–231 cells cultured on 7.5% PCL scaffolds presented a similar cytoplasmic elongation factor than those cultured in 2D, with a value around 1.70, the cells on 15% PCL meshes exhibited a significantly higher cytoplasmic length.

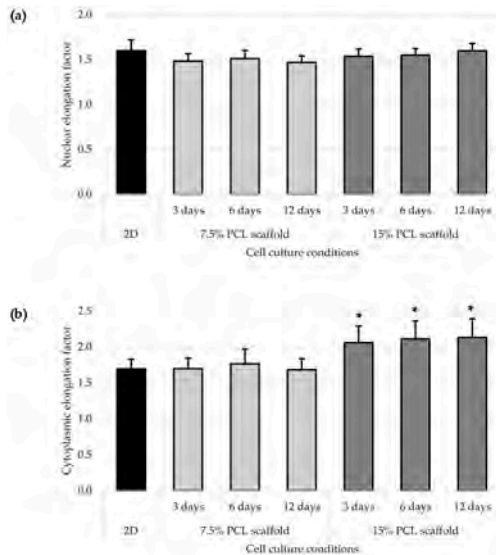


Figure 4. Cell morphology analysis for MDA–MB–231 cells cultured on two-dimensional surfaces (2D) and on 7.5% and 15% PCL scaffolds. Nuclear (a) and cytoplasmic elongation (b) were measured as explained in Section 2.7. Scaffolds values were compared with 2D culture and levels of statistical significance were indicated as * ($p < 0.05$).

As previously mentioned, SEM analysis showed that 15% PCL scaffolds were the only specimen formed exclusively by filaments. Moreover, MDA–MB–231 cells cultured on meshes of 15% PCL exhibited a high cell proliferation (Figure 1) and different cell morphology (Figure 3) compared with 7.5% PCL scaffolds. As the main aim of three-dimensional cell culture is to mimic the extracellular matrix structure and provide a comfortable support to cell growth, meshes from 15% PCL solution were chosen to conduct the further experiments of the present study. From now onwards, 3D culture samples will exclusively refer to cells cultured on 15% PCL scaffolds. As in previous experiments, the effects of culturing cells with those 15% PCL scaffolds were also tested at 3, 6 and 12 days of culture.

3.4. Mammospheres Forming Assay

Breast cancer stem cells possess an anchorage-independent growth, proliferating into mammospheres when cultured on non-adherent surfaces. Hence, Mammospheres Forming Assay was first used to evaluate the spheres forming capacity of cells previously cultured on 2D and 3D supports. The MDA–MB–231 triple negative cell line was seeded as described in “Materials and Methods” section.

Mammospheres from all cell samples did not show qualitative differences regarding morphology and size (Figure 5a–d). However, all three-dimensional cultured cells showed a significantly higher Mammosphere Forming Index (MFI) than 2D samples, reaching the maximum value and significance on 6 days of culture (Figure 5e).

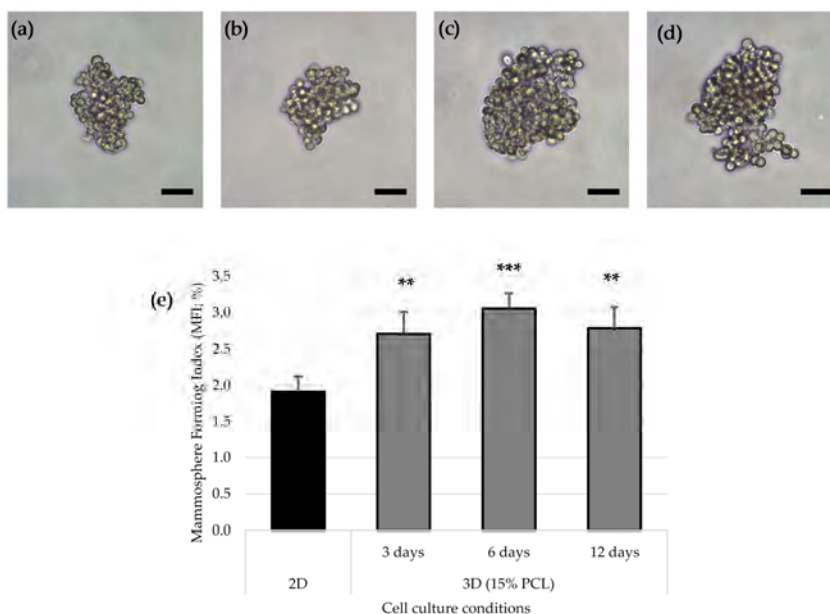


Figure 5. Mammosphere Forming Assay. Mammosphere images of MDA–MB–231 cells previously cultured on 2D surfaces (a) and 15% PCL scaffolds for 3 (b), 6 (c) and 12 days (d). (Scale bars: 50 μ m). Mammosphere Forming Index (MFI) of MDA–MB–231 cell line after 2D or 3D cell culture with 15% PCL scaffolds (e). Significant differences of 3D with regard to 2D cultures are indicated as ** ($p < 0.01$) and *** ($p < 0.001$).

3.5. Aldehyde Dehydrogenase Activity

The aldehyde dehydrogenase (ALDH) family is composed by dehydrogenases enzymes responsible for the oxidation of retinol (vitamin A) to retinoic acid [31], the latter of which is involved in gene expression regulation [32] and embryo development [33]. Moreover, ALDH enzymes have a detoxification role, protecting organisms against damaging aldehydes [34] and cytotoxic agents [35], and have also been demonstrated to regulate hematopoietic stem cells differentiation via retinoic acids production [36]. To corroborate the relative proportion of CSCs in 2D and 3D cultured cells, ALDH activity was quantified as a measure of stem properties. Samples were assessed with ALDEFLUOR assay and the percentage of ALDH-positive cells was determined as shown in Figure 6.

The ALDH-positive subpopulation increased when cells were cultured on PCL scaffolds, compared to monolayer culture (Figure 7). ALDH activity enhancement was observed at 3 and 6 days of cell culture, the latter time point being the one with a significant major percentage. However, the proportion of ALDH + cells after 12 days of culture in 15% PCL scaffolds decreased, with figures close to those of 2D.

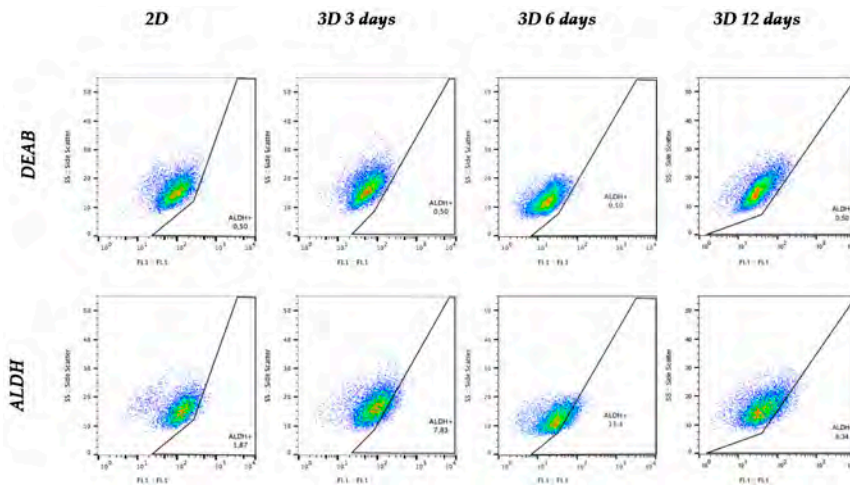


Figure 6. ALDEFUOR assay plots of MDA-MB-231 cells cultured on monolayer (2D) and on 15% PCL scaffolds (3D). Aldehyde dehydrogenase (ALDH) inhibitor (diethylaminobenzaldehyde; DEAB) was processed to determine background fluorescence limit, gating 0.5% ALDH-positive cells for all samples.

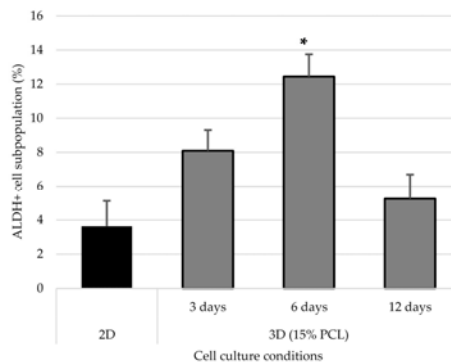


Figure 7. ALDH + cell subpopulation of MDA-MB-231 cells after monolayer culture (2D) or three-dimensional cell culture with 15% PCL scaffolds (3D). (*) Denotes significant ($p < 0.05$) differences between 3D culture at a given time point and 2D.

4. Discussion

Polymer concentration (PCL) has been found to exert a great influence on scaffold architecture. Indeed, 7.5% PCL scaffolds showed polymeric spheres connected to filaments. These structures, previously described in the literature, are called beads and result from low polymer concentration [8,37]. In contrast, no beads were observed in 15% meshes, which also showed an average fiber diameter 2.4-fold higher than that of 7.5% specimens. While performing a direct comparison with values from other studies is difficult owing to the wide range of electrospun parameters used, the significant impact of PCL concentration in acetone on fiber morphology and diameter agrees with most previous studies [7,8,38,39]. Furthermore, pore parameters were also evaluated and, while electrospun meshes

presented similar surface porosity, the average pore area in 15% scaffolds was 3.5-fold larger than that of 7.5% models.

MDA-MB-231 cells were successfully expanded on electrospun mats. Both scaffolds tested (i.e., 7.5% and 15%) showed less cell proliferation compared with the homologous monolayer culture, which was in agreement with previous studies [40]. When scaffolds from different polymer concentrations were compared, microarchitecture traits seemed to influence 3D cell culture efficiency. It is worth mentioning that low filament diameters have been revealed to facilitate cell adhesion and growth [38,41,42] and collagen fibers (the main protein in the extracellular matrix) display small diameters below 100 nm [43]. However, in the current study, the scaffold with the lowest fiber diameter (i.e., 7.5%) also exhibited beads which interfered with cell proliferation. Chen et al. (2007) demonstrated that, despite having smaller fiber diameters, meshes with beads reduce fibroblast growth [38]. In our conditions, beaded scaffolds exhibited a lower surface area-to-volume ratio, providing less material for cell growth. Moreover, interconnected pores with a minimum optimal area are needed to allow cell growth and scaffold infiltration. Small pores of 7.5% scaffolds may also hinder MDA-MB-231 cells' penetration within the mesh structure. Following this hypothesis, most cells would have adhered to the surface and they would hardly have colonized different scaffold depths. With regard to cell morphology, MDA-MB-231 cells seeded on 15% PCL scaffolds presented more cytoplasmic elongations compared with round shaped cells on 7.5% PCL meshes and, specially, flat surfaces. This finding was supported by the higher cytoplasmic elongation factor of 15% PCL mat cells. Cell elongation along scaffold nanofilaments has also been observed in breast cancer cells [27,28], fibroblasts [44] and murine adult neural stem cells [45]. Accordingly, meshes from 15% PCL mimic the physiological environment better as they allow cells to set a structure that 2D monolayers are devoid of. In fact, cytoskeleton reorganization caused by 3D cell culture may regulate gene expression [2].

Taking into account cell proliferation kinetics and morphology changes, scaffold from 15% PCL solution was selected to further accommodate MDA-MB-231 cell culture and evaluate BCSCs niche expansion capacity. The MDA-MB-231 cell line presents low MFI values and can only be propagated few passages on suspension culture due to their moderate e-cadherin expression [46]. However, scaffolds culture improved mammospheres forming ability, particularly after 6 days of culture, resulting in an enlarged tumorigenic [47] and self-renewal potential [48]. Additionally, MDA-MB-231 cells cultured on electrospun mats over the same period showed a significant ALDH-positive population increase in comparison of standard culture, with a conclusive 3.4-fold increase. Greater ALDH activity indicated stem features acquisition since several studies noticed a high ALDH activity on mammary [19], hematopoietic [49] and leukemic stem cells [50]. Taking all described stem features assays into account, the present study has shown that 3D culture with electrospun scaffolds enhances triple negative MDA-MB-231 tumorigenicity and ALDH activity. These rearrangements reach the maximum significance when the culture period lasts 6 days, this time being the one that allows reaching the greatest BCSCs expansion through 3D cell culture. In agreement with our results, different breast cancer cell studies also demonstrated cancer stem cell amplification through PCL scaffolds fabricated by electrospinning [27–29] and by other methods such as additive manufacturing technologies [30].

In conclusion, the current study has revealed the vast potential of poly(ϵ -caprolactone) on the *in vitro* cell culture field. Electrospun PCL solutions resulted in nanofiber production with different architecture traits, demonstrating the high versatility of polymer and technology. Moreover, non-beaded PCL scaffolds have been proven to supply physical support for triple negative breast cancer cell proliferation and elongation. The 3D cell culture expanded the breast cancer stem cell subpopulation, which in turn expressed more malignancy markers and exhibited stem cell characteristics. Therefore, 3D culture with electrospun PCL nanofibers may be useful to maintain the *in vivo* structure and to culture BCSCs, making their expansion and characterization possible. Investigation of this rare subpopulation is much warranted as it could facilitate the development of new specific therapeutic approaches to prevent the high recurrence of tumors such as triple negative breast cancer.

Acknowledgments: This work was supported partially by Spanish grants from Fundación Ramón Areces, Instituto de Salud Carlos III (PI1400329) and Ministerio de Economía Y Competitividad (DPI2013-45201-P; RYC-2014-15581), and the support of the Catalanian government (2014SGR00868). The authors are grateful for the financial support from the University of Girona (MPCUdG2016/036).

Author Contributions: Joaquim Ciurana and Teresa Puig conceived and designed the experiments; Marc Rabionet and Marc Yeste performed the experiments; Marc Rabionet and Marc Yeste analyzed the data; Marc Yeste, Joaquim Ciurana and Teresa Puig contributed reagents/materials/analysis tools; Marc Rabionet, Joaquim Ciurana and Teresa Puig wrote the paper.

Conflicts of Interest: The authors declare no conflict of interest. The founding sponsors had no role in the design of the study; in the collection, analyses, or interpretation of data; in the writing of the manuscript, and in the decision to publish the results.

References

1. Thomas, C.H.; Collier, J.H.; Sfeir, C.S.; Healy, K.E. Engineering gene expression and protein synthesis by modulation of nuclear shape. *Proc. Natl. Acad. Sci. USA* **2002**, *99*, 1972–1977. [[CrossRef](#)] [[PubMed](#)]
2. Vergani, L.; Grattarola, M.; Nicolini, C. Modifications of chromatin structure and gene expression following induced alterations of cellular shape. *Int. J. Biochem. Cell Biol.* **2004**, *36*, 1447–1461. [[CrossRef](#)] [[PubMed](#)]
3. Theocharis, A.D.; Skandalis, S.S.; Gialeli, C.; Karamanos, N.K. Extracellular matrix structure. *Adv. Drug Deliv. Rev.* **2016**, *97*, 4–27. [[CrossRef](#)] [[PubMed](#)]
4. Frantz, C.; Stewart, K.M.; Weaver, V.M. The extracellular matrix at a glance. *J. Cell Sci.* **2010**, *123*, 4195–4200. [[CrossRef](#)] [[PubMed](#)]
5. Knight, E.; Przyborski, S. Advances in 3D cell culture technologies enabling tissue-like structures to be created in vitro. *J. Anat.* **2014**, *227*, 746–756. [[CrossRef](#)] [[PubMed](#)]
6. Li, W.J.; Tuan, R.S. Fabrication and application of nanofibrous scaffolds in tissue engineering. *Curr. Protoc. Cell Biol.* **2009**. [[CrossRef](#)]
7. Bosworth, L.A.; Downes, S. Acetone, a Sustainable Solvent for Electrospinning Poly(ϵ -Caprolactone) Fibres: Effect of Varying Parameters and Solution Concentrations on Fibre Diameter. *J. Polym. Environ.* **2012**, *20*, 879–886. [[CrossRef](#)]
8. Chen, M.; Patra, P.K.; Warner, S.B.; Bhowmick, S. Optimization of electrospinning process parameters for tissue engineering scaffolds. *Biophys. Rev. Lett.* **2006**, *01*, 153–178. [[CrossRef](#)]
9. De Ciurana, J.; Serenó, L.; Vallès, È. Selecting process parameters in RepRap additive manufacturing system for PLA scaffolds manufacture. *Procedia CIRP* **2013**, *5*, 152–157. [[CrossRef](#)]
10. Cipitria, A.; Skelton, A.; Dargaville, T.R.; Dalton, P.D.; Hutmacher, D.W. Design, fabrication and characterization of PCL electrospun scaffolds—A review. *J. Mater. Chem.* **2011**, *21*, 9419–9453. [[CrossRef](#)]
11. Coulembier, O.; Degée, P.; Hedrick, J.L.; Dubois, P. From controlled ring-opening polymerization to biodegradable aliphatic polyester: Especially poly(β -malic acid) derivatives. *Prog. Polym. Sci.* **2006**, *31*, 723–747. [[CrossRef](#)]
12. Woodruff, M.A.; Hutmacher, D.W. The return of a forgotten polymer—Polycaprolactone in the 21st century. *Prog. Polym. Sci.* **2010**, *35*, 1217–1256. [[CrossRef](#)]
13. Lapidot, T.; Sirard, C.; Vormoor, J.; Murdoch, B.; Hoang, T.; Caceres-Cortes, J.; Minden, M.; Paterson, B.; Caligiuri, M.A.; Dick, J.E. A cell initiating human acute myeloid leukaemia after transplantation into SCID mice. *Nature* **1994**, *367*, 645–648. [[CrossRef](#)] [[PubMed](#)]
14. Singh, S.K.; Clarke, I.D.; Terasaki, M.; Bonn, V.E.; Hawkins, C.; Squire, J.; Dirks, P.B. Identification of a cancer stem cell in human brain tumors. *Cancer Res.* **2003**, *63*, 5821–5828. [[PubMed](#)]
15. Kondo, T.; Setoguchi, T.; Taga, T. Persistence of a small subpopulation of cancer stem-like cells in the C6 glioma cell line. *Proc. Natl. Acad. Sci. USA* **2004**, *101*, 781–786. [[CrossRef](#)] [[PubMed](#)]
16. Matsui, W.; Huff, C.A.; Wang, Q.; Malehorn, M.T.; Barber, J.; Tanhehco, Y.; Smith, B.D.; Civin, C.I.; Jones, R.J. Characterization of clonogenic multiple myeloma cells. *Blood* **2004**, *103*, 2332–2336. [[CrossRef](#)] [[PubMed](#)]
17. Al-Hajj, M.; Wicha, M.S.; Benito-Hernandez, A.; Morrison, S.J.; Clarke, M.F. Prospective identification of tumorigenic breast cancer cells. *Proc. Natl. Acad. Sci. USA* **2003**, *100*, 3983–3988. [[CrossRef](#)] [[PubMed](#)]
18. Dontu, G.; Abdallah, W.M.; Foley, J.M.; Jackson, K.W.; Clarke, M.F.; Kawamura, M.J.; Wicha, M.S. In vitro propagation and transcriptional profiling of human mammary stem/progenitor cells. *Genes Dev.* **2003**, *17*, 1253–1270. [[CrossRef](#)] [[PubMed](#)]

19. Ginestier, C.; Hur, M.H.; Charafe-Jauffret, E.; Monville, F.; Dutcher, J.; Brown, M.; Jacquemier, J.; Viens, P.; Kleer, C.G.; Liu, S.; et al. ALDH1 is a marker of normal and malignant human mammary stem cells and a predictor of poor clinical outcome. *Cell Stem Cell* **2007**, *1*, 555–567. [[CrossRef](#)] [[PubMed](#)]
20. Abraham, B.K.; Fritz, P.; McClellan, M.; Hauptvogel, P.; Athelogou, M.; Brauch, H. Prevalence of CD44+/CD24-/low cells in breast cancer may not be associated with clinical outcome but may favor distant metastasis. *Clin. Cancer Res.* **2005**, *11*, 1154–1159. [[PubMed](#)]
21. Diehn, M.; Cho, R.W.; Lobo, N.A.; Kalisky, T.; Dorie, M.J.; Kulp, A.N.; Qian, D.; Lam, J.S.; Ailles, L.E.; Wong, M.; et al. Association of reactive oxygen species levels and radioresistance in cancer stem cells. *Nature* **2009**, *458*, 780–783. [[CrossRef](#)] [[PubMed](#)]
22. Li, X.; Lewis, M.T.; Huang, J.; Gutierrez, C.; Osborne, C.K.; Wu, M.F.; Hilsenbeck, S.G.; Pavlick, A.; Zhang, X.; Chamness, G.C.; et al. Intrinsic Resistance of Tumorigenic Breast Cancer Cells to Chemotherapy. *J. Natl. Cancer Inst.* **2008**, *100*, 672–679. [[CrossRef](#)] [[PubMed](#)]
23. Dent, R.; Trudeau, M.; Pritchard, K.L.; Hanna, W.M.; Kahn, H.K.; Sawka, C.A.; Lickley, L.A.; Rawlinson, E.; Sun, P.; Narod, S.A. Triple-Negative Breast Cancer: Clinical Features and Patterns of Recurrence. *Clin. Cancer Res.* **2007**, *13*, 4429–4434. [[CrossRef](#)] [[PubMed](#)]
24. Carey, L.A.; Dees, E.C.; Sawyer, L.; Gatti, L.; Moore, D.T.; Collichio, F.; Ollila, D.W.; Sartor, C.I.; Graham, M.L.; Perou, C.M. The triple negative paradox: Primary tumor chemosensitivity of breast cancer subtypes. *Clin. Cancer Res.* **2007**, *13*, 2329–2334. [[CrossRef](#)] [[PubMed](#)]
25. Charafe-Jauffret, E.; Ginestier, C.; Iovino, F.; Wicinski, J.; Cervera, N.; Finetti, P.; Hur, M.H.; Diebel, M.E.; Monville, F.; Dutcher, J.; et al. Breast cancer cell lines contain functional cancer stem cells with metastatic capacity and a distinct molecular signature. *Cancer Res.* **2009**, *69*, 1302–1313. [[CrossRef](#)] [[PubMed](#)]
26. Tsuyada, A.; Chow, A.; Wu, J.; Somlo, G.; Chu, P.; Loera, S.; Luu, T.; Li, A.X.; Wu, X.; Ye, W.; et al. CCL2 mediates cross-talk between cancer cells and stromal fibroblasts that regulates breast cancer stem cells. *Cancer Res.* **2012**, *72*, 2768–2779. [[CrossRef](#)] [[PubMed](#)]
27. Feng, S.; Duan, X.; Lo, P.K.; Liu, S.; Liu, X.; Chen, H.; Wang, Q. Expansion of breast cancer stem cells with fibrous scaffolds. *Integr. Biol. (Camb.)* **2013**, *5*, 768–777. [[CrossRef](#)] [[PubMed](#)]
28. Saha, S.; Duan, X.; Wu, L.; Lo, P.K.; Chen, H.; Wang, Q. Electrospun fibrous scaffolds promote breast cancer cell alignment and epithelial-mesenchymal transition. *Langmuir* **2012**, *28*, 2028–2034. [[CrossRef](#)] [[PubMed](#)]
29. Sims-Mourtada, J.; Niamat, R.A.; Samuel, S.; Eskridge, C.; Kmiec, E.B. Enrichment of breast cancer stem-like cells by growth on electrospun polycaprolactone-chitosan nanofiber scaffolds. *Int. J. Nanomed.* **2014**, *9*, 995–1003. [[CrossRef](#)] [[PubMed](#)]
30. Palomeras, S.; Rabionet, M.; Ferrer, I.; Sarrats, A.; Garcia-Romeu, M.L.; Puig, T.; Ciurana, J. Breast Cancer Stem Cell Culture and Enrichment Using Poly(ϵ -Caprolactone) Scaffolds. *Molecules* **2016**, *21*, 537. [[CrossRef](#)] [[PubMed](#)]
31. Duester, G. Families of retinoid dehydrogenases regulating vitamin A function: Production of visual pigment and retinoic acid. *Eur. J. Biochem.* **2000**, *267*, 4315–4324. [[CrossRef](#)] [[PubMed](#)]
32. Duester, G.; Mic, F.A.; Molotkov, A. Cytosolic retinoid dehydrogenases govern ubiquitous metabolism of retinol to retinaldehyde followed by tissue-specific metabolism to retinoic acid. *Chem. Biol. Interact.* **2003**, *143–144*, 201–210. [[CrossRef](#)]
33. Appel, B.; Eisen, J.S. Retinoids run rampant: Multiple roles during spinal cord and motor neuron development. *Neuron* **2003**, *40*, 461–464. [[CrossRef](#)]
34. Vasiliou, V.; Pappa, A. Polymorphisms of human aldehyde dehydrogenases. Consequences for drug metabolism and disease. *Pharmacology* **2000**, *61*, 192–198. [[CrossRef](#)] [[PubMed](#)]
35. Hilton, J. Role of aldehyde dehydrogenase in cyclophosphamide-resistant L1210 leukemia. *Cancer Res.* **1984**, *44*, 5156–5160. [[PubMed](#)]
36. Chute, J.P.; Muramoto, G.G.; Whitesides, J.; Colvin, M.; Safi, R.; Chao, N.J.; McDonnell, D.P. Inhibition of aldehyde dehydrogenase and retinoid signaling induces the expansion of human hematopoietic stem cells. *Proc. Natl. Acad. Sci. USA* **2006**, *103*, 11707–11712. [[CrossRef](#)] [[PubMed](#)]
37. Fong, H.; Chun, I.; Reneker, D. Beaded nanofibers formed during electrospinning. *Polymer* **1999**, *40*, 4585–4592. [[CrossRef](#)]
38. Chen, M.; Patra, P.K.; Warner, S.B.; Bhowmick, S. Role of fiber diameter in adhesion and proliferation of NIH 3T3 fibroblast on electrospun polycaprolactone scaffolds. *Tissue Eng.* **2007**, *13*, 579–587. [[CrossRef](#)] [[PubMed](#)]

39. Dias, J.; Bártolo, P. Morphological Characteristics of Electrospun PCL Meshes—The Influence of Solvent Type and Concentration. *Procedia CIRP* **2013**, *5*, 216–221. [[CrossRef](#)]
40. Bean, A.C.; Tuan, R.S. 3D cell culture and osteogenic differentiation of human bone marrow stromal cells plated onto jet-sprayed or electrospun micro-fiber scaffolds Fiber diameter and seeding density influence chondrogenic differentiation of mesenchymal stem cells seeded on electrospun poly(-caprolactone) scaffolds. *Biomed. Mater* **2015**, *10*, 1–25. [[CrossRef](#)]
41. Szot, C.S.; Buchanan, C.F.; Gatenholm, P.; Rylander, M.N.; Freeman, J.W. Investigation of cancer cell behavior on nanofibrous scaffolds. *Mater. Sci. Eng. C* **2011**, *31*, 37–42. [[CrossRef](#)]
42. Chen, M.; Michaud, H.; Bhowmick, S. Controlled Vacuum Seeding as a Means of Generating Uniform Cellular Distribution in Electrospun Polycaprolactone (PCL) Scaffolds. *J. Biomech. Eng.* **2009**, *131*, 1–8. [[CrossRef](#)] [[PubMed](#)]
43. Barton, S.P.; Marks, R. Measurement of collagen-fibre diameter in human skin. *J. Cutan. Pathol.* **1984**, *11*, 18–26. [[CrossRef](#)] [[PubMed](#)]
44. Li, D.; Wu, T.; He, N.; Wang, J.; Chen, W.; He, L.; Huang, C.; El-Hamshary, H.A.; Al-Deyab, S.S.; Ke, Q.; Mo, X. Three-dimensional polycaprolactone scaffold via needleless electrospinning promotes cell proliferation and infiltration. *Colloids Surf. B* **2014**, *121*, 432–443. [[CrossRef](#)] [[PubMed](#)]
45. Lim, S.H.; Liu, X.Y.; Song, H.; Yarema, K.J.; Mao, H.Q. The effect of nanofiber-guided cell alignment on the preferential differentiation of neural stem cells. *Biomaterials* **2010**, *31*, 9031–9039. [[CrossRef](#)] [[PubMed](#)]
46. Manuel Iglesias, J.; Beloqui, I.; Garcia-Garcia, F.; Leis, O.; Vazquez-Martin, A.; Eguiara, A.; Cufi, S.; Pavon, A.; Menendez, J.A.; Dopazo, J. Mammosphere Formation in Breast Carcinoma Cell Lines Depends upon Expression of E-cadherin. *PLoS ONE* **2013**, *8*, 1–12. [[CrossRef](#)] [[PubMed](#)]
47. Cioce, M.; Gherardi, S.; Viglietto, G.; Strano, S.; Blandino, G.; Muti, P.; Ciliberto, G. Mammosphere-forming cells from breast cancer cell lines as a tool for the identification of CSC-like- and early progenitor-targeting drugs. *Cell Cycle* **2014**, *9*, 2950–2959. [[CrossRef](#)]
48. Shaw, F.L.; Harrison, H.; Spence, K.; Ablett, M.P.; Simoes, B.M.; Farnie, G.; Clarke, R.B. A detailed mammosphere assay protocol for the quantification of breast stem cell activity. *J. Mammary Gland Biol. Neoplasia* **2012**, *17*, 111–117. [[CrossRef](#)] [[PubMed](#)]
49. Hess, D.A.; Meyerrose, T.E.; Wirthlin, L.; Craft, T.P.; Herrbrich, P.E.; Creer, M.H.; Nolte, J.A. Functional characterization of highly purified human hematopoietic repopulating cells isolated according to aldehyde dehydrogenase activity. *Blood* **2004**, *104*, 1648–1655. [[CrossRef](#)] [[PubMed](#)]
50. Pearce, D.J.; Taussig, D.; Simpson, C.; Allen, K.; Rohatiner, A.Z.; Lister, T.A.; Bonnet, D. Characterization of cells with a high aldehyde dehydrogenase activity from cord blood and acute myeloid leukemia samples. *Stem Cells* **2005**, *23*, 752–760. [[CrossRef](#)] [[PubMed](#)]



© 2017 by the authors. Licensee MDPI, Basel, Switzerland. This article is an open access article distributed under the terms and conditions of the Creative Commons Attribution (CC BY) license (<http://creativecommons.org/licenses/by/4.0/>).

Materials Today Bio

FATTY ACID SYNTHASE AS A NOVEL BIOMARKER FOR TRIPLE NEGATIVE BREAST CANCER STEM CELL SUBPOPULATION CULTURED ON ELECTROSPUN SCAFFOLDS

Asynch.CoverPage.ManuscriptDraft

Common.Text.ManuscriptNumber:	MTBIO-D-21-00049
Common.Labels.ArticleType	Research Paper
Common.SubmissionDetails.Keywords:	triple negative breast cancer; three-dimensional cell culture; polycaprolactone; electrospun scaffolds; breast cancer stem cells; fatty acid synthase
Common.SubmissionDetails.CorrespondingAuthor:	Teresa Puig University of Girona: Universitat de Girona SPAIN
Common.SubmissionDetails.FirstAuthor:	Marc Rabionet
Common.SubmissionDetails.OrderOfAuthors:	Marc Rabionet Emma Polonio-Alcalá Joana Relat Marc Yeste Jennifer Sims-Mourtada April M. Kloxin Marta Planas Lidia Feliu Joaquim Ciurana Teresa Puig
Common.SubmissionDetails.Abstract:	<p>There is no targeted therapy for triple negative breast cancer (TNBC), which presents an aggressive profile and poor prognosis. Recent studies noticed the feasibility of breast cancer stem cells (BCSCs), a small population responsible for tumor initiation and relapse, to become a novel target for TNBC treatments. However, new cell culture supports need to be standardized since traditional two-dimensional (2D) surfaces do not maintain the stemness state of cells. Hence, three-dimensional (3D) scaffolds represent an alternative to study <i>in vitro</i> cell behavior without inducing cell differentiation. In this work, electrospun polycaprolactone scaffolds were used to enrich BCSC subpopulation of MDA-MB-231 and MDA-MB-468 TNBC cells, confirmed by the upregulation of several stemness markers and the existence of an epithelial-to-mesenchymal transition within 3D culture. Moreover, 3D-cultured cells displayed a shift from MAPK to PI3K/AKT/mTOR signaling pathways, accompanied by an enhanced EGFR and HER2 activation, especially at early cell culture times. Lastly, the fatty acid synthase (FASN), a lipogenic enzyme overexpressed in several carcinomas, was found to be hyperactivated in stemness-enriched samples. Its pharmacological inhibition led to stemness diminishment, overcoming the BCSC expansion achieved in 3D culture. Therefore, FASN may represent a novel target for BCSC niche in TNBC samples.</p>

FATTY ACID SYNTHASE AS A NOVEL BIOMARKER FOR TRIPLE NEGATIVE BREAST CANCER STEM CELL SUBPOPULATION CULTURED ON ELECTROSPUN SCAFFOLDS

Marc Rabionet^{1,2}, Emma Polonio-Alcalá^{1,2}, Joana Relat³, Marc Yeste⁴, Jennifer Sims-Mourtada⁵, April M. Kloxin⁶, Marta Planas⁷, Lidia Feliu⁷, Joaquim Ciurana^{2,*}, Teresa Puig^{1,*}

¹ New Therapeutic Targets Laboratory (TargetsLab) - Oncology Unit, Department of Medical Sciences, Faculty of Medicine, University of Girona, Emili Grahit 77, 17003 Girona, Spain; m.rabionet@udg.edu (M.R.); emma.polonio@udg.edu (E.P.).

² Product, Process and Production Engineering Research Group (GREP), Department of Mechanical Engineering and Industrial Construction, University of Girona, Maria Aurèlia Capmany 61, 17003 Girona, Spain.

³ Department of Nutrition, Food Sciences and Gastronomy, School of Pharmacy and Food Sciences, Food and Nutrition Torribera Campus, University of Barcelona, Prat de la Riba 171, 08921 Santa Coloma de Gramenet, Spain; jrelat@ub.edu

⁴ Biotechnology of Animal and Human Reproduction (TechnoSperm), Department of Biology, Institute of Food and Agricultural Technology, University of Girona, Pic de Peguera 15, 17003 Girona, Spain; marc.yeste@udg.edu.

⁵ Center for Translational Cancer Research, Helen F Graham Cancer Center and Research Institute, Christiana Care Health Services, Inc, Newark, Delaware, USA; JSimsMourtada@ChristianaCare.org

⁶ Chemical and Biomolecular Engineering, University of Delaware, Newark, DE 19716, USA; akloxin@udel.edu

⁷ LIPPSO, Department of Chemistry, University of Girona, Maria Aurèlia Capmany 69, 17003 Girona, Spain; marta.planas@udg.edu (M.P.); lidia.feliu@udg.edu (L.F.).

* Correspondence: quim.ciurana@udg.edu (J.C.); teresa.puig@udg.edu (T.P.); Tel.: +34-972-418265 (J.C.); +34-972-419628 (T.P.).

ABSTRACT

There is no targeted therapy for triple negative breast cancer (TNBC), which presents an aggressive profile and poor prognosis. Recent studies noticed the feasibility of breast cancer stem cells (BCSCs), a small population responsible for tumor initiation and relapse, to become a novel target for TNBC treatments. However, new cell culture supports need to be standardized since traditional two-dimensional (2D) surfaces do not maintain the stemness state of cells. Hence, three-dimensional (3D) scaffolds represent an alternative to study *in vitro* cell behavior without inducing cell differentiation. In this work, electrospun polycaprolactone scaffolds were used to enrich BCSC subpopulation of MDA-MB-231 and MDA-MB-468 TNBC cells, confirmed by the upregulation of several stemness markers and the existence of an epithelial-to-mesenchymal transition within 3D culture. Moreover, 3D-cultured cells displayed a shift from MAPK to PI3K/AKT/mTOR signaling pathways, accompanied by an enhanced EGFR and HER2 activation, especially at early cell culture times. Lastly, the fatty acid synthase (FASN), a lipogenic enzyme overexpressed in several carcinomas, was found to be hyperactivated in stemness-enriched samples. Its pharmacological inhibition led to stemness diminishment, overcoming the BCSC expansion achieved in 3D culture. Therefore, FASN may represent a novel target for BCSC niche in TNBC samples.

Keywords: triple negative breast cancer; three-dimensional cell culture; polycaprolactone; electrospun scaffolds; breast cancer stem cells; fatty acid synthase

1. Introduction

Breast cancer (BC) is the most common cancer among women worldwide, accounting for 2.1 million diagnoses in 2018 as stated by the International Agency for Research on Cancer (1). Among the different BC clinical subtypes, the Triple Negative Breast Cancer (TNBC) is characterized by the lack of estrogen and progesterone receptors and no overexpression of human epidermal growth factor receptor-2 (HER2), contrary to the other subtypes which

overexpress at least one of these markers (2). This fact prevents the use of targeted therapies and leaves systemic chemotherapy as the sole treatment option for TNBC patients (3). Moreover, TNBC accounts for 15-20% of the BC cases (4) and displays a very aggressive profile. TNBC patients are younger, present a higher relapse rate, and exhibit a greater incidence of metastasis and higher mortality among BC subtypes (5). Unfortunately, despite a very good initial treatment response, there is a 40% of relapse risk in the case tumor is not properly eradicated (6). Within TNBC cells, two main molecular subtypes are represented, basal-like (80%) and mesenchymal-like (also known as claudin-low; 20%), the latter being enriched in stem-like features (7).

Relapse appearance and therapeutic failure are caused in part by cells within the tumor that display stem-like properties, thus termed breast cancer stem cells (BCSCs). Different studies described this subset as a tumor-initiating subpopulation which exhibits radio- (8) and chemoresistance, showing self-renewal capacity and favoring tumor recurrence. Since this malignant subpopulation shares some characteristics similar to mammary stem cells, BCSCs also express pluripotency, self-renewal and stemness markers such as SOX2, SOX4, NANOG, and CD49f (9). *In vitro*, BCSCs possess the capacity to grow in non-adherent conditions forming suspended mammospheres (10) and an enhanced aldehyde dehydrogenase 1 (ALDH1) enzyme activity (11). The CD44⁺/CD24^{-low} cell-surface marker pattern has also been used to isolate BCSCs (12). Besides, epithelial-to-mesenchymal transition (EMT) is known to confer stem-like traits on non-stem cells, facilitating the generation of BCSCs (13). EMT is a well-regulated cell program during embryogenesis and is responsible for the development of many tissues (14). However, cancer epithelial cells can undergo EMT losing epithelial cell polarity and acquiring mesenchymal abilities, such as invasion and migration (15), which can ultimately lead to metastasis. EMT comprises different molecular alterations including the upregulation of several transcription factors such as SNAIL, SLUG, ZEB1, ZEB2, and TWIST. During the acquisition of mesenchymal properties, cells adopt a more invasive phenotype via downregulation of E-cadherin, as this protein is involved in the establishment of cell-cell adhesion (16). This fact is accompanied by the overexpression of the mesenchymal protein vimentin, which contributes to cytoskeleton organization and focal adhesion stability (17).

Along with BCSCs presence, it is known that cancer cells also suffer from metabolism deregulation to deal with the high demand of the uncontrolled cell growth. In particular, the enzyme fatty acid synthase (FASN) is found overactivated in cancer cells in contrast with its low expression in normal tissue (except in lipogenic tissues such as liver, adipose tissue (18) and lactating mammary glands (19)), where diet regulates its expression. In cancer cells, FASN is responsible for the synthesis of almost all the fatty acids *de novo* (20), mainly phospholipids which can act not only as structural pieces but also as signaling molecules (21). For this reason, FASN has become a unique oncologic target whose inhibition has been demonstrated to hinder tumor progression (22–24) and overcome resistance to chemotherapeutic agents (25, 26), by disrupting lipid membrane synthesis, protein palmitoylation, and signaling of major oncogenic pathways (27). (-)-epigallocatechin-3-gallate (EGCG), the most abundant catechin in green tea, belongs to the early generation of FASN inhibitors (28). Despite its effect on EGFR-HER2, MAPK, and PI3K/AKT/mTOR signaling pathways among others, apoptosis after EGCG treatment occurs through FASN inhibition (23, 29). The aforementioned off-target toxicity, along with other bioavailability limitations, led to the production of new FASN inhibitors. For instance, the EGCG-analogue G28 shows more specificity and enhanced FASN inhibitory activity (30), even in TNBC models (31). In fact, mounting evidence supports that lipid metabolism disorders exert a great impact on CSC niche. Overexpression of FASN was detected on induced pluripotent stem cells (32) and its expression has been associated with the

level of stemness markers in glioma stem cells (33). Its inhibition has led to the decrease of several stemness features (33–36), indicating a role in stemness maintenance. Taking all this into account, FASN is suggested to be a more vulnerable target in CSCs than in normal cancer cells (37).

Despite the importance of BCSCs in the oncologic research field, their investigation faces some limitations. They represent a low percentage within the tumor or cell line (12, 38) and, most importantly, *in vitro* two-dimensional (2D) cell culture surfaces induce their differentiation, losing their stem-like state (39). In 2D supports, cells can only grow by forming a monolayer, adopting a flattened morphology which results in cytoskeleton remodeling. Cell shape variations can modify gene and protein expression (40, 41) leading to, for instance, BCSC differentiation. Aside from the lack of three-dimensionality, stiffness also represents a significant gap between traditional *in vitro* cell culture supports and physiological surroundings. Mammalian cells are generally attached to soft surfaces such as another similar cell or the extracellular matrix (ECM), in contrast with the rigidity of 2D surfaces used for *in vitro* studies (42). It has been reported that microenvironment stiffness can have a great mechanical impact on the cell, including changes in morphology, motility, proliferation, protein expression, and spreading (43, 44). Three-dimensional (3D) cell culture supports have emerged as an alternative to reinstate a physiological-like structure and overcome the above-mentioned issues. Among them, scaffolds offer a physical structure made by a network of polymeric filaments, which mimics ECM architecture (45). Over the past decade, electrospinning (ES) technology has been proposed to fit scaffolds manufacturing demands thanks to its customizability and the capacity to fabricate small diameter fibers (46, 47). This manufacturing process, combined with the use of viscoelastic and biocompatible polymers such as poly(ϵ -caprolactone) (PCL) (48), allows the production of ECM-like structures suitable for 3D cell culture. Interestingly, a previous investigation revealed that the use of 15% PCL ES scaffolds enhanced the mammospheres forming capacity and ALDH activity of the TNBC MDA-MB-231 cell line, indicating a BCSCs expansion (49). This fact, corroborated by more works which used scaffolds for expanding cancer stem features (50–52), empowers the use of PCL scaffolds as a 3D culture support to enrich and study BCSCs subpopulation.

All things considered, the BCSC population could become a potential target for BC treatment, in particular for TNBC subtype. To overcome *in vitro* limitations, the present study validated the stemness-enriching capacity of 15% PCL ES scaffolds with mesenchymal-like MDA-MB-231 and basal-like MDA-MB-468 TNBC cells. Furthermore, alterations in common signaling pathways were analyzed, and FASN expression and inhibition were evaluated in order to be proposed as a novel biomarker for TNBC stemness-enriched samples.

2. Materials and methods

2.1. Scaffolds manufacture

Scaffolds were manufactured through electrospinning technology, as previously described (107). Briefly, poly(ϵ -caprolactone) (PCL; 80,000 g/mol; Sigma-Aldrich, St. Louis, MO, USA) and acetone (PanReac AppliChem, Gatersleben, Germany) were used to create a 15% w/v PCL solution. A solution volume of 5 ml was processed through an electrospinning apparatus (Spraybase, Dublin, Ireland) and an 18 G needle emitter located 10 cm above the stationary collector. A voltage of 7 kV was applied and the flow rate was fixed at 6 ml/h by the Syringe Pump Pro software (New Era Pump Systems, Farmingdale, NY, USA). Produced meshes were cut into squares with a scalpel.

2.2. Dynamic Mechanical Analysis

Scaffolds mechanical profile was measured by dynamic mechanical analysis (DMA) employing the Mettler Toledo DMA/SDTA861e instrument (Columbus, OH, USA). Scaffolds were cut into 5.5 mm x 5.5 mm squares with a thickness of 0.39 mm and a large tension clamp was used as a sample holder. The geometry factor was 2582.89 1/m. The storage modulus (E') and tan delta ($\tan \delta$) were analyzed and plotted.

2.3. Three-dimensional cell culture

Mesenchymal-like MDA-MB-231 and basal-like MDA-MB-468 TNBC cells were used in this study. For scaffolds seeding, PCL meshes were sterilized by immersion into 70% ethanol/water solution overnight, washed three times with phosphate-buffered saline (PBS; Gibco) and finally exposed to germicidal UV light for 30 min. Sterilized scaffolds were placed onto non-adherent cell culture microplates (Sartstedt, Nümbrecht, Germany) and soaked in culture medium for 30 min at 37 °C prior cell seeding to favor cell attachment. Corresponding cell density was prepared in a small volume of medium (see **Table S1**). Cell suspension was pipetted drop by drop onto the scaffold center. Afterwards, scaffolds were incubated for 3 h at 37 °C and 5% CO₂ atmosphere to allow cell attachment; culture medium was subsequently added. For cell detachment, scaffolds were once washed with PBS and transferred into new wells to collect only those cells that attached to PCL filaments. Cells from 2D culture and scaffolds were detached with trypsin-EDTA (Cultek) at 37 °C and 5% CO₂ atmosphere. More details can be found in **SI Appendix**.

2.4. Mammosphere forming assay

After cell detachment, 2,000 cells were seeded onto a 6-well non-adherent cell culture microplate (Sarstedt) and incubated for 7 days at 37 °C and 5% CO₂. Cells were cultured with DMEM/F12 medium (HyClone) supplemented with B27 (Gibco), hEGF and hFGF (20 ng/ml; Milteny Biotec, Bergisch Gladbach, Germany), 1% L-glutamine and 1% sodium pyruvate (Gibco). After incubation, spherical mammospheres with a minimum diameter of 50 μm were counted. The following equation was used to calculate the Mammosphere Forming Index (MFI) of each culture condition:

$$MFI (\%) = \frac{n^{\circ} \text{ mammospheres}}{n^{\circ} \text{ seeded cells}} \times 100$$

2.5. ALDEFLUOR™ assay

ALDEFLUOR™ kit (STEMCELL Technologies, Vancouver, Canada) was used to determine the ALDH enzyme activity, following the company guidelines. Cells were detached from the culture plastic (2D samples) and PCL scaffolds (3D) as previously described, PBS-rinsed and 200,000 cells were resuspended in 500 μl of ALDEFLUOR™ assay buffer. Afterwards, 2.5 μl of ALDEFLUOR™ Reagent (BAAA) was added to each cell suspension and 250 μl of the suspension was immediately transferred to a new tube with 2.5 μl of the ALDH inhibitor diethylaminobenzaldehyde (DEAB) to consider background fluorescence. All samples were incubated for 45 min at 37 °C in the dark. Cells were then centrifuged, washed, and analyzed with a Cell Lab Quanta flow cytometer (Beckman Coulter Inc., Miami, FL, USA) to quantify the ALDH-positive cell population. More details can be found in **SI Appendix**.

2.6. Quantitative real-time PCR analysis

Once trypsinized, 2D- and 3D-cultured cells were suspended with 750 μL of Qiazol (Qiagen, Hilden, Germany). Total RNA from each sample was isolated using a RNeasy Mini Kit (Qiagen) following the instructions provided by the manufacturer. After extraction, RNA amount and purity were determined by spectroscopy (NanoDrop™ One Microvolume UV-Vis spectrophotometer, Thermo Fisher Scientific, Waltham, MA, USA). RNA was reverse-transcribed into complementary DNA using High Capacity cDNA Archive Kit (Applied Biosystems, Foster City, CA, USA). Gene expression levels were assessed using QuantStudio 3 Real-Time PCR System (Applied Biosystems) with qPCRBIO SyGreen Mix Lo-ROX (PCR Biosystems, London, UK). Gene expression levels were quantified by double delta Ct analysis method and normalized to the housekeeping gene *GAPDH*. More details can be found in **SI Appendix** and **Table S2**.

2.7. *CD44⁺/CD24^{-low}* analysis

After detachment, cells were washed with PBS containing 10% FBS and resuspended at a density of 2×10^6 cells/mL in cold PBS with 10% FBS. Cells were stained with allophycocyanin (APC)-conjugated CD44 and fluorescein isothiocyanate (FITC)-conjugated CD24 (Abcam, Cambridge, MA, USA) for 30 min in the dark at room temperature. Samples were centrifuged, washed, and passed through a BD Falcon cell strainer cap tube (BD, Franklin Lakes, NJ, USA) for fluorescence-activated cell sorting analysis. Samples were analyzed on a fluorescence-activated cell sorting LSRFortessa flow cytometer (BD) and were gated on an unstained control. Compensation was performed with single stained cells to decrease overlaps of fluorophore emission spectrums.

2.8. Western blot

After culture, the cell pellet was PBS-rinsed and lysed in ice-cold lysis buffer (Cell Signaling Technology, Inc., Danvers, MA, USA) with 100 $\mu\text{g}/\text{mL}$ phenylmethylsulfonyl fluoride (PMSF; Sigma-Aldrich) by vortexing every 5 min for 30 min. Total protein content of each lysate was determined by Lowry-based DC Protein Assay (Bio-Rad Laboratories, Inc., Hercules, CA, USA). Equal amounts of protein (10 μg) were heated in Lithium Dodecyl Sulfate (LDS) Sample Buffer with Sample Reducing Agent (Invitrogen, Carlsbad, CA, USA) for 10 min at 70 °C, electrophoresed on 7.5% sodium dodecyl sulphate polyacrylamide gels (Bio-Rad Laboratories, Inc.), and transferred onto nitrocellulose membranes (Thermo Fisher Scientific). Blots were incubated at room temperature for 3 h in blocking buffer [5% bovine serum albumin (BSA) in tris-buffered saline with 0.1% Tween (TBS-T)] to avoid non-specific antibody binding. Afterwards, membranes were incubated overnight at 4 °C with the appropriate primary antibody diluted in blocking buffer (see **Table S3**). Specific horseradish peroxidase (HRP)-conjugated secondary antibody was incubated for 1 h at room temperature. Immune complexes were detected using a chemiluminescent HRP Substrate [Clarity™ Western ECL Substrate (Bio-Rad Laboratories, Inc.) or SuperSignal™ West Femto (Thermo Fisher Scientific)] and a ChemiDoc™ Imaging System (Bio-Rad Laboratories, Inc.). Western blot analyses were repeated at least three times and representative results are shown. Protein bands were quantified by densitometric analysis using Image Lab™ Software (Bio-Rad Laboratories, Inc.). The expression ratios were determined after normalizing against individual GAPDH levels.

2.9. FASN activity

Cells were cultured on 2D wells and 3D scaffolds for 6 days as previously described in 4.3 section. For the last 6 h, medium was replaced by DMEM supplemented with 1% lipoprotein-deficient FBS (Sigma-Aldrich) and 0.5 $\mu\text{Ci}/\text{mL}$ ($1,2\text{-}^{14}\text{C}$) acetic acid sodium salt (53.9 mCi/mmol ; Perkin Elmer Biosciences, Waltham, MA, USA). Cells were harvested and washed twice with PBS (500 μL) and once with methanol:PBS (2:3; 500 μL). The pellet was resuspended in 0.2 M NaCl (100 μL) and lysed with freeze-thaw cycles. Lipids from cell debris were extracted by centrifugation (2000 G, 5 min) with chloroform:methanol (2:1; 350 μL) and KOH 0.1 M (25 μL). The organic phase recovered was then washed with chloroform:methanol:water (3:48:47; 100 μL) and evaporated in a Speed-vac Plus SC110A (Savant Instruments Pvt. Ltd., Hyderabad, India). The dried pellets were resuspended in ethanol and transferred to a vial for radioactive counting. The total protein content in cell debris was quantified with the Bradford assay (Thermo Fisher Scientific).

2.10. Cell viability assay

After 6 days of culture on 2D and 3D supports, fresh medium along with the corresponding concentrations of doxorubicin (TEDEC-Meiji Farma, Alcalá de Henares, Spain), paclitaxel (Accord Healthcare Ltd., Thaltej, India), EGCG (Sigma-Aldrich) or G28 were added to the cultures. Following a 48-h treatment, a colorimetric MTT assay (3-(4,5-dimethyl-2-thiazolyl)-2,5-diphenyl-2H-tetrazolium bromide; Sigma-Aldrich) was used to measure cell viability. More details can be found in **SI Appendix**.

2.11. Statistical analysis

All data are expressed as mean \pm standard error of the mean (SEM). Data were analyzed using IBM SPSS (SPSS Inc., Chicago, IL, USA). When data normality and homogeneity of variances were confirmed through Shapiro-Wilk and Levene tests, a linear mixed model followed by post-hoc Sidak test were carried out. If data did not fulfil with parametric assumptions, they were tested with Scheirer-Ray-Hare and Mann-Whitney tests. The level of significance was set at $p < 0.05$. All observations were confirmed by at least three independent experiments.

3. Results and discussion

3.1. Stiffness characterization of electrospun PCL scaffolds

Since the stiffness of the cell culture support can have a great impact on the cell, a dynamic mechanic analysis (DMA) was performed on the 15% PCL scaffolds to characterize their viscoelastic behavior. Elastic response of the material can be defined by the storage modulus (E'), shown in **Figure 1A**, which measures the capacity of the material to store elastic energy. Meshes showed an E' value of approximately 6.64 MPa at room temperature (25 $^{\circ}\text{C}$) and around 5 MPa at a physiological one (37 $^{\circ}\text{C}$). Meanwhile, E' values from polystyrene (PS), the main component of 2D culture surfaces, are reported to range from 1300 to 3000 MPa at room temperature in the literature (53, 54). Hence, lower E' values of PCL meshes indicate that this material shows reduced solid-like properties and lower strength and mechanical rigidity. Consequently, produced PCL scaffolds represent a softer cell culture support, although they are stiffer compared with breast cancer tissue, whose E' values vary from 10 to 40 kPa (55). Previous studies using fibroblasts reported that cells generate more traction force and

develop a broader and flatter morphology on stiff surfaces (43). In this context, cell responses on PCL nanofibers are likely influenced by both the stiffness and three-dimensionality of these fibers, where elongated morphologies have been observed for MDA-MB-231 and MDA-MB-468 cells in previous studies (49, 56).

The loss tangent (or tan delta; $\text{Tan } \delta$) is the ratio of loss modulus (E'') and storage modulus (E'), which indicate the viscosity of material and elastic properties, respectively. Interestingly, $\text{Tan } \delta$ curve peak designates the polymer's glass transition temperature (T_g), the critical temperature at which the transition between glassy and rubbery state occurs (57). As seen in **Figure 1B**, electrospun PCL scaffolds exhibited a glass transition point of -49.68°C , similar to the value of neat PCL (-60°C) (58), and other PCL structures used in the literature (59, 60). Consequently, when working at room or physiologically temperature, 3D PCL scaffolds are above their T_g , exhibiting a more elastic profile compared with PS, whose T_g value is around 100°C (61).

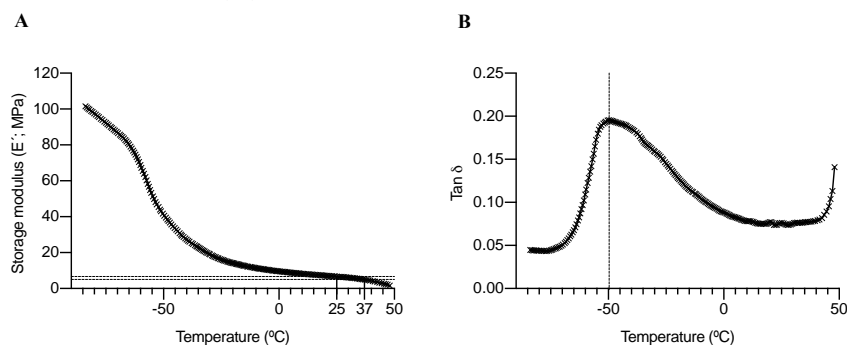


Fig. 1. Dynamic Mechanical Analysis (DMA) for 15% PCL scaffolds. Storage modulus (A) and $\text{Tan } \delta$ (B) of specimens were plotted against temperature.

3.2. Impact of scaffolds culture on MDA-MB-468 BCSC subpopulation

Scaffolds-induced enrichment of BCSC population was previously reported by our research group using mesenchymal-like TNBC MDA-MB-231 cell model, which exhibited greater mammosphere forming capacity and ALDH activity after 3D culture (49). Furthermore, basal-like TNBC MDA-MB-468 cells were proved to adopt a more elongated morphology in ES PCL scaffolds, in disagreement with the flattened morphology on 2D cultures (56). For this reason, we used the same ES scaffold model to culture MDA-MB-468 cell line and analyze the impact on BCSCs through mammospheres forming assay, ALDH activity and $\text{CD44}^+/\text{CD24}^{\text{low}}$ proportion. As shown in **Figure 2A**, cells after 3D culture displayed a significantly higher mammosphere forming index (MFI) when compared with the pertinent monolayer culture, regardless of cell culture time. Moreover, no significant differences were observed within the same cell culture support over time. A time-dependent trend was observed on the ALDH activity (**Fig. 2B**). At early time points (3 and 6 culture days) cells from scaffolds possessed a larger ALDH⁺ subpopulation compared to 2D control. However, after 12 days of incubation the trend was the opposite due to a hyperactivation of ALDH activity on monolayer cells. Representative dot plots are given in **Table S4**. While mRNA *CD44* levels remained broadly stable, lower *CD24* expression was observed in scaffolds culture compared with monolayer control (**Fig. 2C**), which is correlated with increased tumorigenicity (12, 62). To confirm these data, the expression of CD24 and CD44 cell surface markers was assessed through flow

cytometry (**Fig. 2D**). An increase in the CD44⁺/CD24^{-low} population was observed after 3 and 6 days of culture compared with 2D samples. Taking all this into consideration, 3D scaffold culture enlarged the percentage of BCSC-like CD44⁺/CD24^{-low} cells, with decreasing CD24 expression levels, since its basal population are mainly CD44⁺/CD24⁺. Overall, 3D culture on ES 15% PCL scaffolds caused an enrichment of the BCSC subpopulation in the basal-like MDA-MB-468 cell model, especially at early culture times, following the effect previously reported with the mesenchymal-like MDA-MB-231 cells (49).

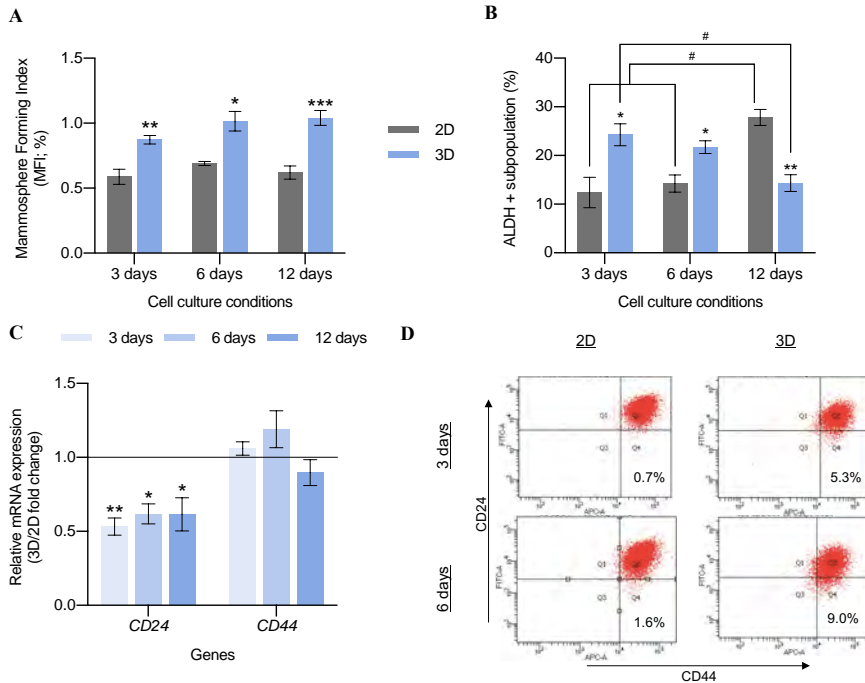


Fig. 2. MDA-MB-468 stemness features after monolayer (2D) and 15% PCL scaffolds (3D) culture. A mammosphere forming assay (**A**), ALDEFLUOR assay (**B**), *CD24* and *CD44* mRNA expression profile (**C**), and protein expression pattern of CD24/CD44 (**D**) are depicted. Gene expression levels were quantified by double delta Ct analysis method and normalized to the housekeeping gene *GAPDH*. Cells were incubated with CD44-APC and CD24-FITC antibodies. Percentage of breast cancer stem-like cells (CD44⁺/CD24^{low/-}) is represented in Q4. Data are representative of three separate experiments. Significant differences of 3D with regard to corresponding 2D cultures are indicated as * ($p < 0.05$), ** ($p < 0.01$) and *** ($p < 0.001$). Significant differences of culture time within same culture support are indicated as # ($p < 0.05$).

3.3. Stemness markers expression and chemoresistance of TNBC models cultured on scaffolds

More stemness features were further analyzed to confirm the expansion of the breast cancer stem cell population when scaffolds were used with the MDA-MB-231 and MDA-MB-468 TNBC models. Expression of the stemness-related genes *SOX2*, *SOX4*, *NANOG* and *CD49f* were examined along time in 2D and 3D-cultured cells (**Fig. 3**). *SOX2* is a transcription factor involved in pluripotency maintenance and self-renewal capacity [66]. In tumoral tissues, it plays a key role in differentiation, invasion, metastasis, and drug resistance [67]. *SOX4* is

another transcription factor related to development processes and progression of cancer [68], and it is used as a CSC-specific marker [52]. NANOG is a key transcription factor involved in self-renewal and pluripotency maintenance in embryonic stem cells. Moreover, it is thought to be regulated by the cooperative action of SOX2 and OCT3/4 [69]. CD49f was found to possess a key role in stemness maintenance through direct regulation of OCT3/4 and SOX2 [70]. MDA-MB-231 cells cultured on scaffolds showed an upregulation of *SOX2* after 3 days of culture, and an overexpression of *SOX4* and *NANOG* after 6 days (**Fig. 3A**). On the other hand, scaffold culture led to an upregulation of *SOX2* and *CD49f* levels on MDA-MB-468 cell model (**Fig. 3B**). Interestingly, *SOX2* and *SOX4* have been related to mammosphere forming capacity [71,72]. However, long incubation periods on scaffolds did not result in the activation of any stemness-related gene and even a downregulation was observed in the case of the mesenchymal-like model (**Fig. 3A**). Therefore, the upregulation of several stemness-related markers proved the BCSC enrichment found in 3D culture at early times.

Another intrinsic characteristic of the BCSC niche is the increased resistance to chemotherapy (69). Concretely, it has been shown that BCSCs display resistance to doxorubicin and paclitaxel (70, 71), two therapeutic agents currently used against TNBC (72). Since the majority of stemness features were found to be upregulated after 6 days of culture in 3D scaffolds, chemoresistance was evaluated at this time. MDA-MB-231 and MDA-MB-468 cells were cultured in tissue culture plastic and 3D 15% PCL scaffolds for 6 days and they were later treated with doxorubicin and paclitaxel for 48 h. As seen in **Figure 3C** and **3D**, both cell models exhibited a significant higher cell survival rate when cultured in scaffolds compared with monolayer culture, after treatment with the two chemoagents. Greater differences between 2D and 3D samples were observed when higher drug concentrations were used, in agreement with other studies (52). *SOX2*, whose expression was upregulated in both cell models when cultured in scaffolds (**Fig. 3A** and **3B**), was linked to drug resistance (64). More specifically, it was found to play a key role in paclitaxel resistance (73), explaining the greatest cell survival of 3D-cultured MDA-MB-468 cells after paclitaxel addition; since this model was the one exhibiting the highest *SOX2* expression (**Fig. 3B**).

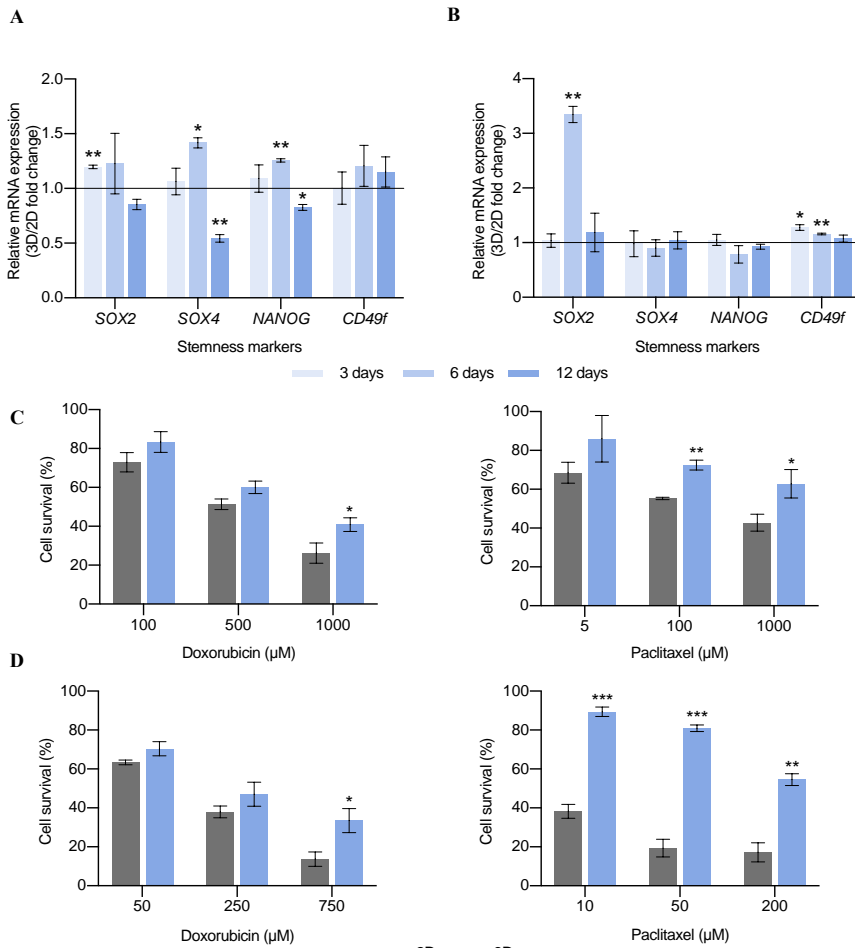


Fig. 3. Stemness features expression analysis. Fold changes in mRNA levels of stemness-related genes in 3D-cultured cells compared to corresponding 2D control for MDA-MB-231 (A) and MDA-MB-468 (B) cell models. Gene expression levels were quantified by double delta Ct analysis method and normalized to the housekeeping gene *GAPDH*. Cell survival plots for MDA-MB-231 (C) and MDA-MB-468 (D) cell models are also depicted. Cells were cultured on monolayer (2D) or in PCL scaffolds (3D) for 6 days and then exposed to the chemoagents doxorubicin or paclitaxel for 48 hours. Data are expressed as percentage of untreated cells as determined by MTT assay. Significant differences of 3D with regard to 2D cultures are indicated as * ($p < 0.05$), ** ($p < 0.01$) and *** ($p < 0.001$).

3.4. Epithelial-to-Mesenchymal Transition (EMT) in scaffolds culture of TNBC cells

The induction of EMT in human mammary epithelial cells is known to increase the BCSC subpopulation (15). We therefore evaluated the expression of several transcription factors that execute EMT, such as *SNAIL*, *SLUG*, *ZEB1*, *ZEB2*, and *TWIST*, in 2D- and 3D-cultured cells. Proteins involved in this process, including E-cadherin and vimentin, were also analysed to determine whether EMT was triggered during 3D culture and may be responsible of the stemness enrichment. In both cell models, *SNAIL* was found to be upregulated at early times of 3D cell culture (**Fig. 4A** and **4B**). *SNAIL* is known to be a prominent EMT initiator since its expression was proven to be sufficient to induce EMT in primary breast cancer cells (74) and drug resistance (75). Moreover, *SNAIL* expression was also associated with self-renewal through *NANOG* activation (76), which was upregulated in 3D-cultured MDA-MB-231 cells (**Fig. 3A**). *SNAIL* is known to bind to and represses its own promoter, indicating the existence of an autoregulatory loop (77). This fact, along with its short half-life (78), proves the time-dependent trend showed in **Figure 4**. In the basal-like cell model, *ZEB2* and *TWIST* were also overexpressed during 3D culture, with greater robustness after 6 days of incubation (**Fig. 4B**). We further measured gene and protein expression of E-cadherin (encoded by *CDH1*) and vimentin (encoded by *VIM*), the two major proteins involved in EMT. 3D cell culture led to a downregulation on *CDH1* gene levels in both cell models (**Fig. 4C** and **4D**). This fact resulted in a decrease of E-cadherin protein expression on the basal-like cells whereas expression in MDA-MB-231 model remained stable, probably because these cells are undergoing an early EMT. *SNAIL*, whose expression was upregulated in 3D culture (**Fig. 4A** and **4B**), has been described as a direct repressor of E-cadherin through histone deacetylase activity (79). Concerning vimentin, its gene expression was found upregulated when MDA-MB-231 cells were cultured on scaffolds for 6 days (**Fig. 4C**). An activation trend was described for protein analysis for both cell models as seen in **Figure 4C** and **4D**.

Considering these data, 3D cell culture with ES PCL scaffolds induced an EMT process to TNBC cells, which acquired a more invasive phenotype and led to an increase of the stemness features. Stiffness reported on PCL scaffolds could play a key role in this EMT induction, since it was proven to be an underlying mediator of TGF- β -driven processes such as EMT through dynamic compression and contraction of cell-matrix interaction (80). Although the expression of structural proteins E-cadherin and vimentin were altered during scaffolds culture, actin and tubulin levels, the main components of the eukaryotic cytoskeleton, were proven to be consistent among the different cell culture supports and incubation period for both cell lines (**Fig. S1**).

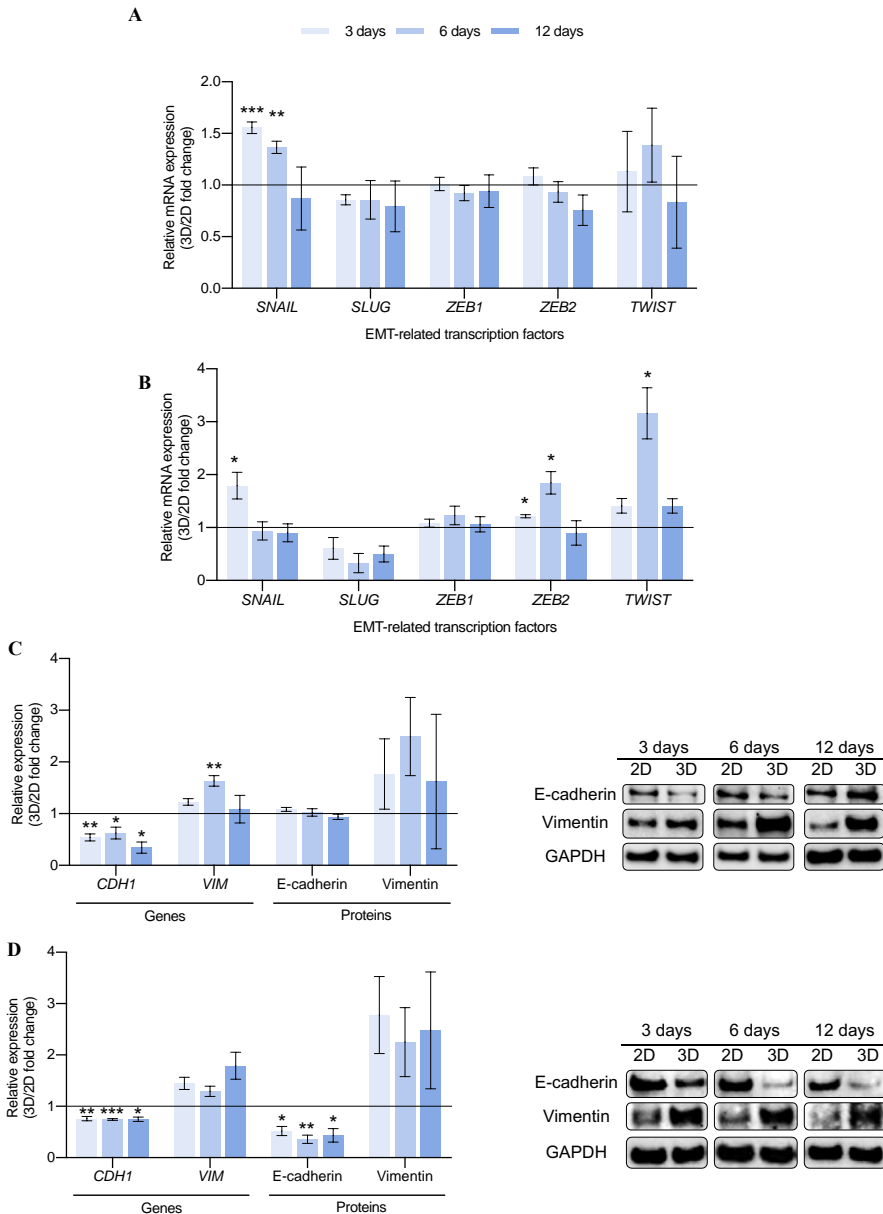


Fig. 4. Epithelial-to-mesenchymal transition (EMT) analysis for MDA-MB-231 (A, C) and MDA-MB-468 (B, D). Fold changes in mRNA levels of EMT-related genes (A, B) and in gene and protein expression of E-cadherin and vimentin (C, D) of cells cultured on ES PCL scaffolds (3D) compared to corresponding 2D control. Gene expression levels were quantified by double delta Ct analysis method. Both gene and protein expression levels were normalized against GAPDH values. Significant differences of 3D with regard to 2D cultures are indicated as * ($p < 0.05$), ** ($p < 0.01$) and *** ($p < 0.001$). A representative Western Blot image for each cell culture condition is shown.

3.5. MAPK and PI3K/AKT/mTOR pathways modulation in scaffolds-cultured TNBC cells

To discern whether cell metabolism is affected during 3D culture and stemness enrichment, MAPK and PI3K/AKT/mTOR pathways, which represent key mechanisms for cells to regulate cell survival, division and motility, were characterized through Western blot. MAPK pathway is involved in both physiological and pathological cell functions, including cell proliferation, differentiation, cell survival, oncogenesis and tumor progression (81). To evaluate the implication of the MAPK pathway in the stem-enriched 3D population, phosphorylated and total protein levels of MAPK, as well as the downstream phospho-S6, were analyzed (**Fig. 5**). Mesenchymal-like model MDA-MB-231 showed a pathway activation after 3 culture days within scaffolds, in accordance with the MAPK phosphorylated levels (**Fig. 5A**), which was not maintained at further culture times. On the other hand, basal-like MDA-MB-468 cell line displayed a clear downregulation of the MAPK pathway along time, even though total MAPK protein levels gradually increased during 3D culture (**Fig. 5B**). We hypothesized that increased activation level of MAPK at early times in MDA-MB-231 model was in part a response to cell cytoskeleton rearrangement on the PCL nanofibers. In fact, MAPK activation was related with cytoskeleton rearrangements in the same breast cancer model to increase the morphological plasticity for metastatic purposes (82). For the other cell culture conditions, MAPK pathway, which regulates cell proliferation, seems downregulated in both TNBC cell lines possibly due to their lower cell growth rate in scaffolds as previously reported in the same 3D model (49, 56). Moreover, decreased MAPK signaling and activation of a quiescent profile has been related to decreased matrix stiffness, a condition found in the used ES PCL scaffolds compared to PS surfaces (**Fig. 1**) (83). Phosphorylated levels of the MAPK-downstream S6 ribosomal protein were found not to be affected by 3D culture (**Fig. 5**). Therefore, differences on cell metabolism during scaffolds culture may be not mediated by p-S6, but probably by MAPK direct modulation of end-point effectors such as transcription factors.

The PI3K/AKT/mTOR signaling pathways play a key role in many physiological and pathological conditions, including cell proliferation, angiogenesis, metabolism, differentiation and survival (84). Interestingly, recent studies have demonstrated its importance in self-renew maintenance and tumorigenicity (85), EMT and radioresistance (86), mammospheres formation (87) and ALDH activity (88). Therefore, the expression and activation of several proteins involved in the PI3K/AKT/mTOR cascade were analyzed (**Fig. 5**). MDA-MB-231 cells showed an increasing activation of PI3K along 3D culture against the stable levels of total protein (**Fig. 5A**). This activation resulted in higher levels of total AKT protein and phosphorylated mTOR after 3 and 6 days of culture within scaffolds, respectively. Regarding the basal-like model MDA-MB-468, higher levels of activated PI3K and mTOR were found after 6 days of culture in scaffolds, accompanied by downregulation of PTEN, the negative regulator of the pathway (**Fig. 5B**). In the light of these results, 3D culture with ES PCL scaffolds led to a mild activation of the PI3K/AKT/mTOR pathway, as proved by the higher phosphorylation level of the downstream complex mTOR after 6 days of culture in both cell models.

In addition to their independent signaling programs, MAPK and PI3K/AKT/mTOR can either positively or negatively intraregulate (89, 90). For instance, in glioblastoma stem-like cells, inactivation of either MAPK or PI3K/mTOR pathway triggered activation of the other, suggesting a mutually inhibitory crosstalk between these two pathways (85). Collectively, hyperactivation of PI3K/AKT/mTOR cascade may inhibit MAPK signaling, leading to a more quiescent culture. Or vice versa, cells adopted a less proliferative profile within 3D surroundings, leading to a MAPK inactivation and triggering PI3K/AKT/mTOR signaling due

to a feedback loop. Contrary to our results, previous works pointed out that 3D culture of HER2+ breast cancer cells in Matrigel or spheres promoted a shift from PI3K/AKT to MAPK signaling (91–93). Overall, this may indicate that cells can adopt different modifications upon 3D culture depending on their molecular subtype and 3D structure type, among other variables.

Not only are receptor tyrosine kinases critical regulators of several cell functions including proliferation, differentiation, and survival (94), but they also have a critical key role in cancer development and progression (95). One of the most important receptors group is the ErbB/HER family, which includes the Epidermal Growth Factor Receptor (EGFR, also known as HER1) and the Human Epidermal growth factor Receptor 2 (HER2) (96). The signal transduction caused by their activation promotes a diverse repertoire of cellular signaling pathways including MAPK or the PI3K/AKT/mTOR pathways (97). As seen in **Figure 5A**, MDA-MB-231 cells underwent a HER2 overexpression and activation after 3 days of culture in scaffolds. Alternatively, EGFR expression seemed stable, with a slight upregulation after 12 days of culture. About MDA-MB-468 cells, activation of EGFR and HER2 was observed after 6 days of culture in scaffolds (**Fig. 5B**). In addition, previous studies already reported overexpression of HER2 in HER2-negative breast and ovarian cancer cells following culture in 3D supports but not in 2D monolayers (91, 93). Activation of HER2 is associated with BCSCs and radioresistance in HER2-negative breast cancer cell models (98), as well as with tight junctions and cell polarity disruption (99).

Considering all these findings, our hypothesis is that upregulation of HER2 alone (MDA-MB-231) or in combination with that of EGFR (MDA-MB-468) may promote PI3K/AKT/mTOR activation during 3D cell culture, in detriment of MAPK signaling. These signaling alterations could be behind BCSC expansion within 3D culture, as PI3K pathway was previously related to the acquisition of CSC-like properties in breast cancer cells (100). Besides, metabolism alterations were mainly found at 3 and 6 culture days, time points were BCSC took the greatest expansion in scaffolds. It is worth noting that HER2 is the preferred dimerization partner, since it possesses a conformation similar to a ligand-activated state (101) and results in greater signal transduction compared with other family members (102). Moreover, HER2 is thought to preferentially form homodimers in 3D suspension culture (91), proving its important role in both cell models. High levels of HER2 are speculated to promote spontaneous dimerization and causing constitutive HER2 activation and signaling (103).

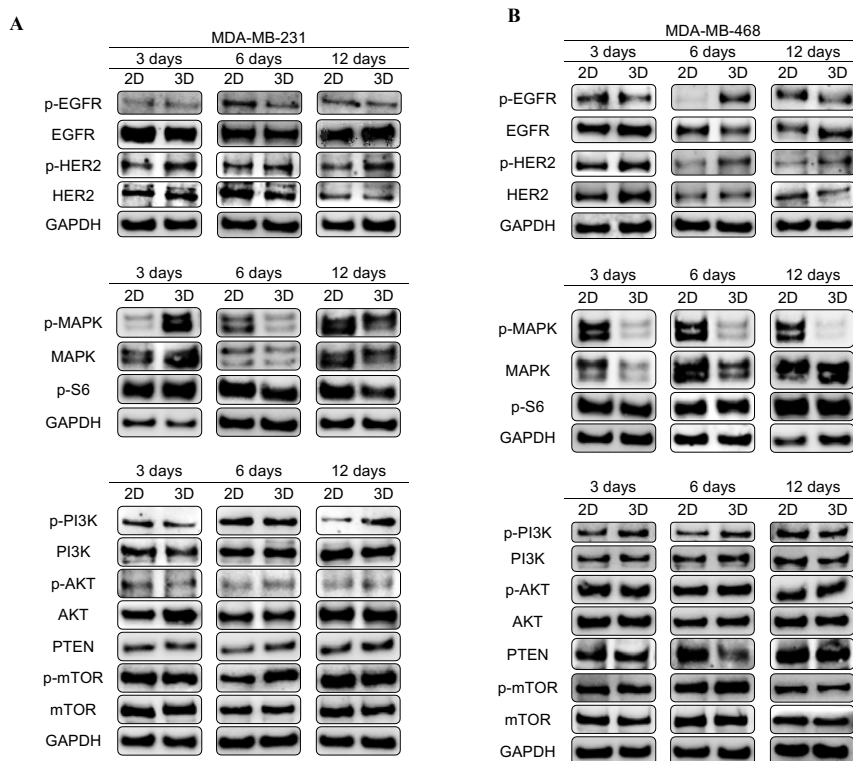


Fig. 5. Characterization of EGFR/HER2, MAPK and PI3K/AKT/mTOR pathways. Phosphorylation state and total protein levels were determined by Western blotting for MDA-MB-231 (A) and MDA-MB-468 (B) cells cultured on ES PCL scaffolds (3D) compared to corresponding 2D control. GAPDH was used as a control of protein loading. Results shown are representative of those obtained from 3 independent experiments.

3.6. Role of Fatty Acid Synthase (*FASN*) enzyme in BCSCs-enriched TNBC samples

3.6.1. *FASN* expression and activity on monolayer and 3D culture

Apart from the relation between stemness and *FASN* (37), *HER2* is proven to stimulate *FASN* expression and post-translational activation by phosphorylation. *FASN*, in turn, contributes to *HER2* activation allowing its incorporation in lipid rafts on the plasma membrane (104). Therefore, gene and protein expression of *FASN* (encoded by *FASN*) was evaluated in 2D and 3D samples to discern a possible role of this enzyme during the acquisition of stemness features within scaffolds culture. As seen in **Figures 6A** and **6B**, *FASN* mRNA levels of both cell models were found slightly upregulated after 6 days of culture within PCL ES scaffolds. This moderate increase resulted in significantly higher protein levels at the aforementioned culture time. Note, *FASN* expression had the same trend in both cell models and it was found upregulated after 6 days of culture in scaffolds, the same incubation period which showed the maximum expansion of stemness features. For this reason, the enzyme activity of *FASN* was also evaluated after 6 days on monolayer or scaffolds culture (**Fig. 6C**). Both cell models showed significantly greater *FASN* activity after their 3D culture. Therefore,

either protein expression or functional FASN activity were determined to be upregulated in MDA-MB-231 and MDA-MB-468 cells following 6 days of culture within PCL meshes.

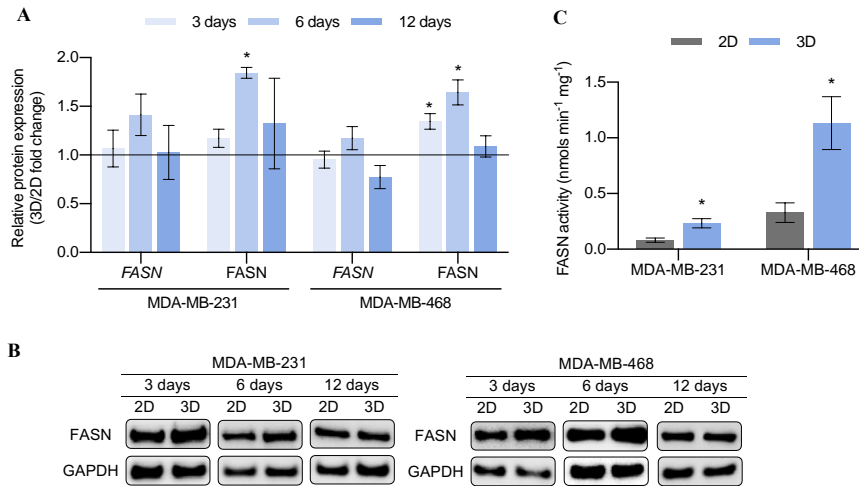


Fig. 6. FASN expression pattern. **(A)** Fold changes in gene and protein expression of FASN for MDA-MB-231 and MDA-MB-468 cells cultured on ES PCL scaffolds (3D) compared to corresponding 2D control. Gene expression levels were quantified by double delta Ct analysis method. Both gene and protein expression levels were normalized against GAPDH values. **(B)** A representative Western Blot image for each cell culture condition is shown. **C** FASN activity analysis for MDA-MB-231 and MDA-MB-468 cells after 6 days of culture on monolayer (2D) and scaffolds (3D). Significant differences of 3D with regard to 2D cultures are indicated as * ($p < 0.05$).

3.6.2. Pharmacological inhibition of FASN on monolayer and 3D culture

In the light of previous results, we wanted to investigate the impact of FASN inhibition on the BCSC-enriched population. Thus, TNBC cells were treated with the FASN inhibitors EGCG and G28 after 6 days of 2D or 3D culture, when both BCSC expansion and FASN hyperactivation took their maximum within scaffolds. Following a 48 h treatment, cell viability was assessed in both cell culture supports (**Fig. 7A** and **7B**). Samples from 2D and 3D culture supports showed a similar behavior. There were no differences regarding inhibitory concentration between the tested TNBC cells cultured on 2D and 3D supports (**Fig. S2**). This data, contrary to the chemoresistance previously reported on 3D-cultured cells (**Fig. 3C** and **3D**), opens the door to propose FASN as a novel target to treat 3D-cultured quiescent and stem-like TNBC populations.

To evaluate the effect on the BCSC niche, cells were treated with IC_{30} and IC_{50} values of EGCG and G28 in 2D- and 3D-cultured samples. After 48 h treatment, the capacity of forming mammospheres was evaluated as a marker of stem-like population. As seen in **Figure 7C** and **7D**, 3D-cultured samples showed significantly higher mammosphere forming capacity confirming the expansion of stemness features in untreated cells. The treatment with EGCG and G28 decreased the MFI values of 3D samples down to similar values of 2D or even lower. It should be noted that G28 exerted a greater impact upon the MDA-MB-231 model, in which 3D samples treated with IC_{50} dosage showed a significantly minor MFI value than the

corresponding 2D control (**Fig. 7C**). On the other hand, basal-like MDA-MB-468 cells in scaffolds underwent a greater MFI decrease when treated with EGCG, also exhibiting an inferior mammosphere forming capacity than 2D cells (**Fig. 7D**). Taking all these findings into account, the inhibition of FASN through EGCG and G28 treatment led to a stemness diminishment, overcoming the BCSC expansion achieved in 3D culture. In a similar fashion, resveratrol, a natural polyphenolic compound, has been proven to suppress tumor stem-like cells growth by inducing pro-apoptotic genes via downregulation of FASN expression, *in vitro* and with mice model (105). Some authors pointed out a possible role of FASN increasing fatty acid levels during tumor cell migration, invasion and metastasis, characteristics of the BCSC niche (106). Despite this report and previous links between FASN and cancer stem-like cells, further investigations are needed to elucidate the mechanism through which stemness diminishes in response to FASN inhibition.

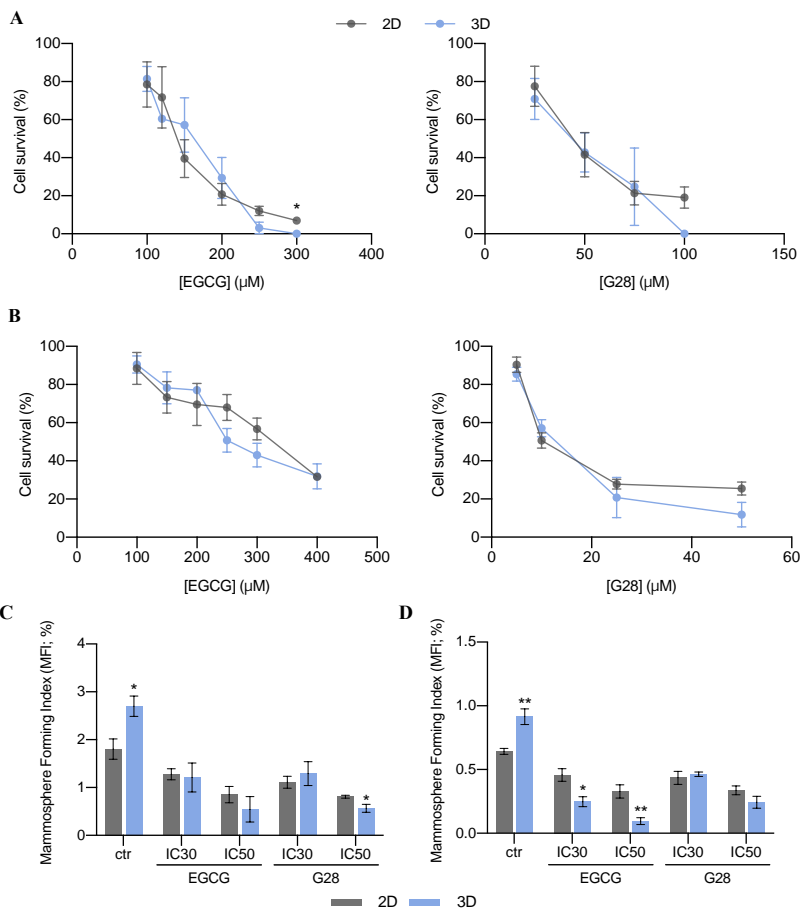


Fig. 7. Cell survival plots (**A, B**) and mammosphere forming assay (**C, D**) for MDA-MB-231 (**A, C**) and MDA-MB-468 (**B, D**) cells after EGCG or G28 treatment. Cells were cultured on monolayer (2D) or in PCL scaffolds (3D) for 6 days and then exposed to the FASN inhibitors EGCG and G28 for 48 h. Cell survival data are expressed as percentage of untreated cells as determined by MTT assay. Significant differences of 3D with regard to corresponding 2D cultures are indicated as * ($p < 0.05$) and ** ($p < 0.01$).

4. Conclusions

ES 15% PCL scaffolds used in the present work have been proven to provide a softer and more elastic 3D network compared with PS surfaces. As demonstrated in previous (49, 56) and current research, 3D culture with this scaffold model led to an enrichment of the BCSC subpopulation in TNBC cells, resulting in higher mammosphere forming capacity, ALDH activity, CD44⁺/CD24^{-low} cell proportion, stemness-related genes expression and chemoresistance, specifically at early culture time points. In addition, EMT was revealed to occur throughout scaffolds culture, which can transform epithelial cancer cells into cancer stem-like cells. Aside from BCSC expansion within scaffolds surroundings, 3D-cultured cells displayed a strong MAPK downregulation alongside a mild PI3K/AKT/mTOR activation, resulting in a quiescent cell profile and the upregulation of the aforementioned stemness features. As hypothesized in **Figure 8**, this signaling switch may be modulated by the described activation of EGFR and HER2, which is proven to favor FASN synthesis, previously related to cancer cells and stemness. To the best of our knowledge, we are the first to define a FASN hyperactivation in stemness-enriched TNBC cells cultured on 3D structures. The addition of two FASN inhibitors led to a similar cell death in monolayer and scaffolds-cultured cells, eluding the cell growth rate dependence of the chemoagents. Moreover, the inhibition of FASN overcame the BCSC enrichment achieved in 3D culture in terms of mammosphere forming capacity, suggesting the possibility to inhibit FASN to treat the cancer stem-like cells. However, more BCSCs markers could be analyzed after FASN inhibition to confirm stemness diminishment, including ALDH activity and CD44⁺/CD24^{-low} status.

Collectively, ES PCL scaffolds represent a potent tool to maintain the stemness features of the sample and expand the BCSC niche of TNBC cells by providing resemblance to a physiological structure. Nanofiber meshes may facilitate research in the cancer stem-like cells field, since novel biomarkers and treatments need to be developed to attack not only the bulk tumor, but also the quiescent and tumor-initiating cells. Notably, FASN deserves further investigation as a novel biomarker for BCSCs-enriched TNBC samples, specially within 3D surroundings. Despite the described links between FASN and stemness, more efforts would be needed to investigate whether BCSCs expansion and signaling switch alongside FASN activation are two independent events occurred in a 3D environment, or there is a causal relation.

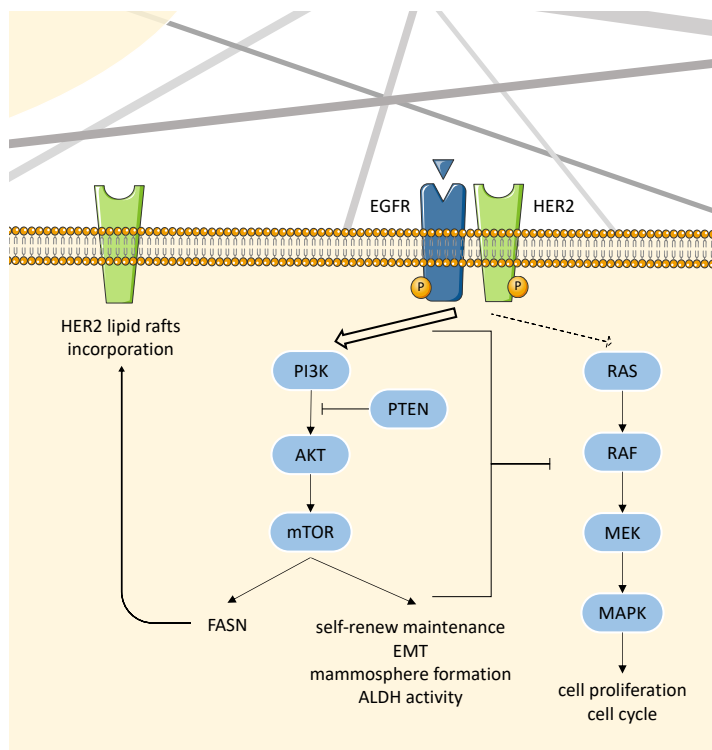


Fig. 8. Schematic representation of TNBC cell metabolism modulation within 3D ES PCL scaffold culture.

5. Acknowledgements

This work was supported by Spanish grants from Fundación Ramón Areces, Instituto de Salud Carlos III (PI1900372) and Ministerio de Economía y Competitividad (DPI2016-77156-R). The authors are grateful to the pre-doctoral grant (IFUdG2017/62), the support of the Catalan Government (2017SGR00385) and Oncolliga Foundation and RadikalSwim (OncoSwim). The authors thank the researcher Sabina Couto-Ovejero and the Research Technical Services from the University of Girona. The authors are also grateful to Lynn Opdenaker and the flow cytometry core at the Cawley Center for Translational Research, Helen F Graham Cancer Center, which is supported by the Delaware INBRE program, with a grant from the National Institute of General Medical Sciences – NIGMS (P20 GM103446) from the National Institutes of Health and the State of Delaware.

6. References

1. J. Ferlay, *et al.*, Estimating the global cancer incidence and mortality in 2018: GLOBOCAN sources and methods. *Int. J. Cancer* **144**, 1941–1953 (2019).
2. C. M. Perou, *et al.*, Molecular portraits of human breast tumours. *Nature* **406**, 747–752 (2000).
3. C. L. Griffiths, J. L. Olin, Triple Negative Breast Cancer: A Brief Review of its Characteristics and Treatment Options. *J. Pharm. Pract.* **25**, 319–323 (2012).
4. K. R. Bauer, M. Brown, R. D. Cress, C. A. Parise, V. Caggiano, Descriptive analysis of estrogen receptor (ER)-negative, progesterone receptor (PR)-negative, and HER2-negative invasive breast cancer, the so-called triple-negative phenotype. *Cancer* **109**, 1721–1728 (2007).

5. R. Dent, *et al.*, Triple-Negative Breast Cancer: Clinical Features and Patterns of Recurrence. *Clin. Cancer Res.* **13** (2007).
6. L. A. Carey, *et al.*, The triple negative paradox: primary tumor chemosensitivity of breast cancer subtypes. *Clin. Cancer Res.* **13**, 2329–34 (2007).
7. A. Prat, *et al.*, Phenotypic and molecular characterization of the claudin-low intrinsic subtype of breast cancer. *Breast Cancer Res.* **12** (2010).
8. M. Diehn, *et al.*, Association of reactive oxygen species levels and radioresistance in cancer stem cells. *Nature* **458**, 780–3 (2009).
9. X. Zhang, K. Powell, L. Li, Breast cancer stem cells: Biomarkers, identification and isolation methods, regulating mechanisms, cellular origin, and beyond. *Cancers (Basel)*. **12**, 1–28 (2020).
10. F. L. Shaw, *et al.*, A detailed mammosphere assay protocol for the quantification of breast stem cell activity. *J. Mammary Gland Biol. Neoplasia* **17**, 111–7 (2012).
11. C. Ginestier, *et al.*, ALDH1 is a marker of normal and malignant human mammary stem cells and a predictor of poor clinical outcome. *Cell Stem Cell* **1**, 555–67 (2007).
12. M. Al-Hajj, M. S. Wicha, A. Benito-Hernandez, S. J. Morrison, M. F. Clarke, Prospective identification of tumorigenic breast cancer cells. *Proc. Natl. Acad. Sci. U. S. A.* **100**, 3983–8 (2003).
13. B. G. Hollier, K. Evans, S. A. Mani, The epithelial-to-mesenchymal transition and cancer stem cells: A coalition against cancer therapies. *J. Mammary Gland Biol. Neoplasia* **14**, 29–43 (2009).
14. S. A. Mani, *et al.*, The Epithelial-Mesenchymal Transition Generates Cells with Properties of Stem Cells. *Cell* **133**, 704–715 (2008).
15. A.-P. Morel, *et al.*, Generation of breast cancer stem cells through epithelial-mesenchymal transition. *PLoS One* **3**, e2888 (2008).
16. J. J. Christiansen, A. K. Rajasekaran, Reassessing epithelial to mesenchymal transition as a prerequisite for carcinoma invasion and metastasis. *Cancer Res.* **66**, 8319–8326 (2006).
17. C. Y. Liu, H. H. Lin, M. J. Tang, Y. K. Wang, Vimentin contributes to epithelial-mesenchymal transition cancer cell mechanics by mediating cytoskeletal organization and focal adhesion maturation. *Oncotarget* **6**, 15966–15983 (2015).
18. H. S. Sul, D. Wang, Nutritional and hormonal regulation of enzymes in fat synthesis: Studies of fatty acid synthase and mitochondrial glycerol-3-phosphate acyltransferase gene transcription. *Annu. Rev. Nutr.* **18**, 331–351 (1998).
19. S. M. Anderson, M. C. Rudolph, J. L. McManaman, M. C. Neville, Key stages in mammary gland development. Secretory activation in the mammary gland: It's not just about milk protein synthesis! *Breast Cancer Res.* **9**, 204 (2007).
20. F. P. Kuhajda, Fatty-acid synthase and human cancer: New perspectives on its role in tumor biology. *Nutrition* **16**, 202–208 (2000).
21. S. F. Jones, J. R. Infante, Molecular pathways: Fatty acid synthase. *Clin. Cancer Res.* **21**, 5434–5438 (2015).
22. S. Bandyopadhyay, *et al.*, Mechanism of apoptosis induced by the inhibition of fatty acid synthase in breast cancer cells. *Cancer Res.* **66**, 5934–5940 (2006).
23. T. Puig, *et al.*, Fatty acid metabolism in breast cancer cells: Differential inhibitory effects of epigallocatechin gallate (EGCG) and C75. *Breast Cancer Res. Treat.* **109**, 471–479 (2008).
24. A. Blancafort, *et al.*, Dual fatty acid synthase and HER2 signaling blockade shows marked antitumor activity against breast cancer models resistant to Anti-HER2 drugs. *PLoS One* **10** (2015).
25. E. Rysman, *et al.*, De novo lipogenesis protects cancer cells from free radicals and chemotherapeutics by promoting membrane lipid saturation. *Cancer Res.* **70**, 8117–26 (2010).
26. A. S. Meena, *et al.*, Inherent and Acquired Resistance to Paclitaxel in Hepatocellular Carcinoma: Molecular Events Involved. *PLoS One* **8**, e61524 (2013).
27. R. Ventura, *et al.*, Inhibition of de novo Palmitate Synthesis by Fatty Acid Synthase Induces Apoptosis in Tumor Cells by Remodeling Cell Membranes, Inhibiting Signaling Pathways, and Reprogramming Gene Expression. *EBioMedicine* **2**, 808–824 (2015).
28. X. Wang, W. Tian, Green tea epigallocatechin gallate: A natural inhibitor of fatty-acid synthase. *Biochem. Biophys. Res. Commun.* **288**, 1200–1206 (2001).
29. D. Chen, *et al.*, EGCG, green tea polyphenols and their synthetic analogs and prodrugs for human cancer prevention and treatment (Adv Clin Chem, 2011).
30. T. Puig, *et al.*, A novel inhibitor of fatty acid synthase shows activity against HER2+ breast cancer xenografts and is active in anti-HER2 drug-resistant cell lines. *Breast Cancer Res.* **13**, R131 (2011).
31. J. Crous-Masó, *et al.*, (–)Epigallocatechin 3-gallate synthetic analogues inhibit fatty acid synthase and show anticancer activity in triple negative breast cancer. *Molecules* **23** (2018).
32. A. Vazquez-Martin, *et al.*, The mitochondrial H⁺-ATP synthase and the lipogenic switch New core components of metabolic reprogramming in induced pluripotent stem (iPS) cells. *Cell Cycle* **12**, 207–218 (2013).
33. Y. Yasumoto, *et al.*, Inhibition of fatty acid synthase decreases expression of stemness markers in glioma stem cells. *PLoS One* **11**, 1–14 (2016).
34. P. R. Pandey, *et al.*, Resveratrol suppresses growth of cancer stem-like cells by inhibiting fatty acid synthase. *Breast Cancer Res Treat* **130**, 387–398 (2011).
35. A. M. Gonzalez-Guerrico, *et al.*, Suppression of endogenous lipogenesis induces reversion of the malignant phenotype and normalized differentiation in breast cancer. *Oncotarget* (2016) <https://doi.org/10.18632/oncotarget.9463>.
36. A. Giró-Perafita, *et al.*, EGCG-Derivative G28 Shows High Efficacy Inhibiting the Mammosphere-Forming Capacity of Sensitive and Resistant TNBC Models. *Molecules* **24**, 1027 (2019).
37. H. Li, Z. Feng, M. L. He, Lipid metabolism alteration contributes to and maintains the properties of cancer stem cells. *Theranostics* **10**, 7053–7069 (2020).
38. E. Charafe-Jauffret, *et al.*, Breast cancer cell lines contain functional cancer stem cells with metastatic capacity and a distinct molecular signature. *Cancer Res.* **69**, 1302–13 (2009).
39. A. Tsuyada, *et al.*, CCL2 mediates cross-talk between cancer cells and stromal fibroblasts that regulates breast cancer stem cells. *Cancer Res.* **72**, 2768–79 (2012).
40. C. H. Thomas, J. H. Collier, C. S. Sfeir, K. E. Healy, Engineering gene expression and protein synthesis by modulation of nuclear shape. *Proc. Natl. Acad. Sci. U. S. A.* **99**, 1972–7 (2002).
41. L. Vergani, M. Grattarola, C. Nicolini, Modifications of chromatin structure and gene expression following induced

- alterations of cellular shape. *Int. J. Biochem. Cell Biol.* **36**, 1447–61 (2004).
42. G. Bao, S. Suresh, Cell and molecular mechanics of biological materials. *Nat. Mater.* **2**, 715–725 (2003).
 43. C.-M. Lo, H.-B. Wang, M. Dembo, Y.-L. Wang, "Cell Movement Is Guided by the Rigidity of the Substrate" (2000).
 44. T. Yeung, *et al.*, Effects of substrate stiffness on cell morphology, cytoskeletal structure, and adhesion. *Cell Motil. Cytoskeleton* **60**, 24–34 (2005).
 45. E. Knight, S. Przyborski, Advances in 3D cell culture technologies enabling tissue-like structures to be created in vitro. *J. Anat.*, 1–11 (2014).
 46. M. Chen, P. K. Patra, S. B. Warner, S. Bhowmick, Optimization of electrospinning process parameters for tissue engineering scaffolds. *Biophys. Rev. Lett.* **01**, 153–178 (2006).
 47. L. A. Bosworth, S. Downes, Acetone, a Sustainable Solvent for Electrospinning Poly(ϵ -Caprolactone) Fibres: Effect of Varying Parameters and Solution Concentrations on Fibre Diameter. *J. Polym. Environ.* **20**, 879–886 (2012).
 48. M. A. Woodruff, D. W. Hutmacher, The return of a forgotten polymer - Polycaprolactone in the 21st century. *Prog. Polym. Sci.* **35**, 1217–1256 (2010).
 49. M. Rabionet, M. Yeste, T. Puig, J. Ciurana, Electrospinning PCL Scaffolds Manufacture for Three-Dimensional Breast Cancer Cell Culture. *Polymers (Basel)*. **9**, 328 (2017).
 50. S. Saha, *et al.*, Electrospun fibrous scaffolds promote breast cancer cell alignment and epithelial-mesenchymal transition. *Langmuir* **28**, 2028–34 (2012).
 51. S. Feng, *et al.*, Expansion of breast cancer stem cells with fibrous scaffolds. *Integr. Biol. (Camb)*. **5**, 768–77 (2013).
 52. J. Sims-Mourtada, R. a. Niamat, S. Samuel, C. Eskridge, E. B. Kmiec, Enrichment of breast cancer stem-like cells by growth on electrospun polycaprolactone-chitosan nanofiber scaffolds. *Int. J. Nanomedicine* **9**, 995–1003 (2014).
 53. P. Russo, D. Acierno, A. Corradi, C. Leonelli, Dynamic-mechanical behavior and morphology of polystyrene/ferroelectric composites: Effects of filler size in *Procedia Engineering*, (Elsevier Ltd, 2011), pp. 1017–1022.
 54. M. Worzakowska, Thermal and mechanical properties of polystyrene modified with esters derivatives of 3-phenylprop-2-en-1-ol. *J. Therm. Anal. Calorim.* **121**, 235–243 (2015).
 55. A. Samani, J. Zubovits, D. Plewes, Elastic moduli of normal and pathological human breast tissues: An inversion-technique-based investigation of 169 samples. *Phys. Med. Biol.* **52**, 1565–1576 (2007).
 56. M. Rabionet, T. Puig, J. Ciurana, Manufacture of PCL scaffolds through electrospinning technology to accommodate triple negative breast cancer cells culture. *Procedia CIRP* **89**, 98–103 (2020).
 57. R. A. L. Jones, *Soft Condensed Matter*, Oxford University Press, Ed. (2002) (January 11, 2021).
 58. L. McKeen, "Renewable Resource and Biodegradable Polymers" in *The Effect of Sterilization on Plastics and Elastomers*, (Elsevier, 2012), pp. 305–317.
 59. S. Tiptakorn, N. Keungputpong, S. Phothiphiphit, S. Rimdusit, Effects of polycaprolactone molecular weights on thermal and mechanical properties of polybenzoxazine. *J. Appl. Polym. Sci.* **132**, n/a-n/a (2015).
 60. D. Priselac, T. Tomašegović, THERMAL, SURFACE AND MECHANICAL PROPERTIES OF PCL/PLA COMPOSITES WITH COCONUT FIBRES AS AN ALTERNATIVE MATERIAL TO PHOTOPOLYMER PRINTING PLATES. *Teh. Glas.* **11**, 111–116 (2017).
 61. J. Rieger, The glass transition temperature of polystyrene. Results of a round robin test. *J. Therm. Anal.* **46**, 965–972 (1996).
 62. S. Schindelmann, *et al.*, Expression profiling of mammary carcinoma cell lines: Correlation of in vitro invasiveness with expression of CD24. *Tumor Biol.* **23**, 139–145 (2002).
 63. S. Okumura-Nakanishi, M. Saito, H. Niwa, F. Ishikawa, Oct-3/4 and Sox2 Regulate Oct-3/4 Gene in Embryonic Stem Cells. *J. Biol. Chem.* **280**, 5307–5317 (2005).
 64. N. Yang, Y. Wang, L. Hui, X. Li, X. Jiang, Silencing SOX2 Expression by RNA Interference Inhibits Proliferation, Invasion and Metastasis, and Induces Apoptosis through MAP4K4/JNK Signaling Pathway in Human Laryngeal Cancer TU212 Cells. *J. Histochem. Cytochem.* **63**, 721–733 (2015).
 65. A. I. Penzo-Méndez, Critical roles for SoxC transcription factors in development and cancer. *Int J Biochem Cell Biol* **42**, 425–428 (2010).
 66. K. R. Yu, *et al.*, CD49f enhances multipotency and maintains stemness through the direct regulation of OCT4 and SOX2. *Stem Cells* **30**, 876–887 (2012).
 67. O. Leis, *et al.*, Sox2 expression in breast tumours and activation in breast cancer stem cells. *Oncogene* **31**, 1354–1365 (2012).
 68. J. Zhang, *et al.*, SOX4 Induces Epithelial-Mesenchymal Transition and Contributes to Breast Cancer Progression. *Cancer Res.* **72**, 4597–4608 (2012).
 69. X. Li, *et al.*, Intrinsic Resistance of Tumorigenic Breast Cancer Cells to Chemotherapy. *JNCI J. Natl. Cancer Inst.* **100**, 672–679 (2008).
 70. M. D. Kars, G. Yıldırım, Determination of the target proteins in chemotherapy resistant breast cancer stem cell-like cells by protein array. *Eur. J. Pharmacol.* **848**, 23–29 (2019).
 71. L. A. Quayle, P. D. Ottewill, I. Holen, Chemotherapy resistance and stemness in mitotically quiescent human breast cancer cells identified by fluorescent dye retention. *Clin. Exp. Metastasis* **35**, 831–846 (2018).
 72. J. Mehanna, F. G. H. Haddad, R. Eid, M. Lambertini, H. R. Kourie, Triple-negative breast cancer: Current perspective on the evolving therapeutic landscape. *Int. J. Womens. Health* **11**, 431–437 (2019).
 73. P. Mukherjee, A. Gupta, D. Chattopadhyay, U. Chatterji, Modulation of SOX2 expression delineates an end-point for paclitaxel-effectiveness in breast cancer stem cells. *Sci. Rep.* **7**, 1–16 (2017).
 74. S. E. Moody, *et al.*, The transcriptional repressor Snail promotes mammary tumor recurrence. *Cancer Cell* **8**, 197–209 (2005).
 75. W. Li, *et al.*, Overexpression of snail accelerates adriamycin induction of multidrug resistance in breast cancer cells. *Asian Pacific J. Cancer Prev.* **12**, 2575–2580 (2011).
 76. C. W. Liu, *et al.*, Snail regulates Nanog status during the epithelial-mesenchymal transition via the Smad1/Akt/GSK3 β signaling pathway in non-small-cell lung cancer. *Oncotarget* **5**, 3880–3894 (2014).
 77. S. Peiró, *et al.*, Snail1 transcriptional repressor binds to its own promoter and controls its expression. *Nucleic Acids Res.* **34**, 2077–2084 (2006).
 78. Y. Wang, J. Shi, K. Chai, X. Ying, B. Zhou, The Role of Snail in EMT and Tumorigenesis. *Curr. Cancer Drug Targets* **13**, 963–972 (2014).
 79. H. Peinado, E. Ballestar, M. Esteller, A. Cano, Snail Mediates E-Cadherin Repression by the Recruitment of the Sin3A/Histone Deacetylase 1 (HDAC1)/HDAC2 Complex. *Mol. Cell. Biol.* **24**, 306–319 (2004).

80. R. G. Wells, D. E. Discher, Matrix elasticity, cytoskeletal tension, and TGF- β : The insoluble and soluble meet. *Sci. Signal.* **1**, pe13 (2008).
81. G. Pearson, *et al.*, Mitogen-activated protein (MAPK) kinase pathways: Regulation and physiological functions. *Endocr. Rev.* **22**, 153–183 (2001).
82. D. A. Rudzka, *et al.*, Migration through physical constraints is enabled by MAPK-induced cell softening via actin cytoskeleton re-organization. *J. Cell Sci.* **132** (2019).
83. P. P. Provenzano, D. R. Inman, K. W. Eliceiri, P. J. Keely, Matrix density-induced mechanoregulation of breast cell phenotype, signaling and gene expression through a FAK-ERK linkage. *Oncogene* **28**, 4326–4343 (2009).
84. C. Porta, C. Paglino, A. Mosca, Targeting PI3K/Akt/mTOR signaling in cancer. *Front. Oncol.* **4** APR (2014).
85. J. Sunayama, *et al.*, Crosstalk between the PI3K/mTOR and MEK/ERK pathways involved in the maintenance of self-renewal and tumorigenicity of glioblastoma stem-like cells. *Stem Cells* **28**, 1930–1939 (2010).
86. L. Chang, *et al.*, Acquisition of epithelial-mesenchymal transition and cancer stem cell phenotypes is associated with activation of the PI3K/Akt/mTOR pathway in prostate cancer radioresistance. *Cell Death Dis.* **4** (2013).
87. J. Zhou, *et al.*, Activation of the PTEN/mTOR/STAT3 pathway in breast cancer stem-like cells is required for viability and maintenance. *Proc. Natl. Acad. Sci. U. S. A.* **104**, 16158–16163 (2007).
88. W. W. Chang, *et al.*, The expression and significance of insulin-like growth factor-1 receptor and its pathway on breast cancer stem/progenitors. *Breast Cancer Res.* **15** (2013).
89. J. Sunayama, *et al.*, Crosstalk Between the PI3K/mTOR and MEK/ERK Pathways Involved in the Maintenance of Self-Renewal and Tumorigenicity of Glioblastoma Stem-Like Cells. *Stem Cells* **28**, 1930–1939 (2010).
90. M. C. Mendoza, E. Emrah Er, J. Blenis, The Ras-ERK and PI3K-mTOR Pathways: Cross-talk and Compensation (2011) <https://doi.org/10.1016/j.tibs.2011.03.006>.
91. M. Pickl, C. H. Ries, Comparison of 3D and 2D tumor models reveals enhanced HER2 activation in 3D associated with an increased response to trastuzumab. *Oncogene* **28**, 461–468 (2009).
92. S. Gangadhara, C. Smith, P. Barrett-Lee, S. Hiscox, 3D culture of Her2+ breast cancer cells promotes AKT to MAPK switching and a loss of therapeutic response. *BMC Cancer* **16** (2016).
93. B. Weigelt, A. T. Lo, C. C. Park, J. W. Gray, M. J. Bissell, HER2 signaling pathway activation and response of breast cancer cells to HER2-targeting agents is dependent strongly on the 3D microenvironment. *Breast Cancer Res Treat* **122**, 35–43 (2010).
94. P. Van Der Geer, T. Hunter, R. A. Lindberg, Receptor protein-tyrosine kinases and their signal transduction pathways. *Annu. Rev. Cell Biol.* **10**, 251–337 (1994).
95. A. C. Porter, R. R. Vaillancourt, Tyrosine kinase receptor-activated signal transduction pathways which lead to oncogenesis. *Oncogene* **17**, 1343–1352 (1998).
96. N. Prenzel, O. M. Fischer, S. Streit, S. Hart, A. Ullrich, The epidermal growth factor receptor family as a central element for cellular signal transduction and diversification in *Endocrine-Related Cancer*, (*Endocr Relat Cancer*, 2001), pp. 11–31.
97. Y. Yarden, G. Pines, The ERBB network: At last, cancer therapy meets systems biology. *Nat. Rev. Cancer* **12**, 553–563 (2012).
98. N. Duru, *et al.*, HER2-associated radioresistance of breast cancer stem cells isolated from HER2-negative breast cancer cells. *Clin. Cancer Res.* **18**, 6634–6647 (2012).
99. S. K. Muthuswamy, D. Li, S. Lelievre, M. J. Bissell, J. S. Brugge, ErbB2, but not ErbB1, reinitiates proliferation and induces luminal repopulation in epithelial acini. *Nat. Cell Biol.* **3**, 785–792 (2001).
100. M. Majumder, *et al.*, COX-2 Induces Breast Cancer Stem Cells via EP4/PI3K/AKT/NOTCH/WNT Axis. *Stem Cells* **34**, 2290–2305 (2016).
101. R. Roskoski, The ErbB/HER family of protein-tyrosine kinases and cancer. *Pharmacol. Res.* **79**, 34–74 (2014).
102. P. J. Brennan, T. Kumogai, A. Berezov, R. Murali, M. I. Greene, HER2/neu: Mechanisms of dimerization/oligomerization. *Oncogene* **19**, 6093–6101 (2000).
103. T. Holbro, G. Civenni, N. E. Hynes, The ErbB receptors and their role in cancer progression. *Exp. Cell Res.* **284**, 99–110 (2003).
104. J. A. Menendez, R. Lupu, Fatty acid synthase and the lipogenic phenotype in cancer pathogenesis. *Nat. Rev. Cancer* **7**, 763–777 (2007).
105. P. R. Pandey, *et al.*, Resveratrol suppresses growth of cancer stem-like cells by inhibiting fatty acid synthase. *Breast Cancer Res. Treat.* **130**, 387–398 (2011).
106. S. Xu, *et al.*, Fatty acid synthase promotes breast cancer metastasis by mediating changes in fatty acid metabolism. *Oncol. Lett.* **21** (2021).
107. M. Rabionet, T. Puig, J. Ciurana, Electrospinning Parameters Selection to Manufacture Polycaprolactone Scaffolds for Three-dimensional Breast Cancer Cell Culture and Enrichment. *Procedia CIRP* **65**, 267–272 (2017).

Supplementary Information for

FATTY ACID SYNTHASE AS A NOVEL BIOMARKER FOR TRIPLE NEGATIVE BREAST CANCER STEM CELL SUBPOPULATION CULTURED ON ELECTROSPUN SCAFFOLDS

Materials and Methods

Three-dimensional cell culture. MDA-MB-231 and MDA-MB-468 TNBC cells were obtained from the American Type Culture Collection (ATCC; Rockville, MD, USA). Both cell lines were routinely grown in Dulbecco's Modified Eagle's Medium (DMEM; Gibco, Waltham, MA, USA) supplemented with 10% fetal bovine serum (FBS; HyClone Laboratories, GE Healthcare, Chicago, IL, USA), 1% L-glutamine, 1% sodium pyruvate (Gibco), and 50 U/ml Pen/Strep (Linus, Cultek, Madrid, Spain). Cells were maintained under sterile conditions at 37 °C and 5% CO₂ atmosphere.

ALDEFLUOR™ assay. Information of a minimum of 10,000 events was recorded and analyzed using FlowJo 10.7 software (FlowJo LLC, Ashland, OR, USA). SS and FL1 dot plots from DEAB samples were created to establish background fluorescence. The ALDH-positive cells' gate was traced, delimiting the rightmost area and including only the 0.5% of total cell population. BAAA samples were equally processed and ALDH-positive cells gates of respective DEAB controls were used to discriminate the percentage of ALDH-positive cells in each sample.

Quantitative real-time PCR analysis. To reverse-transcribe the RNA into complementary DNA, each sample was composed by 1 µg RNA, 2 µL RT Buffer (10X), 0.8 µL dNTP Mix (100 mM), 2 µL RT Random Primers (10X) and 1 µL reverse-transcriptase enzyme (50 U/µL) with a balance of nuclease-free water from the kit. Reverse-transcription was performed at a specific program (25 °C 10 min, 37 °C 120 min, 85 °C for 5 min and 4 °C until finish) with a Veriti 96 Well Thermal Cycler (Applied Biosystems). Resulting cDNA was diluted at 4 ng/µL with nuclease-free water. To assess gene expression levels, 20 ng cDNA were mixed with 5 µL ready-to-use SYBR Green and 0.4 µL of each forward and reverse primer (see **Table S2**).

Cell viability assay. An MTT assay was performed after a 48-h treatment with doxorubicin, paclitaxel, EGCG, or G28. Scaffolds were transferred onto a new microplate to avoid including cells adhered at the bottom of the well. Medium was replaced in 2D and 3D samples by drug-free medium containing 10% MTT solution, and incubation was prolonged for 2 h 30 min at 37 °C. Only metabolically viable cells formed formazan crystals which were dissolved in DMSO (Sigma-Aldrich) under shaking. Four 100 µL aliquots for each well were transferred to a 96 well microplate and absorbance was determined at 570 nm using a Benchmark Plus Microplate Spectrophotometer System (Bio-Rad Laboratories, Inc.). Using treated (T) and control (C) average absorbance values, the percentage of cell survival (CS) at each concentration was calculated from the formula $CS = 100(T/C)$.

Supplementary Tables and Figures

Table S1. Cell densities used for cell seeding experiments. Different cell densities were used in order to achieve a similar confluence after the culture. Since cell adopted a lower cell growth rate within 3D surroundings, higher cell densities were generally used for scaffolds culture.

N° CELLS / CM ²	MDA-MB-231		MDA-MB-468	
	2D	3D	2D	3D
3 days	16,000	16,000	24,000	24,000
6 days	2,400	4,800	8,000	12,000
12 days	120	320	1,600	3,200
8 days (6 culture days + 48h treatment)	1,200	3,000	5,000	8,000

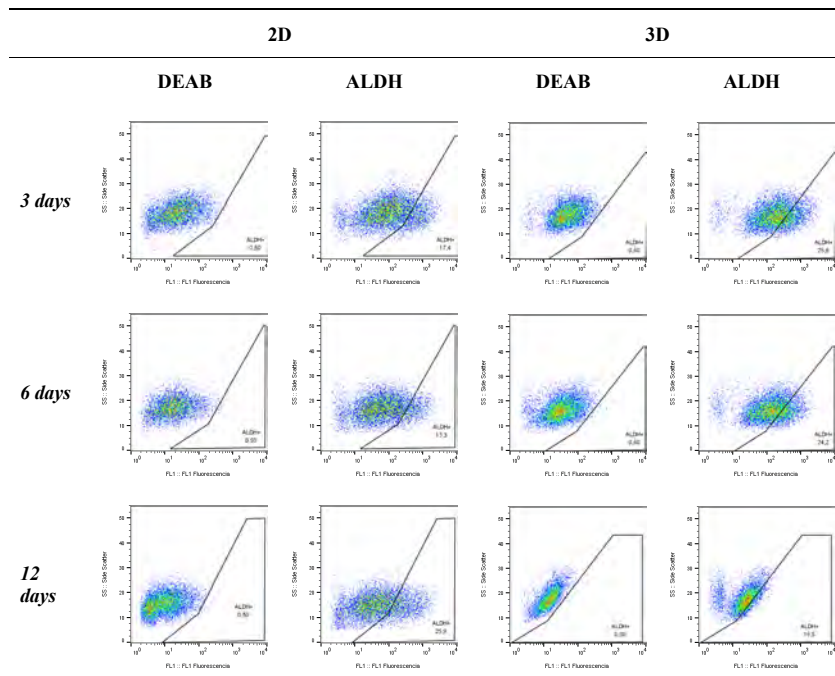
Table S2. List of primers.

Gene	Forward sequence (5'-3')	Reverse sequence (5'-3')
<i>CD24</i>	CCTCCCAGAGTACTTCCAAC	AGTGAGACCACGAAGAGACT
<i>CD44</i>	TGTGGAGGACAGAAAGCCAAG	TCCCAGCTCCCTGTAATGGTT
<i>SOX2</i>	AACCCCAAGATGCACAAC	GCTTAGCCTCGTCGATGAAC
<i>SOX4</i>	CCGGAATTCATGGTGCAGCAAACCAAC	CCGGAATTCAGTAGGTGAAAACCAG
<i>NANOG</i>	AATACCTCAGCCTCCAGCAGATG	TGCGTCACACCATTGCTATTCTTC
<i>CD49f</i>	ATG GAG GAA ACC CTG TGG CT	ACG AGA GCT TGG CTC TTG GA
<i>SNAIL</i>	GCTGCAGGACTCTAATCCAGA	ATCTCCGGAGGTGGGATG
<i>SLUG</i>	GCGATGCCAGTCTAGAAAA	GCAGTGAGGGCAAGAAAAAG
<i>ZEB1</i>	GCCAATAAGCAAACGATTCTG	TTTGCTGGATCACTTCAAG
<i>ZEB2</i>	CCCTTCTGCGACATAAATACG	TGTGATTCATGTGCTGCGAGT
<i>TWIST</i>	AGTACGCCTTCTCGGTCT	CCTTCTCTGGAAACAATGACATC
<i>CDH1</i>	TGGAGGAATTCTTGCTTTGC	CGCTCTCCTCCGAAGAAAC
<i>VIM</i>	AGTCCACTGAGTACCGGAGAC	CATTCACGCATCTGGCGTTC
<i>ACTB</i>	ATTGGCAATGAGCGGTTT	CGTGGATGCCACAGGACT
<i>TUBB</i>	AGGCTACGTGGGAGACTCG	GCCCTGGGCACATATTCT
<i>FASN</i>	CAGGCACACAGATGGAC	CGGAGTGAATCTGGGTTGAT
<i>GAPDH</i>	TCTTCCAGGAGCGAGATC	CAGAGATGATGACCCTTTTG

Table S3. List of antibodies.

Protein	Molecular Weight (kDa)	Reference	Supplier	Dilution	Source			
E-Cadherin	135	3195	Cell Signaling Technology	1:1,000	Rabbit			
Vimentin	57	5741						
Phospho-p44/42 MAPK (Thr202/Tyr204)	42, 44	9101						
p44/42 MAPK	42, 44	9102						
Phospho-S6 ribosomal protein (Ser235/236)	32	2211						
Phospho-PI3 Kinase p85(Tyr458)/p55(Tyr199)	60, 85	4228						
PI3 Kinase p100 α	110	4249						
Phospho-Akt (Ser473)	60	4058						
Akt	60	9272						
PTEN	54	5384						
Phospho-mTOR (Ser2448)	289	2971						
mTOR	289	2983						
Phospho-EGFR (Tyr1068)	175	2234						
EGFR	175	4267						
Phospho-HER2 (Tyr1196)	185	6942						
HER2	185	2165						
FASN	273	3180						
beta-Actin	45	3700				Proteintech	1:50,000	Mouse
alpha-Tubulin	55	3873						
GAPDH	36	60004-1-Ig						
Anti-rabbit IgG, HRP-linked	-	7074	Cell Signaling Technology	1:4,000	Goat			
Anti-mouse IgG, H&L Chain Specific Peroxidase Conjugate	-	401215	Calbiochem	1:5,000				

Table S4. ALDEFLUOR assay plots of MDA-MB-468 cells cultured on tissue microplates (2D) and on 15% PCL ES scaffolds (3D). Aldehyde dehydrogenase (ALDH) inhibitor (diethylaminobenzaldehyde; DEAB) was processed to determine background fluorescence.



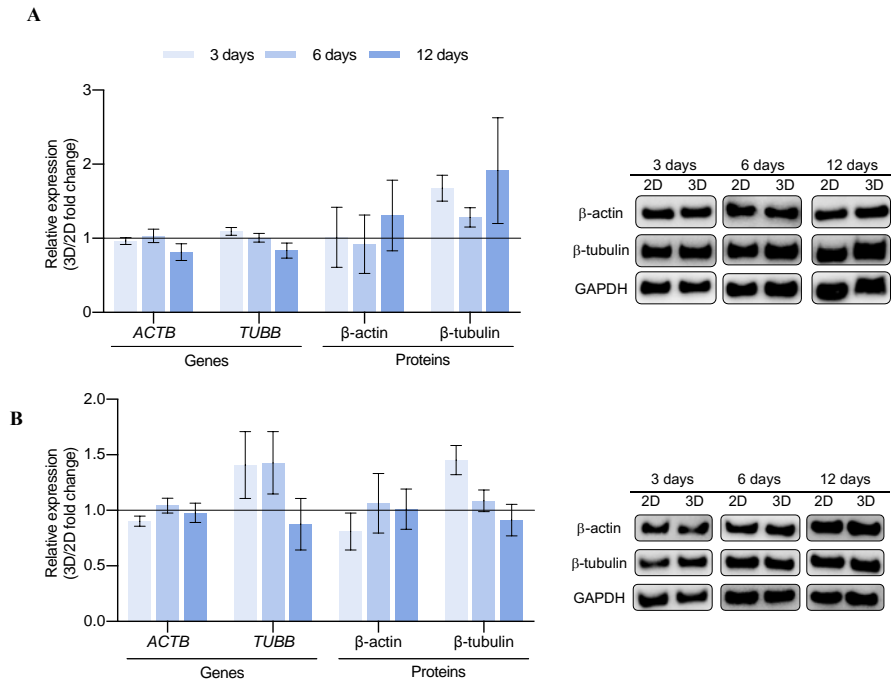


Fig. S1. Fold changes in gene and protein expression of β -actin and β -tubulin for MDA-MB-231 (A) and MDA-MB-468 (B) cells cultured on ES PCL scaffolds (3D) compared to corresponding 2D control. Gene expression levels were quantified by double delta Ct analysis method. Both gene and protein expression levels were normalized against GAPDH values. A representative Western Blot image for each cell culture condition is shown. A slight increase of tubulin expression was found after 3 scaffolds culture days, which may respond to a higher demand of microtubules in scaffolds culture. The polymerization of tubulin results in the formation of microtubules, that form part of the eukaryotic cytoskeleton. This fact might be related to the cytoskeleton remodeling that cells undergo in 3D culture, adopting a more elongated morphology.

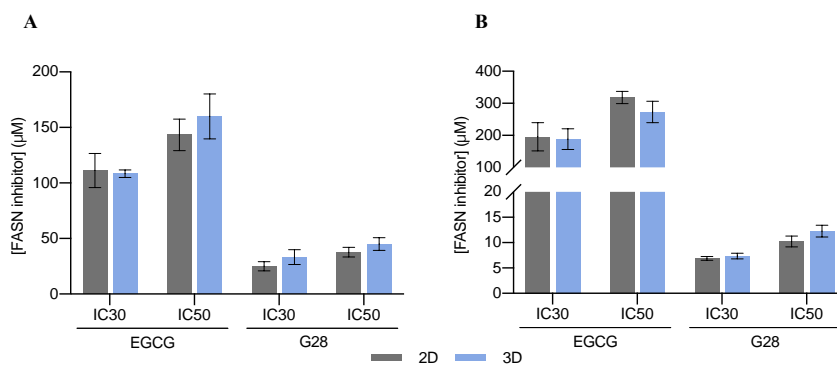


Fig. S2. Average of IC₃₀ and IC₅₀ values (drug concentration that inhibited 30 or 50% of cell viability, respectively) for MDA-MB-231 (**A**) and MDA-MB-468 (**B**). Cells were cultured on monolayer (2D) or in PCL scaffolds (3D) for 6 days and then exposed to the FASN inhibitors EGCG and G28 for 48 h.

CHAPTER 7 Discussion

Discussion

There is no targeted therapy for triple negative breast cancer (TNBC) (19), which presents an aggressive profile and a high recurrence rate (110). These facts highlight the feasibility of breast cancer stem cells (BCSCs), a small subpopulation responsible for tumor initiation and relapse (151), to become a novel target for TNBC. However, BCSC experimentation is hindered by traditional *in vitro* monolayer culture (372). Plastic three-dimensional (3D) supports such as scaffolds have emerged as novel tools for *in vitro* cell culture since they are proven to maintain the stemness features of the sample (330). Therefore, current efforts in the field are focused on the use of biocompatible scaffolds to study the BCSC niche. Present work aims to explore the feasibility of poly(ϵ -caprolactone) (PCL) scaffolds to culture breast cancer cell lines, with particular interest in TNBC models. Hence, the final purpose is to enrich the BCSC subpopulation and properly study its behavior and identify possible targets.

CHAPTER 3 Use and optimization of the fused filament fabrication technology to manufacture PCL scaffolds for 3D cell culture and stemness expansion

Different technologies are available for the manufacture of plastic biocompatible scaffolds. Fused filament fabrication (FFF) technique, which is an additive manufacturing (AM) process, stands for one of the most accessible and simplest options (332). Briefly, the thermoplastic material is melted and deposited in successive layers through a moving, heated printer extruder head, which is moved under computer control to define the printed shape. Final product is usually composed by micrometric fibers. This technology is used by the vast majority of 3D printers (331, 332), representing an open-source and low-cost option that can be easily modified to optimize the quality of the printing (339). Among all the available

polymers, PCL excels due to its biocompatible features, a relatively long-term biodegradability, a lower melting point of 60°C, and the absence of isomers (374). It is therefore not surprising that its use is increasing in tissue engineering (TE), drug delivery, and cell culture (176, 364, 366, 375).

Considering the previous information, RepRap BCN3D+ 3D printer and PCL were chosen to perform the first attempts to manufacture scaffolds for 3D cell culture. Fabrication process usually needs to be optimized depending on the chosen apparatus and polymer, as well as the scaffold design since each cell type requires different scaffold features. Therefore, a novel scaffold parameter selection system was first developed in the form of a sequential flowchart. Several fabrication parameters were gradually optimized step by step: extruder temperature of 85°C, bed temperature of 35°C, deposition velocity of 10 mm/s, and 0.3 mm of layer height. In the case of the design parameters, the following optimal values were determined: filament diameter of 0.3 mm, distance between filaments of 0.7 mm, and three scaffold designs were produced varying the deposition angle between layers (45°, 60°, and 90°). Among the distinct versions, 60° scaffolds accommodated the highest cell growth for breast cancer MCF-7 cells, and 90° version was the optimal for the murine fibroblasts NIH/3T3. The found optimal values are closely related to those defined in other studies that use similar technologies and materials (331, 340). This fact supports the idea of using a single, common methodology to optimize the processing parameters, such as the developed flowchart. Besides, this system makes it easier to adjust scaffold design features according to cell line characteristics. For instance, a tumor and a non-tumor cell line were tested, which resulted in different optimal scaffold design, showing the flexibility of the flowchart described in the present work.

FFF PCL scaffolds adequacy for breast cancer MCF-7 cells was further analyzed. As previously seen, deposition angle design parameter showed a strong influence on cell adhesion and proliferation. Our data pointed out that 60° scaffold exhibited the greatest cell proliferation rate, followed by 45° and 90° model, this last one

showing almost no cell attachment at all probably due to their big pores. In contrast, a previous work using human mesenchymal stem cells (HMSCs) demonstrated that a higher deposition angle provides more space for cells to attach and proliferate (340). This apparent contradiction underlines the fact that specific cells require a different pore size and architecture for optimal attachment, growth, and motility (376). In addition, higher cell proliferation was observed on the scaffolds placed on non-adherent surfaces compared to the ones accommodated in adherent wells. In a non-adherent well, cells only have the possibility of attaching to the PCL filaments of the scaffolds and they are not attracted to the bottom. Besides, MCF-7 cultured in FFF PCL scaffolds displayed a significantly higher capacity to form mammospheres compared to 2D control, revealing a BCSC enrichment. The use of adherent and non-adherent wells did not affect the mammosphere forming index (MFI). Our data agree with prior investigations in which 3D-cultured breast cancer cells exhibited an increased MFI (176, 364), although they used electrospinning scaffolds with thinner filaments.

Taken together, a conventional RepRap 3D printer using FFF has been proved to be suitable to manufacture PCL scaffolds for biomedical applications. A flowchart to optimize the parameters of the whole process has been proposed. This methodology may be further used to set up scaffold manufacturing (both design features and fabrication parameters) when using a 3D printer or any other AM technology and/or materials. Moreover, our results suggest that FFF PCL scaffolds, although they are mostly used for TE applications due to their micrometric fibers and mechanical features (331, 333–335), are also feasible for *in vitro* cell culture and stemness maintenance when using the breast cancer reference model MCF-7.

CHAPTER 4 Use and optimization of electrospinning technology to manufacture PCL scaffolds for 3D cell culture and stemness expansion

Despite the good response of FFF PCL scaffolds in terms of breast cancer cell culture, the use of a new technology to fabricate PLC scaffolds was explored. The goal was to fabricate meshes with smaller porosity and thinner diameters, similar to the native fibrous proteins contained in the physiological extracellular matrix (ECM) (341). The use of a physiological-like scaffold may enhance cell proliferation, maintaining or empowering the stemness-enriching potential previously seen. For this reason, electrospinning (ES) technology was used to manufacture PCL scaffolds due to its capacity of producing nanofibers and its use in the cancer stem cell culture field (176, 364, 373). In fact, there are approximately twice as many publications using ES than FFF for scaffold fabrication (source Pubmed), probably due to the aforementioned differences. In ES, polymer is dissolved and placed in a syringe connected to a metallic needle. A high voltage is applied so the solution becomes charged. When the electric force overcomes the fluid surface tension, a stream of liquid is ejected, which results in the formation of a charged structure called Taylor cone. This formation enables the continuous production of polymer fibers from the needle to the ground collector. When the process is done, the solvent evaporates and nanofibers are randomly formed in the collector. Therefore, the use of voltage in this technique allows the formation of thinner filaments compared with FFF scaffolds. Although a design scaffold step is not possible here, different fabrication parameters lead to distinct scaffolds microarchitectures.

In Chapter 4, a solution of PCL and acetone was electrospun to produce scaffolds that were cut to allow their use in regular 12-well cell culture microplates. ES is a technology highly influenced by fabrication parameters including polymer concentration, applied voltage, and polymer solution flow rate (377–379).

Therefore, different parameters values were tested to reach a stable Taylor cone and a steady stream. In all screening tests, PCL-acetone solution partially solidified in the emitter tip, producing a stalactite-like form, regardless of the different tested room humidity (50-60%) and temperature (19-25°C) values. Acetone was presumably evaporated due to its high volatility producing this lengthened formation at the needle tip. Some authors have electrospun PCL-acetone solutions, but solvent evaporation in the emitter tip was not mentioned since Taylor cone structure was not examined (377–380). A voltage of 7 kV and flow rate of 6 mL/h were found to produce the most stable Taylor cone and manufacturing process. Relation between applied electric field and droplet morphology was superficially studied by Zong *et al.* using polylactic acid (PLA) dissolved in dimethyl formamide (DMF). They pointed out that a too high voltage quickly removes the solution droplet from the tip. Hence, droplet becomes smaller and Taylor cone oscillated due to high voltage and remains unstable (381), a phenomenon observed in our work when using higher voltages. However, fewer differences were observed in droplet morphology varying flow rate parameter compared with voltage.

Regarding the polymer solution, two different concentrations of 7.5 and 15% PCL were processed, producing two distinct scaffold models whose weight and thickness were analyzed. Interestingly, values of scaffolds from different ES process batches did not present significant differences, demonstrating reproducibility among distinct processes in regard to macroscopic characterization. The physical analysis results agreed with the PCL amount in each solution, being the 7.5% scaffold weight the half than 15% model. Both scaffold exemplars were tested with the reference breast cancer model MCF-7 cells. Meshes from 15% PCL solution exhibited a significant cell proliferation increase compared with 7.5% scaffolds. Opposed to these data, a human cancer cell study asserted that higher cell proliferation values can be obtained with small fibers diameters from low biopolymer concentration scaffolds (367). Cell growth differences may be attributed to the mesh microarchitecture. It has been demonstrated that low PCL concentration resulted in scaffolds with spherical structures made by non-

filamented polymer, called beads, which were proven to hinder fibroblast proliferation (377, 380). Cells cultured in both scaffold designs displayed a 3-fold increased MFI compared with monolayer control. These similar values between scaffolds may seem conflicting with the differences previously seen in terms of cell proliferation. It is worth mentioning that, despite their differences on their cell proliferation and structure, both scaffolds provide a 3D environment. This fact allows cells to establish interactions with filaments in different plans of the space, enabling the cytoskeleton reorganization and gene expression regulation.

Compared with the data obtained in the previous chapter, electrospun PCL meshes showed a higher cell proliferation rate than FFF PCL scaffolds using the same cell model. Besides, ES PCL scaffolds led to a 3-fold increased MFI, whereas MCF-7 cells cultured in FFF meshes showed a double MFI increase. In context with literature, Feng *et al.* published a 2-fold MFI increment with MCF-7 cells cultured in electrospun PCL scaffolds (176), the same trend observed by Sims-Mourtada group (364). Therefore, ES PCL scaffolds manufactured in this thesis represent a suitable tool to accommodate breast cancer MCF-7 cells and expand BCSC niche, greater than their FFF counterparts or even ES scaffolds from other literature works.

Some previous works explored the impact of random and aligned ES PCL fibers on cell-substrate response. In fact, ES is a versatile technique with which, with the installation of a special rotating mandrel as a ground collector, aligned fibers can be collected. When using breast cancer cells, a study claimed that cells adopted more elongated morphology in aligned cells compared with random counterparts, as well as a more EMT-like phenotype. Therefore, these data are in agreement with a previous investigation that observed a parallel fiber alignment as a characteristic of ECM produced by primary carcinoma associated fibroblasts of the skin (382). In a similar fashion, Provenzano and colleagues identified parallel collagen fibers perpendicular to the advancing edge of the tumors in a mouse mammary tumor model (383). However, results provided in this work clearly emphasize the use of

random ES PCL fibers in terms of sustaining both breast cancer cell proliferation and BCSC expansion.

Taking into account all data, ES has been proved to be a potent technology useful in diverse fields. Controlling process parameters allows the production of different meshes, demonstrating its potential for nanotechnology research. Moreover, the BCSC-enriching capacity of ES scaffolds may facilitate the development of new therapeutic strategies against this malignant subpopulation.

CHAPTER 5 Evaluation of BCSC and fatty acid synthase (FASN) role in chemosensitive and chemoresistant MDA-MB-231 TNBC cells

Distinct approaches can be done to properly study the BCSC subpopulation in TNBC samples. In previous chapters, the impact of microenvironment on stemness preservation has been described, concluding that ES PCL scaffolds can be used to expand and characterize this malignant subpopulation in breast cancer cells. In other settings, tumors that progress after chemotherapy usually display an enrichment of BCSC features (384, 385). Besides, fatty acid synthase (FASN), the key enzyme for *de novo* lipogenesis, also plays an important role in drug resistance (282, 386, 387) and stemness regulation. Hence, chapter 5 has been focused on the use of the TNBC MDA-MB-231 cells and its resistant derivatives 231DXR (resistant to doxorubicin) and 231PTR (resistant to paclitaxel) to evaluate BCSC population and FASN role in resistance to chemotherapy acquisition. This cell line was chosen since it belongs to the mesenchymal-like (ML) molecular subtype, which represents the 30% of TNBC cases and shows BCSC and epithelial-to-mesenchymal transition (EMT) properties, as well as a poor prognosis (23, 29). Present investigation may elucidate the relationship behind all these elements and describe the potential of FASN and its pharmacological blocking as a novel approach for BCSC niche in TNBC samples.

Results obtained indicated that both 231DXR and 231PTR showed increased ability to form mammospheres under drug treatment compared to chemosensitive cells. ALDH1 activity, a BCSC feature related with chemoresistance in patients (388), was significantly increased in 231DXR cells but the percentage of ALDH-positive cells in 231PTR model remained similar to that in the parental. Overall, 231DXR showed an enlargement of the BCSC niche while intrinsic stemness features of the 231PTR cells were, at least, maintained.

It has been described that induction of EMT can lead to cell dedifferentiation, so cells can acquire BCSC characteristics including chemoresistance (389, 390). Therefore, the expression of some EMT markers was analyzed to know whether the development of this phenotype was due to an EMT process triggered by the addition of chemotherapy drugs. *SNAIL*, an EMT inducer associated with tumor development and relapse (391–393), was found upregulated in 231DXR derivative compared to sensitive cells. In the case of 231PTR model, the expression of *SLUG* was increased, an EMT transcription factor linked to cancer progression and BCSC activity (394). Therefore, resistant cells may have acquired stemness features through an EMT process.

The use of chemotherapeutic drugs counts with undeniable advantages as an antitumor medicine. However, doxorubicin has been showed to promote stemness in murine cell lines (395–397) and increase stemness-related signaling pathways (398), in agreement with our results. Concerning paclitaxel, it has been proved to increase the BCSC population in head and neck cancer cell lines (399); however, non-obvious enrichment was observed after paclitaxel addition in our hands, but a maintenance of the intrinsic stem features of this ML subtype.

FASN overexpression confers many advantages to tumor cells such as the ability to preserve a high proliferation rate and partially regulate drug resistance acquisition (282, 386, 387). In this work, the addition of doxorubicin led to a significantly increase of FASN protein levels in the 231DXR model, which was described to be a

resistance mechanism in breast cancer (400). Gonzalez-Guerrico *et al.* showed that FASN inhibition resulted in the conversion of ML phenotype to a non-malignant one by downregulating EMT markers in a breast cancer model (401). Besides, the FASN inhibitor resveratrol precluded the growth of the CSC population both *in vitro* and *in vivo* using a breast cancer xenograft model (402). FASN expression has also been determined to be crucial in stemness maintenance in glioma (403). In this chapter, the effect of FASN inhibition in a BCSC population was evaluated through the ability to hinder the mammosphere-forming capacity compared to the cytotoxic effect in the non-enriched adherent culture. Among the tested FASN inhibitors, G28 displayed a greater inhibitory effect in the BCSC-enriched spheres culture in both sensitive and resistant cell lines, which was not found when using the chemotherapeutical agents. Interestingly, this proliferation inhibition was equally found in the adherent monolayer culture, which can be considered homologous of the bulk tumor. These results set up the basis for further investigation using FASN inhibitors in combination with chemotherapy to target BCSCs as well as the bulk of the tumor to improve the prognosis of the TNBC patients.

CHAPTER 6 Enrichment of BCSCs in the TNBC cell models MDA-MB-231 (mesenchymal-like) and MDA-MB-468 (basal-like) within 3D ES PCL scaffold culture

The first chapters have been focused on the use and optimization of biocompatible meshes, concluding that PCL scaffolds made by ES technology may serve as an *in vitro* tool to expand the BCSC subpopulation of breast cancer cells. Moreover, the previous chapter pointed out the potential of FASN to target the sphere-forming BCSC niche of TNBC cells. On this account, this chapter aimed to use ES PCL scaffolds to expand and characterize the BCSC portion of TNBC cell models and, eventually, evaluate the potential of FASN to become a target for BCSC-enriched TNBC samples.

Firstly, 7.5 and 15% PCL scaffolds were produced following the ES optimization presented in Chapter 4 and subsequently characterized through several mechanical analyses. Scaffold curves obtained in differential scanning calorimetry (DSC) and thermal gravimetric analysis (TGA) almost overlap raw PCL data, indicating the absence of material modification neither contamination after fabrication process. Moreover, dynamic mechanical analysis (DMA) determined that PCL scaffolds offered a softer and more elastic 3D network compared with traditional polystyrene (PS) *in vitro* surfaces. These differences might be of a value since cells are proven to generate more traction force and develop a broader and flatter morphology on stiff surfaces (321). Finally, scanning electron microscopy (SEM) images were taken to analyze the microstructure of ES PCL scaffolds. Polymer concentration has been found to exert a strong influence on scaffold architecture. Indeed, 7.5% PCL meshes exhibited, apart from filaments with an average diameter of 300 nm, spherical structures made by non-filamentous polymer. These structures, already described in the literature, are known as beads and are resulted from low polymer concentration (380, 404). In contrast, no beads were observed in 15% PCL meshes, which showed an average fiber diameter of 700 nm. While performing a direct comparison with values from other studies is difficult owing to the wide range of ES parameters used, the significant impact of PCL concentration in acetone on fiber morphology and diameter agrees with most previous studies (377, 379, 380, 405). Then, porosity was also evaluated and, although ES scaffolds presented similar surface porosity (22-28%), the average pore area in 15% PCL model was 3.5-fold larger than that of 7.5% PCL specimens. In these settings, cell responses to PCL nanofibers are likely influenced by both the stiffness and three-dimensionality features provided by these scaffolds.

Two TNBC models from distinct molecular subtypes, MDA-MB-231 (mesenchymal-like) and MDA-MB-468 (basal-like), were successfully expanded on the 7.5 and 15% PCL electrospun mats. Both tested scaffolds showed less cell proliferation compared with the homologous monolayer culture, in agreement with previous studies (406). When scaffolds from different polymer concentrations are

compared, microarchitecture traits seem to influence 3D cell culture efficiency. Both cell lines exhibited a higher cell growth rate on 2D control and 15% PCL scaffolds in comparison with the 7.5% PCL samples. It is worth mentioning that low filament diameters facilitates cell adhesion and growth (367, 377, 378) and, in fact, collagen fibers (the main protein in the extracellular matrix) display small diameters below 100 nm (341). However, in the current study, the scaffold model with the lowest fiber diameter (i.e., 7.5% PCL) also exhibited beads which interfered with cell proliferation. Chen *et al.* demonstrated that, despite having smaller fiber diameters, meshes with beads hindered fibroblast growth (377). In our conditions, beaded scaffolds exhibited a lower surface area-to-volume ratio, providing less material for cell growth. Besides, interconnected pores with a minimum optimal area are needed to allow cell growth and scaffold infiltration. Small pores of 7.5% scaffolds may also hinder TNBC cells' penetration within the mesh structure. Following this hypothesis, most cells would have adhered to the surface and they would hardly have colonized different scaffold depths. With regard to cell morphology, both cell lines seeded on 15% PCL scaffolds presented more cytoplasmic elongations compared with the round shape seen on 7.5% PCL meshes and, especially, 2D monolayer culture. This finding is supported by the higher cytoplasmic elongation factor of 15% PCL mat cells. Cell elongation along scaffold nanofilaments has also been observed in other breast cancer cells (176, 373), fibroblasts (407), and murine adult neural stem cells (408).

Considering cell proliferation kinetics and morphology changes, scaffold from 15% PCL solution was selected to further accommodate MDA-MB-231 and MDA-MB-468 cell culture. This scaffold model was the only that provided a suitable 3D environment for TNBC cells to adopt an *in vivo*-like elongated shape, in contrast with the round flattened shape of 2D-cultured cells which has been proved to induce BCSC differentiation (316, 317, 372). 15% PCL scaffold culture led to an enrichment of the BCSC subpopulation at early culture times in both TNBC cells, resulting in higher mammosphere-forming capacity, ALDH1 activity, stemness-related genes expression, and resistance to the chemotherapeutic drugs

doxorubicin and paclitaxel. In the case of the basal-like MDA-MB-468 cell line, a higher CD44⁺/CD24^{-/low} BCSC-like cell proportion was also found in 3D culture. This analysis was not performed with the mesenchymal-like MDA-MB-231 cell model since up to 95% of these cells are CD44⁺/CD24^{-/low} in basal conditions (own data and (409–411)). These arrangements reached the maximum significance when the culture period lasted 6 days, this time being the one that allows the greatest BCSC expansion through 3D cell culture. Overall, when incubation was extended at 12 days, the expression of several stemness markers remained stable or were even downregulated. In addition, EMT was revealed to occur throughout scaffold culture, which can transform epithelial cancer cells to cancer stem-like cells. Softness reported on PCL scaffolds could play a key role in this EMT induction, since it was proven to be an underlying mediator of TFG- β -driven processes such as EMT through dynamic compression and contraction of cell-matrix interaction (412).

Aside from BCSC expansion within ES PCL scaffold surroundings, a metabolic alteration was also found in 3D-cultured TNBC cells. MDA-MB-231 cells underwent a HER2 overexpression and activation in 3D culture, whereas MDA-MB-468 model displayed activation of both EGFR and HER2. The signal transduction caused by the activation of these receptor tyrosine kinases promotes a diverse repertoire of cellular signaling pathways including MAPK and the PI3K/AKT/mTOR pathways (413). Overall, 3D-cultured TNBC cells displayed a strong MAPK downregulation alongside a mild PI3K/AKT/mTOR pathway activation. Considering all these findings, our hypothesis is that upregulation of HER2 alone (MDA-MB-231) or in combination with that of EGFR (MDA-MB-468) may promote PI3K/AKT/mTOR activation during 3D cell culture, in detriment of MAPK signaling (**Figure 15**). Decreased MAPK signaling and activation of a quiescent profile has also been related to decreased matrix stiffness, a condition found in the used ES PCL scaffolds compared with polystyrene surfaces (414). These signaling alterations could be behind BCSC expansion within 3D culture, as PI3K pathway was previously related to the acquisition of CSC-like properties in breast cancer cells (415). Due to their crosstalk (416, 417), hyperactivation of PI3K/AKT/mTOR cascade may inhibit MAPK

signaling, leading to a more quiescent culture since MAPK regulates cell proliferation (53). Or vice versa, cells adopted a less proliferative profile within 3D surroundings, leading to a MAPK inactivation and triggering PI3K/AKT/mTOR signaling due to a feedback loop. Contrary to our results, previous works pointed out that 3D culture of HER2+ breast cancer cells in Matrigel or spheres promoted a shift from PI3K/AKT to MAPK signaling (418–420). However, these investigations also revealed a HER2 hyperactivation within 3D surroundings. This may indicate that cells can adopt different modifications upon 3D culture depending on their molecular subtype and 3D structure type, among other variables.

Apart from the relation between stemness and FASN, seen in the previous chapter and reported by others (402, 403, 421, 422), HER2 is proven to stimulate FASN expression and post-translational activation by phosphorylation. FASN, in turn, contributes to HER2 activation allowing its incorporation in lipid rafts on the plasma membrane (268). According to our results, both TNBC cell models exhibited significantly higher FASN protein and activity levels after 6 days of culture in ES PCL scaffolds, the same incubation period which showed the maximum expansion of stemness features. When TNBC cells were treated with the FASN inhibitors EGCG and G28, similar cell death values were found in monolayer and scaffolds-cultured cells, eluding the cell growth rate dependence of the chemoagents. Finally, the effect of FASN blocking was evaluated on the BCSC niche through the capacity of forming mammospheres. In basal conditions, the mammosphere forming index (MFI) of 3D samples was significantly increased compared with 2D control, in accordance with previous results and BCSC expansion in scaffolds. However, the treatment with EGCG and G28 decreased the MFI values of 3D-cultured cells down to similar values of 2D or even lower. Concretely, G28 exerted a greater impact upon the MDA-MB-231 cells, whereas MDA-MB-468 cells in scaffolds underwent a greater MFI decrease when treated with EGCG. Taking all these findings into account, the inhibition of FASN through EGCG and G28 treatment led to a stemness diminishment, overcoming the BCSC expansion achieved in 3D culture. In a similar fashion, resveratrol, a natural polyphenolic compound, has been proven to

suppress tumor stem-like cells growth by inducing pro-apoptotic genes via downregulation of FASN expression, *in vitro* and in mice model (402). Some authors pointed out a possible role of FASN increasing fatty acid levels during tumor cell migration, invasion, and metastasis, features of the BCSC niche (423). Overall, pharmacological blocking of FASN hindered both the cell growth of the bulk sample and the stemness capacity of the BCSC-enriched cells.

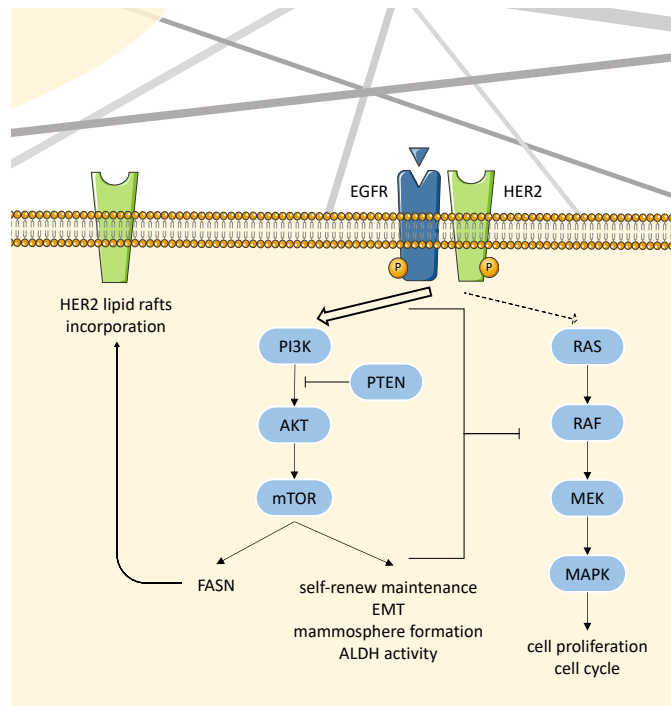


Figure 15. Schematic representation of triple negative breast cancer (TNBC) cell metabolism modulation within three-dimensional (3D) electrospinning (ES) poly(ϵ -caprolactone) (PCL) scaffold culture.

Schematic representation of our hypothesis in which 3D cell culture with ES 15% PCL scaffolds causes an activation of the human epidermal growth factor receptor 2 (HER2) alone (MDA-MB-231 cells, mesenchymal-like) or combined with that of the epidermal growth factor receptor (EGFR; MDA-MB-468 cells, basal-like). This activation trend may stimulate PI3K/AKT/mTOR signaling pathway in detriment of MAPK cascade, leading to a quiescent profile and BCSC features expansion. Due to their crosstalk, hyperactivation of PI3K/AKT/mTOR pathway could inhibit MAPK signaling. Moreover, HER2 is proven to stimulate fatty acid synthase (FASN) expression and post-translational activation by phosphorylation. FASN, in turn, contributes to HER2 activation allowing its incorporation in lipid rafts on the plasma membrane. Abbreviations: AKT (protein kinase B), ALDH (aldehyde dehydrogenase), EMT (epithelial-to-mesenchymal transition), MAPK (mitogen activated protein kinase), MEK (MAPK/ERK kinase), mTOR (mammalian target of rapamycin), PI3K (phosphoinositide-3-kinase), PTEN (phosphatase and tensin homolog), RAF (rapidly accelerated fibrosarcoma), RAS (rat sarcoma). Own elaboration based on observed data.

As a conclusion, 15% PCL ES scaffolds offered a suitable environment to accommodate TNBC cells and, more importantly, to expand their BCSC niche. Our findings open the door to further study FASN as a novel target to treat 3D-cultured quiescent and stem-like TNBC populations. However, further investigations are needed to elucidate the mechanisms through which stemness diminishes in response to FASN inhibition.

Concluding remarks

Collectively, PCL scaffolds represent a potent tool to maintain the stemness features of the sample and expand the BCSC niche of TNBC cells by providing resemblance to a physiological structure. In particular, meshes produced with ES technology displayed the greatest potential to accommodate breast cancer cell culture alongside a BCSC expansion. Therefore, the use of micro- and nanofibers may facilitate research in the cancer stem-like cell field, since novel biomarkers and treatments need to be developed to attack not only the bulk tumor, but also the quiescent and tumor-initiating cells. Notably, FASN deserves further investigation as a novel biomarker for BCSC-enriched TNBC samples, especially within 3D surroundings. Despite the described links between FASN and stemness, more efforts would be needed to investigate whether BCSC expansion and signaling switch alongside FASN activation are two independent events occurred in a 3D environment, or there is a causal relation.

Limitations of the study

At the conclusion of the present research, it is necessary to point out some limitations that have not been possible to control in the presented thesis due to available amount of time, resources, and intrinsic nature of the investigation.

As in most biomedical investigations, the choice of the used cell models is a critical step. In our case, the non-TNBC reference breast cancer cell line MCF-7 was chosen for the initial studies due to its presence in a wide range of 3D culture studies. Therefore, once a 3D cell culture protocol was optimized, two different TNBC models were selected: MDA-MB-231 and MDA-MB-468. Each of them belongs to one TNBC molecular subtype (mesenchymal-like and basal-like, respectively) with the aim to have the whole molecular representation of the TNBC disease. Some differences were observed between these two cell models, e.g., upregulation of different stemness and EMT markers, EGFR activation state of 3D-cultured cells, and distinct impact of EGCG and G28 on mammospheres-forming cells. However, since only one cell line of each molecular subtype was tested, aforementioned differences cannot be directly associated to each category. The use of more cell lines of each subtype would improve the understanding, such as DU4475 and HCC1806 for mesenchymal-like group, and BT549 and HCC1395 for the basal-like one. However, more biological details including critical cell mutations should be considered.

Another significant limitation of our study is the number of scaffold designs tested, especially in the electrospinning section. Only two different ES scaffold models were tested, varying the concentration of PCL (i.e., 7.5 and 15% PCL). Low polymer concentration meshes exhibited reduced cell proliferation and elongation even though they displayed the thinnest filaments, which is preferred for cell growth. However, non-filamented beads that hinder cell growth were also present in the 7.5% PCL scaffolds structure. Since beads formation is related to the use of a low

polymer concentration solution, an intermediate PCL concentration (between 7.5 and 15%) may have been explored to manufacture fibers thinner than the ones present in 15% PCL model but without the appearance of beads. By doing so, we may have been able to produce a scaffold model that enable a higher cell proliferation rate maintaining the cell elongation factor. Despite this limitation, ES 15% PCL scaffold successfully accommodates the culture of TNBC cells, as well as a significant expansion of the BCSC niche.

Finally, the mechanism with which scaffolds increased the BCSC subset could not be fully analyzed. As discussed before, changes in cytoplasm and nucleus shape are thought to be behind stemness upregulation, since cells undergo a complex cytoskeleton reorganization that leads to gene and protein regulation (316, 317). However, increases in BCSC population in 3D culture could result from either increased proliferation of BCSCs or inhibition of their differentiation. To comprehend this matter, further studies can be performed to determine the proliferation rates of BCSC and non-BCSC subpopulation in the sample using, for example, flow cytometry. The combination of 5-ethynyl-2'-deoxyuridine (EdU) incorporation assay with CD44⁺/CD24^{-/low} or ALDH⁺ staining would determine the proliferation rate of both cell subpopulations. This is an approach already performed by another group that cultured breast cancer cells in ES PCL scaffolds. Authors determined that, in their conditions, BCSC and non-BCSC cell niches showed similar cell growth kinetics and, therefore, stemness enrichment was likely due to a differentiation reduction (364).

CHAPTER 8 Conclusions

The general conclusion of this thesis is that fused filament fabrication (FFF) and electrospinning (ES) apparatus have been successfully optimized to manufacture poly(ϵ -caprolactone) (PCL) scaffolds suitable for *in vitro* three-dimensional (3D) breast cancer cell culture and stemness maintenance. Among them, the use of 15% PCL ES scaffold shows the highest potential to expand the breast cancer stem cell (BCSC) subpopulation of the triple negative breast cancer (TNBC) cells MDA-MB-231 (mesenchymal-like subtype) and MDA-MB-468 (basal-like). Additionally, the fatty acid synthase (FASN) enzyme, involved in the *de novo* lipogenesis and drug resistance acquisition, is overexpressed and hyperactivated in the stemness-enriched 3D TNBC samples, and its blocking overcome the BCSC expansion achieved in scaffold culture in terms of mammosphere forming capacity. Our findings encourage the use of PCL scaffolds to maintain the *in vivo* structure and culture BCSCs, making their expansion and characterization possible. Investigation of this rare cancer subpopulation is much warranted as it could facilitate the development of new specific therapeutic approaches to attack malignant and recurrent tumors such as TNBC. FASN has been postulated as a feasible target for BCSC-enriched TNBC samples, however, further studies should be performed to elucidate the potential of its inhibition. The specific conclusions for each objective are listed below:

- I. **Use and optimization of fused filament fabrication (FFF) technology to manufacture polycaprolactone (PCL) scaffolds for 3D cell culture and stemness expansion**
 - a. Design and fabrication parameters of the FFF RepRap 3D printer were optimized to produce PCL scaffolds suitable for 3D cell culture, following a detailed and unidirectional flowchart.
 - b. Produced FFF PCL scaffolds were suitable for 3D cell growth of the tumoral breast cancer cell model MCF-7 and non-tumoral murine fibroblasts NIH/3T3.

- c. FFF PCL scaffolds with a deposition angle between layers of 60° and placed in non-adherent wells resulted in the MCF-7 highest cell proliferation rate.
- d. MCF-7 cells cultured on FFF PCL scaffolds exhibited a greater mammosphere forming capacity than monolayer-cultured cells, revealing a possible BCSC enrichment.

II. **Use and optimization of electrospinning (ES) technology to manufacture PCL scaffolds for 3D cell culture and stemness expansion**

- a. The manufacture of two different ES scaffolds (7.5 and 15% PCL) was achieved after optimization of the ES process and using acetone as a solvent.
- b. Scaffolds of 7.5% PCL solution were less heavy and thinner than 15% ones, in agreement with the PCL amount in each solution.
- c. In all culture conditions, 15% PCL scaffolds showed a significant higher MCF-7 cell proliferation compared with 7.5% specimens.
- d. ES PCL scaffold culture of MCF-7 cells led to a 3-fold increased mammosphere forming index (MFI) compared with 2D-cultured cells, indicating a BCSC enrichment.
- e. MCF-7 cells cultured in ES PCL scaffolds, especially 15% PCL model, showed higher cell proliferation rate and greater BCSC expansion than the ones seeded on FFF PCL counterparts.

III. **Evaluation of BCSC and fatty acid synthase (FASN) role in chemosensitive and chemoresistant MDA-MB-231 TNBC cells**

- a. Doxorubicin-resistant MDA-MB-231 (231DXR) cells showed an expansion of BCSC attributes whereas paclitaxel-resistant derivative (231PTR) maintained the stemness features of the parental cell line. FASN protein levels were significantly increased in the 231DXR model when treated with doxorubicin.

- b. The epithelial-to-mesenchymal (EMT) transcription factors *SNAIL* and *SLUG* were upregulated in the 231DXR and 231PTR model, respectively.
- c. FASN inhibitor G28 displayed a greater inhibitory effect in BCSC-enriched spheres culture in both sensitive and resistant cell lines.
- d. Data from this chapter provide a rationale to suppress FASN as a potential strategy to target BCSCs to improve the prognosis of TNBC patients.

IV. **Enrichment of BCSCs in the TNBC cell models MDA-MB-231 (mesenchymal-like) and MDA-MB-468 (basal-like) within 3D ES PCL scaffold culture**

- a. ES PCL scaffolds provided a softer and more elastic 3D network compared with polystyrene surfaces. Meshes from 7.5% PCL solution exhibited filaments with an average diameter of 300 nm alongside the presence of beads, whereas 15% PCL scaffolds uniquely showed 700 nm average diameter fibers.
- b. TNBC MDA-MB-231 and MDA-MB-468 cells showed a higher cell growth rate when cultured on 15% PCL scaffolds compared with the 7.5% PCL model, as well as a strongest cytoplasmic elongation.
- c. 3D cell culture with 15% PCL scaffolds led to a BCSC enrichment at early culture times in both TNBC cell models, resulting in higher MFI, ALDH1 activity, stemness markers expression, and resistance to the chemotherapeutic drugs doxorubicin and paclitaxel. EMT was revealed to occur throughout scaffold culture, transforming epithelial cancer cells to cancer stem-like cells.
- d. 3D-cultured cells displayed a HER2 activation, accompanied by an EGFR overexpression in the MDA-MB-468 model, which resulted in MAPK to PI3K/AKT/mTOR switching.
- e. FASN was found overexpressed and hyperactivated in stemness-enriched TNBC cells cultured on 3D structures.

- f. The addition of the FASN inhibitors EGCG and G28 led to a similar cell death in monolayer and scaffold-cultured TNBC cells. FASN inhibition also overcame the BCSC enrichment achieved in 3D culture in terms of mammosphere forming capacity.

CHAPTER 9 Future directions

Results presented in this work clearly empower the use of PCL scaffolds as a tool to expand and study the BCSC niche of TNBC samples. Hence, PCL meshes, especially the ones produced with ES technology, would allow researchers to further investigate the BCSC niche and provide a more detailed understanding of their behavior. This upgrade would ultimately enable the development of targeted therapies against this malignant subpopulation.

In a more specific sense, our data pointed out the importance of FASN in the stem-like cells. Regarding its potential as a therapeutical target for BCSC niche in TNBC disease, more efforts should be done to corroborate this hypothesis. In tested conditions, TNBC cells enriched in BCSCs showed both a strong overexpression and a hyperactivation of FASN. Future studies can be focused on discerning whether its upregulation is directly linked to the activation of HER2 downstream signaling determined in 3D conditions, which has been previously related to FASN stimulation (268).

What is more interesting about FASN role is that its pharmacological inhibition hindered the cell growth of both the bulk sample and the BCSC niche. The impact of FASN blockade upon BCSC-like population has been evaluated through the mammospheres forming assay. Nonetheless, the expression of more stem markers after FASN inhibition can be assessed to confirm the BCSC reduction, such as ALDH1 activity, CD44⁺/CD24^{-/low} proportion, and expression of stemness- and EMT-related genes. Following up, the combinatorial use of systemic chemotherapy drugs and FASN inhibitors should be explored, since it may provide therapeutic benefit.

Lastly, it is worth noting the versatility displayed by the FFF and ES technologies and their produced scaffolds, which exhibited very different fiber and pore architectures. Besides, different breast cancer cell lines were cultured on them, along with a non-tumoral fibroblast cell model. All things considered, presented scaffolds may be further customized and used for a wide range of applications and

cell types, including stemness maintenance, tissue engineering, coculture, and drug screening. Optimization flowchart presented in Chapter 3 is a good example of standardized processes that can be useful for people from diverse research fields. For instance, and close to our scope, the use of PCL scaffolds to culture breast cancer cells resistant to some of the current drugs can be helpful to discern the role of BCSC niche in the resistance acquisition process. Moreover, samples from patients' biopsies might be cultured on PCL scaffolds to better characterize the tumor and perform a personalized drug screening.

CHAPTER 10 References

1. Cancer. *World Heal. Organ.* (2021) (March 1, 2021).
2. Understanding cancer. *Natl. Cancer Institute, NIH* (2015) (March 2, 2021).
3. H. Sung, *et al.*, Global cancer statistics 2020: GLOBOCAN estimates of incidence and mortality worldwide for 36 cancers in 185 countries. *CA. Cancer J. Clin.* (2021) <https://doi.org/10.3322/caac.21660> (March 3, 2021).
4. R. Clèries, *et al.*, Predicting the cancer burden in Catalonia between 2015 and 2025: the challenge of cancer management in the elderly. *Clin. Transl. Oncol.* **20**, 647–657 (2018).
5. D. Hanahan, R. A. Weinberg, The hallmarks of cancer. *Cell* **100**, 57–70 (2000).
6. D. Hanahan, R. A. Weinberg, Hallmarks of cancer: The next generation. *Cell* **144**, 646–674 (2011).
7. G. K. Reeves, K. Pirie, J. Green, D. Bull, V. Beral, Reproductive factors and specific histological types of breast cancer: prospective study and meta-analysis. *Br. J. Cancer* **100**, 538–544 (2009).
8. A. Howell, *et al.*, “Risk determination and prevention of breast cancer” (2014) (March 5, 2021).
9. K. D. Miller, *et al.*, Cancer treatment and survivorship statistics, 2016. *CA. Cancer J. Clin.* **66**, 271–289 (2016).
10. C. Sotiropoulos, L. Pusztai, Gene-expression signatures in breast cancer. *N. Engl. J. Med.* **360**, 790–800 (2009).
11. L. A. Carey, *et al.*, Race, Breast Cancer Subtypes, and Survival in the Carolina Breast Cancer Study. *JAMA* **295**, 2492 (2006).
12. O. Abe, *et al.*, Relevance of breast cancer hormone receptors and other factors to the efficacy of adjuvant tamoxifen: Patient-level meta-analysis of randomised trials. *Lancet* **378**, 771–784 (2011).
13. F. Lumachi, Current medical treatment of estrogen receptor-positive breast cancer. *World J. Biol. Chem.* **6**, 231 (2015).
14. D. J. Slamon, *et al.*, Human breast cancer: Correlation of relapse and survival with amplification of the HER-2/neu oncogene. *Science (80-)*. **235**, 182–191 (1987).
15. C. J. Witton, J. R. Reeves, J. J. Going, T. G. Cooke, J. M. S. Barlett, Expression of the HER1-4 family of receptor tyrosine kinases in breast cancer. *J. Pathol.* **200**, 290–297 (2003).
16. C. L. Arteaga, *et al.*, Treatment of HER2-positive breast cancer: current status and future perspectives. *Nat. Rev. Clin. Oncol.* **9**, 16–32 (2011).
17. K. R. Bauer, M. Brown, R. D. Cress, C. A. Parise, V. Caggiano, Descriptive analysis of estrogen receptor (ER)-negative, progesterone receptor (PR)-negative, and HER2-negative invasive breast cancer, the so-called triple-negative phenotype. *Cancer* **109**, 1721–1728 (2007).
18. R. Dent, *et al.*, Triple-Negative Breast Cancer: Clinical Features and Patterns of Recurrence. *Clin. Cancer Res.* **13** (2007).
19. C. L. Griffiths, J. L. Olin, Triple Negative Breast Cancer: A Brief Review of its Characteristics and Treatment Options. *J. Pharm. Pract.* **25**, 319–323 (2012).
20. L. A. Carey, *et al.*, The triple negative paradox: primary tumor

- chemosensitivity of breast cancer subtypes. *Clin. Cancer Res.* **13**, 2329–34 (2007).
21. C. M. Perou, *et al.*, Molecular portraits of human breast tumours. *Nature* **406**, 747–752 (2000).
 22. T. Sørli, *et al.*, Gene expression patterns of breast carcinomas distinguish tumor subclasses with clinical implications. *Proc. Natl. Acad. Sci. U. S. A.* **98**, 10869–10874 (2001).
 23. A. Prat, *et al.*, Phenotypic and molecular characterization of the claudin-low intrinsic subtype of breast cancer. *Breast Cancer Res.* **12** (2010).
 24. C. M. Perou, A. L. Borresen-Dale, Systems biology and genomics of breast cancer. *Cold Spring Harb. Perspect. Biol.* **3**, 1–17 (2011).
 25. F. Bertucci, P. Finetti, D. Birnbaum, Basal Breast Cancer: A Complex and Deadly Molecular Subtype. *Curr. Mol. Med.* **12**, 96–110 (2012).
 26. M. C. U. Cheang, *et al.*, Basal-like breast cancer defined by five biomarkers has superior prognostic value than triple-negative phenotype. *Clin. Cancer Res.* **14**, 1368–1376 (2008).
 27. S. Krishnamurthy, R. Poornima, V. R. Challa, Y. G. B. Goud, Triple Negative Breast Cancer - Our Experience and Review. *Indian J. Surg. Oncol.* **3**, 12–16 (2012).
 28. C. M. Perou, Molecular Stratification of Triple-Negative Breast Cancers. *Oncologist* **15**, 39–48 (2010).
 29. A. Prat, C. M. Perou, Deconstructing the molecular portraits of breast cancer. *Mol. Oncol.* **5**, 5–23 (2011).
 30. B. D. B. Lehmann, *et al.*, Identification of human triple-negative breast cancer subtypes and preclinical models for selection of targeted therapies. *J. Clin. Invest.* **121**, 2750–2767 (2011).
 31. T. Sørli, *et al.*, Repeated observation of breast tumor subtypes in independent gene expression data sets. *Proc. Natl. Acad. Sci. U. S. A.* **100**, 8418–8423 (2003).
 32. D. C. Koboldt, *et al.*, Comprehensive molecular portraits of human breast tumours. *Nature* **490**, 61–70 (2012).
 33. P. Van Der Geer, T. Hunter, R. A. Lindberg, Receptor protein-tyrosine kinases and their signal transduction pathways. *Annu. Rev. Cell Biol.* **10**, 251–337 (1994).
 34. N. Prenzel, O. M. Fischer, S. Streit, S. Hart, A. Ullrich, The epidermal growth factor receptor family as a central element for cellular signal transduction and diversification in *Endocrine-Related Cancer*, (Endocr Relat Cancer, 2001), pp. 11–31.
 35. A. C. Porter, R. R. Vaillancourt, Tyrosine kinase receptor-activated signal transduction pathways which lead to oncogenesis. *Oncogene* **17**, 1343–1352 (1998).
 36. G. Carpenter, L. King, S. Cohen, Epidermal growth factor stimulates phosphorylation in membrane preparations in vitro [21]. *Nature* **276**, 409–410 (1978).
 37. R. Roskoski, ErbB/HER protein-tyrosine kinases: Structures and small molecule inhibitors. *Pharmacol. Res.* **87**, 42–59 (2014).

38. R. Roskoski, The ErbB/HER family of protein-tyrosine kinases and cancer. *Pharmacol. Res.* **79**, 34–74 (2014).
39. P. J. Brennan, T. Kumogai, A. Berezov, R. Murali, M. I. Greene, HER2/neu: Mechanisms of dimerization/oligomerization. *Oncogene* **19**, 6093–6101 (2000).
40. Y. Yarden, The EGFR family and its ligands in human cancer: Signalling mechanisms and therapeutic opportunities. *Eur. J. Cancer* **37**, 3–8 (2001).
41. D. Zhang, *et al.*, Neuregulin-3 (NRG3): A novel neural tissue-enriched protein that binds and activates ErbB4. *Proc. Natl. Acad. Sci. U. S. A.* **94**, 9562–9567 (1997).
42. D. Harari, *et al.*, Neuregulin-4: A novel growth factor that acts through the ErbB-4 receptor tyrosine kinase. *Oncogene* **18**, 2681–2689 (1999).
43. J. Baselga, S. M. Swain, Novel anticancer targets: Revisiting ERBB2 and discovering ERBB3. *Nat. Rev. Cancer* **9**, 463–475 (2009).
44. N. E. Hynes, H. A. Lane, ERBB receptors and cancer: The complexity of targeted inhibitors. *Nat. Rev. Cancer* **5**, 341–354 (2005).
45. M. F. Rimawi, R. Schiff, C. K. Osborne, Targeting HER2 for the treatment of breast cancer. *Annu. Rev. Med.* **66**, 111–128 (2015).
46. B. Singh, G. Carpenter, R. J. Coffey, EGF receptor ligands: Recent advances [version 1; referees: 3 approved]. *F1000Research* **5** (2016).
47. R. Pinkas-Kramarski, *et al.*, Diversification of Neu differentiation factor and epidermal growth factor signaling by combinatorial receptor interactions. *EMBO J.* **15**, 2452–2467 (1996).
48. E. Tzahar, *et al.*, A hierarchical network of interreceptor interactions determines signal transduction by Neu differentiation factor/neuregulin and epidermal growth factor. *Mol. Cell. Biol.* **16**, 5276–5287 (1996).
49. P. Seshacharyulu, *et al.*, Targeting the EGFR signaling pathway in cancer therapy. *Expert Opin. Ther. Targets* **16**, 15–31 (2012).
50. R. Nahta, L. X. H. Yuan, B. Zhang, R. Kobayashi, F. J. Esteva, Insulin-like growth factor-I receptor/human epidermal growth factor receptor 2 heterodimerization contributes to trastuzumab resistance of breast cancer cells. *Cancer Res.* **65**, 11118–11128 (2005).
51. A. Citri, Y. Yarden, EGF–ERBB signalling: towards the systems level. *Nat. Rev. Mol. Cell Biol.* **7**, 505–516 (2006).
52. J. Schlessinger, D. Bar-Sagi, Activation of Ras and other signaling pathways by receptor tyrosine kinases in *Cold Spring Harbor Symposia on Quantitative Biology*, (Cold Spring Harbor Laboratory Press, 1994), pp. 173–179.
53. G. Pearson, *et al.*, Mitogen-activated protein (MAPK) kinase pathways: Regulation and physiological functions. *Endocr. Rev.* **22**, 153–183 (2001).
54. C. Porta, C. Paglino, A. Mosca, Targeting PI3K/Akt/mTOR signaling in cancer. *Front. Oncol.* **4** APR (2014).
55. F. Janku, T. A. Yap, F. Meric-Bernstam, Targeting the PI3K pathway in cancer: Are we making headway? *Nat. Rev. Clin. Oncol.* **15**, 273–291 (2018).
56. P. Kumar, R. Aggarwal, An overview of triple-negative breast cancer. *Arch.*

- Gynecol. Obstet.* **293**, 247–269 (2016).
57. G. J. Morris, *et al.*, Differences in breast carcinoma characteristics in newly diagnosed African-American and Caucasian patients: A single-institution compilation compared with the national cancer institute's surveillance, epidemiology, and end results database. *Cancer* **110**, 876–884 (2007).
 58. P. Neven, Brouckaert, Wildiers, Floris, Update on triple-negative breast cancer: prognosis and management strategies. *Int. J. Womens. Health* **4**, 511 (2012).
 59. M. Dowsett, *et al.*, Retrospective analysis of time to recurrence in the ATAC trial according to hormone receptor status: An hypothesis-generating study. *J. Clin. Oncol.* **23**, 7512–7517 (2005).
 60. R. C. Millikan, *et al.*, Epidemiology of basal-like breast cancer. *Breast Cancer Res. Treat.* **109**, 123–139 (2008).
 61. A. I. Phipps, *et al.*, Reproductive history and oral contraceptive use in relation to risk of triple-negative breast cancer. *J. Natl. Cancer Inst.* **103**, 470–477 (2011).
 62. X. R. Yang, *et al.*, Associations of Breast Cancer Risk Factors With Tumor Subtypes: A Pooled Analysis From the Breast Cancer Association Consortium Studies. *Artic. / JNCI* **103**, 250 (2011).
 63. S. R. Lakhani, *et al.*, The pathology of familial breast cancer: Predictive value of immunohistochemical markers estrogen receptor, progesterone receptor, HER-2, and p53 in patients with mutations in BRCA1 and BRCA2. *J. Clin. Oncol.* **20**, 2310–2318 (2002).
 64. D. P. Atchley, *et al.*, Clinical and pathologic characteristics of patients with BRCA-positive and BRCA-negative breast cancer. *J. Clin. Oncol.* **26**, 4282–4288 (2008).
 65. F. J. Couch, *et al.*, Inherited mutations in 17 breast cancer susceptibility genes among a large triple-negative breast cancer cohort unselected for family history of breast cancer. *J. Clin. Oncol.* **33**, 304–311 (2015).
 66. S. P. Shah, *et al.*, The clonal and mutational evolution spectrum of primary triple-negative breast cancers. *Nature* **486**, 395–399 (2012).
 67. L. Vona-Davis, *et al.*, Triple-negative breast cancer and obesity in a rural appalachian population. *Cancer Epidemiol. Biomarkers Prev.* **17**, 3319–3324 (2008).
 68. A. M. Gonzalez-Angulo, *et al.*, Incidence and outcome of BRCA mutations in unselected patients with triple receptor-negative breast cancer. *Clin. Cancer Res.* **17**, 1082–1089 (2011).
 69. M. Aapro, H. Wildiers, Triple-negative breast cancer in the older population. *Ann. Oncol.* **23** (2012).
 70. N. U. Lin, *et al.*, Sites of distant recurrence and clinical outcomes in patients with metastatic triple-negative breast cancer: High incidence of central nervous system metastases. *Cancer* **113**, 2638–2645 (2008).
 71. M. Smid, *et al.*, Subtypes of breast cancer show preferential site of relapse. *Cancer Res.* **68**, 3108–3114 (2008).
 72. H. Kennecke, *et al.*, Metastatic behavior of breast cancer subtypes. *J. Clin. Oncol.* **28**, 3271–3277 (2010).

73. K. D. Voduc, *et al.*, Breast cancer subtypes and the risk of local and regional relapse. *J. Clin. Oncol.* **28**, 1684–1691 (2010).
74. E. Montagna, *et al.*, Breast cancer subtypes and outcome after local and regional relapse. *J. Clin. Oncol.* **29**, 1076–1076 (2011).
75. T. O. Nielsen, *et al.*, Immunohistochemical and Clinical Characterization of the Basal-Like Subtype of Invasive Breast Carcinoma. *Clin. Cancer Res.* **10**, 5367–5374 (2004).
76. Y. Yamamoto, *et al.*, Clinical significance of basal-like subtype in triple-negative breast cancer in *Breast Cancer*, (Springer, 2009), pp. 260–267.
77. R. Gerhard, *et al.*, Immunohistochemical features of claudin-low intrinsic subtype in metaplastic breast carcinomas. *Breast* **21**, 354–360 (2012).
78. J. Choi, W. H. Jung, J. S. Koo, Clinicopathologic features of molecular subtypes of triple negative breast cancer based on immunohistochemical markers. *Histol. Histopathol.* **27**, 1481–1493 (2012).
79. C. Liedtke, *et al.*, Response to neoadjuvant therapy and long-term survival in patients with triple-negative breast cancer. *J. Clin. Oncol.* **26**, 1275–1281 (2008).
80. S. Aebi, T. Davidson, G. Gruber, F. Cardoso, Primary breast cancer: Esmo clinical practice guidelines for diagnosis, treatment and follow-up. *Ann. Oncol.* **22** (2011).
81. W. J. Gradishar, *et al.*, Breast cancer, version 3.2020. *JNCCN J. Natl. Compr. Cancer Netw.* **18**, 452–478 (2020).
82. M. Kyndi, *et al.*, Estrogen receptor, progesterone receptor, HER-2, and response to postmastectomy radiotherapy in high-risk breast cancer: The Danish Breast Cancer Cooperative Group. *J. Clin. Oncol.* **26**, 1419–1426 (2008).
83. M. E. Straver, *et al.*, The 70-gene signature as a response predictor for neoadjuvant chemotherapy in breast cancer. *Breast Cancer Res. Treat.* **119**, 551–558 (2010).
84. J. Huober, *et al.*, Effect of neoadjuvant anthracycline-taxane-based chemotherapy in different biological breast cancer phenotypes: Overall results from the GeparTrio study. *Breast Cancer Res. Treat.* **124**, 133–140 (2010).
85. D. A. Berry, *et al.*, Estrogen-receptor status and outcomes of modern chemotherapy for patients with node-positive breast cancer. *J. Am. Med. Assoc.* **295**, 1658–1667 (2006).
86. C. M, *et al.*, Adjuvant chemotherapy in oestrogen-receptor-poor breast cancer: patient-level meta-analysis of randomised trials. *Lancet* **371**, 29–40 (2008).
87. L. Yin, J. J. Duan, X. W. Bian, S. C. Yu, Triple-negative breast cancer molecular subtyping and treatment progress. *Breast Cancer Res.* **22**, 61 (2020).
88. J. A. Bauer, *et al.*, Identification of markers of taxane sensitivity using proteomic and genomic analyses of breast tumors from patients receiving neoadjuvant paclitaxel and radiation. *Clin. Cancer Res.* **16**, 681–690 (2010).
89. N. Juul, *et al.*, Assessment of an RNA interference screen-derived mitotic

- and ceramide pathway metagene as a predictor of response to neoadjuvant paclitaxel for primary triple-negative breast cancer: A retrospective analysis of five clinical trials. *Lancet Oncol.* **11**, 358–365 (2010).
90. D. A. Gewirtz, A critical evaluation of the mechanisms of action proposed for the antitumor effects of the anthracycline antibiotics adriamycin and daunorubicin. *Biochem. Pharmacol.* **57**, 727–741 (1999).
 91. D. Edwardson, *et al.*, Role of Drug Metabolism in the Cytotoxicity and Clinical Efficacy of Anthracyclines. *Curr. Drug Metab.* **16**, 412–426 (2015).
 92. O. Abe, *et al.*, Effects of chemotherapy and hormonal therapy for early breast cancer on recurrence and 15-year survival: An overview of the randomised trials. *Lancet* **365**, 1687–1717 (2005).
 93. O. Metzger-Filho, *et al.*, Dissecting the heterogeneity of triple-negative breast cancer. *J. Clin. Oncol.* **30**, 1879–1887 (2012).
 94. R. Rouzier, *et al.*, Breast cancer molecular subtypes respond differently to preoperative chemotherapy. *Clin. Cancer Res.* **11**, 5678–5685 (2005).
 95. M. Martin, *et al.*, Molecular and genomic predictors of response to single-agent doxorubicin (ADR) versus single-agent docetaxel (DOC) in primary breast cancer (PBC). *J. Clin. Oncol.* **28**, 502–502 (2010).
 96. M. Martin, *et al.*, Genomic predictors of response to doxorubicin versus docetaxel in primary breast cancer. *Breast Cancer Res. Treat.* **128**, 127–136 (2011).
 97. L. A. Smith, *et al.*, Cardiotoxicity of anthracycline agents for the treatment of cancer: Systematic review and meta-analysis of randomised controlled trials. *BMC Cancer* **10** (2010).
 98. A. S. Fauci, S. M. Wolff, J. S. Johnson, Effect of Cyclophosphamide upon the Immune Response in Wegener's Granulomatosis. *N. Engl. J. Med.* **285**, 1493–1496 (1971).
 99. K. Nakatsukasa, *et al.*, Docetaxel and cyclophosphamide as neoadjuvant chemotherapy in HER2-negative primary breast cancer. *Breast Cancer* **24**, 63–68 (2017).
 100. S. J. Isakoff, Triple-negative breast cancer: Role of specific chemotherapy agents. *Cancer J.* **16**, 53–61 (2010).
 101. G. Von Minckwitz, *et al.*, Neoadjuvant carboplatin in patients with triple-negative and HER2-positive early breast cancer (GeparSixto; GBG 66): A randomised phase 2 trial. *Lancet Oncol.* **15**, 747–756 (2014).
 102. J. Zhang, *et al.*, Cisplatin and gemcitabine as the first line therapy in metastatic triple negative breast cancer. *Int. J. Cancer* **136**, 204–211 (2015).
 103. B. Jovanovic, *et al.*, A randomized phase II neoadjuvant study of cisplatin, paclitaxel with or without everolimus in patients with stage II/III triple-negative breast cancer (TNBC): Responses and long-term outcome correlated with increased frequency of DNA damage response gene mutations, TNBC subtype, AR status, and Ki67. *Clin. Cancer Res.* **23**, 4035–4045 (2017).
 104. Q. Li, *et al.*, A phase II study of capecitabine plus cisplatin in metastatic

- triple-negative breast cancer patients pretreated with anthracyclines and taxanes. *Cancer Biol. Ther.* **16**, 1746–1753 (2015).
105. E. Amir, *et al.*, Prospective study evaluating the impact of tissue confirmation of metastatic disease in patients with breast cancer. *J. Clin. Oncol.* **30**, 587–592 (2012).
 106. B. P. Schneider, K. D. Miller, Angiogenesis of breast cancer. *J. Clin. Oncol.* **23**, 1782–1790 (2005).
 107. K. Miller, *et al.*, Paclitaxel plus Bevacizumab versus Paclitaxel Alone for Metastatic Breast Cancer. *N. Engl. J. Med.* **357**, 2666–2676 (2007).
 108. N. J. Robert, *et al.*, RIBBON-1: Randomized, double-blind, placebo-controlled, phase III trial of chemotherapy with or without bevacizumab for first-line treatment of human epidermal growth factor receptor 2-negative, locally recurrent or metastatic breast cancer. *J. Clin. Oncol.* **29**, 1252–1260 (2011).
 109. H. D. Bear, *et al.*, Bevacizumab Added to Neoadjuvant Chemotherapy for Breast Cancer. *N. Engl. J. Med.* **366**, 310–320 (2012).
 110. D. Cameron, *et al.*, Adjuvant bevacizumab-containing therapy in triple-negative breast cancer (BEATRICE): Primary results of a randomised, phase 3 trial. *Lancet Oncol.* **14**, 933–942 (2013).
 111. R. B. D’Agostino, Changing End Points in Breast-Cancer Drug Approval — The Avastin Story. *N. Engl. J. Med.* **365**, e2 (2011).
 112. Home - ClinicalTrials.gov (March 19, 2021).
 113. B. D. Lehmann, J. A. Pietenpol, Identification and use of biomarkers in treatment strategies for triple-negative breast cancer subtypes. *J. Pathol.* **232**, 142–150 (2014).
 114. T. A. Buchholz, *et al.*, Epidermal growth factor receptor expression correlates with poor survival in patients who have breast carcinoma treated with doxorubicin-based neoadjuvant chemotherapy. *Cancer* **104**, 676–681 (2005).
 115. H. S. Park, *et al.*, High EGFR gene copy number predicts poor outcome in triple-negative breast cancer. *Mod. Pathol.* **27**, 1212–1222 (2014).
 116. L. A. Carey, *et al.*, TBCRC 001: Randomized phase II study of cetuximab in combination with carboplatin in stage IV triple-negative breast cancer. *J. Clin. Oncol.* **30**, 2615–2623 (2012).
 117. S. Y. Cho, Identification of ERBB pathway-activated cells in triple-negative breast cancer. *Genomics and Informatics* **17** (2019).
 118. J. Baselga, *et al.*, Phase II and tumor pharmacodynamic study of gefitinib in patients with advanced breast cancer. *J. Clin. Oncol.* **23**, 5323–5333 (2005).
 119. B. Corkery, J. Crown, M. Clynes, N. O’Donovan, Epidermal growth factor receptor as a potential therapeutic target in triple-negative breast cancer. *Ann. Oncol.* **20**, 862–867 (2009).
 120. M. De Vos, V. Schreiber, F. Dantzer, The diverse roles and clinical relevance of PARPs in DNA damage repair: Current state of the art. *Biochem. Pharmacol.* **84**, 137–146 (2012).
 121. K. A. Gelmon, *et al.*, Olaparib in patients with recurrent high-grade serous or poorly differentiated ovarian carcinoma or triple-negative breast

- cancer: A phase 2, multicentre, open-label, non-randomised study. *Lancet Oncol.* **12**, 852–861 (2011).
122. R. S. Finn, *et al.*, Dasatinib, an orally active small molecule inhibitor of both the src and abl kinases, selectively inhibits growth of basal-type/"triple-negative" breast cancer cell lines growing in vitro. *Breast Cancer Res. Treat.* **105**, 319–326 (2007).
 123. D. Tryfonopoulos, *et al.*, Src: A potential target for the treatment of triple-negative breast cancer. *Ann. Oncol.* **22**, 2234–2240 (2011).
 124. M. N. Fornier, *et al.*, A phase I study of dasatinib and weekly paclitaxel for metastatic breast cancer. *Ann. Oncol.* **22**, 2575–2581 (2011).
 125. L. H. Saal, *et al.*, PIK3CA mutations correlate with hormone receptors, node metastasis, and ERBB2, and are mutually exclusive with PTEN loss in human breast carcinoma. *Cancer Res.* **65**, 2554–2559 (2005).
 126. S. L. Ellard, *et al.*, Randomized phase II study comparing two schedules of everolimus in patients with recurrent/metastatic breast cancer: NCIC clinical trials group IND.163. *J. Clin. Oncol.* **27**, 4536–4541 (2009).
 127. V. N. Barton, *et al.*, Androgen Receptor Biology in Triple Negative Breast Cancer: a Case for Classification as AR+ or Quadruple Negative Disease. *Horm. Cancer* **6**, 206–213 (2015).
 128. A. S. Doane, *et al.*, An estrogen receptor-negative breast cancer subset characterized by a hormonally regulated transcriptional program and response to androgen. *Oncogene* **25**, 3994–4008 (2006).
 129. A. Gucalp, *et al.*, Phase II trial of bicalutamide in patients with androgen receptor-positive, estrogen receptor-negative metastatic breast cancer. *Clin. Cancer Res.* **19**, 5505–5512 (2013).
 130. T. A. Traina, *et al.*, Enzalutamide for the treatment of androgen receptor-expressing triple-negative breast cancer. *J. Clin. Oncol.* **36**, 884–890 (2018).
 131. J. P. Persijn, E. Engelsman, Oestrogen and androgen receptors in breast cancer and response to endocrine therapy. *Br. Med. J.* **4**, 503 (1975).
 132. R. M. Bryan, *et al.*, Androgen receptors in breast cancer. *Cancer* **54**, 2436–2440 (1984).
 133. Y. W. Zhao, *et al.*, Identification, cloning, and expression of human estrogen receptor- α 36, a novel variant of human estrogen receptor- α 66. *Biochem. Biophys. Res. Commun.* **336**, 1023–1027 (2005).
 134. Z. Y. Wang, *et al.*, A variant of estrogen receptor- α , hER- α 36: Transduction of estrogen- and antiestrogen-dependent membrane-initiated mitogenic signaling. *Proc. Natl. Acad. Sci. U. S. A.* **103**, 9063–9068 (2006).
 135. X. T. Zhang, *et al.*, A positive feedback loop of ER- α 36/EGFR promotes malignant growth of ER-negative breast cancer cells. *Oncogene* **30**, 770–780 (2011).
 136. J. Gibson, Anti-PD-L1 for metastatic triple-negative breast cancer. *Lancet Oncol.* **16**, e264 (2015).
 137. P. García-Tejido, M. L. Cabal, I. P. Fernández, Y. F. Pérez, Tumor-infiltrating lymphocytes in triple negative breast cancer: The future of immune targeting. *Clin. Med. Insights Oncol.* **10**, 31–39 (2016).
 138. R. Nanda, *et al.*, Pembrolizumab in patients with advanced triple-negative

- breast cancer: Phase Ib keynote-012 study. *J. Clin. Oncol.* **34**, 2460–2467 (2016).
139. , Atezolizumab Extends Survival for Breast Cancer. *Cancer Discov.* **7**, OF10 (2017).
140. D. G. Song, *et al.*, Effective adoptive immunotherapy of triple-negative breast cancer by folate receptor-alpha redirected CAR T cells is influenced by surface antigen expression level. *J. Hematol. Oncol.* **9** (2016).
141. H. Mao, *et al.*, New Insights of CTLA-4 into Its Biological Function in Breast Cancer. *Curr. Cancer Drug Targets* **10**, 728–736 (2010).
142. T. Reya, S. J. Morrison, M. F. Clarke, I. L. Weissman, Stem cells, cancer, and cancer stem cells. *Nature* **414**, 105–11 (2001).
143. J. Furth, M. C. Kahn, C. Breedis, The Transmission of Leukemia of Mice with a Single Cell. *Am. J. Cancer* **31**, 276–282 (1937).
144. K. Ishibashi, Studies on the number of cells necessary for the transplantation of Yoshida sarcoma; transmission of the tumor with a single cell. *Gan* **41**, 1–14 (1950).
145. H. B. Hewitt, Studies of the quantitative transplantation of mouse sarcoma. *Br. J. Cancer* **7**, 367–83 (1953).
146. W. R. Bruce, H. Van Der Gaag, A quantitative assay for the number of murine lymphoma cells capable of proliferation in vivo. *Nature* **199**, 79–80 (1963).
147. I. Wodinsky, C. Foley, C. J. Kensler, Spleen colony studies of leukemia L1210. VI. Quantitation of the surviving population of frozen-thawed L1210 cells using the spleen colony assay. *Cryobiology* **4**, 333–336 (1968).
148. D. E. Bergsagel, F. A. Valeriote, Growth Characteristics of a Mouse Plasma Cell Tumor. *Cancer Res.* **28** (1968).
149. C. H. Park, D. E. Bergsagel, E. A. McCulloch, Mouse myeloma tumor stem cells: A primary cell culture assay. *J. Natl. Cancer Inst.* **46**, 411–422 (1971).
150. D. Bonnet, J. E. Dick, Human acute myeloid leukemia is organized as a hierarchy that originates from a primitive hematopoietic cell. *Nat. Med.* **3**, 730–7 (1997).
151. M. Al-Hajj, M. S. Wicha, A. Benito-Hernandez, S. J. Morrison, M. F. Clarke, Prospective identification of tumorigenic breast cancer cells. *Proc. Natl. Acad. Sci. U. S. A.* **100**, 3983–8 (2003).
152. E. L.-H. Leung, *et al.*, Non-small cell lung cancer cells expressing CD44 are enriched for stem cell-like properties. *PLoS One* **5**, e14062 (2010).
153. G. F. Weber, *et al.*, Absence of the CD44 gene prevents sarcoma metastasis. *Cancer Res.* **62**, 2281–6 (2002).
154. H. Ponta, L. Sherman, P. A. Herrlich, CD44: from adhesion molecules to signalling regulators. *Nat. Rev. Mol. Cell Biol.* **4**, 33–45 (2003).
155. D. Naor, S. B. Wallach-Dayana, M. A. Zahalka, R. V. Sionov, Involvement of CD44, a molecule with a thousand faces, in cancer dissemination. *Semin. Cancer Biol.* **18**, 260–7 (2008).
156. H. J. Lee, *et al.*, CD24, a novel cancer biomarker, predicting disease-free survival of non-small cell lung carcinomas: a retrospective study of prognostic factor analysis from the viewpoint of forthcoming (seventh)

- new TNM classification. *J. Thorac. Oncol.* **5**, 649–57 (2010).
157. J. Zheng, *et al.*, NDRG2 inhibits hepatocellular carcinoma adhesion, migration and invasion by regulating CD24 expression. *BMC Cancer* **11**, 251 (2011).
 158. G. Kristiansen, *et al.*, CD24 expression is a new prognostic marker in breast cancer. *Clin. Cancer Res.* **9**, 4906–13 (2003).
 159. E. Park, *et al.*, Prognostic significance of stem cell-related marker expression and its correlation with histologic subtypes in lung adenocarcinoma. *Oncotarget* **7**, 42502–42512 (2016).
 160. H. Schabath, S. Runz, S. Joumaa, P. Altevogt, CD24 affects CXCR4 function in pre-B lymphocytes and breast carcinoma cells. *J. Cell Sci.* **119**, 314–25 (2006).
 161. G. Honeth, *et al.*, The CD44+/CD24- phenotype is enriched in basal-like breast tumors. *Breast Cancer Res.* **10**, R53 (2008).
 162. E. Mylona, *et al.*, The clinicopathologic and prognostic significance of CD44+/CD24(-/low) and CD44-/CD24+ tumor cells in invasive breast carcinomas. *Hum. Pathol.* **39**, 1096–102 (2008).
 163. C. H. Stuelten, *et al.*, Complex display of putative tumor stem cell markers in the NCI60 tumor cell line panel. *Stem Cells* **28**, 649–60 (2010).
 164. A. Jaggupilli, E. Elkord, Significance of CD44 and CD24 as Cancer Stem Cell Markers: An Enduring Ambiguity. *Clin. Dev. Immunol.* **2012**, 1–11 (2012).
 165. J. I. Lopez, *et al.*, CD44 attenuates metastatic invasion during breast cancer progression. *Cancer Res.* **65**, 6755–63 (2005).
 166. C. Sheridan, *et al.*, CD44+/CD24- breast cancer cells exhibit enhanced invasive properties: an early step necessary for metastasis. *Breast Cancer Res.* **8**, R59 (2006).
 167. C. M. Fillmore, C. Kuperwasser, Human breast cancer cell lines contain stem-like cells that self-renew, give rise to phenotypically diverse progeny and survive chemotherapy. *Breast Cancer Res.* **10**, R25 (2008).
 168. S. Ricardo, *et al.*, Breast cancer stem cell markers CD44, CD24 and ALDH1: expression distribution within intrinsic molecular subtype. *J. Clin. Pathol.* **64**, 937–46 (2011).
 169. J. P. Chute, *et al.*, Inhibition of aldehyde dehydrogenase and retinoid signaling induces the expansion of human hematopoietic stem cells. *Proc. Natl. Acad. Sci. U. S. A.* **103**, 11707–12 (2006).
 170. C. Ginestier, *et al.*, ALDH1 is a marker of normal and malignant human mammary stem cells and a predictor of poor clinical outcome. *Cell Stem Cell* **1**, 555–67 (2007).
 171. S. Liu, *et al.*, Breast Cancer Stem Cells Transition between Epithelial and Mesenchymal States Reflective of their Normal Counterparts. *Stem Cell Reports* **2**, 78–91 (2014).
 172. X. Zhang, K. Powell, L. Li, Breast cancer stem cells: Biomarkers, identification and isolation methods, regulating mechanisms, cellular origin, and beyond. *Cancers (Basel)*. **12**, 1–28 (2020).
 173. S. Okumura-Nakanishi, M. Saito, H. Niwa, F. Ishikawa, Oct-3/4 and Sox2 Regulate Oct-3/4 Gene in Embryonic Stem Cells. *J. Biol. Chem.* **280**, 5307–

- 5317 (2005).
174. N. Yang, Y. Wang, L. Hui, X. Li, X. Jiang, Silencing SOX2 Expression by RNA Interference Inhibits Proliferation, Invasion and Metastasis, and Induces Apoptosis through MAP4K4/JNK Signaling Pathway in Human Laryngeal Cancer TU212 Cells. *J. Histochem. Cytochem.* **63**, 721–733 (2015).
 175. A. I. Penzo-Méndez, Critical roles for SoxC transcription factors in development and cancer. *Int J Biochem Cell Biol* **42**, 425–428 (2010).
 176. S. Feng, *et al.*, Expansion of breast cancer stem cells with fibrous scaffolds. *Integr. Biol. (Camb)*. **5**, 768–77 (2013).
 177. D. J. Rodda, *et al.*, Transcriptional regulation of Nanog by OCT4 and SOX2. *J. Biol. Chem.* **280**, 24731–24737 (2005).
 178. G.-Q. Ling, D.-B. Chen, B.-Q. Wang, L.-S. Zhang, Expression of the pluripotency markers Oct3/4, Nanog and Sox2 in human breast cancer cell lines. *Oncol. Lett.* **4**, 1264–1268 (2012).
 179. K. Friedrichs, *et al.*, High Expression Level of $\alpha 6$ Integrin in Human Breast Carcinoma Is Correlated with Reduced Survival. *Cancer Res.* **55** (1995).
 180. K. R. Yu, *et al.*, CD49f enhances multipotency and maintains stemness through the direct regulation of OCT4 and SOX2. *Stem Cells* **30**, 876–887 (2012).
 181. Z. L. Yang, Q. Zheng, J. Yan, Y. Pan, Z. G. Wang, Upregulated CD133 expression in tumorigenesis of colon cancer cells. *World J. Gastroenterol.* **17**, 932–937 (2011).
 182. M. Schneider, *et al.*, Characterization of colon cancer cells: A functional approach characterizing CD133 as a potential stem cell marker. *BMC Cancer* **12** (2012).
 183. S. Ma, Biology and clinical implications of CD133+ liver cancer stem cells. *Exp. Cell Res.* **319**, 126–132 (2013).
 184. P. C. Hermann, *et al.*, Distinct Populations of Cancer Stem Cells Determine Tumor Growth and Metastatic Activity in Human Pancreatic Cancer. *Cell Stem Cell* **1**, 313–323 (2007).
 185. S. Rutella, *et al.*, Cells with characteristics of cancer stem/progenitor cells express the CD133 antigen in human endometrial tumors. *Clin. Cancer Res.* **15**, 4299–4311 (2009).
 186. L. Tume, K. Paco, R. Ubidia-Incio, J. Moya, CD133 in breast cancer cells and in breast cancer stem cells as another target for immunotherapy. *Gac. Mex. Oncol.* **15**, 22–30 (2016).
 187. P. Xia, CD133 mRNA may be a suitable prognostic marker for human breast cancer. *Stem Cell Investig.* **4** (2017).
 188. G. Dontu, *et al.*, In vitro propagation and transcriptional profiling of human mammary stem / progenitor cells. *genes Dev.* **17**, 1253–1270 (2003).
 189. F. L. Shaw, *et al.*, A detailed mammosphere assay protocol for the quantification of breast stem cell activity. *J. Mammary Gland Biol. Neoplasia* **17**, 111–117 (2012).
 190. J. Manuel Iglesias, *et al.*, Mammosphere Formation in Breast Carcinoma Cell Lines Depends upon Expression of E-cadherin. *PLoS One* **8**, 1–12 (2013).

191. R. Wang, *et al.*, Comparison of mammosphere formation from breast cancer cell lines and primary breast tumors. *J. Thorac. Dis.* **6**, 829–837 (2014).
192. T. Bonnefoix, P. Bonnefoix, P. Verdiel, J. J. Sotto, Fitting limiting dilution experiments with generalized linear models results in a test of the single-hit Poisson assumption. *J. Immunol. Methods* **194**, 113–119 (1996).
193. J. E. Dick, M. Bhatia, O. Gan, U. Kapp, J. C. Y. Wang, Assay of human stem cells by repopulation of NOD/SCID mice. *Stem Cells* **15**, 199–207 (1997).
194. T. M. Phillips, W. H. McBride, F. Pajonk, The response of CD24-/low/CD44+ breast cancer-initiating cells to radiation. *J. Natl. Cancer Inst.* **98**, 1777–1785 (2006).
195. C. Lagadec, *et al.*, Survival and self-renewing capacity of breast cancer initiating cells during fractionated radiation treatment. *Breast Cancer Res.* **12** (2010).
196. F. Karimi-Busheri, A. Rasouli-Nia, J. R. Mackey, M. Weinfeld, Senescence evasion by MCF-7 human breast tumor-initiating cells. *Breast Cancer Res.* **12** (2010).
197. F. Yu, *et al.*, let-7 Regulates Self Renewal and Tumorigenicity of Breast Cancer Cells. *Cell* **131**, 1109–1123 (2007).
198. S. P. Zielske, A. C. Spalding, M. S. Wicha, T. S. Lawrence, Ablation of breast cancer stem cells with radiation. *Transl. Oncol.* **4**, 227–233 (2011).
199. X. Li, *et al.*, Intrinsic Resistance of Tumorigenic Breast Cancer Cells to Chemotherapy. *JNCI J. Natl. Cancer Inst.* **100**, 672–679 (2008).
200. P. Zou, *et al.*, P57 Kip2 and p27 Kip1 cooperate to maintain hematopoietic stem cell quiescence through interactions with Hsc70. *Cell Stem Cell* **9**, 247–261 (2011).
201. F. Staud, P. Pavek, Breast cancer resistance protein (BCRP/ABCG2). *Int. J. Biochem. Cell Biol.* **37**, 720–725 (2005).
202. M. Dean, ABC transporters, drug resistance, and cancer stem cells. *J. Mammary Gland Biol. Neoplasia* **14**, 3–9 (2009).
203. M. A. Goodell, K. Brose, G. Paradis, A. S. Conner, R. C. Mulligan, Isolation and functional properties of murine hematopoietic stem cells that are replicating in vivo. *J. Exp. Med.* **183**, 1797–1806 (1996).
204. P. E. Mirkes, A. Ellison, S. A. Little, Role of aldehyde dehydrogenase (ALDH) in the detoxication of cyclophosphamide (CP) in rat embryos. *Adv. Exp. Med. Biol.* **284**, 85–95 (1991).
205. C. H. Chang, *et al.*, Mammary Stem Cells and Tumor-Initiating Cells Are More Resistant to Apoptosis and Exhibit Increased DNA Repair Activity in Response to DNA Damage. *Stem Cell Reports* **5**, 378–391 (2015).
206. S. Liu, S. G. Clouthier, M. S. Wicha, Role of microRNAs in the regulation of breast cancer stem cells. *J. Mammary Gland Biol. Neoplasia* **17**, 15–21 (2012).
207. S. Palomeras, S. Ruiz-Martínez, T. Puig, Targeting Breast Cancer Stem Cells to Overcome Treatment Resistance. *Molecules* **23**, 2193 (2018).
208. A. Matsumoto, *et al.*, P57 Is required for quiescence and maintenance of

- adult hematopoietic stem cells. *Cell Stem Cell* **9**, 262–271 (2011).
209. S. Takeishi, *et al.*, Ablation of Fbxw7 Eliminates Leukemia-Initiating Cells by Preventing Quiescence. *Cancer Cell* **23**, 347–361 (2013).
210. D. Moreno-Lorenzana, *et al.*, CDKIs p18INK4c and p57Kip2 are involved in quiescence of CML leukemic stem cells after treatment with TKI. *Cell Cycle* **15**, 1276–1287 (2016).
211. J. Gasca, *et al.*, Loss of FBXW7 and accumulation of MCL1 and PLK1 promote paclitaxel resistance in breast cancer. *Oncotarget* **7**, 52751–52765 (2016).
212. C. Naujokat, R. Steinhart, Salinomycin as a Drug for Targeting Human Cancer Stem Cells. *J. Biomed. Biotechnol.* **2012**, 1–17 (2012).
213. W. Yue, *et al.*, Inhibition of the autophagic flux by salinomycin in breast cancer stem-like/progenitor cells interferes with their maintenance. *Autophagy* **9**, 714–29 (2013).
214. C. Gong, *et al.*, Markers of tumor-initiating cells predict chemoresistance in breast cancer. *PLoS One* **5** (2010).
215. P. S. Oak, *et al.*, Combinatorial treatment of mammospheres with trastuzumab and salinomycin efficiently targets HER2-positive cancer cells and cancer stem cells. *Int. J. Cancer* **131**, 2808–2819 (2012).
216. M. Kai, *et al.*, Targeting breast cancer stem cells in triple-negative breast cancer using a combination of LBH589 and salinomycin. *Breast Cancer Res. Treat.* **151**, 281–294 (2015).
217. R. Lamb, *et al.*, Antibiotics that target mitochondria effectively eradicate cancer stem cells, across multiple tumor types: treating cancer like an infectious disease. *Oncotarget* **6**, 4569–84 (2015).
218. J. M.-M. Kwok, *et al.*, Thiostrepton selectively targets breast cancer cells through inhibition of forkhead box M1 expression. *Mol. Cancer Ther.* **7**, 2022–32 (2008).
219. N. Yang, *et al.*, Inhibition of Sonic Hedgehog Signaling Pathway by Thiazole Antibiotic Thiostrepton Attenuates the CD44+/CD24-Stem-Like Population and Sphere-Forming Capacity in Triple-Negative Breast Cancer. *Cell. Physiol. Biochem.* **38**, 1157–70 (2016).
220. H. Yin, J. Glass, The phenotypic radiation resistance of CD44 +/CD24 -or low breast cancer cells is mediated through the enhanced activation of ATM signaling. *PLoS One* **6** (2011).
221. A. K. Croker, A. L. Allan, Inhibition of aldehyde dehydrogenase (ALDH) activity reduces chemotherapy and radiation resistance of stem-like ALDH hiCD44 + human breast cancer cells. *Breast Cancer Res. Treat.* **133**, 75–87 (2012).
222. J. Li, *et al.*, Polymer-lipid hybrid anti-HER2 nanoparticles for targeted salinomycin delivery to HER2-positive breast cancer stem cells and cancer cells. *Int. J. Nanomedicine* **12**, 6909–6921 (2017).
223. P. Liu, *et al.*, Liposome encapsulated Disulfiram inhibits NFκB pathway and targets breast cancer stem cells in vitro and in vivo. *Oncotarget* **5**, 7471–85 (2014).
224. D. Coradini, C. Pellizzaro, G. Miglierini, M. G. Daidone, A. Perbellini,

- Hyaluronic acid as drug delivery for sodium butyrate: improvement of the anti-proliferative activity on a breast-cancer cell line. *Int. J. Cancer* **81**, 411–6 (1999).
225. R. E. Eliaz, F. C. Szoka, Liposome-encapsulated doxorubicin targeted to CD44: a strategy to kill CD44-overexpressing tumor cells. *Cancer Res.* **61**, 2592–601 (2001).
226. E. Auzenne, *et al.*, Hyaluronic acid-paclitaxel: antitumor efficacy against CD44(+) human ovarian carcinoma xenografts. *Neoplasia* **9**, 479–86 (2007).
227. N.-K. Han, *et al.*, Hyaluronan-conjugated liposomes encapsulating gemcitabine for breast cancer stem cells. *Int. J. Nanomedicine* **11**, 1413–25 (2016).
228. J. P. Thiery, Epithelial-mesenchymal transitions in development and pathologies. *Curr. Opin. Cell Biol.* **15**, 740–746 (2003).
229. A. Singh, J. Settleman, EMT, cancer stem cells and drug resistance: An emerging axis of evil in the war on cancer. *Oncogene* **29**, 4741–4751 (2010).
230. M. A. Huber, N. Kraut, H. Beug, Molecular requirements for epithelial-mesenchymal transition during tumor progression. *Curr. Opin. Cell Biol.* **17**, 548–558 (2005).
231. G. Moreno-Bueno, F. Portillo, A. Cano, Transcriptional regulation of cell polarity in EMT and cancer. *Oncogene* **27**, 6958–6969 (2008).
232. J. J. Christiansen, A. K. Rajasekaran, Reassessing epithelial to mesenchymal transition as a prerequisite for carcinoma invasion and metastasis. *Cancer Res.* **66**, 8319–8326 (2006).
233. C. Y. Liu, H. H. Lin, M. J. Tang, Y. K. Wang, Vimentin contributes to epithelial-mesenchymal transition cancer cell mechanics by mediating cytoskeletal organization and focal adhesion maturation. *Oncotarget* **6**, 15966–15983 (2015).
234. J. P. Thiery, Epithelial-mesenchymal transitions in tumour progression. *Nat. Rev. Cancer* **2**, 442–54 (2002).
235. S. Kotiyal, S. Bhattacharya, Breast cancer stem cells, EMT and therapeutic targets. *Biochem. Biophys. Res. Commun.* **453**, 112–116 (2014).
236. R. Kalluri, R. A. Weinberg, The basics of epithelial-mesenchymal transition. *J. Clin. Invest.* **119**, 1420–1428 (2009).
237. T. Brabletz, To differentiate or not-routes towards metastasis. *Nat. Rev. Cancer* **12**, 425–436 (2012).
238. M. Balic, *et al.*, Most early disseminated cancer cells detected in bone marrow of breast cancer patients have a putative breast cancer stem cell phenotype. *Clin. Cancer Res.* **12**, 5615–5621 (2006).
239. M. A. Watson, *et al.*, Isolation and molecular profiling of bone marrow micrometastases identifies TWIST1 as a marker of early tumor relapse in breast cancer patients. *Clin. Cancer Res.* **13**, 5001–5009 (2007).
240. C. Raimondi, *et al.*, Epithelial-mesenchymal transition and stemness features in circulating tumor cells from breast cancer patients. *Breast Cancer Res. Treat.* **130**, 449–455 (2011).

241. M. Yu, *et al.*, Circulating breast tumor cells exhibit dynamic changes in epithelial and mesenchymal composition. *Science* (80-.). **339**, 580–584 (2013).
242. R. Liu, *et al.*, The Prognostic Role of a Gene Signature from Tumorigenic Breast-Cancer Cells. *N. Engl. J. Med.* **356**, 217–226 (2007).
243. S. A. Mani, *et al.*, The epithelial-mesenchymal transition generates cell with properties of stem cells. *Cell* **133**, 704–715 (2008).
244. M. Luo, M. Brooks, M. S. Wicha, Epithelial-mesenchymal plasticity of breast cancer stem cells: implications for metastasis and therapeutic resistance. *Curr. Pharm. Des.* **21**, 1301–10 (2015).
245. S. Liu, *et al.*, Breast cancer stem cells are regulated by mesenchymal stem cells through cytokine networks. *Cancer Res.* **71**, 614–624 (2011).
246. M. Magni, *et al.*, Induction of cyclophosphamide-resistance by aldehyde-dehydrogenase gene transfer. *Blood* **87**, 1097–1103 (1996).
247. J. S. Moreb, C. Maccow, M. Schweder, J. Hecomovich, Expression of antisense RNA to aldehyde dehydrogenase class-1 sensitizes tumor cells to 4-hydroperoxycyclophosphamide in vitro. *J. Pharmacol. Exp. Ther.* **293**, 390–396 (2000).
248. M. Zhang, R. L. Atkinson, J. M. Rosen, Selective targeting of radiation-resistant tumor-initiating cells. *Proc. Natl. Acad. Sci. U. S. A.* **107**, 3522–3527 (2010).
249. C. J. Creighton, *et al.*, Residual breast cancers after conventional therapy display mesenchymal as well as tumor-initiating features. *Proc. Natl. Acad. Sci. U. S. A.* **106**, 13820–13825 (2009).
250. F. Schmitt, S. Ricardo, A. F. Vieira, M. R. Dionísio, J. Paredes, Cancer stem cell markers in breast neoplasias: Their relevance and distribution in distinct molecular subtypes. *Virchows Arch.* **460**, 545–553 (2012).
251. F. P. Kuhajda, Fatty-acid synthase and human cancer: New perspectives on its role in tumor biology. *Nutrition* **16**, 202–208 (2000).
252. E. Currie, A. Schulze, R. Zechner, T. C. Walther, R. V. Farese, Cellular fatty acid metabolism and cancer. *Cell Metab.* **18**, 153–161 (2013).
253. S. J. Wakil, Fatty Acid Synthase, A Proficient Multifunctional Enzyme. *Biochemistry* **28**, 4523–4530 (1989).
254. U. S. Shah, *et al.*, Fatty acid synthase gene overexpression and copy number gain in prostate adenocarcinoma. *Hum. Pathol.* **37**, 401–409 (2006).
255. A. K. Witkiewicz, *et al.*, Co-expression of fatty acid synthase and caveolin-1 in pancreatic ductal adenocarcinoma: Implications for tumor progression and clinical outcome. *Cell Cycle* **7**, 3021–3025 (2008).
256. D. Veigel, *et al.*, Fatty acid synthase is a metabolic marker of cell proliferation rather than malignancy in ovarian cancer and its precursor cells. *Int. J. Cancer* **136**, 2078–2090 (2015).
257. Y. Y. Zaytseva, *et al.*, Increased expression of fatty acid synthase provides a survival advantage to colorectal cancer cells via upregulation of cellular respiration. *Oncotarget* **6**, 18891–18904 (2015).
258. A. KATSURADA, *et al.*, Effects of nutrients and hormones on transcriptional

- and post-transcriptional regulation of acetyl-CoA carboxylase in rat liver. *Eur. J. Biochem.* **190**, 435–441 (1990).
259. H. S. Sul, D. Wang, Nutritional and hormonal regulation of enzymes in fat synthesis: Studies of fatty acid synthase and mitochondrial glycerol-3-phosphate acyltransferase gene transcription. *Annu. Rev. Nutr.* **18**, 331–351 (1998).
260. S. M. Anderson, M. C. Rudolph, J. L. McManaman, M. C. Neville, Key stages in mammary gland development. Secretory activation in the mammary gland: It's not just about milk protein synthesis! *Breast Cancer Res.* **9**, 204 (2007).
261. H. Macias, L. Hinck, Mammary gland development. *Wiley Interdiscip. Rev. Dev. Biol.* **1**, 533–557 (2012).
262. J. A. Menendez, R. Lupu, Fatty acid synthase and the lipogenic phenotype in cancer pathogenesis. *Nat. Rev. Cancer* **7**, 763–777 (2007).
263. R. Ventura, *et al.*, Inhibition of de novo Palmitate Synthesis by Fatty Acid Synthase Induces Apoptosis in Tumor Cells by Remodeling Cell Membranes, Inhibiting Signaling Pathways, and Reprogramming Gene Expression. *EBioMedicine* **2**, 808–824 (2015).
264. S. F. Jones, J. R. Infante, Molecular pathways: Fatty acid synthase. *Clin. Cancer Res.* **21**, 5434–5438 (2015).
265. R. Flavin, S. Peluso, P. L. Nguyen, M. Loda, Fatty acid synthase as a potential therapeutic target in cancer. *Futur. Oncol.* **6**, 551–562 (2010).
266. L. Weiss, *et al.*, Fatty-Acid Biosynthesis in Man, a Pathway of Minor Importance Purification, Optimal Assay Conditions, and Organ Distribution of Fatty-Acid Synthase. *Biol. Chem. Hoppe. Seyler.* **367**, 905–912 (1986).
267. E. S. Pizer, R. J. Kurman, G. R. Pasternack, F. P. Kuhajda, Expression of fatty acid synthase is closely linked to proliferation and stromal decidualization in cycling endometrium. *Int. J. Gynecol. Pathol.* **16**, 45–51 (1997).
268. J. A. Menendez, R. Lupu, Fatty acid synthase and the lipogenic phenotype in cancer pathogenesis. *Nat. Rev. Cancer* **7**, 763–777 (2007).
269. M. Schweizer, K. Roder, L. Zhang, S. S. Wolf, Transcription factors acting on the promoter of the rat fatty acid synthase gene in *Biochemical Society Transactions*, (Biochem Soc Trans, 2002), pp. 1070–1072.
270. J. Swierczynski, Leptin and age-related down-regulation of lipogenic enzymes genes expression in rat white adipose tissue in *Journal of Physiology and Pharmacology*, (2006), pp. 85–102.
271. J. V. Swinnen, *et al.*, Overexpression of fatty acid synthase is an early and common event in the development of prostate cancer. *Int. J. Cancer* **98**, 19–22 (2002).
272. C. Kumar-Sinha, K. Woods Ignatoski, M. E. Lippman, S. P. Ethier, A. M. Chinnaiyan, Transcriptome Analysis of HER2 Reveals a Molecular Connection to Fatty Acid Synthesis. *Cancer Res.* **63**, 132–139 (2003).
273. J. A. Menendez, I. Mehmi, V. A. Verma, P. K. Teng, R. Lupu, Pharmacological inhibition of fatty acid synthase (FAS): A novel therapeutic approach for breast cancer chemoprevention through its ability to suppress Her-2/neu (erbB-2) oncogene-induced malignant transformation. *Mol. Carcinog.* **41**,

- 164–178 (2004).
274. T. V. D. Sande, E. D. Schrijver, W. Heyns, G. Verhoeven, J. Swinnen, Advances in Brief Role of the Phosphatidylinositol 3-Kinase / PTEN / Akt Kinase Pathway in the Overexpression of Fatty Acid Synthase in LNCaP Prostate Cancer Cells 1 (2002).
275. H. Q. Wang, *et al.*, Positive feedback regulation between AKT activation and fatty acid synthase expression in ovarian carcinoma cells. *Oncogene* **24**, 3574–3582 (2005).
276. H. Heemers, *et al.*, Androgens stimulate lipogenic gene expression in prostate cancer cells by activation of the sterol regulatory element-binding protein cleavage activating protein/sterol regulatory element-binding protein pathway. *Mol. Endocrinol.* **15**, 1817–1828 (2001).
277. S. Bandyopadhyay, *et al.*, Mechanism of apoptosis induced by the inhibition of fatty acid synthase in breast cancer cells. *Cancer Res.* **66**, 5934–5940 (2006).
278. T. Puig, *et al.*, Fatty acid metabolism in breast cancer cells: Differential inhibitory effects of epigallocatechin gallate (EGCG) and C75. *Breast Cancer Res. Treat.* **109**, 471–479 (2008).
279. A. Blancafort, *et al.*, Dual fatty acid synthase and HER2 signaling blockade shows marked antitumor activity against breast cancer models resistant to anti-HER2 drugs. *PLoS One* **10**, e0131241 (2015).
280. C. D. Browne, E. J. Hindmarsh, J. W. Smith, Inhibition of endothelial cell proliferation and angiogenesis by orlistat, a fatty acid synthase inhibitor. *FASEB J.* **20**, 2027–2035 (2006).
281. F. Seguin, *et al.*, The fatty acid synthase inhibitor orlistat reduces experimental metastases and angiogenesis in B16-F10 melanomas. *Br. J. Cancer* **107**, 977–987 (2012).
282. E. Rysman, *et al.*, De novo lipogenesis protects cancer cells from free radicals and chemotherapeutics by promoting membrane lipid saturation. *Cancer Res.* **70**, 8117–8126 (2010).
283. A. S. Meena, *et al.*, Inherent and Acquired Resistance to Paclitaxel in Hepatocellular Carcinoma: Molecular Events Involved. *PLoS One* **8**, e61524 (2013).
284. J. A. Menendez, L. Vellon, R. Colomer, R. Lupu, Pharmacological and small interference RNA-mediated inhibition of breast cancer-associated fatty acid synthase (oncogenic antigen-519) synergistically enhances Taxol (Paclitaxel)-induced cytotoxicity. *Int. J. Cancer* **115**, 19–35 (2005).
285. A. Giró-Perafita, *et al.*, Preclinical Evaluation of Fatty Acid Synthase and EGFR Inhibition in Triple Negative Breast Cancer. *Clin. Cancer Res.* **22**, 4687–4697 (2016).
286. F. P. Kuhajda, *et al.*, Fatty acid synthesis: A potential selective target for antineoplastic therapy. *Proc. Natl. Acad. Sci. U. S. A.* **91**, 6379–6383 (1994).
287. J. A. Menendez, R. Lupu, Fatty acid synthase-catalyzed de novo fatty acid biosynthesis: From anabolic-energy-storage pathway in normal tissues to jack-of-all-trades in cancer cells. *Arch. Immunol. Ther. Exp. (Warsz)*. **52**, 414–426 (2004).

288. K. Simons, J. L. Sampaio, Membrane organization and lipid rafts. *Cold Spring Harb. Perspect. Biol.* **3**, 1–17 (2011).
289. F. Mollinedo, C. Gajate, Lipid rafts as major platforms for signaling regulation in cancer. *Adv. Biol. Regul.* **57**, 130–146 (2015).
290. T. Maier, S. Jenni, N. Ban, Architecture of mammalian fatty acid synthase at 4.5 Å resolution. *Science (80-.)*. **311**, 1258–1262 (2006).
291. J.-N. Li, *et al.*, “Pharmacological Inhibition of Fatty Acid Synthase Activity Produces Both Cytostatic and Cytotoxic Effects Modulated by p53 1” (2001).
292. E. S. Pizer, *et al.*, Malonyl-Coenzyme-A Is a Potential Mediator of Cytotoxicity Induced by Fatty-Acid Synthase Inhibition in Human Breast Cancer Cells and Xenografts. *Cancer Res.* **60** (2000).
293. T. Puig, *et al.*, Novel inhibitors of fatty acid synthase with anticancer activity. *Clin. Cancer Res.* **15**, 7608–7615 (2009).
294. J. Relat, *et al.*, Different fatty acid metabolism effects of (-)-epigallocatechin-3-gallate and C75 in adenocarcinoma lung cancer. *BMC Cancer* **12**, 280 (2012).
295. D. Vance, *et al.*, Inhibition of fatty acid synthetases by the antibiotic cerulenin. *Biochem. Biophys. Res. Commun.* **48**, 649–656 (1972).
296. H. Funabashi, *et al.*, Binding site of cerulenin in fatty acid synthetase. *J. Biochem.* **105**, 751–755 (1989).
297. F. P. Kuhajda, Synthesis and antitumor activity of an inhibitor of fatty acid synthase. *Proc. Natl. Acad. Sci.* **97**, 3450–3454 (2000).
298. E. S. Pizer, *et al.*, Inhibition of Fatty Acid Synthesis Delays Disease Progression in a Xenograft Model of Ovarian Cancer. *Cancer Res.* **56** (1996).
299. A. R. Rendina, D. Cheng, Characterization of the inactivation of rat fatty acid synthase by C75: Inhibition of partial reactions and protection by substrates. *Biochem. J.* **388**, 895–903 (2005).
300. P. M. Alli, M. L. Finn, E. M. Jaffee, J. M. McFadden, F. P. Kuhajda, Fatty acid synthase inhibitors are chemopreventive for mammary cancer in neu-N transgenic mice. *Oncogene* **24**, 39–46 (2005).
301. T. M. Loftus, *et al.*, Reduced food intake and body weight in mice treated with fatty acid synthase inhibitors. *Science (80-.)*. **288**, 2379–2381 (2000).
302. T. Puig, *et al.*, Fatty acid metabolism in breast cancer cells: Differential inhibitory effects of epigallocatechin gallate (EGCG) and C75. *Breast Cancer Res. Treat.* **109**, 471–479 (2008).
303. D. Chen, *et al.*, *EGCG, green tea polyphenols and their synthetic analogs and prodrugs for human cancer prevention and treatment* (Adv Clin Chem, 2011).
304. G. Oliveras, *et al.*, Novel anti-fatty acid synthase compounds with anti-cancer activity in HER2+ breast cancer. *Ann. N. Y. Acad. Sci.* **1210**, 86–92 (2010).
305. J. Crous-Masó, *et al.*, (-)-Epigallocatechin 3-gallate synthetic analogues inhibit fatty acid synthase and show anticancer activity in triple negative breast cancer. *Molecules* **23** (2018).
306. T. Puig, *et al.*, A novel inhibitor of fatty acid synthase shows activity against

- HER2+ breast cancer xenografts and is active in anti-HER2 drug-resistant cell lines. *Breast Cancer Res.* **13**, R131 (2011).
307. A. Blancafort, *et al.*, Dual fatty acid synthase and HER2 signaling blockade shows marked antitumor activity against breast cancer models resistant to Anti-HER2 drugs. *PLoS One* **10** (2015).
308. S. Ringer, Concerning the Influence exerted by each of the Constituents of the Blood on the Contraction of the Ventricle. *J. Physiol.* **3**, 380–393 (1882).
309. G. Gey, W. Coffman, M. Kubicek, Tissue culture studies of the proliferative capacity of cervical carcinoma and normal epithelium. *Cancer Res.* **12**, 264–265 (1952).
310. R. L. Ehrmann, G. O. Gey, The Growth of Cells on a Transparent Gel of Reconstituted Rat-Tail Collagen. *JNCI J. Natl. Cancer Inst.* **16**, 1375–1403 (1956).
311. E. Polonio-Alcalá, M. Rabionet, S. Ruiz-Martínez, J. Ciurana, T. Puig, Three-Dimensional Manufactured Supports for Breast Cancer Stem Cell Population Characterization. *Curr. Drug Targets* **20**, 839–851 (2019).
312. C. F. Amstein, P. A. Hartman, Adaptation of plastic surfaces for tissue culture by glow discharge. *J. Clin. Microbiol.* **2**, 46–54 (1975).
313. J. A. Ryhan, Evolution of Cell Culture Surfaces. *Biofiles* **3**, 21–24 (2008).
314. C. Frantz, K. M. Stewart, V. M. Weaver, The extracellular matrix at a glance. *J. Cell Sci.* **123**, 4195–200 (2010).
315. A. D. Theocharis, S. S. Skandalis, C. Gialeli, N. K. Karamanos, Extracellular matrix structure. *Adv. Drug Deliv. Rev.* **97**, 4–27 (2016).
316. C. H. Thomas, J. H. Collier, C. S. Sfeir, K. E. Healy, Engineering gene expression and protein synthesis by modulation of nuclear shape. *Proc. Natl. Acad. Sci. U. S. A.* **99**, 1972–7 (2002).
317. L. Vergani, M. Grattarola, C. Nicolini, Modifications of chromatin structure and gene expression following induced alterations of cellular shape. *Int. J. Biochem. Cell Biol.* **36**, 1447–61 (2004).
318. F. Xu, A. E. K. J. L. Burg, Three-dimensional polymeric systems for cancer cell studies. 135–143 (2007).
319. J. S. Hale, *et al.*, The malignant social network The malignant social network Cell-cell adhesion and communication in cancer stem cells. **6918** (2016).
320. G. Bao, S. Suresh, Cell and molecular mechanics of biological materials. *Nat. Mater.* **2**, 715–725 (2003).
321. C.-M. Lo, H.-B. Wang, M. Dembo, Y.-L. Wang, “Cell Movement Is Guided by the Rigidity of the Substrate” (2000).
322. T. Yeung, *et al.*, Effects of substrate stiffness on cell morphology, cytoskeletal structure, and adhesion. *Cell Motil. Cytoskeleton* **60**, 24–34 (2005).
323. B. A. Reynolds, S. Weiss, Clonal and population analyses demonstrate that an EGF-responsive mammalian embryonic CNS precursor is a stem cell. *Dev. Biol.* **175**, 1–13 (1996).
324. S. Weiss, *et al.*, Is there a neural stem cell in the mammalian forebrain? *Trends Neurosci.* **19**, 387–93 (1996).
325. F. L. Shaw, *et al.*, A detailed mammosphere assay protocol for the

- quantification of breast stem cell activity. *J. Mammary Gland Biol. Neoplasia* **17**, 111–7 (2012).
326. O. WICHTERLE, D. LÍM, Hydrophilic Gels for Biological Use. *Nature* **185**, 117–118 (1960).
327. J. Ciurana, C. A. Rodríguez, Trends in nanomaterials and processing for drug delivery of polyphenols for cancer and other treatments. *Curr. Drug Targets* (2015) (January 10, 2017).
328. K. Saha, J. F. Pollock, D. V Schaffer, K. E. Healy, Designing synthetic materials to control stem cell phenotype. *Curr. Opin. Chem. Biol.* **11**, 381–387 (2007).
329. H. K. Kleinman, G. R. Martin, Matrigel: basement membrane matrix with biological activity. *Semin. Cancer Biol.* **15**, 378–86 (2005).
330. E. Knight, S. Przyborski, Advances in 3D cell culture technologies enabling tissue-like structures to be created in vitro. *J. Anat.*, 1–11 (2014).
331. M. Domingos, *et al.*, Polycaprolactone Scaffolds Fabricated via Bioextrusion for Tissue Engineering Applications. *Int. J. Biomater.* **2009**, 1–9 (2009).
332. J. De Ciurana, L. Serenó, È. Vallès, Selecting process parameters in RepRap additive manufacturing system for PLA scaffolds manufacture in *Procedia CIRP*, (2013), pp. 152–157.
333. P. Bartolo, M. Domingos, a. Gloria, J. Ciurana, BioCell Printing: Integrated automated assembly system for tissue engineering constructs. *CIRP Ann. - Manuf. Technol.* **60**, 271–274 (2011).
334. Y. J. Tan, X. Tan, W. Y. Yeong, S. B. Tor, Additive Manufacturing of Patient-Customizable Scaffolds for Tubular Tissues Using the Melt-Drawing Method. *Mater. (Basel, Switzerland)* **9** (2016).
335. A. Rathore, M. Cleary, Y. Naito, K. Rocco, C. Breuer, Development of tissue engineered vascular grafts and application of nanomedicine. *Wiley Interdiscip. Rev. Nanomedicine Nanobiotechnology* **4**, 257–272 (2012).
336. A. Giró Perafita, M. Rabionet, T. Puig, J. Ciurana, Optimization of Poly(ϵ -caprolactone) Scaffolds Suitable for 3D Cancer Cell Culture. *Procedia CIRP* **49**, 61–66 (2016).
337. M. Rabionet, *et al.*, Design of a Scaffold Parameter Selection System with Additive Manufacturing for a Biomedical Cell Culture. *Materials (Basel)*. **11**, 1427 (2018).
338. S. J. Hollister, R. D. Maddox, J. M. Taboas, Optimal design and fabrication of scaffolds to mimic tissue properties and satisfy biological constraints. *Biomaterials* **23**, 4095–4103 (2002).
339. O. A. Mohamed, S. H. Masood, J. L. Bhowmik, Experimental Investigations of Process Parameters Influence on Rheological Behavior and Dynamic Mechanical Properties of FDM Manufactured Parts. *Mater. Manuf. Process.* **31**, 1983–1991 (2016).
340. M. Domingos, *et al.*, The first systematic analysis of 3D rapid prototyped poly(ϵ -caprolactone) scaffolds manufactured through BioCell printing: the effect of pore size and geometry on compressive mechanical behaviour and in vitro hMSC viability. *Biofabrication* **5**, 045004 (2013).

341. S. P. Barton, R. Marks, Measurement of collagen-fibre diameter in human skin. *J. Cutan. Pathol.* **11**, 18–26 (1984).
342. B. D. Ratner, S. J. Bryant, Biomaterials: Where we have been and where we are going. *Annu. Rev. Biomed. Eng.* **6**, 41–75 (2004).
343. J. Ciurana, Designing, prototyping and manufacturing medical devices: An overview. *Int. J. Comput. Integr. Manuf.* **27**, 901–918 (2014).
344. T. W. Gilbert, T. L. Sellaro, S. F. Badylak, Decellularization of tissues and organs. *Biomaterials* **27**, 3675–3683 (2006).
345. P. M. Crapo, T. W. Gilbert, S. F. Badylak, An overview of tissue and whole organ decellularization processes. *Biomaterials* **32**, 3233–3243 (2011).
346. H. Breme, V. Biehl, J. Helsen, “Metals and implants” in *Metals as Biomaterials*, (1998), pp. 37–72.
347. S. H. Alavi, A. Kheradvar, Metal mesh scaffold for tissue engineering of membranes. *Tissue Eng. - Part C Methods* **18**, 293–301 (2012).
348. J. Li, H. Yuan, A. Chandrakar, L. Moroni, P. Habibovic, 3D porous Ti6Al4V-beta-tricalcium phosphate scaffolds directly fabricated by additive manufacturing. *Acta Biomater.* **126**, 496–510 (2021).
349. P. Bartolo, *et al.*, Biomedical production of implants by additive electrochemical and physical processes. *CIRP Ann. - Manuf. Technol.* **61**, 635–655 (2012).
350. M. Wang, Developing bioactive composite materials for tissue replacement. *Biomaterials* **24**, 2133–2151 (2003).
351. K. Y. Lee, *et al.*, Ceramic bioactivity: Progresses, challenges and perspectives. *Biomed. Mater.* **1** (2006).
352. S. V. Dorozhkin, Bioceramics of calcium orthophosphates. *Biomaterials* **31**, 1465–1485 (2010).
353. L. L. Hench, J. Wilson, *An Introduction to Bioceramics* (WORLD SCIENTIFIC, 1993) <https://doi.org/10.1142/2028>.
354. G. Binyamin, B. M. Shafi, C. M. Mery, Biomaterials: A primer for surgeons. *Semin. Pediatr. Surg.* **15**, 276–283 (2006).
355. R. Shu, R. McMullen, M. J. Baumann, L. R. McCabe, Hydroxyapatite accelerates differentiation and suppresses growth of MC3T3-E1 osteoblasts. *J. Biomed. Mater. Res. - Part A* **67**, 1196–1204 (2003).
356. B. Annaz, K. A. Hing, M. Kayser, T. Buckland, L. Di Silvio, Porosity variation in hydroxyapatite and osteoblast morphology: A scanning electron microscopy study. *J. Microsc.* **215**, 100–110 (2004).
357. L. Sun, *et al.*, Gene expressions of Collagen type I, ALP and BMP-4 in osteo-inductive BCP implants show similar pattern to that of natural healing bones. *Mater. Sci. Eng. C* **29**, 1829–1834 (2009).
358. J. Wang, J. de Boer, K. de Groot, Proliferation and differentiation of osteoblast-like MC3T3-E1 cells on biomimetically and electrolytically deposited calcium phosphate coatings. *J. Biomed. Mater. Res. A* **90**, 664–670 (2009).
359. K. Jurczyk, K. Niespodziana, M. U. Jurczyk, M. Jurczyk, Synthesis and characterization of titanium-45S5 Bioglass nanocomposites. *Mater. Des.* **32**, 2554–2560 (2011).

360. J. Jagur-Grodzinski, Polymers for tissue engineering, medical devices, and regenerative medicine. Concise general review of recent studies. *Polym. Adv. Technol.* **17**, 395–418 (2006).
361. M. Domingos, *et al.*, Evaluation of in vitro degradation of pcl scaffolds fabricated via bioextrusion. part 1: Influence of the degradation environment. *Virtual Phys. Prototyp.* **5**, 65–73 (2010).
362. A. Cipitria, A. Skelton, T. R. Dargaville, P. D. Dalton, D. W. Hutmacher, Design, fabrication and characterization of PCL electrospun scaffolds—a review. *J. Mater. Chem.* **21**, 9419–9453 (2011).
363. R. R. Duling, R. B. Dupaix, N. Katsube, J. Lannutti, Mechanical characterization of electrospun polycaprolactone (PCL): a potential scaffold for tissue engineering. *J. Biomech. Eng.* **130**, 011006 (2008).
364. J. Sims-Mourtada, R. a. Niamat, S. Samuel, C. Eskridge, E. B. Kmiec, Enrichment of breast cancer stem-like cells by growth on electrospun polycaprolactone-chitosan nanofiber scaffolds. *Int. J. Nanomedicine* **9**, 995–1003 (2014).
365. S. Palomeras, *et al.*, Breast cancer stem cell culture and enrichment using poly(ϵ -caprolactone) scaffolds. *Molecules* (2016).
366. B. M. Baker, N. L. Nerurkar, J. A. Burdick, D. M. Elliott, R. L. Mauck, Fabrication and modeling of dynamic multipolymer nanofibrous scaffolds. *J. Biomech. Eng.* **131**, 101012 (2009).
367. C. S. Szot, C. F. Buchanan, P. Gatenholm, M. N. Rylander, J. W. Freeman, Investigation of cancer cell behavior on nanofibrous scaffolds. *Mater. Sci. Eng. C* **31**, 37–42 (2011).
368. S. Hinderer, *et al.*, Engineering of fibrillar decorin matrices for a tissue-engineered trachea. *Biomaterials* **33**, 5259–5266 (2012).
369. Y. Qian, *et al.*, The effect of hyaluronan on the motility of skin dermal fibroblasts in nanofibrous scaffolds. *Int. J. Biol. Macromol.* **79**, 133–143 (2015).
370. S. G. Wise, *et al.*, A multilayered synthetic human elastin/polycaprolactone hybrid vascular graft with tailored mechanical properties. *Acta Biomater.* **7**, 295–303 (2011).
371. E. Charafe-Jauffret, *et al.*, Breast Cancer Cell Lines Contain Functional Cancer Stem Cells with Metastatic Capacity and a Distinct Molecular Signature. *Cancer Res.* **69**, 1302–1313 (2009).
372. A. Tsuyada, *et al.*, CCL2 mediates cross-talk between cancer cells and stromal fibroblasts that regulates breast cancer stem cells. *Cancer Res.* **72**, 2768–79 (2012).
373. S. Saha, *et al.*, Electrospun fibrous scaffolds promote breast cancer cell alignment and epithelial-mesenchymal transition. *Langmuir* **28**, 2028–34 (2012).
374. M. A. Woodruff, D. W. Hutmacher, The return of a forgotten polymer - Polycaprolactone in the 21st century. *Prog. Polym. Sci.* **35**, 1217–1256 (2010).
375. G. Xiang Gu, *et al.*, Three-Dimensional-Printing of Bio-Inspired Composites. *J. Biomech. Eng.* **138**, 021006 (2016).

376. C. S. Ranucci, A. Kumar, S. P. Batra, P. V. Moghe, Control of hepatocyte function on collagen foams: Sizing matrix pores toward selective induction of 2-D and 3-D cellular morphogenesis. *Biomaterials* **21**, 783–793 (2000).
377. M. Chen, P. K. Patra, S. B. Warner, S. Bhowmick, Role of fiber diameter in adhesion and proliferation of NIH 3T3 fibroblast on electrospun polycaprolactone scaffolds. *Tissue Eng.* **13**, 579–87 (2007).
378. M. Chen, H. Michaud, S. Bhowmick, Controlled Vacuum Seeding as a Means of Generating Uniform Cellular Distribution in Electrospun Polycaprolactone (PCL) Scaffolds. *J Biomech Eng* **131**, 1–8 (2009).
379. L. A. Bosworth, S. Downes, Acetone, a Sustainable Solvent for Electrospinning Poly(ϵ -Caprolactone) Fibres: Effect of Varying Parameters and Solution Concentrations on Fibre Diameter. *J. Polym. Environ.* **20**, 879–886 (2012).
380. M. Chen, P. K. Patra, S. B. Warner, S. Bhowmick, Optimization of electrospinning process parameters for tissue engineering scaffolds. *Biophys. Rev. Lett.* **01**, 153–178 (2006).
381. X. Zong, *et al.*, Structure and process relationship of electrospun bioabsorbable nanofiber membranes. *Polymer (Guildf)*. **43**, 4403–4412 (2002).
382. M. D. Amatangelo, D. E. Bassi, A. J. P. Klein-Szanto, E. Cukierman, Stroma-derived three-dimensional matrices are necessary and sufficient to promote desmoplastic differentiation of normal fibroblasts. *Am. J. Pathol.* **167**, 475–488 (2005).
383. P. P. Provenzano, *et al.*, Collagen reorganization at the tumor-stromal interface facilitates local invasion. *BMC Med.* **4** (2006).
384. C. J. Creighton, *et al.*, Residual breast cancers after conventional therapy display mesenchymal as well as tumor-initiating features. *Proc. Natl. Acad. Sci. U. S. A.* **106**, 13820–13825 (2009).
385. S. J. Vidal, V. Rodriguez-Bravo, M. Galsky, C. Cordon-Cardo, J. Domingo-Domenech, Targeting cancer stem cells to suppress acquired chemotherapy resistance. *Oncogene*, 1–13 (2013).
386. H. Liu, *et al.*, Fatty acid synthase causes drug resistance by inhibiting TNF- α and ceramide production. *J. Lipid Res.* **54**, 776–85 (2013).
387. X. Wu, L. Qin, V. Fako, J.-T. Zhang, Molecular mechanisms of fatty acid synthase (FASN)-mediated resistance to anti-cancer treatments. *Adv. Biol. Regul.* **54**, 214–21 (2014).
388. T. Tanei, *et al.*, Association of breast cancer stem cells identified by aldehyde dehydrogenase 1 expression with resistance to sequential paclitaxel and epirubicin-based chemotherapy for breast cancers. *Clin. Cancer Res.* **15**, 4234–4241 (2009).
389. S. A. Mani, *et al.*, The epithelial-mesenchymal transition generates cells with properties of stem cells. *Cell* **133**, 704–15 (2008).
390. A.-P. Morel, *et al.*, Generation of breast cancer stem cells through epithelial-mesenchymal transition. *PLoS One* **3**, e2888 (2008).
391. S. E. Moody, *et al.*, The transcriptional repressor Snail promotes mammary tumor recurrence. *Cancer Cell* **8**, 197–209 (2005).

392. H. D. Tran, *et al.*, Transient SNAIL1 expression is necessary for metastatic competence in breast cancer. *Cancer Res.* **74**, 6330–6340 (2014).
393. X. Ye, *et al.*, Distinct EMT programs control normal mammary stem cells and tumour-initiating cells. *Nature* **525**, 256–260 (2015).
394. S. Phillips, C. Kuperwasser, SLUG: Critical regulator of epithelial cell identity in breast development and cancer <http://www.tandfonline.com/doi/pdf/10.4161/19336918.2014.972740>. *Cell Adhes. Migr.* **8**, 578–587 (2014).
395. J. A. Kruger, *et al.*, mice Characterization of stem cell – like cancer cells in immune-competent mice. **108**, 3906–3912 (2012).
396. A. Bandyopadhyay, *et al.*, Doxorubicin in combination with a small TGF β inhibitor: A potential novel therapy for metastatic breast cancer in mouse models. *PLoS One* **5** (2010).
397. X. Zhuang, *et al.*, Doxorubicin-enriched, ALDH(br) mouse breast cancer stem cells are treatable to oncolytic herpes simplex virus type 1. *BMC Cancer* **12**, 549 (2012).
398. O. Tudoran, *et al.*, Regulation of stem cells-related signaling pathways in response to doxorubicin treatment in Hs578T triple-negative breast cancer cells. *Mol. Cell. Biochem.* **409**, 163–176 (2015).
399. A. L. Silva Galbiatti-Dias, *et al.*, Relationship between CD44high/CD133high/CD117high cancer stem cells phenotype and Cetuximab and Paclitaxel treatment response in head and neck cancer cell lines. *Am. J. Cancer Res.* **8**, 1633–1641 (2018).
400. H. Liu, Y. Liu, J.-T. Zhang, A new mechanism of drug resistance in breast cancer cells: fatty acid synthase overexpression-mediated palmitate overproduction. *Mol. Cancer Ther.* **7**, 263–70 (2008).
401. A. M. Gonzalez-Guerrico, *et al.*, Suppression of endogenous lipogenesis induces reversion of the malignant phenotype and normalized differentiation in breast cancer. *Oncotarget* **7**, 71151–71168 (2016).
402. P. R. Pandey, *et al.*, Resveratrol suppresses growth of cancer stem-like cells by inhibiting fatty acid synthase. *Breast Cancer Res Treat* **130**, 387–398 (2011).
403. Y. Yasumoto, *et al.*, Inhibition of fatty acid synthase decreases expression of stemness markers in glioma stem cells. *PLoS One* **11** (2016).
404. H. Fong, I. Chun, D. . Reneker, Beaded nanofibers formed during electrospinning. *Polymer (Guildf)*. **40**, 4585–4592 (1999).
405. J. Dias, P. Bártolo, Morphological Characteristics of Electrospun PCL Meshes – The Influence of Solvent Type and Concentration. *Procedia CIRP* **5**, 216–221 (2013).
406. A. C. Bean, R. S. Tuan, 3D cell culture and osteogenic differentiation of human bone marrow stromal cells plated onto jet-sprayed or electrospun micro-fiber scaffolds Fiber diameter and seeding density influence chondrogenic differentiation of mesenchymal stem cells seeded on electrospun poly(-caprolactone) scaffolds. *Biomed. Mater* **10** (2015).
407. D. Li, *et al.*, Three-dimensional polycaprolactone scaffold via needleless electrospinning promotes cell proliferation and infiltration. *Colloids*

- Surfaces B Biointerfaces* **121**, 432–443 (2014).
408. S. H. Lim, X. Y. Liu, H. Song, K. J. Yarema, H.-Q. Mao, The effect of nanofiber-guided cell alignment on the preferential differentiation of neural stem cells. *Biomaterials* **31**, 9031–9 (2010).
409. W. Li, *et al.*, Unraveling the roles of CD44/CD24 and ALDH1 as cancer stem cell markers in tumorigenesis and metastasis. *Sci. Rep.* **7**, 13856 (2017).
410. L. Feng, *et al.*, Identification of new cancer stem cell markers and signaling pathways in HER-2-positive breast cancer by transcriptome sequencing. *Int. J. Oncol.* **55**, 1013–1018 (2019).
411. S. Yousefnia, K. Ghaedi, F. Seyed Forootan, M. H. Nasr Esfahani, Characterization of the stemness potency of mammospheres isolated from the breast cancer cell lines. *Tumor Biol.* **41** (2019).
412. R. G. Wells, D. E. Discher, Matrix elasticity, cytoskeletal tension, and TGF- β : The insoluble and soluble meet. *Sci. Signal.* **1**, pe13 (2008).
413. Y. Yarden, G. Pines, The ERBB network: At last, cancer therapy meets systems biology. *Nat. Rev. Cancer* **12**, 553–563 (2012).
414. P. P. Provenzano, D. R. Inman, K. W. Eliceiri, P. J. Keely, Matrix density-induced mechanoregulation of breast cell phenotype, signaling and gene expression through a FAK-ERK linkage. *Oncogene* **28**, 4326–4343 (2009).
415. M. Majumder, *et al.*, COX-2 Induces Breast Cancer Stem Cells via EP4/PI3K/AKT/NOTCH/WNT Axis. *Stem Cells* **34**, 2290–2305 (2016).
416. J. Sunayama, *et al.*, Crosstalk Between the PI3K/mTOR and MEK/ERK Pathways Involved in the Maintenance of Self-Renewal and Tumorigenicity of Glioblastoma Stem-Like Cells. *Stem Cells* **28**, 1930–1939 (2010).
417. M. C. Mendoza, E. Emrah Er, J. Blenis, The Ras-ERK and PI3K-mTOR Pathways: Cross-talk and Compensation (2011) <https://doi.org/10.1016/j.tibs.2011.03.006>.
418. M. Pickl, C. H. Ries, Comparison of 3D and 2D tumor models reveals enhanced HER2 activation in 3D associated with an increased response to trastuzumab. *Oncogene* **28**, 461–468 (2009).
419. S. Gangadhara, C. Smith, P. Barrett-Lee, S. Hiscox, 3D culture of Her2+ breast cancer cells promotes AKT to MAPK switching and a loss of therapeutic response. *BMC Cancer* **16** (2016).
420. B. Weigelt, A. T. Lo, C. C. Park, J. W. Gray, M. J. Bissell, HER2 signaling pathway activation and response of breast cancer cells to HER2-targeting agents is dependent strongly on the 3D microenvironment. *Breast Cancer Res Treat* **122**, 35–43 (2010).
421. T. Wang, *et al.*, JAK/STAT3-Regulated Fatty Acid β -Oxidation Is Critical for Breast Cancer Stem Cell Self-Renewal and Chemoresistance. *Cell Metab.* **27**, 136-150.e5 (2018).
422. H. Li, Z. Feng, M. L. He, Lipid metabolism alteration contributes to and maintains the properties of cancer stem cells. *Theranostics* **10**, 7053–7069 (2020).
423. S. Xu, *et al.*, Fatty acid synthase promotes breast cancer metastasis by mediating changes in fatty acid metabolism. *Oncol. Lett.* **21** (2021).

CHAPTER 11 Annex

Part of the Introduction has been expanded, adapted, and published as a review in the following publication.

Polonio-Alcalá, E., Rabionet, M., Ruiz-Martínez, S., Ciurana, J., & Puig, T. Three-Dimensional Manufactured Supports for Breast Cancer Stem Cell Population Characterization. *Current drug targets*. Vol. 20, Issue 8 (2019), 839–851.

<http://dx.doi.org/10.1016/j.ins.2011.12.012>

Received: July 24, 2018

Revised: November 03, 2018

Accepted: November 07, 2018

©2019 Bentham Science Publishers

Abstract

Breast Cancer (BC) is the most common cancer among women and the second cause of female death for cancer. When the tumor is not correctly eradicated, there is a high relapse risk and incidence of metastasis. Breast Cancer Stem Cells (BCSCs) are responsible for initiating tumors and are resistant to current anticancer therapies being in part responsible for tumor relapse and metastasis. The study of BCSCs is limited due to their low percentage within both tumors and established cell models. Hence, three-dimensional (3D) supports are presented as an interesting tool to keep the stem-like features in 3D cell culture. In this review, several 3D culture systems are discussed. Moreover, scaffolds are presented as a tool to enrich in BCSCs in order to find new specific therapeutic strategies against this malignant subpopulation. Anticancer treatments focused on BCSCs could be useful for BC patients, with particular interest in those that progress to current therapies.

Keywords:

Breast cancer; additive manufacturing; breast cancer stem cells biomarkers; cancer stem cells; electrospinning; fused filament fabrication; scaffolds; three-dimensional cell culture..

